Journal of Energy Storage 181 (2026) 124299

Contents lists available at ScienceDirect

Journal of Energy Storage

journal homepage: www.elsevier.com/locate/est

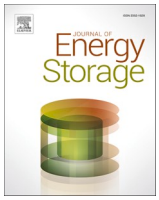

Review Article

Energy and exergy optimization of multilevel power converters in renewable energy systems: A review of AI-driven control strategies

Gowthamraj Rajendran [a,*], Darius Andriukaitis [a,*], Reiko Raute [b], Vytautas Markevičius [a], Dangirutis Navikas [a], Mindaugas Žilys [a], Algimantas Valinevičius [a], Roman Šotner [c], Jan Jerabek [c], Ladislav Polak [c]

[a] Department of Electronics Engineering, Faculty of Electrical and Electronics Engineering Kaunas University of Technology, Studentu St. 50, LT-51368 Kaunas, Lithuania
[b] Department of Electrical Engineering, Faculty of Engineering, University of Malta Msida Campus (Main Campus), MSD, 2080 Msida, Malta
[c] Faculty of Electrical Engineering and Communication, Brno University of Technology, 616 00 Brno, Czech Republic

ARTICLE INFO

Keywords:
Multilevel converters
Modular multilevel converters (MMCs)
Artificial intelligence–based control
Renewable energy systems
Power electronic converters

ABSTRACT

The rapid expansion of renewable energy generation and energy-storage deployment has increased the demand for power conversion systems that combine high efficiency, reduced thermal stress, extended storage lifetime, reliable grid interaction, and adaptive real-time operation. Multilevel converter topologies, including neutral-point-clamped, active-neutral-point-clamped, flying-capacitor, cascaded H-bridge, T-type, and modular multilevel converters, provide improved waveform quality, lower semiconductor voltage stress, reduced filtering requirements, and enhanced scalability. Wide-bandgap devices, particularly gallium nitride and silicon carbide, further enable higher switching frequencies, lower losses, increased power density, and more compact converter designs. However, converter topology, semiconductor characteristics, storage dynamics, thermal behavior, and control implementation are strongly interdependent and therefore require integrated optimization. This review critically examines energy and exergy optimization in energy-storage-integrated multilevel converters from a converter-control co-design perspective. The literature is systematically classified according to converter topology, semiconductor technology, storage characteristics, control method, artificial-intelligence technique, validation approach, and reported performance metrics. An exergy-based framework is introduced to distinguish conventional energy losses from degradation of useful energy potential, including contributions from semiconductor losses, passive components, storage irreversibility, thermal gradients, circulating currents, capacitor-voltage imbalance, auxiliary consumption, and control-dependent switching activity. Conventional, nonlinear, predictive, and AI-assisted control strategies are compared in terms of efficiency, harmonic distortion, dynamic response, robustness, computational burden, thermal-stress mitigation, storage degradation, and real-time feasibility. The analysis shows that converter topology and control strategy should be optimized concurrently. Redundant switching states in active-neutral-point-clamped and modular multilevel converters can improve capacitor-voltage regulation and thermal distribution, but at the cost of greater sensing, computation, and implementation complexity. GaN devices support high-frequency and high-power-density operation but impose stricter requirements on control latency, parasitic-aware design, electromagnetic compatibility, gate driving, and thermal management. AI-assisted model predictive control and reinforcement learning offer adaptive and multi-objective capabilities, although their deployment remains constrained by limited training data, poor generalization, stability verification, computational demand, and embedded hardware limitations. The review identifies persistent gaps in standardized datasets, benchmark conditions, experimentally validated exergy assessment, and reproducible converter-control-storage co-design. Future research should emphasize exergy-aware predictive control, degradation-conscious dispatch, Pareto-based co-optimization, digital-twin-assisted monitoring, and standardized hardware-in-the-loop and experimental validation.

* Corresponding authors.
E-mail addresses: gowthamraj.rajendran@ktu.lt (G. Rajendran), darius.andriukaitis@ktu.lt (D. Andriukaitis), reiko.raute@um.edu.mt (R. Raute), vytautas.markevicius@ktu.lt (V. Markevičius), dangirutis.navikas@ktu.lt (D. Navikas), mindaugas.zilys@ktu.lt (M. Žilys), algimantas.valinevicius@ktu.lt (A. Valinevičius), sotner@vut.cz (R. Šotner), jerabekj@vut.cz (J. Jerabek), polakl@vut.cz (L. Polak).

https://doi.org/10.1016/j.est.2026.124299
Received 20 April 2026; Received in revised form 20 July 2026; Accepted 17 August 2026
Available online 31 August 2026
2352-152X/© 2026 The Authors. Published by Elsevier Ltd. This is an open access article under the CC BY license (http://creativecommons.org/licenses/by/4.0/).

1. Introduction

Advanced societies exhibit a profound dependence on continuous and substantial energy supplies, making the reliable operation of energy systems essential for sustaining economic, industrial, and social functions. The escalating demand for energy and energy-dependent services is driving significant transformations within energy infrastructures, influenced by technological innovation, evolving environmental conditions, and shifting regulatory and policy frameworks. These simultaneous changes create intricate interdependencies between energy generation, distribution networks, resource availability, and environmental sustainability. Consequently, there is an increasing need for the development of resilient, flexible, and efficient energy systems capable of accommodating rising demand while minimizing ecological impact. Addressing these challenges requires integrated strategies that encompass advanced technological solutions, robust system planning, and sustainable resource management, thereby ensuring long-term energy security and supporting the overarching objectives of sustainable societal development [1]. Rapid technological advancements and ongoing developments in energy systems are giving rise to novel and increasingly complex risks, many of which are difficult to anticipate and manage using conventional approaches. These emerging challenges span technical, operational, and cybersecurity domains, and may significantly impact the stability, reliability, and resilience of energy infrastructures if left unaddressed. Consequently, there is a growing imperative to implement adaptive strategies, advanced monitoring, and robust risk management frameworks that can respond dynamically to evolving threats. Ensuring system stability, safety, and resilience in this context requires a multidisciplinary approach that integrates technological innovation, predictive analytics, regulatory oversight, and proactive operational practices, thereby safeguarding energy supply continuity while supporting sustainable and secure energy system development [2]. The energy sector remains the largest contributor to global greenhouse gas (GHG) emissions, playing a central role in climate change and environmental degradation. In 2019, global net anthropogenic GHG emissions increased by approximately 11% relative to 2010, reflecting continued reliance on fossil-fuel-based energy generation and industrial processes [3]. Rising concentrations of greenhouse gases (GHGs) are exerting profound and multifaceted impacts on the global environment, including land degradation in arid, semi-arid, and dry sub-humid regions [4], disruption of food production and distribution systems [5,6], and increased risks to human health, security, and socio-economic stability [7]. The continued accumulation of GHGs has also contributed to the transgression of multiple planetary boundaries [8], emphasizing the urgent need for coordinated mitigation and adaptation strategies. Concurrently, the intensification of extreme weather events, such as prolonged droughts, catastrophic floods, and large-scale wildfires, further amplifies environmental vulnerability by altering the transport, fate, and accumulation of inorganic and organic contaminants across terrestrial and aquatic ecosystems [9]. In response to these pressing challenges, the Paris Agreement [10] established a global framework aiming to limit the rise in average global temperatures to well below 2 °C, with efforts to restrict warming to 1.5 °C above pre-industrial levels. Realizing these objectives necessitates substantial reductions in carbon-intensive energy generation, large-scale adoption of renewable energy technologies, improvements in energy efficiency, and the implementation of integrated policies that align environmental sustainability with economic and social development goals. Recent analyses by the World Meteorological Organization (WMO) [11] indicate that 2024 is the warmest year on record, marking the first annual exceedance of the 1.5 °C threshold. These unprecedented warming underscores the critical need to accelerate decarbonization, develop resilient low-carbon energy systems, and implement adaptive strategies to safeguard both ecological integrity and human well-being in the face of accelerating climate change. The United Nations Sustainable Development Goals (SDGs) [12] underscore the imperative to address the adverse impacts of climate change while achieving air quality standards that safeguard public health. Concurrently, there remains a pressing need to improve access to clean water and sanitation globally. In response, an increasing number of studies have focused on the design and analysis of 100% renewable energy (RE) systems as a means to establish sustainable and resilient energy infrastructures [13]. These investigations aim to identify strategies that simultaneously mitigate climate change, reduce air pollution, alleviate energy poverty, and optimize the economic efficiency of energy systems [14–16].

This growing environmental and energy concern has accelerated the global shift toward the integration of renewable energy sources-such as wind, solar, hydro, and tidal power, within modern power generation and distribution infrastructures. These clean and sustainable energy sources play a pivotal role in ensuring environmental protection by significantly reducing carbon emissions and minimizing pollution, while also fostering economic growth through long-term energy cost savings, diversification of energy supply, and the creation of new employment opportunities. According to projections from the International Energy Agency (IEA), renewable energy technologies are expected to account for more than 90% of new global power generation capacity by the end of this decade, establishing renewables as the dominant sector in future energy systems [17]. This rapid expansion underscores the increasing importance of renewable energy in addressing global electricity demands and meeting international climate objectives, particularly those outlined in the Paris Agreement, which emphasize deep decarbonization and the transition toward sustainable and resilient energy infrastructures. Moreover, the large-scale integration of renewable energy sources within modern power grids contributes not only to enhancing system reliability and operational flexibility but also to accelerating technological innovation across multiple sectors of the energy economy. The deployment of advanced power conversion technologies, multilevel inverters, energy storage systems, and intelligent grid management strategies facilitates the stable and efficient incorporation of intermittent renewable sources such as solar photovoltaic and wind energy, thereby mitigating variability, enhancing grid resilience, and ensuring a continuous and secure power supply. These technological advancements are further complemented by predictive analytics, real-time monitoring, and demand-side management techniques, which optimize energy flow, prevent overloads, and enable adaptive responses to fluctuations in both generation and consumption. In addition to technical benefits, the expansion of renewable energy infrastructures generates substantial socio-economic advantages. It stimulates sustainable industrial growth, fosters regional and national economic development, and creates employment opportunities in emerging sectors such as renewable technology manufacturing, installation, operation, and maintenance. By reducing dependence on fossil fuels, these developments also enhance energy security, promote diversification of the energy mix, and contribute to the establishment of a circular, resource-efficient economy. Furthermore, the large-scale deployment of renewables plays a critical role in achieving global climate targets, supporting carbon neutrality commitments, and advancing environmental sustainability by curbing greenhouse gas emissions and minimizing ecological impacts. Collectively, these advancements represent a pivotal step toward the realization of a sustainable global energy transition, one that harmonizes environmental stewardship, economic competitiveness, and energy security while laying the groundwork for resilient and low-carbon energy systems in the decades to come [9,18].

A socio-technical transition typically depends on the availability of novel technologies or alternative practices that are often already developed but remain confined to niche applications; the central challenge then becomes creating the conditions for these innovations to diffuse, gain socio-political legitimacy, and ultimately displace the incumbent, unsustainable regime [19]. A major impediment to the uptake of such technologies is their misalignment with existing infrastructures, institutions, and market structures. Furthermore, successful implementation frequently requires complementary

technologies or systems that may be absent, scarce, or economically unviable. Battery-electric vehicles (BEVs) provide a salient example, as their widespread diffusion is contingent upon both cost-competitive battery technologies and the rollout of reliable, accessible charging infrastructure [20]. The ongoing transformation of the energy sector, marked by the large-scale deployment of diverse renewable energy (RE) technologies—suggests that contemporary society may be entering a new phase in the evolution of its energy system [21]. Empirically, this is reflected in the fact that, in 2024, renewable sources constituted 92.5% of all newly installed power generation capacity [22]. International collaboration in technological innovation has the potential to further accelerate global energy transitions; however, for such collaboration to induce systemic change, partnerships must transcend isolated pilot projects and local initiatives, expanding their geographical scope and institutional reach [23]. When transitioning toward an energy system that is compatible with climate neutrality and the elimination of air pollution, it is imperative that all energy-using sectors undergo a sustainable transformation [24]. These sectors include power generation [25,26], heating and cooling [27,28], transport [29,30], industry [31,32], desalination [33,34], as well as carbon dioxide removal (CDR) technologies [35,36]. In the literature, agriculture [37], fishing, and military [38] are in some cases treated as separate energy sectors due to their distinct output characteristics and operational profiles; however, in this review their energy use is accounted for within the broader conventional sectors rather than analyzed as standalone sectors. The interaction and coordinated integration of these sectors, commonly referred to as sector coupling [39–42], represents a central strategy for achieving deep decarbonization. Sector coupling generally entails the electrification of end-use energy demand outside the traditional power sector, enabled by a rapidly increasing share of renewable electricity. This is realized through, inter alia, battery electric vehicles (BEVs) in the transport sector, electric heat pumps for space and water heating, and electrolyzers for hydrogen production, which can subsequently be used for the synthesis of e-fuels and e-chemicals [43]. Such cross-sectoral integration enhances system flexibility, facilitates the integration of high penetrations of variable renewable energy, and supports the temporal and spatial balancing of supply and demand through conversion and storage pathways (e.g., power-to-gas, and power-to-liquids). Within this context, e-fuels and e-chemicals play a pivotal role in the defossilisation of hard-to-abate segments, notably long-distance aviation, maritime transport, and the provision of carbon-containing industrial feedstocks [44,45]. In these applications, direct electrification is often technically constrained or economically suboptimal, thereby increasing the relevance of high-energy-density synthetic fuels. The principal e-fuels and e-chemicals considered in this study are e-hydrogen, e-methane, e-Fischer-Tropsch liquids (e-FTL), e-ammonia, and e-methanol. These energy carriers can be utilized either as drop-in or near drop-in substitutes in existing fuel infrastructures and conversion technologies, or as feedstocks in established industrial processes. Collectively, sector coupling strategies and the deployment of e-fuels and e-chemicals constitute a coherent framework for the transition to a climate-neutral, low-pollution energy system. Solar photovoltaic (PV) technology has become a central option for expanding low-carbon electricity supply due to its modularity, broad geographic applicability, and comparatively low operational burdens. PV installations can be deployed across a broad range of scales, from distributed rooftop systems to utility-scale power plants. During operation, photovoltaic systems generate electricity without direct combustion-related emissions and generally require limited water consumption and routine maintenance, making them well aligned with decarbonization, resource-efficiency, and energy-security objectives. The relative strengths of PV are further clarified when contrasted with limitations associated with other low-carbon pathways. Bioenergy-based options may face constraints related to sustainable feedstock availability, land-use competition, and non-negligible lifecycle emissions depending on supply chains and conversion routes. Large hydropower can deliver firm renewable generation but is often linked to substantial site dependence, ecological disturbance, resettlement concerns, and long development timelines. Nuclear power provides dispatchable low-carbon electricity yet is frequently characterized by high capital intensity, extended planning and construction periods, and unresolved societal and institutional challenges related to long-term waste management and public acceptance. In addition, indirect electrification routes, particularly hydrogen and synthetic fuels are important for applications where direct electrification is technically difficult; however, they are generally subject to significant conversion losses across production, processing, storage, and end-use. These efficiency penalties, combined with infrastructure requirements and current cost levels, imply that such carriers are best prioritized for hard-to-abate segments rather than as broad substitutes for direct electricity supply. Within this framing, expanding solar PV and using the generated electricity directly wherever feasible constitutes a comparatively resource-efficient pathway, while complementary vectors (e.g., hydrogen and e-fuels) can be reserved for sectors that lack practical direct-electrification alternatives [46–48]. According to IRENA, global renewable power capacity reached 4448 GW by the end of 2024, with solar representing the largest share at 1865 GW [49]. Consistent with this trend, Fernández [50] reports a continuous rise in cumulative solar PV deployment since 2000; by 2024, global installed PV capacity had reached 1865 GW, including approximately 452 GW of newly added capacity in that year. These developments confirm the increasingly prominent role of PV in power-system decarbonization and capacity expansion. At the same time, higher PV penetration intensifies operational and integration challenges, particularly those arising from the temporal misalignment between solar generation, concentrated around midday and demand profiles that may peak in the morning and evening. A key manifestation of this mismatch is the emergence of PV electricity production that cannot be productively utilized during periods of high output. The literature has described this outcome using various terms, including dumped energy [51], excess or unusable energy [52,53], surplus energy [54,55], and redundant energy [56,57]. In the context of distributed PV systems, redundant (or wasted) energy can be defined as the share of electricity generation that exceeds instantaneous on-site demand and cannot be absorbed through available flexibility options, thereby necessitating curtailment or resulting in non-harvested generation. In PV-battery configurations, redundancy most commonly occurs when PV output exceeds load while the battery has reached full state of charge, leaving additional generation without an available sink. As deployment continues to scale, mitigating redundant PV generation through storage expansion, flexible demand, and enabling grid and market arrangements become increasingly important to maximize energy utilization and improve overall system efficiency. Battery energy storage systems (BESS) constitute a key flexibility option in renewable-based energy systems specifically for solar PV systems by enabling the temporal redistribution of electricity, capturing surplus renewable generation and supplying it during periods of elevated demand. Consequently, a substantial body of research has addressed both optimal battery sizing and operational scheduling, reporting improvements in economic performance, system efficiency, and environmental outcomes. Zhu et al. [58], for example, demonstrated that optimized battery dispatch in a hybrid PV-battery-diesel architecture can yield an 8.52% reduction in carbon emissions. In a related vein, Elsanabary et al. and Niveditha et al. [59,60] showed that appropriately sized, grid-connected PV-wind-battery systems can reduce grid reliance and operational interruptions, while improving continuity of supply through coordinated power management. Despite these advantages, degradation remains a major constraint on the long-term viability of battery-based energy-storage systems, as cycling intensity, depth of discharge, and operating temperature can accelerate capacity fade, increase internal resistance, shorten service life, and raise lifecycle costs. To mitigate this, degradation-aware energy management strategies have gained attention. In [61], deep reinforcement learning was employed to derive adaptive control policies aimed at improving grid interaction while

extending battery service life. Although such approaches are promising, their translation to practice can be hindered by computational overheads, data requirements, and challenges associated with dependable real-time implementation in operational settings. To further situate these emerging directions within the broader scholarly landscape, a bibliometric analysis was conducted using VOSviewer, a software tool used for constructing and visualizing bibliometric networks. It helps analyze relationships in scientific literature based on data such as keyword co-occurrence, citations, and co-authorship. By creating visual maps, VOSviewer enables researchers to identify key themes, research clusters, and connections within a field. The keyword co-occurrence network and the accompanying word cloud provide a concise thematic synthesis of the reviewed corpus by highlighting the most frequently occurring keywords and visualizing their co-occurrence relationships, thereby delineating the principal research clusters and their interconnections. Fig. 1 shows a keyword co-occurrence network from VOSviewer software that summarizes how major topics in the renewable energy literature are related. Each node represents an author keyword, with larger nodes indicating higher occurrence across the dataset, while links denote keywords that appear together within the same publications; the resulting edge density provides a proxy for thematic proximity. The color partitions correspond to communities of closely associated keywords, thereby outlining the principal research domains and their interconnections. The network is structured around renewable energy as the most central and frequently occurring concept, reflecting its role as an overarching framework that connects multiple subfields. Around this hub, technology-focused groupings are clearly visible, with solar power and photovoltaic forming a prominent cluster linked to terms that capture performance, conversion, and deployment contexts, suggesting sustained attention to both system-level evaluation and application-driven studies. A complementary cluster centered on wind power indicates continued activity in wind energy research, including modeling and operational analysis. In addition, a strongly connected region associated with power systems and renewable energy sources highlights the growing emphasis on integration challenges, including planning, reliability, and the operational implications of high penetrations of variable generation. A further salient feature is the appearance of a distinct methodological cluster involving artificial intelligence, machine learning, and forecasting, indicating increasing adoption of data-driven techniques for prediction, optimization, and operational decision-making in renewable energy systems. Connections to terms related to efficiency, environmental performance, and emissions-related

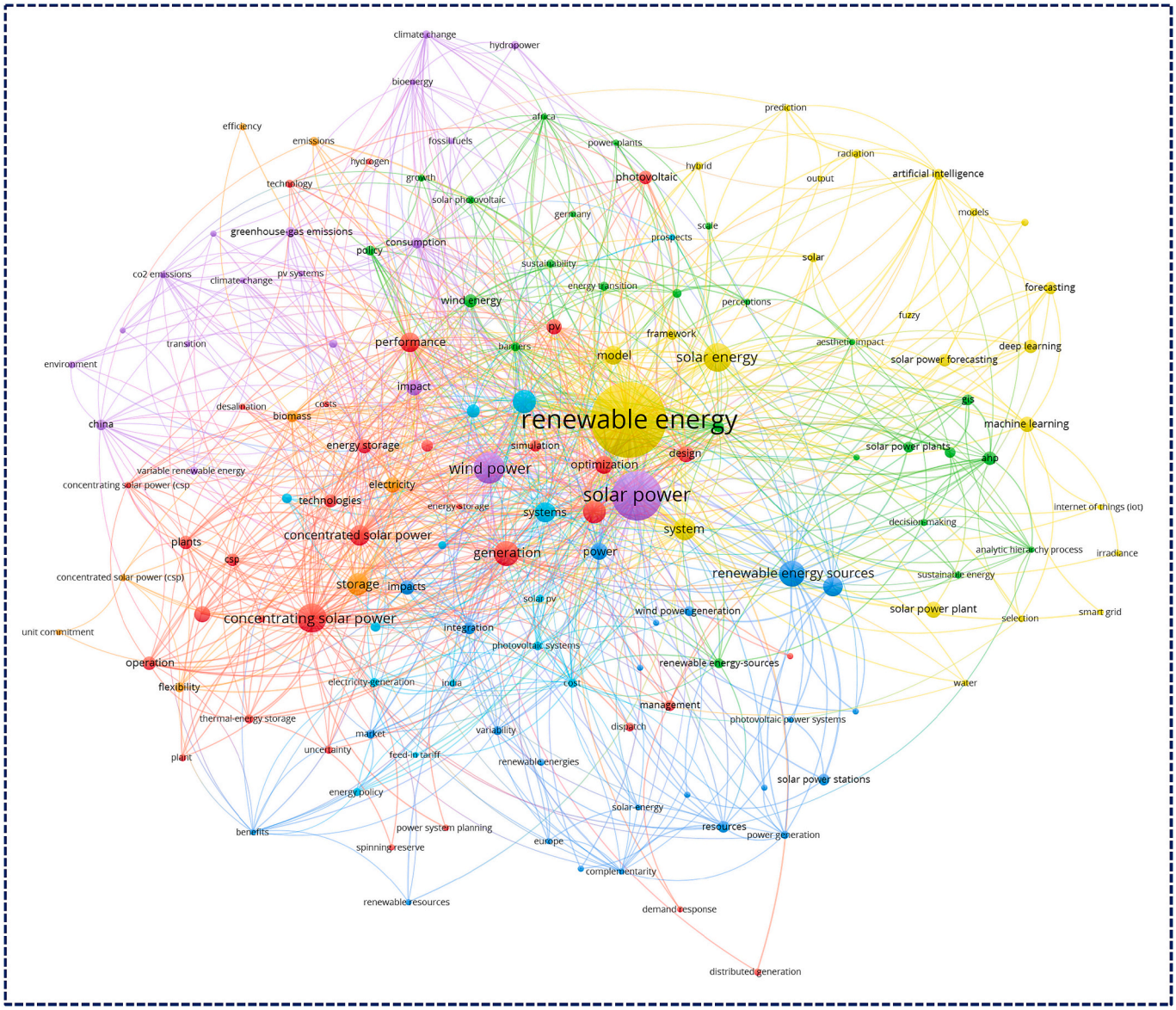

Fig. 1. Keyword co-occurrence network highlighting major research themes in renewable energy.

considerations point to ongoing interest in sustainability-oriented assessment alongside technical advancement. Overall, the extensive cross-links between clusters suggest that current research increasingly adopts multidisciplinary perspectives, coupling renewable generation technologies with grid integration, advanced analytics, and sustainability evaluation to address the broader requirements of energy transition planning and operation.

The increasing deployment of solar photovoltaic (PV) systems has intensified the demand for advanced power conversion technologies capable of delivering high efficiency, superior power quality, and robust grid compliance under variable operating conditions. PV penetration continues to rise in both centralized and distributed configurations, power electronic interfaces increasingly govern system-level performance, influencing voltage regulation, harmonic behavior, transient response, and operational reliability. Consequently, progress in both semiconductor device technologies and converter architecture has become a key enabler for next-generation PV energy conversion systems. In this context, recent advances in wide-bandgap (WBG) semiconductor devices, particularly gallium nitride (GaN), have introduced new possibilities for high-performance PV power converters. Owing to their low on-state resistance, reduced parasitic capacitances, high electron mobility, and negligible reverse recovery losses, GaN power devices enable significantly higher switching frequencies with reduced conduction and switching losses compared with conventional silicon devices. These characteristics support increased power density, faster dynamic response, and reduced passive component size, making GaN-based converters attractive for PV applications such as high-frequency DC-DC conversion stages, microinverters, and string inverters. However, the fast-switching transitions associated with GaN devices also pose design challenges related to gate-drive implementation, electromagnetic interference, voltage overshoot, layout sensitivity, and long-term reliability. Addressing these challenges requires careful device-circuit co-design and robust control strategies, particularly for grid-connected PV systems operating under stringent power quality and electromagnetic compatibility requirements. Building upon these device-level developments, multilevel power converter architectures have emerged as a practical solution for achieving high-quality voltage synthesis and scalability toward medium- and high-power PV applications. Among the various multilevel topologies, the modular multilevel converter (MMC) has gained considerable attention due to its modular structure, flexible scalability, and ability to produce near-sinusoidal output waveforms with low harmonic distortion. These features make MMCs well suited for large-scale grid-connected PV plants and medium-voltage applications. Nevertheless, MMC-based PV systems introduce additional technical complexities, including submodule capacitor voltage balancing, circulating current suppression, fault detection and protection, and thermal management across a large number of distributed submodules. The potential integration of GaN devices into MMC submodules offers opportunities for improved switching performance and power density, but remains constrained by device voltage ratings, cost considerations, and the increased sensitivity of fast-switching devices to parasitic effects and electromagnetic interference in modular, large-scale converter installations [62,63].

Existing reviews generally address multilevel converter topologies, wide-bandgap semiconductor technologies, energy storage systems, and artificial-intelligence-based control as largely independent research domains. This fragmented treatment limits a comprehensive understanding of how converter architecture, semiconductor switching characteristics, storage dynamics, thermal behavior, sensing requirements, computational latency, and controller design interact to determine overall system performance. Moreover, the literature has predominantly focused on first-law energy efficiency, with comparatively less attention devoted to exergy destruction, entropy generation, and the loss of useful work potential in integrated energy-storage-converter systems. A further limitation is the lack of consistent comparative frameworks that jointly account for conversion efficiency, power quality, thermal loading, storage lifetime, control robustness, computational burden, and implementation cost. These limitations highlight the need for a unified converter-control co-design framework incorporating energy, exergy, thermal, reliability, and real-time implementation criteria.

The originality of this review arises from the integrated treatment of energy storage characteristics, multilevel converter topology, semiconductor technology, exergy performance, thermal behavior, and artificial-intelligence-assisted control within a unified converter-control co-design framework. In contrast to studies that examine converter hardware and control development independently, this review evaluates the physical, computational, thermal, and operational interactions that collectively influence system-level performance.

The principal contributions of this review are summarized as follows:

1. A structured comparative assessment of neutral-point-clamped, active neutral-point-clamped, T-type, flying-capacitor, cascaded H-bridge, and modular multilevel converter topologies using consistent criteria, including conversion efficiency, switching frequency, semiconductor voltage stress, harmonic performance, voltage-balancing requirements, power density, thermal-stress distribution, scalability, cost, and implementation complexity.
2. A comparative evaluation of silicon, silicon carbide, and gallium nitride semiconductor technologies that relates device-level conduction and switching characteristics to converter efficiency, thermal loading, electromagnetic interference, passive-component requirements, switching-frequency capability, and control latency.
3. An exergy-based analytical framework for integrated energy-storage-converter systems that incorporates exergy balance, exergy efficiency, entropy generation, component-level exergy destruction, and potential pathways for reducing useful-energy degradation.
4. A systematic comparison of conventional linear, nonlinear, predictive, artificial-intelligence-based, and AI-assisted control strategies with respect to model dependence, transient response, harmonic mitigation, constraint handling, robustness, computational burden, thermal-stress management, and embedded implementation feasibility.
5. A converter-control co-design formulation that jointly accounts for converter topology, semiconductor selection, passive-component sizing, energy-storage capacity, switching frequency, sensing architecture, controller parameters, computational platform, thermal constraints, and reliability requirements.
6. A multi-objective optimization perspective that integrates energy loss, exergy destruction, semiconductor thermal stress, storage degradation, power quality, control robustness, execution time, and economic cost within a common decision-making framework.
7. The identification of methodological and implementation gaps, including inconsistent test conditions, limited experimental validation, restricted access to open datasets, insufficient AI generalization, inadequate stability verification, and the absence of standardized exergy-aware benchmarking procedures.

Motivated by these research gaps, this review provides a comprehensive and critical synthesis of energy-storage-integrated multilevel power conversion systems, with particular emphasis on the interactions among converter topology, semiconductor technology, storage behavior, thermal performance, exergy efficiency, and advanced control strategies. The analysis is organized across device, converter, storage, control, and system levels. At the device level, the review examines silicon, silicon carbide, and gallium nitride technologies in relation to conduction and switching losses, thermal characteristics, packaging, parasitic effects, and switching-frequency capability. At the converter level, it evaluates neutral-point-clamped, active neutral-point-clamped, T-type, flying-capacitor, cascaded H-bridge, and modular multilevel topologies with respect to efficiency, harmonic performance, voltage balancing, scalability, thermal-stress distribution, and implementation complexity. At the storage and system levels, the review considers

storage dynamics, degradation, bidirectional power flow, grid interaction, and reliability. Conventional, nonlinear, predictive, and artificial-intelligence-assisted control methods are further assessed in terms of robustness, computational burden, constraint handling, thermal management, storage lifetime, and real-time feasibility. Through this integrated assessment, the review establishes a converter-control co-design perspective for improving the energy, exergy, thermal, and operational performance of renewable-energy-integrated storage systems.

The literature review was undertaken using Scopus, Web of Science, IEEE Xplore, and ScienceDirect, encompassing peer-reviewed journal articles and conference papers published between January 2000 and December 2025. The search was updated in March 2026 to incorporate the most recent studies relevant to the scope of the review. A structured search strategy was applied using Boolean combinations of keywords associated with energy-storage systems, multilevel power converters, wide-bandgap semiconductor technologies, artificial intelligence, model predictive control, energy and exergy efficiency, entropy generation, thermal management, and converter-control co-design. Studies were considered eligible when they investigated energy-storage-integrated power conversion systems and provided sufficient technical detail regarding converter topology, semiconductor technology, storage characteristics, control architecture, operating conditions, validation procedures, or quantitative performance indicators. Publications were excluded from the comparative analysis when they lacked methodological transparency, quantitative evidence, technical relevance, or a direct connection to integrated converter-control-storage systems. Duplicate records were removed before title and abstract screening, after which potentially relevant publications underwent full-text assessment according to predefined eligibility criteria. The selected studies were systematically categorized according to converter topology, semiconductor technology, storage type, control strategy, artificial-intelligence method, validation approach, and reported performance metrics. Methodological quality was assessed based on the clarity of the system configuration, completeness of the operating conditions, reproducibility of the control formulation, availability of quantitative results, and rigor of the validation procedure. Studies supported primarily by conceptual or descriptive evidence were retained for contextual discussion, whereas direct technical comparisons were limited to publications presenting adequate analytical, simulation-based, hardware-in-the-loop, experimental, or field-validation evidence.

2. Energy storage technologies and renewable-energy integration

2.1. Current global energy-storage landscape

The global energy-storage sector is undergoing a marked transition from a system historically dominated by pumped-hydroelectric storage toward a more diversified portfolio that increasingly incorporates electrochemical, thermal, mechanical, and chemical storage technologies [64]. Pumped hydro continues to account for a substantial share of cumulative installed storage capacity because of its large unit size, long operational lifetime, and ability to provide multi-hour or multi-day energy delivery. Nevertheless, cumulative installed capacity alone does not adequately represent contemporary deployment patterns. Recent market growth is increasingly driven by battery energy storage systems, particularly utility-scale lithium-ion projects co-located with solar and wind generation, together with distributed systems deployed in residential, commercial, industrial, and microgrid applications [65]. The scale of energy-storage deployment should be characterized using both power capacity and energy capacity. Power capacity, expressed in gigawatts, defines the maximum instantaneous charging or discharging capability of the system and is particularly relevant to frequency regulation, ramp-rate control, voltage support, reserve provision, and peak-power management. Energy capacity, expressed in gigawatt-hours, indicates the total quantity of electricity that can be stored and therefore determines the duration for which rated power can be sustained. For example, a system rated at 100 MW/400 MWh can theoretically deliver its rated output for four hours. Reporting storage deployment solely in terms of gigawatts may therefore obscure substantial differences between high-power, short-duration systems and lower-power installations designed for extended energy delivery [66]. Utility-scale storage systems are generally connected at transmission, distribution, or large renewable-generation sites and are deployed for bulk energy shifting, renewable-energy firming, congestion management, reserve provision, capacity adequacy, and ancillary services. These installations commonly range from tens of megawatts to portfolio-scale developments approaching the gigawatt level. By contrast, distributed storage includes residential batteries, commercial and industrial systems, community storage, telecommunications backup units, electric-vehicle-integrated storage, and microgrid-based installations. Although individual distributed systems are relatively small, aggregation through virtual power plants can provide substantial dispatchable capacity and enable coordinated participation in energy and ancillary-service markets [67]. Storage duration provides an additional basis for classification. Short-duration storage generally supplies power for periods ranging from a few seconds to approximately four hours and is well suited to frequency regulation, renewable-power smoothing, voltage support, peak shaving, and intraday balancing. Lithium-ion batteries, supercapacitors, and flywheels are prominent in this category because of their rapid response and high round-trip efficiency. Long-duration energy storage is intended to sustain discharge over extended periods, commonly beyond eight to ten hours, and is increasingly considered for multi-day balancing, resilience, renewable-energy shifting, capacity adequacy, and reduced dependence on fossil-fuel-based peaking generation. Candidate technologies include pumped hydro, compressed-air storage, flow batteries, sodium-based batteries, thermal storage, gravity storage, hydrogen, and other power-to-X pathways [68]. Accordingly, the current storage landscape should not be interpreted exclusively through the historical dominance of pumped hydro. Pumped storage remains essential for large-scale and long-duration applications, whereas electrochemical storage now represents a major share of new installations because of its modularity, rapid deployment, controllability, and suitability for both centralized and distributed applications. The resulting global portfolio is increasingly differentiated by power rating, energy capacity, response speed, discharge duration, cycling intensity, siting flexibility, cost structure, and grid-service capability [69].

2.2. Electrochemical storage trends

Lithium-ion batteries currently dominate electrochemical energy-storage deployment because of their high round-trip efficiency, rapid dynamic response, modular construction, mature manufacturing infrastructure, and declining system cost. Within this category, lithium iron phosphate batteries have become particularly important for stationary storage. Compared with nickel-rich lithium-ion chemistries, LFP generally provides lower gravimetric and volumetric energy density but offers improved thermal stability, long cycle life, reduced dependence on cobalt and nickel, and favorable performance under frequent cycling. These characteristics are well aligned with stationary applications, where installation footprint and mass are generally less restrictive than in transport applications. Other lithium-ion chemistries, including nickel manganese cobalt, nickel cobalt aluminum, lithium manganese oxide, and lithium titanate, remain relevant where specific combinations of energy density, power capability, low-temperature performance, rapid charging, safety, and cycle life are required [70,71]. Nickel-rich chemistries provide comparatively high energy density but normally impose more demanding thermal-management and safety requirements. Lithium titanate offers excellent power capability, rapid charging, and extended cycle life, although its comparatively low energy density and higher cost limit widespread deployment. Chemistry

selection should therefore be based on the intended duty cycle, depth of discharge, operating temperature, calendar-aging behavior, safety requirements, expected project lifetime, and replacement cost rather than on energy density alone. Sodium-ion batteries are emerging as a promising alternative for stationary storage because sodium is abundant, geographically distributed, and less exposed to the supply constraints associated with lithium, nickel, and cobalt [72,73]. Sodium-ion systems may offer favorable low-temperature performance, enhanced safety, and potentially lower material costs. Their present limitations include lower energy density, less mature manufacturing capacity, and limited long-term operational data compared with established lithium-ion technologies. However, these constraints are less critical in stationary applications, making sodium-ion batteries increasingly relevant for renewable-energy buffering, distributed storage, microgrids, and selected long-duration applications. Vanadium redox flow batteries store energy in liquid electrolytes circulated through electrochemical stacks. Their principal advantage is the independent scaling of power and energy capacity: stack size determines power capability, whereas electrolyte volume determines stored energy. This separation enables flexible duration design and supports frequent deep cycling with comparatively limited electrode degradation [74]. Vanadium redox flow batteries also offer low fire risk, long service life, and the possibility of electrolyte recovery and reuse. Their wider adoption is constrained by low energy density, pumping requirements, system complexity, and sensitivity to vanadium cost. These characteristics make the technology particularly suitable for stationary applications requiring extended discharge duration, frequent cycling, and long operational life [75]. Hybrid battery-supercapacitor storage systems combine the comparatively high energy density of batteries with the high-power density and rapid response of supercapacitors. In such configurations, the battery supplies the average and low-frequency components of the power demand, while the supercapacitor absorbs rapid fluctuations, regenerative pulses, and short-duration transients. Appropriate power-splitting control can reduce battery current ripple, peak current, thermal stress, and high-frequency cycling, thereby improving dynamic performance and extending battery service life. These advantages are particularly relevant to renewable-energy systems, electric-vehicle charging stations, traction applications, and DC microgrids. However, hybridization also introduces additional converter stages, sensing requirements, control complexity, cost, and energy-management challenges [76,77]. Long-duration electrochemical storage encompasses flow batteries, sodium-based systems, zinc-based batteries, metal-air batteries, and other aqueous or non-aqueous chemistries designed for extended discharge and high cycling endurance. Their development is motivated by the need to shift renewable generation over periods exceeding the conventional two- to four-hour operating range of lithium-ion systems. Nevertheless, the suitability of each technology depends on round-trip efficiency, self-discharge, auxiliary power demand, material availability, operational lifetime, safety, energy density, and levelized cost of storage. Long-duration storage should therefore be assessed as a portfolio of technologies matched to specific operating requirements rather than as a single uniform category [78].

2.3. Energy-storage services

Energy-storage systems can provide a broad range of services across generation, transmission, distribution, microgrid, and end-user levels. Their technical and economic value depends not only on installed capacity but also on response time, discharge duration, converter rating, state-of-charge availability, control architecture, market access, and degradation cost. Frequency regulation requires rapid adjustment of active power to compensate for short-term imbalances between generation and demand. Converter-interfaced battery systems are well suited to this function because their charging and discharging power can be modified within milliseconds [79]. However, continuous regulation introduces frequent shallow cycling and high-frequency current variations. Effective implementation therefore requires state-of-charge recovery, power-reserve management, and degradation-aware dispatch. Peak shaving reduces the maximum power drawn from the network or delivered through constrained infrastructure. The storage system discharges during periods of high demand and recharges during lower-demand intervals. This service can reduce demand charges, defer network reinforcement, limit transformer and feeder loading, and reduce reliance on high-cost peaking generation. Its effectiveness depends on accurate load forecasting, sufficient energy capacity, and appropriate coordination between power and energy constraints [80]. Renewable-power smoothing mitigates rapid variations in photovoltaic and wind generation. The storage system absorbs power during upward generation ramps and injects power during downward ramps, thereby reducing the rate of change observed at the point of grid connection. Although smoothing is primarily power intensive, prolonged weather-related fluctuations may also require substantial energy capacity. Energy shifting transfers electricity from periods of surplus generation or low market prices to periods of elevated demand or higher prices. Unlike frequency regulation, energy shifting requires sufficient stored energy to sustain multi-hour discharge. Its economic and technical performance depends on discharge duration, round-trip efficiency, forecast accuracy, storage degradation, and electricity-price differentials [81,82]. Reserve provision requires the storage system to maintain sufficient charging or discharging capability to respond to contingencies, generator outages, network disturbances, or forecast errors. Upward reserve can be provided by discharging or reducing charging demand, whereas downward reserve can be delivered by increasing charging power or reducing discharge. Reserve participation requires the supervisory controller to maintain an appropriate state-of-charge margin rather than maximizing short-term energy-market revenue. Voltage support is achieved through the controlled exchange of reactive power and, where necessary, active power at the point of connection [83,84]. Converter-interfaced storage can operate across multiple quadrants of the active-reactive power plane, subject to current and apparent-power limits. Local voltage regulation is particularly valuable in distribution networks with high photovoltaic penetration, reverse power flow, weak-grid conditions, and limited reactive-power capability. Black-start operation enables the restoration of de-energized network sections without reliance on an external grid voltage. A storage system providing black-start capability must energize transformers, establish voltage and frequency, supply auxiliary loads, tolerate inrush current, and coordinate the sequential reconnection of generation and demand. This function requires sufficient stored energy, grid-forming control, robust protection, and adequate short-term converter overcurrent capability [85].

Grid-forming operation allows the storage converter to establish the voltage and frequency reference rather than merely following an externally imposed waveform. Grid-forming controllers can provide virtual inertia, fast frequency response, damping, voltage regulation, and stable operation in weak or islanded networks. Their implementation requires coordinated current limiting, fault ride-through, synchronization, state-of-charge management, and reliable transitions between grid-connected and islanded modes [86]. Microgrid resilience involves maintaining critical loads during network interruptions and supporting system recovery after disturbances. Storage contributes by balancing local generation and demand, stabilizing voltage and frequency, enabling islanded operation, reducing dependence on diesel generation, and supplying uninterrupted power to priority loads [87]. Resilience-oriented sizing differs from purely economic sizing because sufficient energy must be reserved for uncertain outage duration and critical-load requirements. These services are strongly interdependent. A single storage system may participate simultaneously in frequency regulation, energy arbitrage, peak shaving, reserve provision, voltage support, and resilience enhancement. Effective service stacking therefore requires supervisory optimization that accounts for converter limits, state-of-charge constraints, storage degradation, forecast uncertainty, market obligations, and potential conflicts among operating objectives [88].

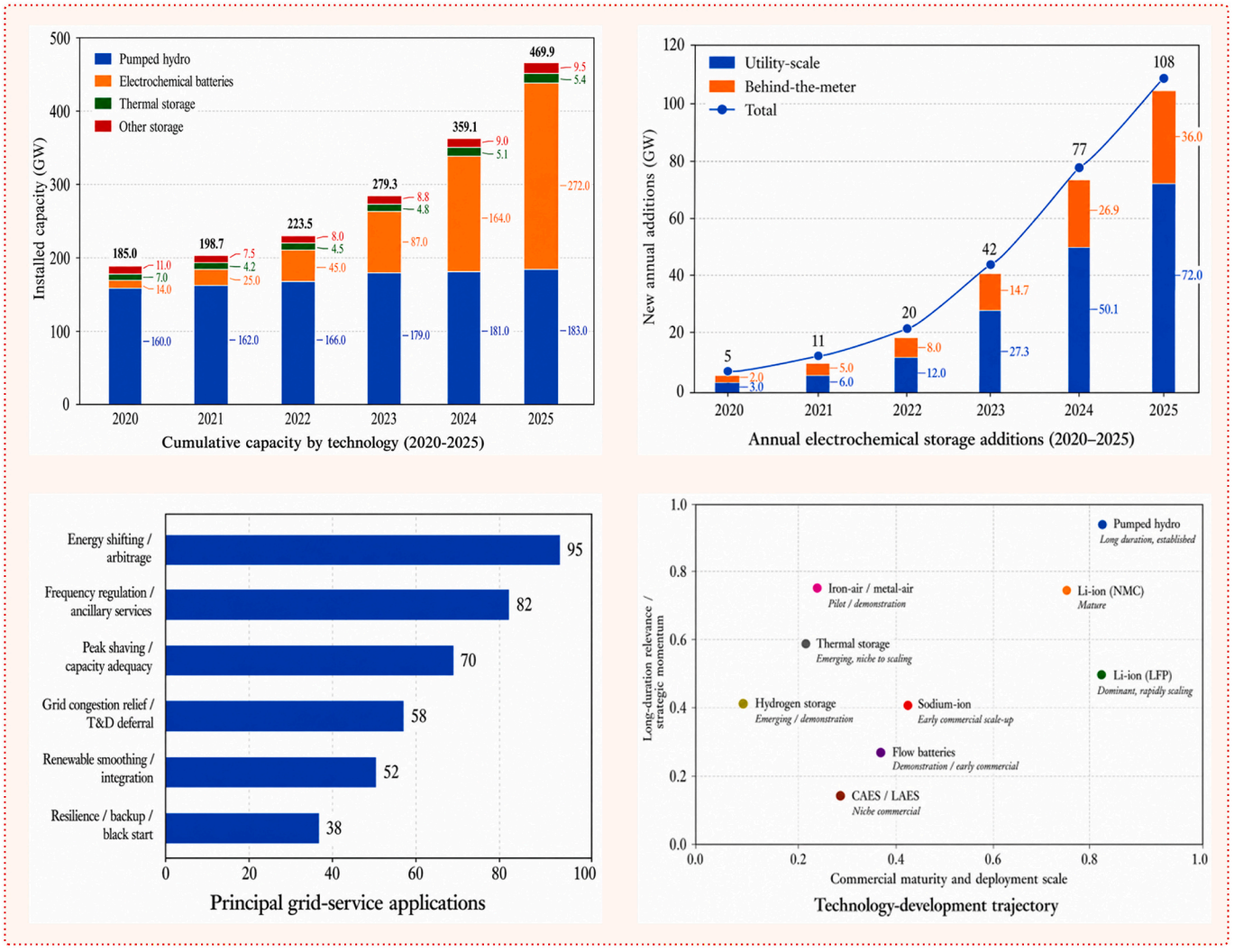

Fig. 2. Global energy-storage deployment, applications, and technology positioning during 2020–2025. (a) Cumulative installed capacity by storage technology; (b) annual electrochemical storage additions by utility-scale and behind-the-meter segments; (c) principal grid-service applications; and (d) technology positioning according to commercial maturity and long-duration relevance [89].

Fig. 2 shows rapid growth in electrochemical storage, led by utility-scale deployment, while pumped hydro remains dominant in cumulative capacity. Energy shifting, frequency regulation, and peak shaving represent the principal applications. The technology map indicates that lithium-ion systems are commercially mature, whereas flow batteries, sodium-ion, hydrogen, thermal storage, and metal-air technologies occupy emerging or specialized long-duration roles.

2.4. Coupling between energy storage and power converters

The power converter is not merely an interface between the storage device and the electrical network. Its topology, switching frequency, modulation strategy, control bandwidth, current-regulation performance, thermal design, and auxiliary consumption directly affect the electrochemical, thermal, and lifetime behavior of the storage system [90]. Consequently, the ESS and converter should be treated as a coupled electro-thermal-control system. Battery current ripple is influenced by converter switching, DC-link dynamics, passive-filter design, interleaving, modulation, and controller performance. High-frequency ripple increases the root-mean-square battery current and may produce additional ohmic and electrochemical losses. Low-frequency ripple, particularly the second-harmonic component associated with single-phase power conversion, may propagate into the battery when the DC-link buffering stage is insufficient [91]. Excessive ripple can increase heat generation, promote non-uniform current distribution, and accelerate degradation mechanisms. Multiphase interleaving, active ripple cancellation, optimized modulation, appropriate passive-component sizing, and hybridization with supercapacitors can reduce the ripple imposed on the battery. Depth of discharge is determined by the energy-management strategy and converter power commands. Operation over a wide state-of-charge range increases usable energy but generally accelerates cycle-related degradation. Restricting the operating window can extend storage lifetime, although it reduces available capacity and may limit revenue generation. The preferred depth-of-discharge range therefore depends on battery chemistry, temperature, cycling frequency, service requirements, replacement cost, and project lifetime. State of charge estimation is closely linked to converter measurements and operating conditions. Current-sensor bias, voltage-measurement error, parameter uncertainty, and unaccounted converter losses can produce cumulative estimation errors. In addition, multi-service operation requires the converter controller to preserve sufficient upward and downward power flexibility. State-of-charge management should therefore be integrated with dispatch optimization rather than treated as an independent battery-management function. State of health describes

progressive changes in usable capacity, internal resistance, power capability, and degradation state [92]. Converter operating profiles influence state of health through current magnitude, current slew rate, switching ripple, temperature, depth of discharge, and time spent at high or low states of charge. Health-aware control can incorporate degradation indicators into the dispatch objective so that short-term efficiency and market value are balanced against long-term loss of storage capability. Thermal gradients arise from non-uniform cell resistance, unequal electrical loading, differences in cooling paths, module placement, and heat transferred from adjacent converter components. High current and current ripple increase internal battery losses, while semiconductor and magnetic-component losses can elevate enclosure temperature. Uneven thermal distribution accelerates cell imbalance because degradation rate and internal resistance are temperature dependent. Converter and battery thermal systems should therefore be designed jointly using coordinated airflow, liquid-cooling paths, temperature monitoring, thermal isolation, and temperature-aware derating [93]. Cycle life is governed by the number, depth, rate, and temperature of charge-discharge cycles. Converter control determines the instantaneous C-rate, frequency of power reversals, and distribution between shallow and deep cycling. Aggressive provision of grid services may increase short-term utilization but reduce battery lifetime. Degradation-conscious control can limit peak current, smooth power references, avoid unnecessary state-of-charge reversals, and allocate high-frequency transients to auxiliary storage elements. Electrochemical degradation includes solid-electrolyte interphase growth, lithium plating, electrolyte decomposition, active-material loss, particle cracking, and increased internal resistance. These mechanisms are affected by current rate, temperature, state of charge, rest duration, depth of discharge, and current-ripple characteristics. Converter-induced electrical stress should therefore be translated into electrochemical degradation variables rather than represented solely through conversion efficiency. A control strategy that minimizes semiconductor losses may not necessarily minimize storage degradation if it increases peak current, ripple, or operation at unfavourable states of charge. Auxiliary cooling demand also contributes to the total energy consumption and exergy destruction of the integrated system. Higher semiconductor switching and conduction losses increase converter cooling requirements, while aggressive battery operation increases the demand placed on the storage thermal-management system. Fans, pumps, chillers, control electronics, and conditioning systems reduce net delivered energy and may become particularly significant under partial-load operation [94,95]. System performance should therefore be evaluated using net conversion efficiency that includes converter, storage, and auxiliary losses rather than semiconductor efficiency alone. The interaction between the storage system and power converter demonstrates the need for coordinated design and control. Converter topology, semiconductor technology, switching frequency, passive-component sizing, modulation method, storage chemistry, energy-management strategy, cooling architecture, and degradation model should be optimized jointly. Such a converter-control co-design approach enables simultaneous improvement of conversion efficiency, exergy performance, thermal loading, power quality, storage lifetime, reliability, and lifecycle cost. The influence of the power converter on storage-system performance is governed not only by the control strategy and operating conditions, but also by the structural characteristics of the selected converter topology. Split-DC-link configurations require effective neutral-point and capacitor-voltage regulation, whereas cascaded architectures depend on coordinated power allocation among distributed storage modules. Modular converter structures introduce additional requirements associated with circulating-current suppression, submodule-voltage balancing, and distributed state-of-charge management. Flying-capacitor converters similarly require continuous regulation of intermediate capacitor voltages, while single-stage and multistage interfaces differ in the extent to which storage-side voltage variations can be decoupled from grid-side power regulation. These topology-dependent characteristics directly influence storage-current ripple, module utilization, thermal loading, fault-containment capability, auxiliary power demand, and degradation behavior [96].

2.5. Converter-control co-design for energy storage systems

The increasing functional complexity of energy-storage-integrated power conversion systems has revealed the limitations of conventional sequential design methodologies, in which the converter hardware and control architecture are developed as largely independent subsystems. Although such an approach may provide satisfactory performance under nominal conditions, it does not adequately represent the strong interdependence among converter topology, semiconductor switching behavior, storage dynamics, thermal loading, component aging, and grid-support requirements. Converter-control co-design addresses this limitation by integrating hardware configuration, modulation strategy, control objectives, and storage constraints within a unified design framework [97]. The converter topology determines the available switching states, voltage levels, current paths, semiconductor stress distribution, internal balancing requirements, and fault-management capability. The control architecture governs the extent to which these structural characteristics are effectively utilized across varying operating conditions. Converter performance is therefore influenced not only by the physical configuration of the power stage, but also by the ability of the controller to exploit topology-specific degrees of freedom. This interaction is particularly significant in multilevel converter structures, including neutral-point-clamped, active-neutral-point-clamped, T-type, flying-capacitor, and modular multilevel converters, where redundant switching states can be used to improve waveform quality, regulate capacitor voltages, redistribute semiconductor losses, and mitigate thermal imbalance [98].

In energy-storage applications, converter operation directly affects the electrical, thermal, and electrochemical stress imposed on the storage medium. High-frequency current ripple, abrupt charge-discharge transitions, prolonged operation near state-of-charge limits, and repeated deep cycling may contribute to temperature rise, internal resistance growth, capacity degradation, and accelerated aging [99]. Converter control should therefore extend beyond conventional objectives such as current tracking and DC-link voltage regulation. Storage-side current quality, state-of-charge boundaries, thermal constraints, and degradation-sensitive operating conditions should also be incorporated into the control formulation. A coordinated co-design framework enables the simultaneous consideration of conversion efficiency, current-ripple suppression, switching-loss minimization, semiconductor thermal balancing, capacitor-voltage regulation, and storage-lifetime preservation. Predictive control is particularly suitable for this purpose because electrical, thermal, and storage-related variables can be evaluated within a common optimization process [100,101]. Each candidate control action can therefore be assessed according to its influence on tracking performance, converter losses, switching activity, battery stress, and junction-temperature variation. The adoption of wide-bandgap semiconductor devices further reinforces the need for coordinated converter and control development. Silicon carbide and gallium nitride devices enable higher switching frequencies, reduced switching losses, and increased power density [102,103]. However, these advantages may be accompanied by greater electromagnetic interference, increased insulation stress, higher sensitivity to gate-drive design, and additional high-frequency components at the storage interface. An appropriate system configuration should be derived through the integrated evaluation of semiconductor characteristics, switching frequency, passive-component design, filtering requirements, modulation strategy, thermal constraints, and storage-side operating conditions. Thermal performance constitutes another critical element of converter-control co-design. Uneven semiconductor loss distribution can produce localized hot spots and repetitive junction-temperature cycling, particularly in converter structures with multiple conduction

paths and redundant switching combinations. Thermal-aware control can redistribute switching and conduction losses among semiconductor devices without significantly degrading output waveform quality [104]. When coordinated with battery-temperature limits and auxiliary cooling requirements, such strategies can improve the reliability of the complete energy-storage conversion system rather than optimizing the power converter in isolation. The required converter-control co-design strategy also depends on the operational function of the energy-storage system. Frequency regulation, synthetic inertia, and fast reserve provision require rapid bidirectional power exchange and high dynamic bandwidth. In contrast, peak shaving and energy shifting emphasize sustained efficiency and thermal stability over extended operating periods. Grid-forming operation introduces additional requirements related to voltage regulation, weak-grid stability, fault-current limitation, synchronization, and transient power support [105]. Converter ratings, control bandwidth, thermal margins, and storage operating windows should therefore be selected according to the intended service portfolio rather than a single rated operating point.

Data-driven methods can further support converter-control co-design through online parameter estimation, thermal-state prediction, degradation assessment, and adaptive tuning of control priorities. Nevertheless, such methods should remain constrained by converter switching feasibility, storage safety limits, thermal boundaries, and grid-code requirements. Hybrid physics-informed approaches are particularly appropriate because they preserve model-based interpretability while introducing adaptive decision-making capability [106]. Converter-control co-design establishes an integrated framework for the coordinated selection of converter topology, semiconductor technology, modulation strategy, control architecture, storage characteristics, and thermal-management provisions. This approach enables concurrent improvement of conversion efficiency, mitigation of electrochemical and thermal stresses, enhancement of operational reliability, and extension of service life in energy-storage systems deployed for renewable-energy integration and advanced grid-support functions.

2.6. Research gaps and emerging requirements

Despite advances in energy-storage technologies, converter topologies, and intelligent control methods, the literature remains fragmented across storage, power conversion, thermal management, and grid-support functions. Many studies examine these elements independently, limiting the assessment of their combined influence on efficiency, degradation, reliability, and system-level performance. A key limitation is the insufficient integration of battery aging and thermal dynamics into converter-control design [107,108]. Existing methods frequently emphasize current tracking, voltage regulation, and harmonic reduction, while current-ripple-induced heating, state-of-health variation, electrochemical degradation, and cooling demand receive less attention. This may improve short-term dynamic performance without ensuring long-term operational durability. The system-level benefits of wide-bandgap semiconductor devices also require more comprehensive evaluation. Although SiC and GaN devices can improve switching efficiency and power density, their effects on electromagnetic interference, insulation stress, common-mode behavior, storage-side ripple, and thermal-management requirements are not consistently quantified [109]. Another limitation is the absence of standardized criteria for evaluating converter-control co-design. Reported studies use different combinations of efficiency, harmonic distortion, switching loss, thermal variation, state-of-charge deviation, and degradation indicators, which complicates direct comparison [110]. Unified electrical, thermal, electrochemical, reliability, and exergy-based metrics are therefore required. The increasing use of grid-forming storage converters introduces additional challenges related to voltage regulation, virtual inertia, weak-grid stability, fault-current limitation, and black-start capability [111]. These functions require coordinated consideration of converter ratings, control bandwidth, protection requirements, thermal constraints, and storage availability.

Artificial intelligence and data-driven methods offer potential for adaptive control, degradation prediction, and thermal-state estimation. However, their application remains limited by model interpretability, training-data dependence, computational burden, and uncertain behavior outside the training domain [112,113]. Physics-informed and constraint-aware approaches are therefore necessary for reliable implementation. These gaps highlight the need for integrated design and assessment frameworks that coordinate converter topology, semiconductor technology, control architecture, storage degradation, thermal management, and grid-service requirements [114,115]. Such frameworks are essential for improving efficiency, reliability, and service life in renewable-energy-integrated storage systems.

3. Power converter technologies

Power electronics constitutes a fundamental enabling technology that interfaces electrical energy sources with end-use systems by providing efficient power conversion, regulation, and control. In practical applications, electrical energy is processed through multiple conversion stages, which are realized using power electronic converters incorporating semiconductor switching devices. To date, these converters have predominantly relied on silicon (Si)-based power semiconductor technologies. Conventional silicon power semiconductor switches (CPSS) have maintained a dominant position in the power electronics market due to their technological maturity, reliability, and cost effectiveness [116]. Nevertheless, a key limitation of Si-based devices is the considerable energy loss incurred during operation, which restricts achievable efficiency and power density [117–119]. CPSS are extensively employed in a wide range of applications, including power supplies for computing systems, industrial motor drives, power conversion units such as inverters, rectifiers, and voltage regulators, electric vehicles (EVs), and renewable energy systems (RES) [120]. In these systems, energy dissipation represents a critical design concern, as it directly influences thermal management requirements, system size, and overall reliability [121]. Semiconductor losses are generally categorized into conduction and switching losses. Conduction losses are governed primarily by the device on-state characteristics, particularly the on-state resistance or forward voltage drop, whereas switching losses arise from non-ideal turn-on and turn-off transitions involving simultaneous voltage and current overlap. Minimizing total device loss therefore requires a reduction in both on-state resistance and switching transition times. However, the intrinsic material properties of Si impose fundamental constraints to the extent to which these parameters can be optimized simultaneously, particularly under high-voltage, high-current, and high-frequency operating conditions. As result, Si-based devices face challenges related to increased power dissipation, limited thermal capability, and reduced efficiency at elevated switching frequencies [122].

The growing demand for compact, high-efficiency, and high-power-density power electronic systems has driven the need for devices capable of operating at higher voltages, switching frequencies, and junction temperatures than those attainable with conventional Si technology. Historically, power converter designs based on CPSS have involved inherent trade-offs among efficiency, cost, switching frequency, and physical size, largely dictated by device limitations and associated passive components [123]. The term CPSS refers specifically to Si-based power semiconductor devices, which continue to form the backbone of many existing power electronic converters. However, for advanced high-power and high-frequency applications, Si technology is approaching its theoretical performance limits, as illustrated by commonly reported material capability comparisons presented in Fig. 4, thereby motivating a transition toward alternative semiconductor materials [124,125]. In this context, wide bandgap (WBG) semiconductors have emerged as promising candidates capable of overcoming the limitations of Si and enabling significant improvements in converter

performance [126]. Accordingly, this review focuses on next-generation WBG power device technologies, with particular emphasis on gallium nitride (GaN), and its application in modern power electronic converters. Several WBG semiconductor materials have been investigated for power electronic applications, including silicon carbide (SiC), gallium nitride (GaN), diamond, and aluminum nitride (AlN) [127,128]. Among these, SiC and GaN have reached the highest levels of technological maturity and commercial adoption, making them the most viable alternatives to Si-based devices in contemporary power electronic converters (PECs) [129–131]. Comparative evaluations of their theoretical material properties, presented in Fig. 4, demonstrate that both SiC and GaN possess significantly wider bandgaps and higher critical electric fields than Si, enabling higher breakdown voltages and reliable operation at elevated temperatures [132–135]. In addition, SiC exhibits high thermal conductivity, which supports efficient heat dissipation and improved thermal management in high-power applications, while GaN is characterized by high electron mobility and saturation velocity, rendering it particularly well suited for high frequency switching applications. These advantageous material properties allow WBG devices to employ thinner drift regions and higher doping concentrations, resulting in substantially lower specific on-resistance and reduced conduction losses compared with CPSS. Consequently, the integration of WBG semiconductor devices in PECs enables higher efficiency, increased power density, and reduced converter size. The selection of power semiconductor switches is largely dictated by the required drain-source blocking voltage (V_{ds}) and the performance targets of the intended application. For low- to medium-voltage conversion stages, typically on the order of 100–600 V, gallium nitride (GaN) devices are often preferred because their wide-bandgap properties enable fast switching and low switching losses, supporting high-frequency, high-power-density designs. For higher-voltage operation, particularly around 1200 V and above, silicon carbide (SiC) devices are generally more appropriate due to their higher blocking capability and proven suitability for high-power conversion. Despite the growing adoption of wide-bandgap technologies, silicon (Si) IGBTs/MOSFETs remain widely used in industrial converters owing to their maturity, established supply chains, and favorable cost-performance balance. In addition, increasing attention has been directed toward hybrid converter topologies that combine WBG devices with Si MOSFETs, aiming to exploit the advantages of WBG switching where most beneficial while retaining the economic and practical benefits of conventional silicon devices. Fig. 3 provides a visual representation of the most frequently occurring terms in the literature on GaN-based power converters for solar photovoltaic applications, thereby highlighting the principal themes within this research domain.

The prominence of terms such as “converter,” “power,” “switching,” “high frequency,” “efficiency,” “design,” and “control” indicates that the literature primarily emphasizes improvements in conversion efficiency and power density through higher switching frequencies, optimized converter architectures, and advanced control methodologies. The dominance of keywords such as converter, power, switching, high frequency, efficiency, design, and control indicates that the current research landscape is primarily driven by the pursuit of higher conversion efficiency and power density through elevated switching frequencies, optimized converter architectures, and increasingly sophisticated control methodologies. The strong representation of GaN-based, gallium nitride, and HEMTs further signals the continued migration from silicon toward wide-bandgap (WBG) semiconductor devices, motivated by GaN's favorable switching characteristics,

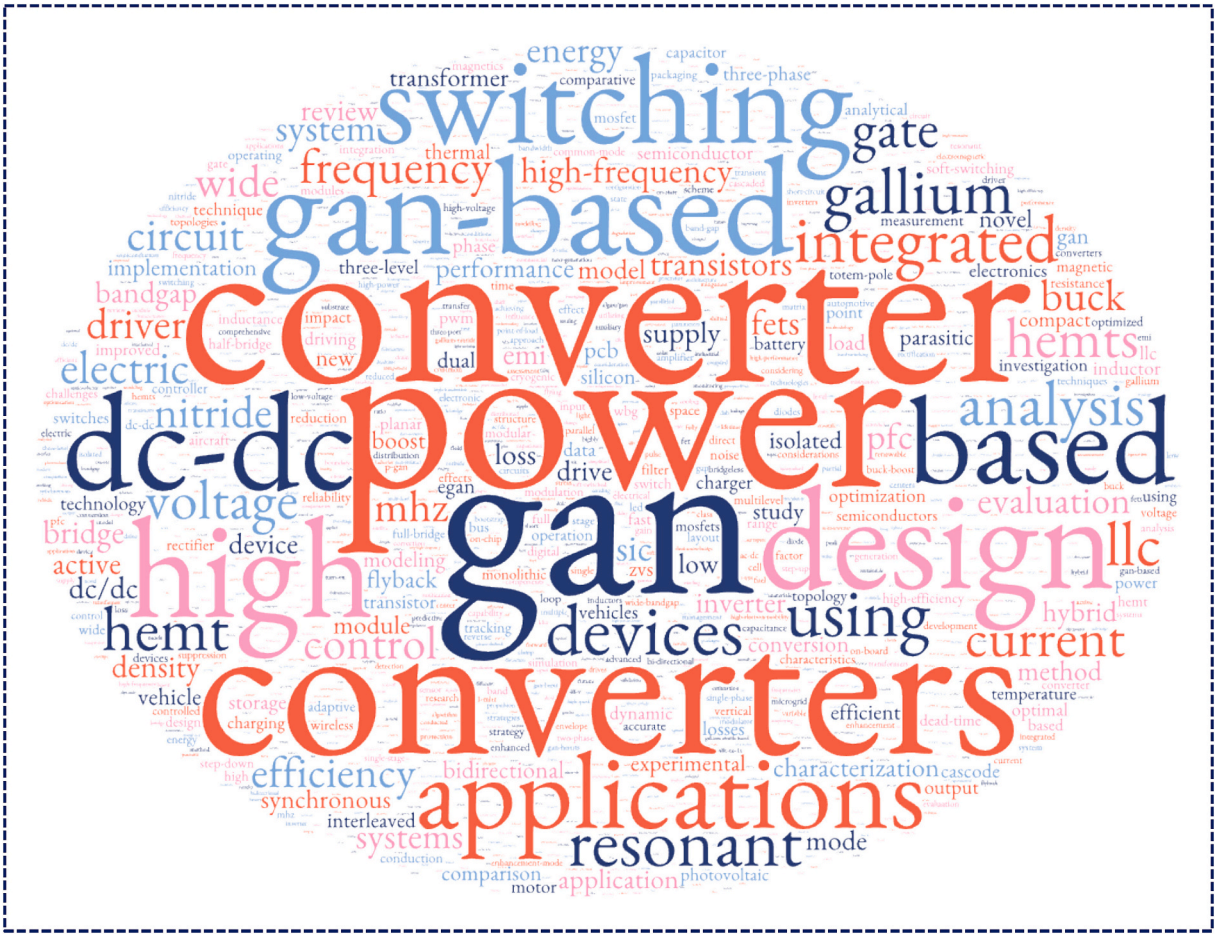

Fig. 3. Word cloud showing key power electronics research trends with emphasis on GaN-based converters for solar PV systems.

particularly reduced parasitic capacitances and gate charge which enable low-loss operation at substantially higher frequencies than conventional Si MOSFETs. In solar photovoltaic (PV) power-conditioning systems, these device attributes are being translated into tangible system-level benefits, most notably within high-frequency DC- DC stages (e.g., boost, interleaved, and isolated resonant structures such as LLC/CLLC and dual-active-bridge families) and module-level power electronics (MLPE) implementations, including microinverters and power optimizers. The resulting increase in feasible switching frequency supports meaningful reductions in passive component size and energy storage requirements, thereby improving volumetric power density and facilitating compact, lightweight PV converter designs while maintaining high efficiency across wide operating conditions, including partial-load and dynamically varying irradiance typical of field operation. Concurrently, the presence of terms associated with analysis, modeling, loss evaluation, and control suggests that the literature is not limited to performance enhancement but also addresses practical design constraints introduced by fast GaN switching transitions, including electromagnetic interference (EMI) management, gate-driver and protection converter-control co-design, thermal pathways and packaging, and layout-sensitive parasitic interactions.

Gallium nitride (GaN) power devices are realized in both lateral and vertical device architectures, each addressing different power and voltage requirements. Lateral GaN devices represent the most mature technology and are predominantly employed in high-frequency, low- to medium-power applications, whereas vertical GaN structures offer a promising pathway toward high-power and high-voltage operation by enabling vertical current flow and enhanced electric field management. Although vertical GaN devices are not yet commercially available, extensive research efforts are currently focused on material growth, device fabrication, and reliability enhancement to facilitate their future commercialization and to fully exploit the superior intrinsic properties of GaN [136,137]. GaN power transistors can be classified according to their operating mode as normally-ON (depletion-mode) or normally-OFF (enhancement-mode) devices. Conventional GaN heterojunction field-effect transistors (HFETs), based on an AlGaN/GaN heterostructure, form a high-density two-dimensional electron gas (2DEG) at the heterointerface, which acts as a low-resistance conduction channel between the drain and source. Silicon substrates are commonly used for GaN epitaxial growth, although alternative substrates such as silicon carbide and diamond have also been investigated to improve thermal performance. The presence of the 2DEG results in depletion-mode operation, whereby the device conducts at zero gate bias. While this characteristic is advantageous for certain radio-frequency applications, normally-ON GaN devices are generally unsuitable for power electronic converters, particularly for voltage-source topologies, due to safety and controllability concerns during start-up or in the event of gate-drive failure. For this reason, normally OFF GaN devices are strongly preferred in power electronic applications, as they provide inherently safer operation and simplify gate-driver design. Significant research activity has therefore been directed toward the development of enhancement-mode GaN transistors. One commercially adopted approach is the cascode configuration, in which a depletion-mode GaN HFET is connected in series with a low-voltage enhancement-mode silicon MOSFET. This arrangement produces a normally-OFF composite device, with the silicon MOSFET controlling the gate potential of the GaN HFET. During conduction, both devices carry the same channel current, while in the off state the blocking voltage is shared between them. Despite their practicality, cascode GaN devices introduce additional packaging complexity and parasitic inductances associated with the series connection, which may adversely affect high-speed switching behavior. Commercial 600-V GaN-on-Si cascode devices, such as those offered by Transphorm, exemplify this approach, where threshold-voltage engineering is used to achieve enhancement-mode operation [138]. At present, the majority of commercially available GaN power devices are lateral enhancement-mode high-electron-mobility transistors (*E*-HEMTs) [138]. Compared with conventional silicon MOSFETs, lateral GaN devices exhibit substantially lower gate-source (C_{gs}) and gate-drain (C_{gd}) capacitances, resulting in a significantly reduced total gate charge. Since gate charge directly influences switching speed and gate-driver losses, GaN devices can achieve faster switching transitions and higher switching efficiency [139]. In addition, GaN possesses advantageous intrinsic material properties, including high electron mobility, a wide bandgap, a high critical electric field, and a high saturation drift velocity, which collectively support high-performance power switching applications [140,141]. Comparative assessments of wide-bandgap (WBG) semiconductors indicate that GaN outperforms silicon and silicon carbide in terms of electron mobility, energy bandgap, and breakdown electric field strength [142]. However, GaN exhibits lower thermal conductivity than both silicon and silicon carbide, which can limit heat dissipation from the device junction to the package and heat sink. Consequently, GaN devices typically exhibit higher thermal resistance, leading to elevated junction temperatures for a given power dissipation. It should be noted that thermal performance is strongly influenced by packaging technology and substrate selection. The saturation drift velocity of GaN is comparable to that of silicon carbide, supporting high-field carrier transport. Fig. 4 presents a normalized comparison of key material properties for Si, SiC, and GaN that directly influence power-device performance. The energy bandgap and breakdown electric field are substantially higher for GaN and SiC than for Si, enabling higher blocking capability and lower specific on resistance through thinner drift regions. GaN exhibits strong carrier transport (high electron mobility and saturation velocity), supporting fast switching and high-frequency, high-power-density conversion. SiC combines a high breakdown field with superior thermal conductivity, which improves heat removal and is advantageous for high-power, high-voltage modules. Fig. 4 demonstrates the superior material characteristics of wide-bandgap semiconductors relative to silicon and emphasizes the complementary advantages of GaN for high-speed switching and SiC for high-voltage operation and effective thermal management.

A further advantage of GaN technology is its low drain-source on-resistance ($R_{ds_{on}}$), which enables significantly smaller chip areas, often by an order of magnitude compared with silicon devices of equivalent voltage and current ratings [144]. This reduction in chip size directly contributes to lower conduction losses and supports compact, high-power-density converter designs. As a result, GaN-based devices can reduce cooling and heat-sink requirements, which is advantageous for applications seeking high efficiency and reduced system cost [145,146]. Although GaN devices currently incur higher costs than conventional silicon devices and, in certain applications, SiC-based alternatives, ongoing advances in material growth, wafer-scale fabrication, device packaging, and manufacturing throughput are expected to reduce

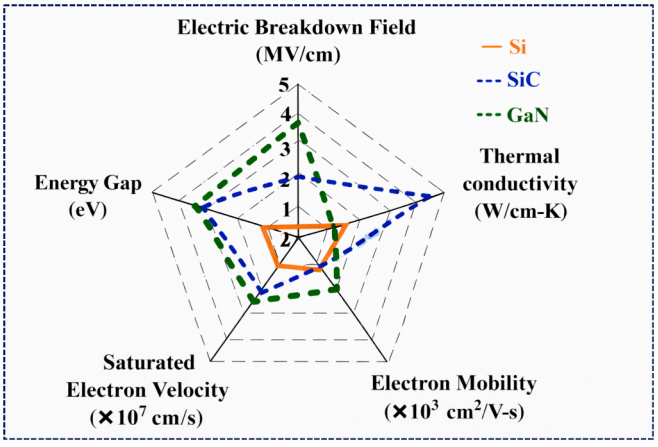

Fig. 4. Comparison of key material properties of silicon (Si), silicon carbide (SiC), and gallium nitride (GaN) [143].

production costs and strengthen their commercial competitiveness [147]. In comparison with silicon carbide MOSFETs, GaN devices exhibit a stronger positive temperature coefficient of $R_{ds_{on}}$, which facilitates current sharing in parallel device configurations, an important consideration in high-power applications [148]. Moreover, GaN devices typically require lower gate-drive voltages than SiC MOSFETs for comparable current levels [149,150]. The combination of a high breakdown electric field and high electron mobility enables GaN devices to operate at switching frequencies significantly higher than those achievable with silicon-based devices, making them well suited to high-frequency applications, including electric and hybrid-electric vehicle powertrains and renewable energy conversion systems, particularly solar photovoltaic systems [143,151]. The superior switching performance of GaN *E*-HEMTs is largely attributed to their extremely low input, output, and Miller capacitances, with reported input capacitance values several tens of times lower than those of silicon MOSFETs. These characteristics reduce gate-drive losses and switching delays, while the inherently low parasitic inductance of GaN devices further minimizes switching losses [152].

As shown in Fig. 5, hard-switching turn-on, the drain-source voltage (V_{DS}) collapses while the drain current (I_D) rises toward the load current (I_{Load}). The overlap of $V_{DS}$and I_D produces turn-on switching energy, represented as the V/ILoss region. In addition, part of the turn-on energy is associated with charging and discharging the device output capacitances, captured by the capacitive terms $E_{\text{oss}}$and E_{qoss}. For the GaN HEMT, the total turn-on loss is primarily governed by the capacitive energy (E_{oss}, E_{qoss}) and the voltage-current overlap during the transition. For the SiC MOSFET, an additional contribution arises from reverse-recovery effects (E_{qrr}) of the body diode or external antiparallel diode, which introduces a recovery current component during commutation. This increases the effective current during the voltage fall, enlarging the overlap region and thereby raising the overall turn-on energy relative to the GaN case under comparable conditions.

The device-level switching-loss mechanisms discussed above have a direct and cumulative impact on the performance of power-electronic converters, where semiconductor devices undergo repetitive commutation under high voltage and current stress. In such converters, the instantaneous turn-on and turn-off energies, originating from the overlap of V_{DS} and I_D as well as from output-capacitance-related components (E_{oss} and E_{qoss}), translate into average switching losses that scale proportionally with the switching frequency. In the case of SiC MOSFETs, the additional reverse-recovery-related energy (E_{qrr}) further elevates the effective commutation current during turn-on, which can exacerbate switching losses, increase junction temperature, and impose stricter thermal management requirements. These factors ultimately constrain the maximum achievable switching frequency and influence converter efficiency, electromagnetic interference (EMI) performance, and passive component sizing. These considerations are particularly critical in the DC-AC conversion stage of solar photovoltaic (PV) systems, where inverter operation must accommodate wide variations in input voltage and power due to changing irradiance and temperature conditions. Under such dynamic operating scenarios, switching losses can constitute a significant portion of the total inverter loss, especially during partial-load operation. Therefore, the intrinsic switching behavior of the selected power semiconductor technology plays a pivotal role in determining the overall efficiency, power density, and reliability of PV inverters, reinforcing the importance of linking device-level loss mechanisms to system-level DC-AC conversion performance.

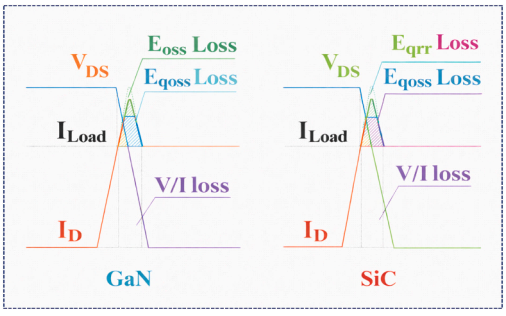

Fig. 5. Hard-switching turn-on loss comparison of GaN HEMT and SiC MOSFET [153].

The growing penetration of solar photovoltaic (PV) generation is accelerating the transition from centralized electricity production toward distributed energy resources integrated at the distribution level. From an energy conversion perspective, PV arrays inherently supply DC power, and their electrical characteristics vary with irradiance and temperature. As a result, practical PV integration requires a power-electronic interface capable of both conditioning the DC output and delivering AC power compatible with utility grids and conventional loads. In grid-connected PV systems, DC-AC conversion is typically realized through a DC-link voltage-source inverter (VSI). The inverter regulates the DC-link and injects a controlled AC current (or voltage) using high-frequency modulation, while meeting stringent requirements on power quality and grid compliance. This includes limiting harmonic distortion through appropriate filtering, ensuring accurate synchronization via grid-referenced control, and maintaining stable operation under irradiance fluctuations and grid disturbances. In addition, the inverter is often required to support protective and supervisory functions such as anti-islanding, over/under-voltage and frequency protection, and controlled power ramping, in accordance with applicable grid codes. Although DC microgrids can reduce the number of conversion stages for native DC sources and loads and avoid issues associated with reactive power and synchronization within the local network, most existing electricity infrastructures, particularly in residential and legacy distribution systems remain predominantly AC-based. Therefore, efficient and reliable DC-to-AC conversion remains a critical enabling function for large-scale PV deployment, ensuring that solar-generated DC power can be delivered to AC networks with high efficiency, low distortion, and robust dynamic performance.

Multilevel inverters (MLIs) have emerged as a prominent solution for high-power DC-AC conversion due to their capability to synthesize staircase waveforms with superior spectral quality and reduce semiconductor stress. Relative to conventional two-level inverters, MLIs can achieve lower total harmonic distortion (THD) with smaller output filters, reduced dv/dt and common-mode voltage (CMV), lower electromagnetic interference (EMI), and improved loss distribution, which collectively support enhanced thermal performance and efficiency. These advantages have stimulated extensive research toward new MLI structures and control strategies aimed at improving performance, scalability, and implementation feasibility. Despite the substantial progress in MLI topologies, input-side conditioning remains a major obstacle, particularly for solar photovoltaic (PV) system applications [154,155]. A considerable portion of the reported MLI configurations assume a stiff and regulated DC input, an assumption that is seldom satisfied in practice. In solar PV systems, the DC output voltage varies with irradiance and temperature, which can degrade the inverter's modulation range, compromise output regulation, and complicate compliance with grid power-quality requirements. To mitigate these issues, DC-DC converters are frequently employed as front-end stages to provide voltage regulation and step-up/step-down capability prior to the MLI stage, thereby enabling stable DC-link operation under variable PV conditions. Several studies have attempted to incorporate voltage-conditioning functionality into MLI architecture to facilitate direct interfacing with solar PV sources. However, many of these solutions are constrained to single-source integration and provide only boost operation, limiting their applicability across wide operating ranges. Alternative approaches combine multiple PV strings by cascading DC-DC converters before the MLI stage to enable buck-boost operation and multi-input capability. While effective in principle, such arrangements

generally increase component count and introduce additional conduction and switching losses, which translate into higher cost, reduced power density, and lower overall efficiency [156]. More recent efforts have investigated converter structures that integrate DC-DC conversion and multilevel inversion within a unified DC-AC interface for solar PV applications. Although these designs can improve functional integration, they often face limitations in the number of input ports, attainable voltage levels, or phase configurations. Moreover, many multiport modular multilevel solutions employ low-frequency transformers to achieve voltage scaling and input isolation. While this approach provides modularity, it also results in increased size, weight, and cost, in addition to higher losses. Transformer-less multiport alternatives can alleviate these drawbacks but frequently sacrifice modularity and scalability, restricting their suitability to low- and medium-voltage PV systems. The key design considerations in multilevel converter topologies for grid-connected applications encompass leakage current mitigation and reduction of common-mode voltage (CMV), along with cost optimization achieved by minimizing the number of passive components and switching devices. Effective capacitor voltage regulation, including voltage balancing and ripple suppression, is essential for stable operation. In addition, the converter must accommodate a wide input voltage range, which may necessitate the adoption of either single-stage or multi-stage configurations. Reliability aspects such as fault classification, detection, and the implementation of fault-tolerant designs are also critical to ensure continuous and robust system performance, as illustrated in Fig. 6.

In addition, integrating multiple PV inputs introduces the challenge of maintaining DC-link capacitor voltage balance in multilevel inverter structures. Series-connected capacitor arrangements are commonly used to distribute the DC-link voltage among switching devices; however, unequal power extraction from PV strings and asymmetric operating conditions can cause voltage imbalance. Such imbalance degrades output waveform quality and increases semiconductor stress. Maintaining capacitor voltage balance typically requires advanced modulation and control strategies, which further increase system complexity. Accordingly, a rigorous and structured synthesis of multilevel inverter-based DC-AC conversion for solar PV systems is necessary to establish clear design guidelines and to articulate the practical trade-offs among competing approaches. Core technical considerations, including front-end voltage conditioning under irradiance-dependent PV variability, multi-input integration, DC-link capacitor voltage balancing, and the implications of modularity and isolation strategies directly govern achievable efficiency, power density, power quality, and control complexity. Consolidating these aspects within a unified perspective facilitates objective comparison of existing MLI configurations, clarifies their limitations under realistic operating conditions, and delineates the most relevant directions for advancing high-performance PV inverter interfaces for AC grid integration. Despite the well-established advantages of multilevel inverters (MLIs), several technical barriers remain during their design and practical deployment. These include the non-trivial selection of an appropriate topology for a targeted voltage-power range, the requirement to maintain stable DC-link capacitor voltages (notably in neutral-point-clamped and flying-capacitor families), and the development of high-performance modulation and control schemes capable of ensuring low distortion under operating uncertainties. In practice, additional implementation factors such as device dead time, parameter drift, component tolerances, and parasitic inductances can degrade waveform quality and complicate compliance with electromagnetic compatibility (EMC) and grid interconnection requirements. To address these challenges, current research efforts emphasize (i) the development of topologies with reduced component count and improved voltage utilization, (ii) enhanced balancing and control strategies including optimized PWM/SVPWM, predictive control, and observer-based approaches, and (iii) the integration of device- and system-level considerations to improve efficiency and reliability. In this context, the adoption of wide-bandgap (WBG) semiconductors, particularly silicon carbide (SiC) and gallium nitride (GaN), has significantly influenced the evolution of MLI technology. Compared with silicon devices, WBG switches exhibit higher breakdown strength, faster switching transitions, and improved high-temperature capability, enabling operation at higher switching frequencies with reduced switching energy and improved thermal margins. These characteristics can reduce passive-component size, including filter requirements, and ease heat-sinking demands, thereby increasing the achievable power density while preserving power quality. Moreover, the benefits of WBG devices interact strongly with multilevel converter operation, where switching loss distribution, commutation behavior, and voltage balancing dynamics collectively determine overall performance. SiC MOSFETs are particularly suitable for medium- and high-voltage MLIs due to their high blocking capability and robust thermal properties, whereas GaN HEMTs are attractive for lower- to medium-voltage MLIs that prioritize very high switching frequency and fast transient response. SiC and GaN power devices support operation at elevated switching frequencies with comparatively lower switching energy and improved thermal capability, thereby reducing heat generation and easing cooling requirements. This enables higher converter efficiency and facilitates compact implementations through the downsizing of passive components such as inductors, capacitors, and EMI filters. In multilevel inverter (MLI) systems, where voltage is synthesized through multiple discrete levels and switching events are distributed among several devices, the use of wide-bandgap switches can further improve performance by reducing per-device stress while maintaining high-quality output waveforms. When applied to dynamic MLI operation-in which switching states are continuously adjusted to regulate power flow and maintain internal capacitor voltage balance-the fast transition characteristics of SiC and GaN devices provide additional benefits. Higher

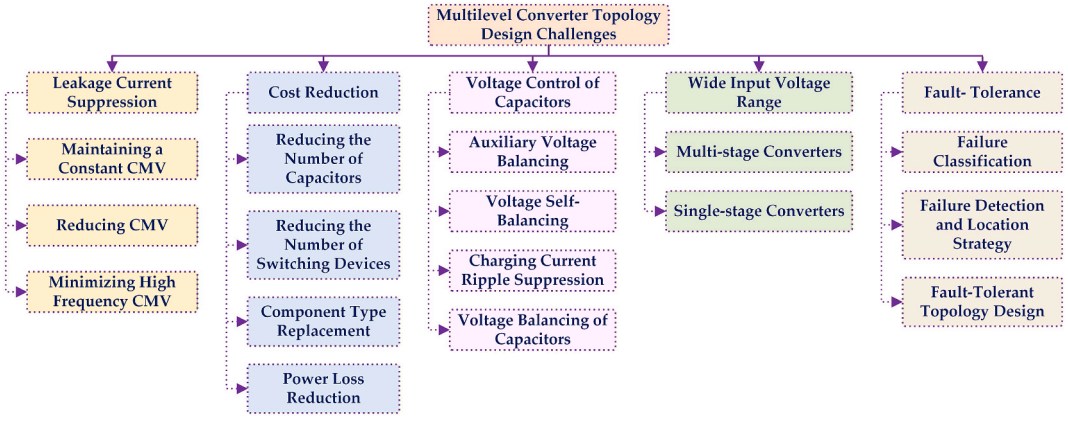

Fig. 6. Design challenges in multilevel converter topologies [154].

effective switching frequency and improved commutation behavior can support finer voltage-step resolution and enhanced harmonic performance, which may reduce filtering requirements without imposing a proportional penalty in switching losses. Moreover, improved efficiency and higher allowable junction temperatures can lower thermal design margins and simplify packaging, contributing to increased power density and improved scalability. Collectively, these attributes strengthen the feasibility of modular, high-performance MLI platforms that achieve efficient DC-AC conversion while enabling cost-effective scaling across a broad range of power levels and application requirements [157]. Within the inverter-based category, multilevel inverter (MLI) structures are widely adopted because they synthesize the output voltage using multiple discrete levels, thereby improving waveform quality relative to two level inverters. By increasing the number of available voltage steps, MLIs can reduce harmonic distortion, lower dv/dt stress across machine terminals and grid interfaces and distribute voltage stress among semiconductor devices. These characteristics make MLIs particularly suitable for medium and high-power conversion where device voltage ratings, switching losses, and filter size impose practical constraints. Among established MLI families, cascaded H bridge (CHB), flying capacitor (FC), and neutral point clamped (NPC) topologies are most frequently reported due to their maturity and scalability [158,159]. The CHB topology is formed by connecting multiple single phase H bridge cells in series, with each cell contributing an additional voltage level. This modular structure enables straightforward extension to higher voltage levels by adding identical submodules, and it supports redundancy through reconfiguration or bypass of faulty cells. CHB converters are especially attractive when multiple isolated DC sources are naturally available, such as segmented photovoltaic strings or distributed storage modules, because each cell can be supplied independently. The modular arrangement also provides flexibility in control, since the switching states of individual cells can be coordinated to shape the output waveform and manage cell level voltages where applicable. The FC topology generates multiple voltage levels using a set of floating capacitors that serve as intermediate voltage sources. Different switching combinations insert selected capacitor voltages into the output, producing a stepped waveform. A distinctive feature of FC converters is the presence of redundant switching states, which can be used to achieve secondary objectives such as capacitor voltage regulation while maintaining the desired output level. However, maintaining stable capacitor voltages typically requires additional sensing and balancing control, and the number of capacitors increases rapidly with the number of levels, which can influence converter size, cost, and long-term reliability. The NPC topology, also referred to as diode clamped multilevel conversion, produces intermediate voltage levels by clamping the phase output to the split DC link through clamping devices. This approach enables voltage sharing among devices, allowing higher output voltages with moderate device blocking ratings. NPC converters are therefore commonly considered for medium voltage operation and high-power conversion. A key technical challenge is regulation of the neutral point potential, since unequal charging and discharging of the DC link capacitors can lead to neutral point drift, which degrades waveform quality and limits the modulation range. Neutral point balancing is therefore a central requirement in NPC control design, particularly under asymmetric loading, reactive power exchange, or dynamic operating conditions. Hybrid converter-based configurations combine structural elements from two or more conventional inverter families to exploit complementary advantages. Hybrid multilevel arrangements may integrate a CHB stage with an NPC stage, combine switched capacitor concepts with cascaded cells, or introduce auxiliary networks to improve voltage utilization and extend operating range. Such combinations are generally motivated by the desire to reduce component count, improve fault tolerance, enhance voltage boosting capability, or relax internal voltage balancing requirements while maintaining multilevel voltage synthesis capability. Hybrid structures also introduce additional control degrees of freedom that can be leveraged to improve dynamic performance, although this comes with increased coordination complexity. Structure based categorization highlights how voltage levels are generated and how semiconductor devices, passive elements, and energy storage components are arranged within the converter. This perspective is useful for comparing scalability, redundancy potential, voltage stress distribution, balancing requirements, and modulation complexity across MLI families. Renewable energy source-based categorization, in contrast, focuses on how renewable generators are incorporated into the converter architecture. In such configurations, distributed DC sources such as photovoltaic strings may be directly interfaced through cascaded or modular multilevel structures, enabling source level modularity and potentially reducing the need for additional conversion stages. At the same time, source variability and mismatch can introduce additional coordination requirements, including power sharing among modules and management of unequal DC voltages, which must be addressed by the converter control strategy. The increasing integration of renewable energy sources necessitates advanced power conversion and control frameworks to ensure reliable and efficient system operation. A generalized architecture of distributed renewable energy systems is presented in Fig. 7, where photovoltaic and wind generation units are interfaced with the grid through multilevel power converters. These converters enable efficient DC–AC conversion, facilitate bidirectional power flow, and support both grid-connected and islanded modes of operation. Energy storage systems are incorporated to address the variability of renewable generation, providing functionalities such as energy buffering, peak shaving, and load leveling. On the demand side, the system accommodates residential users, distributed loads, and electric vehicle charging infrastructure, including vehicle-to-grid interaction. Furthermore, architecture extends to electrified transportation applications, demonstrating the adaptability of multilevel converter-based systems across diverse operating conditions. These integrated configurations highlight the role of multilevel converters in improving operational flexibility, power quality, and overall system reliability in distributed renewable energy networks.

3.1. Single stage inverter

A single-stage grid-connected inverter architecture, as shown in Fig. 8, integrates multiple power processing and control functions within a single conversion unit. The photovoltaic (PV) array delivers DC power to a full-bridge inverter through a DC-link capacitor, facilitating direct power conversion. In this configuration, the inverter simultaneously performs maximum power point tracking (MPPT), voltage adaptation, DC–AC conversion, and regulation of the injected grid current, thereby eliminating the need for a dedicated intermediate DC–DC stage. An LCL filter is employed to attenuate switching harmonics and ensure compliance with power quality standards. Measurement signals are utilized for feedback control, while the generated power is either supplied to local loads or injected into the utility grid [160]. This approach reduces component count and can improve efficiency and power density; however, it also couples the DC side energy extraction dynamics with the AC side grid current regulation, which introduces specific design constraints. A defining characteristic of single-phase grid connected conversion is the presence of a second harmonic power component at twice the grid frequency. As a result, the instantaneous power transferred to the grid is not constant, even under steady irradiance and constant average power delivery. For a unity power factor operating condition, the grid voltage and current can be represented as

$$v_g(t) = V_m \sin(\omega_{grid} t) \text{ and } i_g(t) = I_m \sin(\omega_{grid} t) \tag{1}$$

respectively. The instantaneous power is then

$$p_{grid}(t) = v_g(t) i_g(t) = V_m I_m \sin^2(\omega_{grid} t) \tag{2}$$

which can be rewritten using $\sin^2(x) = \frac{1}{2}[1 - \cos(2x)]$ as

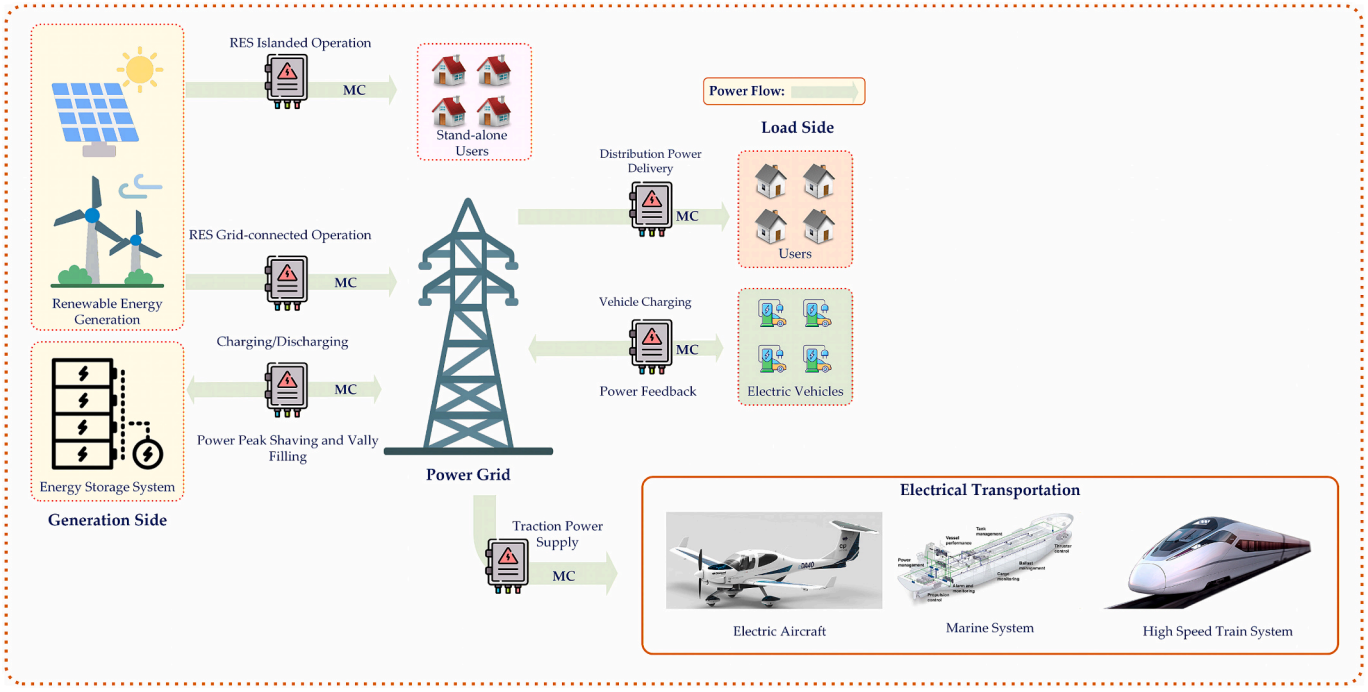

Fig. 7. Distributed renewable energy system with multilevel power converters.

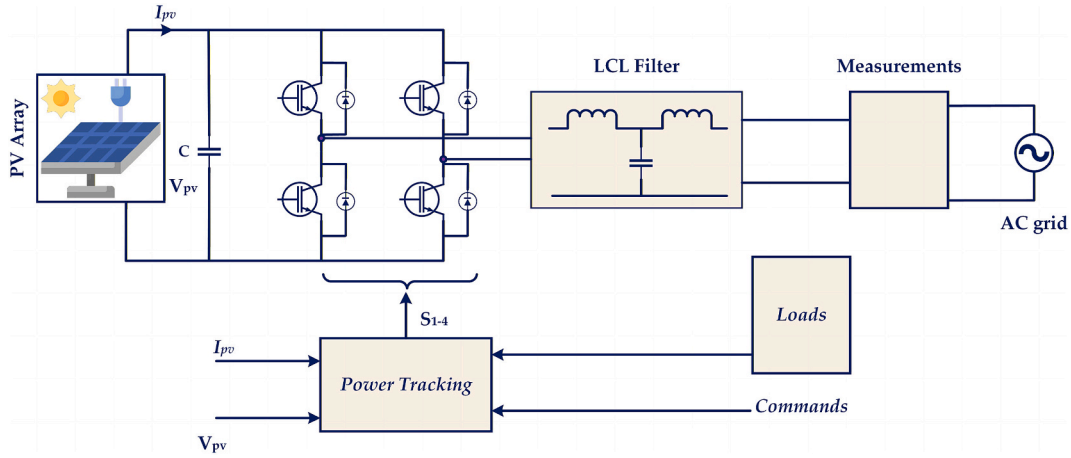

Fig. 8. Single-stage inverter topology.

$$p_{grid}(t) = \frac{V_m I_m}{2}\left[1 - \cos\left(2\omega_{grid}t\right)\right] \tag{3}$$

where ω_{grid} is the grid angular frequency. Eqs. (1)–(2) indicate that the delivered power consists of an average component and a ripple component at $2\omega_{grid}$. This double frequency power ripple must be buffered by the DC link energy storage element, typically a capacitor, resulting in a second harmonic voltage ripple on the DC side. If the DC link is not adequately dimensioned or regulated, the ripple can propagate to the PV operating point and degrade maximum power point tracking accuracy, while also increasing current stress and reducing lifetime of passive components. Therefore, DC link design and control bandwidth are critical aspects of single stage inverters. Historically, line frequency transformers have been used to provide galvanic isolation and voltage matching between the PV source and the grid. While robust, these transformers operate at the fundamental grid frequency and therefore add considerable mass and volume, and they introduce additional copper and core losses that can reduce peak conversion efficiency [161]. For this reason, many contemporary designs avoid line frequency transformers in favor of high frequency isolated solutions or transformer less implementations. High frequency transformers significantly reduce magnetic size due to operation at elevated frequencies, whereas transformer less topologies improve power density and efficiency by removing the isolation stage, although they impose additional requirements for leakage current mitigation and compliance with safety and electromagnetic compatibility standards [162–167]. In single stage inverters, the energy transfer and buffering function is typically realized using an inductor or a high frequency transformer, which may also provide isolation when required. Buck boost derived single stage inverter topologies are frequently investigated because they offer step up and step-down voltage capability without a line frequency transformer, thereby allowing greater flexibility in accommodating variations in PV array voltage. Nevertheless, integrating MPPT and grid current regulation within a single power stage results in coupled control objectives. The practical DC input voltage range is often limited because the inverter must maintain the PV array at its optimal operating point

while simultaneously producing the required grid voltage and current waveform. Achieving stringent harmonic limits and high-power factor under wide operating conditions can also be more challenging due to this coupling. Scalability is another important consideration. As power rating increases, the entire power is processed through a single set of switching devices and passive components, which increases current stress, conduction and switching losses, and thermal management requirements. These factors can constrain the practical power capacity of single stage designs and reduce efficiency at higher ratings. Consequently, single stage inverters are most commonly applied in low to medium power systems with moderate input voltage variation and compact design priorities. For applications requiring wide PV voltage operating range, stringent power quality, and higher power levels, multistage architectures are often preferred because they offer improved decoupling between MPPT and grid current control, enhanced scalability, and greater design flexibility [168].

3.2. Multi-stage inverter

A multi-stage grid-connected inverter architecture, as depicted in Fig. 9, employs two or more cascaded power conversion stages between the DC source and the AC grid, allowing functional separation of key control and energy conversion tasks. In typical photovoltaic (PV) applications, the initial DC-DC stage is responsible for voltage conditioning, which may involve step-up or buck–boost operation, as well as maximum power point tracking (MPPT) to ensure optimal energy extraction. In certain configurations, this stage additionally provides galvanic isolation through the integration of a high-frequency transformer. The conditioned DC output is subsequently delivered to a DC-AC inverter stage, which ensures grid synchronization and regulates the injected current. An LCL filter is incorporated to mitigate switching harmonics and maintain compliance with grid power quality requirements. System measurements are utilized for closed-loop control, while the generated power can be either consumed by local loads or supplied to the utility grid [169]. In a conventional two stage structure, the DC-DC front end regulates the PV array operating point and generates a controlled DC link voltage. This regulated intermediate bus decouples source side dynamics from grid side control. As a result, the inverter stage can be designed primarily for sinusoidal current injection and compliance with grid code requirements, while the DC-DC stage maintains maximum power extraction under irradiance and temperature variation. This functional separation generally improves controllability, facilitates independent tuning of the two control loops, and enhances transient performance compared with single stage solutions, particularly under rapid input fluctuations. Multistage inverters can be implemented as isolated or non-isolated systems. In non-isolated configurations, the elimination of transformer isolation can improve conversion efficiency and reduce cost and volume. However, the absence of galvanic isolation imposes additional constraints on grounding strategy, leakage current mitigation, and safety compliance, and may limit the practical input voltage operating range depending on the topology and grid connection requirements [169]. In isolated configurations, a high frequency transformer is typically incorporated within the DC-DC stage. Because the transformer operates at elevated switching frequency, it can provide voltage scaling and galvanic isolation with significantly reduced size and weight compared with line frequency transformers. The regulated DC link produced by the first stage is then processed by the inverter stage to generate a full wave sinusoidal output synchronized with the grid frequency. Buck boost derived DC-DC stages are commonly used in multistage PV systems because they provide flexibility in accommodating wide variations in PV array voltage while maintaining a stable DC link. By ensuring an appropriate DC link level, the inverter stage can operate within a favorable modulation range, which supports lower harmonic distortion and improved current control. The second stage, typically implemented as a full bridge or three phase voltage source inverters, converts the regulated DC bus into an AC waveform and injects a controlled sinusoidal grid current at the line frequency, while the switching actions are realized at a substantially higher carrier frequency to shape the output spectrum [169]. The principal advantages of multistage architecture include an extended DC input voltage range, improved power quality, enhanced scalability to higher power levels, and the ability to incorporate galvanic isolation when required. In addition, distributing the conversion function across stages can reduce peak device stress within each stage and allow component selection to be optimized according to voltage and current demands. These benefits are balanced by an increase in component count and control complexity, as well as additional conduction and switching losses associated with cascaded power processing. Consequently, multistage inverter architectures are generally preferred in applications requiring wide operating range and high-power quality, whereas single stage solutions remain attractive where compactness and minimal hardware are primary objectives. Fig. 9 illustrates a typical two-stage grid-connected photovoltaic inverter. The PV array supplies a variable DC voltage to the first stage, which is a DC-DC converter responsible for maximum power point tracking and voltage regulation or boosting. This stage generates a controlled DC-link voltage that stabilizes the system despite variations in irradiance and temperature. The regulated DC-link feeds the second stage, a DC-AC inverter, which converts the DC power into a sinusoidal AC waveform synchronized with the grid. This stage controls the injected grid current to ensure proper power transfer, high power factor operation, and compliance with harmonic standards.

3.3. Half-bridge diode clamped inverters

Three level half bridge diode clamped inverters are frequently employed in single phase transformer less grid connected photovoltaic

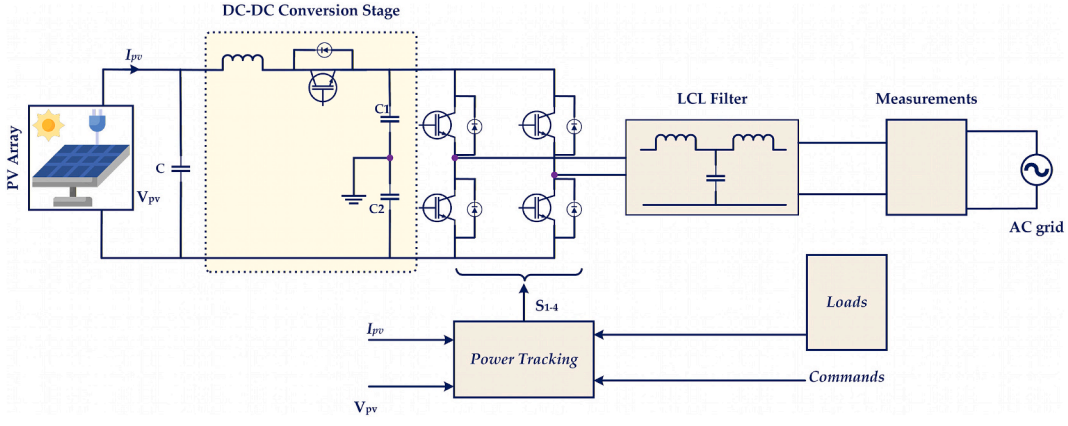

Fig. 9. Multi-stage inverter topology.

systems, where high efficiency and compact implementation are important. The topology is formed by a split DC link, typically realized using two series connected capacitors, and a set of clamping diodes that provide a controlled connection to the midpoint of the DC bus. This configuration enables the synthesis of three output voltage levels, commonly $+V_{dc}/2$, 0, and $-V_{dc}/2$, which improves output waveform quality compared with a two-level inverter and supports lower current harmonic distortion for a given switching frequency [170]. The output voltage is determined by the active switching state. When the upper devices are turned on, the output terminal is connected to the positive half of the DC link, and a positive voltage level is applied to the grid interface. When the lower devices are turned on, the output is connected to the negative half of the DC link, and a negative voltage level is produced. A zero-voltage level is obtained by clamping the output node to the DC link midpoint through the diode clamping path using the appropriate switch combination. The availability of the zero level increases control flexibility and reduces dv/dt at the output, which can decrease device stress and relax the requirements on the grid side filter. Transformer less photovoltaic systems are sensitive to leakage current because parasitic capacitances exist between the PV array and earth. Variations in common mode voltage can drive displacement currents through these capacitances, contributing to electromagnetic interference and raising safety concerns. In half bridge diode clamped structures, the midpoint of the split DC link can be referenced to ground, which stabilizes the common mode potential and reduces the magnitude of capacitive earth leakage current. This feature is frequently cited as an advantage of the topology for transformer less operation, since it supports reduced electromagnetic emissions and improved compliance with leakage current limits [171]. For power injection into the utility grid, the DC link voltage must exceed the grid voltage peak by a sufficient margin to ensure controllability under the chosen modulation strategy. In addition, maintaining balanced capacitor voltages across the split DC link is important because any imbalance alters the intended voltage levels, degrades harmonic performance, and may introduce low frequency distortion components. Practical implementations therefore employ modulation and control methods that regulate grid current while supporting DC link capacitor voltage balancing and synchronization with the grid voltage. A half-bridge diode-clamped three-level inverter topology, as shown in Fig. 10, enables multilevel voltage generation using a split DC-link configuration. The photovoltaic (PV) arrays provide the DC input, which is divided into multiple voltage levels through the use of clamping diodes. The switching devices (S1–S4) operate in a coordinated manner to produce three distinct output voltage levels, thereby improving waveform quality compared to conventional two-level inverters. The clamping diodes (D1 and D2) ensure proper voltage sharing across the switches and limit voltage stress. This configuration reduces harmonic distortion and switching losses, resulting in enhanced efficiency and improved power quality. The AC output generated is then delivered to the grid through an interface inductance.

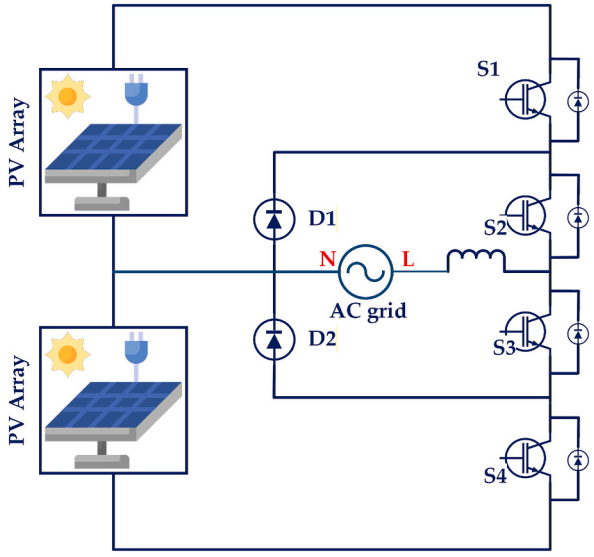

Fig. 10. Half-bridge diode-clamped three-level inverter [172].

3.4. Full-bridge single-leg clamped inverters

Full bridge single leg clamped inverter topologies are widely considered for transformer less residential photovoltaic systems because they enhance common mode voltage management and reduce leakage current without the use of galvanic isolation. The structure can be viewed as a modified full bridge inverter in which an additional clamping leg is introduced to control the connection of the AC side to the midpoint of a split DC link. In the configuration reported in Fig. 11, auxiliary bidirectional switches $S_1$and $S_2$and clamping diodes $D_1$and $D_2$are integrated with the conventional bridge switches S_4, S_5, and $S_6$to provide a controlled current path to and from the DC link midpoint [173]. The main full bridge stage generates the required AC output voltage through appropriate switching of the bridge devices, while the clamping leg regulates the midpoint current and constrains common mode voltage variations. This function is particularly important in transformer less PV systems because parasitic capacitances between the PV array and earth can drive displacement currents when the common mode voltage varies rapidly. By actively clamping the inverter output with respect to the DC link midpoint during specific switching intervals, the topology reduces high frequency common mode voltage transitions and therefore suppresses leakage current and associated electromagnetic interference. The additional bidirectional path also enables more controlled charging and discharging of the DC link capacitors, which supports voltage balancing and stable operation under varying power flow conditions. From a practical perspective, full bridge single leg clamped inverters are typically deployed at residential power levels where leakage current mitigation, efficiency, and compliance with safety requirements are critical. Reported implementations indicate that transformer less PV systems employing this class of inverter are commonly designed for ratings on the order of 1.5 kW and above, where the additional semiconductor devices and associated control complexity can be justified by improved performance and reduced filter burden [174]. Nevertheless, the topology requires coordinated modulation to ensure correct commutation of the bidirectional switches, maintain DC link capacitor voltage balance, and avoid unintended circulating currents, especially during grid disturbances and rapid irradiance changes.

A full-bridge single-leg clamped inverter topology, as shown in Fig. 11, employs a split DC-link configuration with capacitors to generate multiple voltage levels from the photovoltaic (PV) source. The inverter utilizes a combination of main switches (S1–S6) and clamping diodes (D1 and D2) to achieve controlled voltage synthesis and balanced operation. The clamping branch enables intermediate voltage levels, reducing voltage stress across the switches and improving output waveform quality. By appropriately coordinating the switching states, the topology produces a multilevel AC output with lower harmonic distortion compared to conventional two-level inverters.

3.5. Neutral point clamping converter

Neutral point clamped (NPC) inverters were originally introduced as multilevel converter structures in which series connected semiconductor devices are coordinated through voltage clamping to intermediate nodes of a split direct current link [176,177]. This arrangement enables the synthesis of stepped output waveforms while distributing the blocking voltage among devices, thereby extending the achievable output voltage using devices with moderate voltage ratings. Since their widespread adoption in the 1980s, NPC inverters have remained among the most established multilevel topologies for medium and high-power

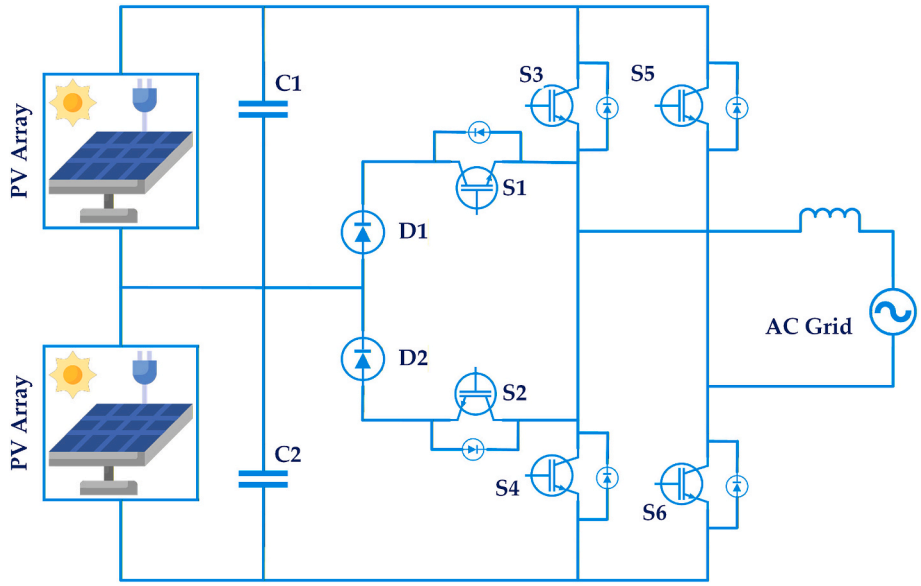

Fig. 11. Full bridge single-leg clamped inverter topology [175].

conversion. Their capability to generate multilevel voltages with improved spectral quality has motivated extensive use in power conditioning interfaces, where reduced total harmonic distortion, lower dv/dt, and improved conversion efficiency are desirable. Owing to these characteristics, NPC converters have been deployed in a broad range of applications, including uninterruptible power supplies, grid connected photovoltaic systems, wind turbine interfaces, variable speed motor drives, conveyor systems, and industrial installations across the power, mining, petrochemical, hydrogen, and electric vehicle sectors [178,179]. The practical relevance of NPC inverters is largely attributed

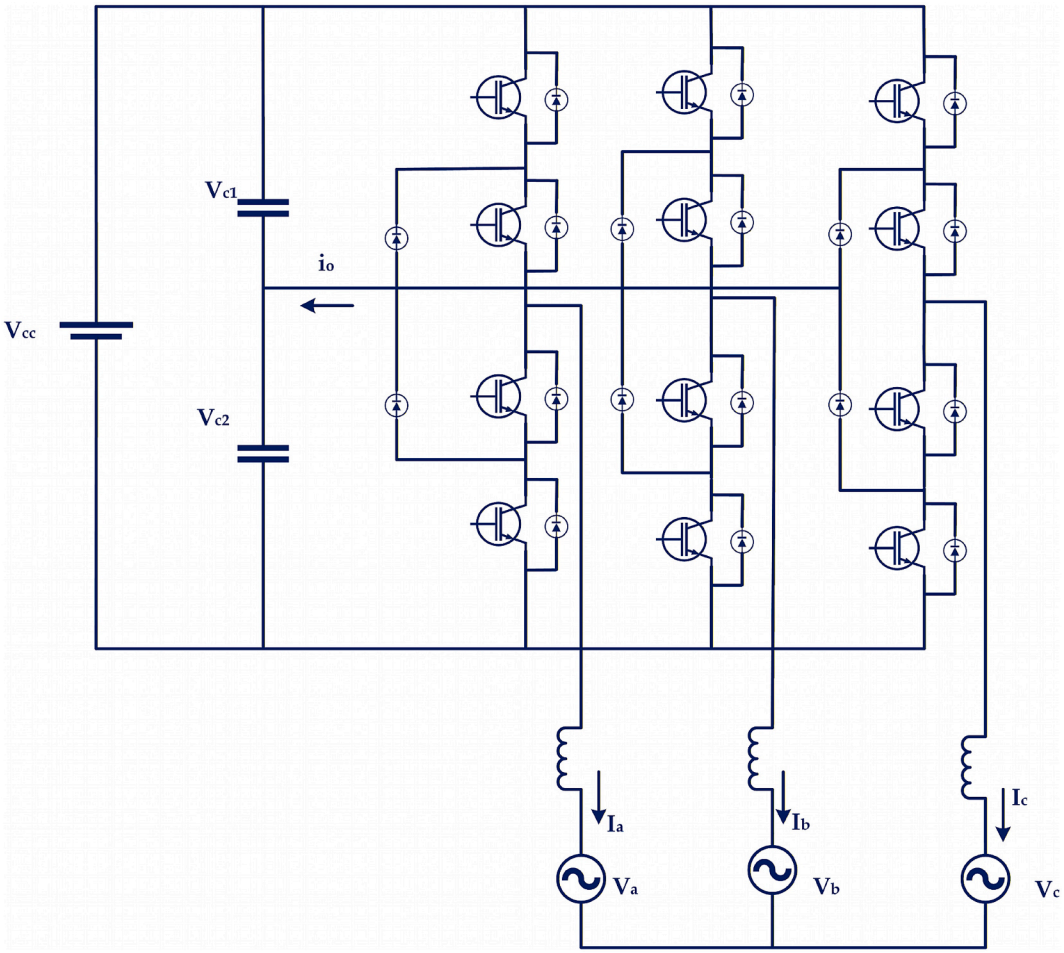

Fig. 12. Neutral point clamping converter topology.

to three technical advantages. First, the multilevel output reduces harmonic content relative to two level conversion, which may relax output filter requirements and reduce current ripple. Second, the split DC link structure lowers voltage stress on individual switches, contributing to improved device utilization and potentially enhanced reliability. Third, the availability of intermediate voltage levels supports improved power factor control and more flexible voltage synthesis, which is beneficial in grid connected and load interfacing applications. These attributes have led to the dominance of the three-level NPC topology in many medium voltage implementations. Notwithstanding these benefits, NPC inverters impose several design and operational challenges that are particularly relevant when the topology is adopted in power conditioning interfaces. A principal limitation is the need for active neutral point voltage regulation. Under practical operating conditions, unequal capacitor charging and discharging can cause neutral point drift, which degrades waveform quality, restricts the feasible modulation range, and may introduce uneven voltage stress across devices. Maintaining stable neutral point potential typically requires sophisticated modulation and control strategies, as well as accurate sensing and compensation mechanisms. In addition, conventional NPC implementations are frequently limited to three level operations in practical systems. Extending the diode clamped structure beyond three levels increases clamping component count and control complexity, while also intensifying balancing and protection requirements. These constraints often limit scalability and can lead to unresolved imbalance related performance limitations in reported implementations.

Within the literature on NPC inverter-based power conditioning interfaces, several representative implementations illustrate both the strengths and remaining limitations of the topology. Da Silva et al. [180] evaluated a three-phase system employing dual three level NPC inverters, as illustrated in Fig. 12, implemented using 1.3 kV insulated gate bipolar transistor switches. The study demonstrated feasible multilevel operation with improved waveform quality, but retained limitations associated with three level neutral point balancing. Akbari and Zare Ghaleh Seyyedi [181] proposed an NPC based configuration aimed at mitigating selected operational indices, including those related to unbalanced conditions. While improvements were reported in specific aspects, voltage imbalance effects persisted, indicating the continuing importance of neutral point regulation and structural scalability. Dietrich et al. [182] introduced a hybrid NPC arrangement using 10 kV insulated gate bipolar transistor devices together with filtering networks, including inductor capacitor resistor low pass filtering and damping resistor based passive filtering, to mitigate waveform distortion and neutral point related issues. Although the hybrid approach improved harmonic performance, its reliance on high voltage devices increased cost and did not fully eliminate constraints associated with device availability and economic feasibility. Campanhol et al. [183] developed a distributed generation architecture in which NPC inverters were connected in parallel and series to provide bidirectional interfacing between grid and microgrid operation. The proposed structure improved operating flexibility and addressed selected functional limitations, yet the overall system remained constrained by device rating requirements and associated cost considerations. Ramasamy and Krishnasamy [184], shown in Fig. 12, proposed an NPC based configuration designed to manage voltage stress and support operation under unbalanced conditions. Although the topology improved device stress distribution, the associated three phase rectifier stage introduced additional harmonic distortion, leading to elevated THD and incomplete mitigation of higher order waveform quality limitations. More recently, Madhusoodhanan et al. [185] presented a medium voltage NPC based interface employing 15 kV silicon carbide devices. The introduction of wide bandgap switches improved voltage capability, reduced losses, and enhanced thermal margins, thereby addressing several device and efficiency related constraints. However, the absence of additional cascading or higher-level extension meant that limitations associated with three level neutral point balancing and waveform synthesis remained. Consistent with the scope of this review, the discussion is restricted to NPC inverter-based power conditioning interface technologies, emphasizing their demonstrated advantages in medium and high-power conversion and the persistent challenges associated with neutral point balancing, limited scalability beyond three levels, dependence on high voltage devices, and the resulting implications for waveform quality and implementation cost.

The Neutral Point Clamped (NPC) inverter continues to be a widely employed topology in medium- and high-power conversion systems; however, its practical deployment is constrained by several inherent limitations. A key challenge is the neutral point voltage imbalance, which arises due to unequal capacitor charging and discharging dynamics, leading to voltage drift, increased stress on semiconductor devices, and degradation of output waveform quality. Furthermore, the NPC topology exhibits non-uniform distribution of switching and conduction losses, resulting in thermal imbalance and potentially reduced system reliability. Its limited scalability beyond three levels, together with the dependence on high-voltage semiconductor devices, further restricts its applicability in higher voltage domains while contributing to increased system cost and design complexity. To address these challenges, advanced three-level converter topologies, notably the Active Neutral Point Clamped (ANPC) inverter and the T-type converter, have been developed. The ANPC topology as shown in Fig. 13 extends the conventional NPC structure by replacing passive clamping diodes with actively controlled switches, thereby increasing the number of available switching states and enabling enhanced operational flexibility. This structural modification facilitates effective regulation of the neutral point voltage, ensuring improved voltage balancing under both steady-state and transient operating conditions. In addition, the ANPC configuration enables optimized distribution of switching and conduction losses among semiconductor devices, thereby improving thermal performance, reducing localized stress, and enhancing overall system efficiency. The availability of redundant switching states further supports the implementation of advanced modulation strategies, contributing to reduced harmonic distortion and improved dynamic performance. Moreover, the capability to employ lower voltage-rated devices in series configurations makes ANPC converters particularly suitable for medium-voltage applications, offering a favorable balance between performance, efficiency, and device utilization. In comparison, the T-type converter represents an alternative three-level topology that prioritizes reduced conduction losses and improved efficiency. By substituting clamping diodes with actively controlled bidirectional switches, the T-type structure minimizes the number of semiconductor devices in the current conduction path, thereby achieving lower conduction losses and enhanced efficiency, particularly at elevated switching frequencies. The T-type converter topology configuration is illustrated in Fig. 14. This configuration also contributes to reduced thermal stress and increased power density, making it well suited for compact and high-efficiency system designs. Nevertheless, the T-type converter generally requires high-speed semiconductor devices, such as silicon carbide (SiC) or gallium nitride (GaN), to fully realize its performance advantages. Additionally, similar to the NPC topology, it remains susceptible to neutral point voltage imbalance, especially under dynamic or unbalanced operating conditions. Despite the performance improvements offered by ANPC and T-type converters, both topologies introduce increased control complexity, necessitating precise gate signal coordination and the adoption of advanced modulation techniques to ensure reliable and efficient operation. Moreover, challenges related to scalability, device cost, and implementation complexity persist, particularly in high-voltage applications. Among the available three-level topologies, the ANPC inverter is generally regarded as the most effective, owing to its superior capability in neutral point voltage regulation, balanced loss distribution, and thermal management. These attributes make it a highly suitable and efficient solution for modern power conditioning interfaces in medium-voltage applications.

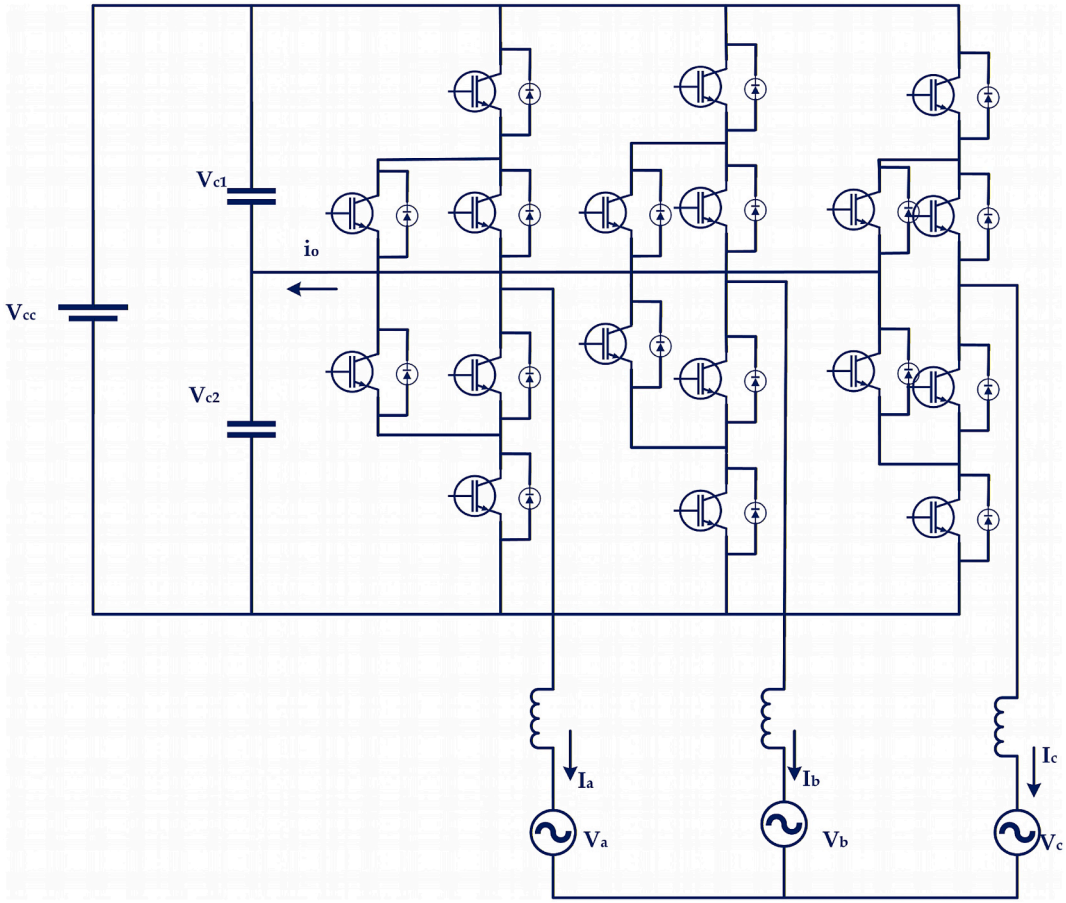

Fig. 13. Active neutral point clamping converter topology.

3.6. Flying capacitor (FC) inverter

The flying capacitor (FC) inverter, originally introduced by Meynard and Foch [186], is a multilevel converter topology that resembles the Neutral Point Clamped inverter in terms of switch configuration, but replaces clamping diodes with floating capacitors to generate intermediate voltage levels. By exploiting redundant switching states and multiple voltage vectors, the FC inverter can synthesize stepped output waveforms with low harmonic distortion and improved spectral performance. The availability of redundant states also enables flexible control of active and reactive power, which is advantageous in applications requiring dynamic voltage regulation and compensation. Since the topology does not depend on a neutral point, it inherently avoids neutral point voltage drift and balancing issues that are frequently encountered in NPC converters, particularly under unbalanced or distorted load conditions. This structural characteristic simplifies certain aspects of DC link voltage management while maintaining the benefits of multilevel operation, such as reduced device voltage stress and lower dv/dt. Despite these technical advantages, the practical implementation of FC inverters is strongly influenced by the significant number of capacitors required to achieve higher voltage levels. As the number of output levels increases, the flying capacitor count grows rapidly, resulting in higher system cost, increased physical size and weight, and greater mechanical and wiring complexity. In medium voltage systems, these disadvantages are amplified by insulation coordination requirements, thermal management constraints, and spatial limitations within converter enclosures. Each capacitor must be designed to withstand specified voltage stress and ripple current, and its lifetime is highly dependent on temperature rise and electrical loading. Consequently, reliability, maintenance, and replacement considerations become critical in long term operation. These factors collectively limit scalability and practical feasibility, often reflected in implementation constraints associated with IP1, which denotes Implementation Phase 1, representing the initial stage of system deployment and operational validation [187].

Voltage balancing of the flying capacitors represents another major technical challenge. Although redundant switching states provide theoretical capability for active balancing the capacitor voltages are inherently dynamic and influenced by load current direction, modulation index, switching sequence, and operating frequency. Under transient operating conditions, rapid load variations, or nonlinear loading, voltage imbalance and ripples may increase significantly. Such deviations can distort the synthesized voltage steps, increase total harmonic distortion, and produce unequal voltage stress across semiconductor devices. In medium voltage applications, switching frequencies are typically kept relatively low to reduce switching losses and improve efficiency. However, lower switching frequency leads to increased capacitor voltage ripple, which generally requires larger capacitance values to maintain acceptable ripple and distortion limits. The need for higher capacitance further increases cost and volume and introduces design tradeoffs among efficiency, harmonic performance, and passive component sizing. Moreover, sophisticated balancing algorithms often require additional sensing circuits, digital control resources, and real time computation, thereby increasing implementation complexity and potentially affecting robustness over a wide operating range. From a performance perspective, the multilevel structure of the FC inverter reduces voltage stress on individual switching devices by distributing the total DC link voltage across multiple levels. This feature enables the use of devices with lower voltage ratings or improves reliability margins when higher rated devices are employed. In addition, the

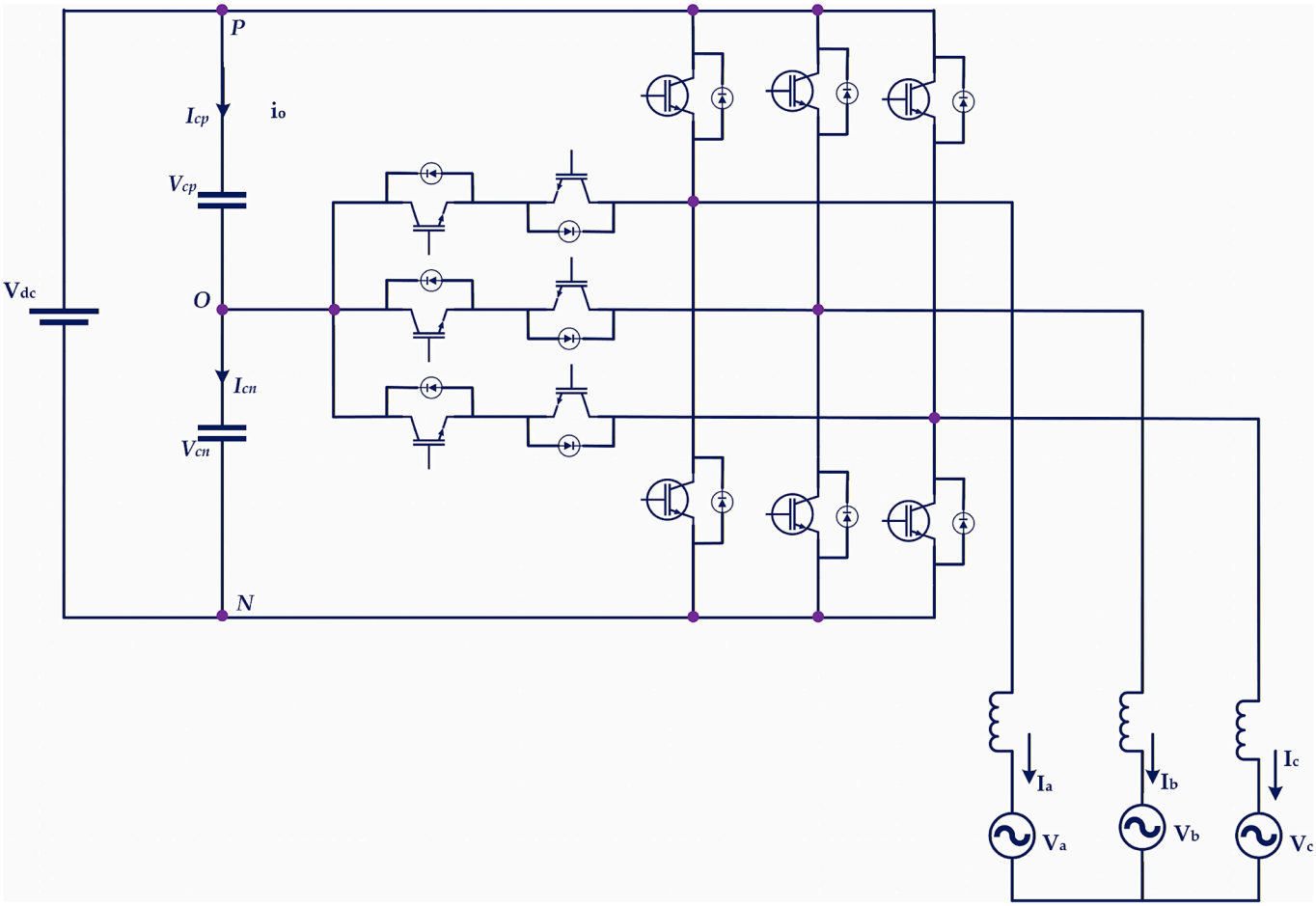

Fig. 14. Three level T-type converter.

step voltage waveform reduces dv/dt stress on connected equipment, which is particularly beneficial in motor drive applications where insulation aging and bearing currents are major concerns. The more uniform distribution of switching losses among devices can also improve thermal management and extend converter lifetime. These advantages make the FC topology attractive for certain medium voltage applications, especially high-speed drives and systems requiring improved waveform quality. Several research contributions have examined FC based converter configurations with different performance objectives and varying degrees of success. Karmiris et al. [188] proposed an FC based system intended to mitigate voltage sags at the Point of Common Coupling and reduce load current harmonics. Although current harmonic reduction was demonstrated, the reported results indicated distorted output waveforms and insufficient capacitor voltage balancing, highlighting persistent challenges in capacitor management and output quality that affect IP3 and IP8, which correspond to advanced stages of the implementation phase, particularly in terms of performance optimization and system stability. The limitations suggest that achieving simultaneous voltage support and high-quality current compensation requires more advanced control coordination. A cascaded symmetric flying capacitor configuration was introduced in [189] with the objective of reducing semiconductor count and improving efficiency while enabling reactive power regulation. The cascaded arrangement contributed to improved structural organization and effectively addressed certain capacitor voltage balancing and modularity challenges associated with IP3 and IP4, corresponding to performance optimization and operational refinement within the implementation phase. However, performance under nonlinear loading remained limited, and comprehensive mitigation of both voltage and current disturbances was not fully achieved. High DC link capacitance requirements continued to impose feasibility constraints associated with IP1 and influenced dynamic performance linked to IP8. Humayun et al. [190] focused on reducing the number of semiconductor devices to enhance compactness and potentially decrease losses. While this approach improved hardware simplicity, it did not completely resolve cost and scalability limitations. Furthermore, the relatively low switching frequency restricted dynamic response and harmonic shaping capability, thereby limiting the effectiveness of disturbance mitigation and leaving IP8 related performance gaps. In renewable energy applications, Falehi and Rafiee [191] employed an FC based converter to improve Fault Ride Through capability in Doubly Fed Induction Generator systems. Their work demonstrated enhanced response during grid disturbances, addressing specific voltage disturbance requirements. Nevertheless, challenges associated with current distortion, robust capacitor voltage balancing during fault conditions, and the relatively high passive and active component count remained insufficiently addressed, indicating unresolved issues linked to IP3 and IP1. González and Valla [192], as illustrated in Fig. 15, proposed an FC based converter that achieved effective current harmonic compensation and ensured self-balancing of flying capacitor voltages through an appropriate modulation strategy. This approach improved capacitor voltage regulation performance associated with IP3 and strengthened current related disturbance mitigation. However, voltage related disturbances were not comprehensively treated, limiting applicability in scenarios where simultaneous voltage and current conditioning are required and leaving IP8 related constraints. Research on FC inverters continues to concentrate on reducing capacitor requirements, enhancing voltage balancing robustness with reduced sensing and computational burden, and

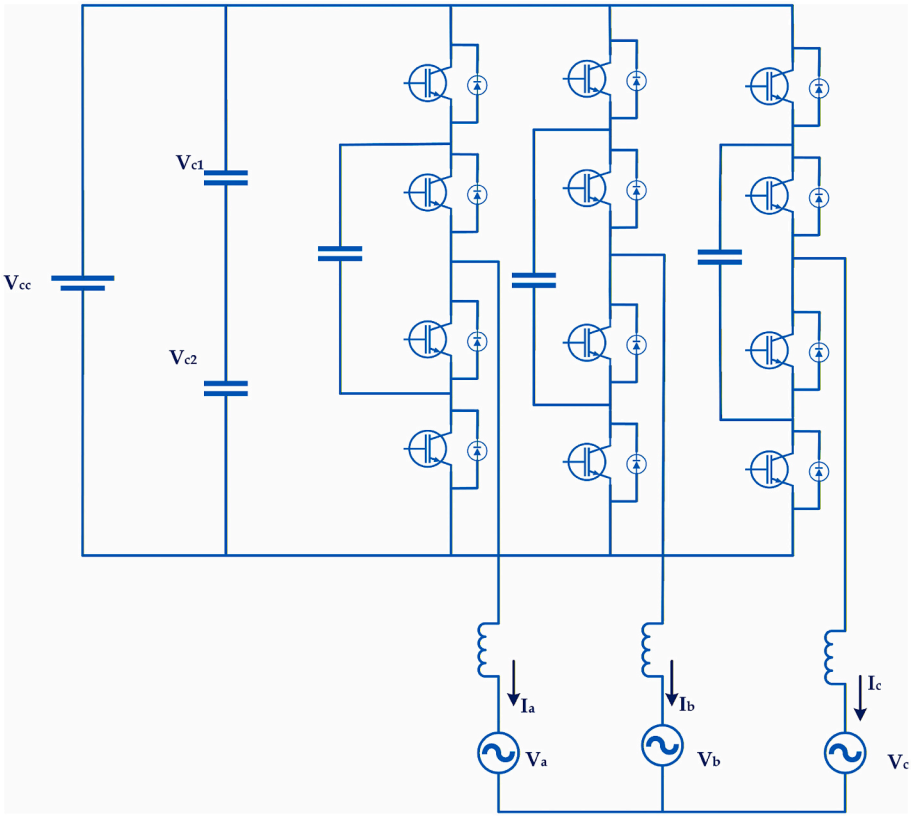

Fig. 15. Flying capacitor inverter topology [193].

developing advanced modulation strategies capable of maintaining waveform quality under nonlinear and dynamic operating conditions. Such developments are essential for improving feasibility, reliability, and performance in medium voltage implementations while preserving the inherent advantages of multilevel operation.

3.7. Cascaded H-bridge inverter

The cascaded H bridge (CHB) inverter was initially reported by Marchesoni et al. [194] and later extended by Peng et al. [195], who emphasized the use of multiple isolated DC sources and demonstrated parallel operation to support reactive power exchange. Espinoza and Joos [196] further established that CHB based converters can be configured to operate as static reactive power compensators when integrated in series with the utility grid, thereby positioning the topology as a flexible platform for grid support and power conditioning functions. A defining feature of the CHB inverter is its cell based modular structure, where each H bridge module is supplied by an independent DC source and contributes a controllable voltage step to the synthesized output. By connecting identical modules, the CHB inverter can generate a high number of voltage levels with comparatively low device voltage stress, enabling medium voltage operation using mature semiconductor ratings. The modularity also facilitates scalability, redundancy, and maintainability, since failed modules can often be bypassed or replaced without redesigning the entire system. Compared with flying capacitor converters, CHB implementations avoid extensive capacitor banks and the associated voltage ripple and balancing burden. Relative to Neutral Point Clamped structures, CHB inverters eliminate the need for neutral point voltage stabilization, which simplifies modulation and control under a wide range of loading conditions. These structural advantages contribute to reduced harmonic distortion and improved waveform quality, supporting IP8 related performance targets, while also enabling high conversion efficiency and favorable thermal distribution, which aligns with IP4. The repeated cell architecture and the absence of neutral point constraints typically yield a more straightforward converter structure, supporting IP3.

Notwithstanding these advantages, CHB converters impose a fundamental requirement for multiple isolated DC sources. Depending on the application, these sources may be realized through isolated transformers, dedicated rectifier stages, distributed energy storage elements, or renewable energy sub arrays. This requirement can increase capital cost, system footprint, and design complexity, particularly when galvanic isolation and coordinated voltage regulation are necessary. Furthermore, unequal DC source voltages or mismatched power availability among cells can degrade waveform symmetry, increase distortion, and introduce uneven device stress. Consequently, practical CHB systems often require additional control layers for DC link regulation, source balancing, and fault management, especially in grid connected operation. A number of studies have investigated CHB based converters for improved power quality and grid support. Badawi et al. [197] developed a seven level CHB inverter employing carrier shifted pulse width modulation to reduce voltage and current harmonic content. Their results indicate improved harmonic performance consistent with IP8 objectives. However, maintaining stable and balanced module voltages remained a challenge, illustrating that voltage coordination among CHB cells can still impose implementation constraints associated with IP3. Liu et al. [198] proposed a modular CHB configuration capable of regulating both active and reactive power, enabling controllable power exchange with the grid and supporting improved distribution level operational objectives. Their approach directly addressed active and reactive power regulation requirements corresponding to ER2, where ER denotes Engineering Requirements, and further contributed to enhancing distribution efficiency and power flow management objectives associated with EG3 and ER3, with EG representing Engineering Goals. Amaral et al. [199] introduced a CHB based architecture incorporating a solid-state transformer and multiple maximum power point

tracking units to improve energy extraction under partial shading conditions in photovoltaic systems, thereby addressing ER1. While this design enhances energy harvesting and provides additional flexibility for distributed generation integration, it also increases physical size and control complexity, contributing to feasibility concerns linked to EG1, EG6, and IP1 due to added conversion stages and coordination requirements. Umuhoza et al. [200] investigated the use of silicon carbide devices in CHB converters for medium voltage operation. Wide bandgap devices enabled improved switching performance and, in certain configurations, reduced the number of required H bridge modules for a target voltage rating, thereby mitigating hardware burden associated with IP1. The reported system achieved total harmonic distortion of approximately 3.05% with the aid of passive filtering, indicating improved compliance with waveform quality objectives related to IP8 and grid integration expectations associated with EG7. Zhang et al. [201] applied a CHB based converter in wind turbine systems to improve reliability and promote balanced power sharing among converter modules, supporting ER3 related objectives. Their analysis also identified envelope oscillations under specific operating conditions, corresponding to EG8. To mitigate these oscillations, additional synchronization and control elements such as phase locked loops were required, increasing control complexity in line with EG6 considerations. Muneer et al. [202], as illustrated in Fig. 16, presented a CHB based converter designed to address a wider set of disturbances, including voltage and current harmonics, voltage sags and swells, and reactive power demand. The controller was based on second order sliding mode control using a super twisting algorithm, providing strong dynamic disturbance rejection and enabling broad compensation capability, effectively supporting IP8. The principal drawback was the elevated system size and cost resulting from the increased number of modules and associated auxiliary circuitry, reinforcing IP1 related feasibility limitations. Chakrabarty and Adda [203] proposed a seven-level reduced structure dual cell H-bridge multilevel inverter intended for weak distribution networks. The reported performance achieved total harmonic distortion and individual total unbalance distortion below 1%, indicating strong waveform quality improvement and partial fulfillment of IP8 requirements. The reduced structure design also aimed to moderate hardware overhead, contributing to improved feasibility relative to conventional CHB realizations and addressing IP1 more effectively. In addition, operation at unity power factor supports efficient grid interfacing and reduces reactive power burden on the upstream network. The literature collectively indicates that CHB inverters offer a compelling combination of modularity, scalability, and high-quality multilevel waveform synthesis for medium voltage and high-power applications. At the same time, the reliance on multiple isolated DC sources and the associated coordination and balancing requirements remain key practical constraints that influence cost, complexity, and system integration.

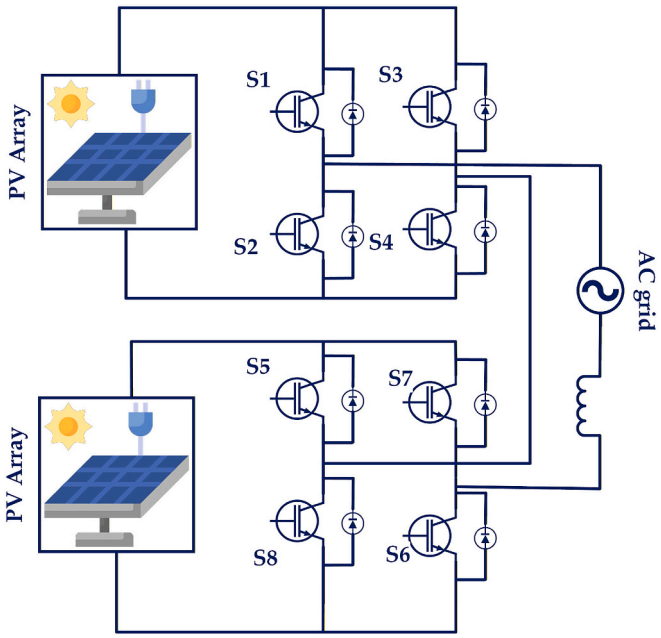

Fig. 16. Cascaded H-bridge inverter topology [204].

3.8. Switching based classification of inverters

Inverters may be classified not only by topology or number of conversion stages, but also by the switching approach used to commutate the power semiconductor devices. Under this classification, inverter systems are commonly grouped into hard switching and soft switching categories. This distinction applies to both single stage and multistage implementations and is primarily determined by the voltage and current conditions at the switching instants. The chosen switching mechanism has a direct impact on switching losses, electromagnetic interference, semiconductor stress, thermal loading, and the practical switching frequency range, all of which are critical in grid connected power conversion. Hard switching inverters commutate semiconductor devices under simultaneous non-zero voltage and non-zero current. During turn on and turn off transitions, the overlap of device voltage and current produces switching energy loss, which increases with switching frequency and can become a dominant contributor to total losses in high frequency operation. In addition, the steep voltage and current transitions associated with hard commutation led to high dv/dt and di/dt, which excite parasitic inductances and capacitances in device packages, interconnections, and converter layouts. This interaction can produce voltage overshoot, oscillatory ringing, and transient current spikes, increasing electrical stress on the switching devices and potentially accelerating degradation. From an electromagnetic compatibility perspective, these fast transitions also increase conducted and radiated emissions and may require additional filtering, shielding, or damping networks to meet regulatory limits. In grid connected photovoltaic inverters, rapid common mode voltage transitions can further increase leakage current through parasitic capacitances, which imposes additional constraints on grounding, filter design, and protection coordination. Although hard switching pulse width modulation inverters remain widely adopted due to their structural simplicity and well-established control frameworks, they often involve a tradeoff between efficiency and passive component size. Increasing switching frequency can reduce the volume of magnetic components and filters, but at the expense of higher switching loss and thermal stress, whereas lowering the switching frequency improves efficiency but typically increases the size and weight of passive components. Soft switching inverters mitigate these limitations by shaping the commutation process such that switching transitions occur when either the device voltage or the device current is near zero. The two principal soft switching modes are zero voltage switching and zero current switching. In zero voltage switching, the switch transitions when the voltage across it approaches zero, which reduces turn on loss and limits dv/dt related stress. In zero current switching, commutation occurs when the current through the device approaches zero, thereby reducing turn off loss and limiting di dt related stress. By reducing the energy dissipated during each commutation event, soft switching enables higher frequency operation without proportional increases in switching loss, supporting higher power density and improved efficiency.

Soft switching behavior is typically realized through resonant or quasi resonant techniques in which inductors and capacitors form controlled resonant paths during switching transitions. Many practical designs augment conventional PWM converters with auxiliary resonant branches, additional switches, or diodes to establish the required commutation intervals while maintaining regulation capability. The literature reports a wide range of such configurations. High step-up multi-

input inverter structures with soft switching have been proposed to improve conversion efficiency while limiting circulating currents that otherwise increase conduction losses. High frequency resonant inverters operating under zero current switching control have also been investigated to reduce switching stress under fast commutation. In addition, single stage flyback derived inverter configurations employing capacitive commutation principles have been explored to achieve soft switching with comparatively compact structures. Hybrid arrangements that integrate transition assisted PWM stages with a full bridge inverter have been developed to combine the steady state controllability of PWM with reduced commutation loss and improved electromagnetic behavior. The selection between hard switching and soft switching strategies is therefore application dependent. Soft switching offers clear advantages in terms of switching loss reduction, electromagnetic performance, and device stress mitigation, particularly at high switching frequencies. However, these benefits are accompanied by increased circuit complexity, additional passive or auxiliary components, and tighter design requirements to maintain soft switching over variations in operating conditions. Hard switching remains attractive where simplicity, predictable switching frequency, and lower component count are prioritized, whereas soft switching is often justified in grid connected systems that demand very high efficiency and power density under stringent electromagnetic compatibility constraints.

3.9. Diode clamped inverter

The diode-clamped multilevel inverter, widely referred to as the Neutral Point Clamped (NPC) inverter, was introduced to enable high-voltage power conversion using semiconductor devices with moderate voltage ratings [205]. The fundamental three-level diode-clamped multilevel inverter (DCMLI), illustrated in Fig. 17, generates three discrete voltage levels by employing a split DC-link structure. In the conventional three-level configuration, the DC bus is divided by two series-connected capacitors, establishing a neutral midpoint. The topology comprises four unidirectional active switches and clamping diodes that connect the switching nodes to the intermediate DC-link points. The clamping diodes are arranged to share the blocking voltage and to fix the potential of the switching node to predefined capacitor voltages [206]. Through appropriate switching combinations, the inverter synthesizes output voltage levels of $+V_{dc}/2$, 0, and $-V_{dc}/2$. The positive level is obtained when the upper switch pair is gated, the negative level when the lower switch pair is activated, and the zero level when the inner switches clamp the output to the neutral point of the DC link. A significant advantage of the DCMLI lies in its inherent voltage-sharing capability. For an m-level diode-clamped inverter, each active device is required to withstand approximately $V_{dc}/(m-1)$, thereby reducing device voltage stress and enabling medium- and high-voltage operation without the need for extremely high-voltage-rated semiconductors [207]. However, the clamping diodes must be appropriately rated to withstand reverse voltage stress under all operating conditions. In high-voltage and high-frequency applications, diode reverse recovery presents a critical design consideration. During pulse width modulation (PWM) operation, reverse recovery currents of the clamping diodes may introduce additional switching losses and voltage overshoot, which increase stress on active devices and reduce overall efficiency [208]. Consequently, careful device selection and optimized modulation strategies are required to mitigate these effects. The DCMLI topology has achieved widespread industrial adoption owing to its relatively simple structure, high power capability, and favorable efficiency characteristics. It is extensively employed in applications such as high-voltage motor drives, static VAR compensators, renewable energy grid interfaces, and back-to-back converter systems [208]. The presence of a single DC bus facilitates integration into high-voltage systems and simplifies implementation in adjustable-speed drive applications. Despite these advantages, several technical challenges remain. Maintaining voltage balance across the DC-link capacitors is essential, as imbalance leads to distortion of the output waveform and uneven distribution of voltage stress among devices. Under transient conditions or asymmetric loading, improper power flow management may result in overcharging or undercharging of individual capacitor segments [206]. Therefore, advanced control and modulation techniques are often required to stabilize the neutral-point voltage and ensure reliable operation [209]. These balancing and control requirements represent key design challenges in practical DCMLI implementations. A diode-clamped inverter, as shown in Fig. 17 employs a split DC-link and clamping diodes to generate multiple voltage levels. This configuration reduces device voltage stress and improves output waveform quality, although capacitor voltage balancing remains a key challenge.

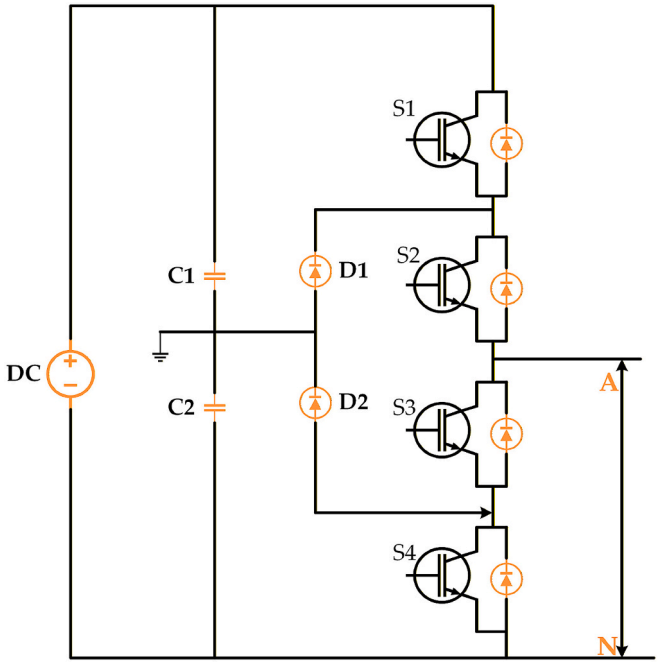

Fig. 17. Diode clamped inverter topology [210].

3.10. Modular multilevel inverter

The modular multilevel converter (MMC), classified as a voltage source inverter, has emerged as a key topology in modern power electronics owing to its scalability, modularity, and superior output performance. The evolution of MMC technology can be traced to early multilevel converter concepts developed in the 1970s, where stepped voltage waveforms were generated through series-connected inverter structures. Subsequent advancements introduced modified multilevel configurations, ultimately leading to the development of modular converter architectures. The MMC topology was later formally established with well-defined structural and operational principles, enabling its widespread adoption in high-power and high-voltage applications [211]. In recent decades, MMCs have gained considerable attention in renewable energy systems and grid integration applications. They are extensively utilized in high-voltage direct current (HVDC) transmission systems, particularly for offshore wind farms and large-scale photovoltaic (PV) installations, where efficient long-distance power transmission and grid stability are essential. Additionally, MMCs are applied in medium-voltage drives, flexible AC transmission systems (FACTS), D-STATCOM, and power quality improvement systems. Their capability to support bidirectional power flow and provide flexible control makes them highly suitable for modern power systems characterized by a high penetration of renewable energy sources. The structural architecture of the MMC offers several technical and economic advantages. Its modular configuration enables scalable voltage levels, allowing operation at high

voltages without the need for bulky transformers. This feature is particularly advantageous in renewable energy applications, where efficiency, compactness, and reliability are critical. The use of submodules (SMs) as fundamental building blocks facilitates the generation of high-quality staircase voltage waveforms with reduced harmonic distortion, lower electromagnetic interference, and improved overall system efficiency. Furthermore, the modular design enhances system redundancy and simplifies maintenance, contributing to reduced lifecycle costs. Recent research trends between 2020 and 2025 have focused on enhancing the functionality, intelligence, and adaptability of MMC-based systems for renewable energy integration. One significant development is the incorporation of energy storage within the MMC structure, enabling the concept of MMC with integrated energy storage. This approach allows the converter to perform both power conversion and energy buffering, thereby mitigating the variability and intermittency associated with renewable energy sources. In addition, advanced energy management strategies have been proposed to coordinate power exchange between submodule capacitors, storage elements, and renewable sources, improving system flexibility and operational efficiency [212,213].

Another important area of research involves the development of advanced control and modulation techniques. Methods such as model predictive control, optimization-based control strategies, and reduced-switching-frequency modulation have been introduced to enhance dynamic performance, reduce switching losses, and improve efficiency. These approaches are particularly relevant in weak grid conditions, where stability and fast dynamic response are critical. Moreover, the development of multi-terminal HVDC (MT-HVDC) systems based on MMC technology has gained significant attention, as it enables the interconnection of multiple renewable energy sources and facilitates the creation of more flexible and resilient grid infrastructures. Reliability, protection, and fault management have also become key research priorities in recent years. The increasing penetration of converter-based renewable energy systems has necessitated the development of advanced protection schemes tailored to MMC characteristics. Research efforts are focused on improved fault detection techniques, enhanced fault ride-through capabilities, and robust protection strategies to ensure stable operation under grid disturbances. Additionally, hybrid and advanced submodule topologies have been proposed to improve efficiency, enhance fault tolerance, and reduce system losses. Despite these advancements, MMCs continue to present certain challenges. The control of MMC systems is inherently complex, requiring simultaneous regulation of output currents, circulating currents, DC-link voltage, and capacitor voltage balancing across numerous submodules. Furthermore, the requirement for large submodule capacitances to limit voltage ripple remains a significant design constraint, impacting system size and cost. Consequently, ongoing research is directed toward reducing capacitance requirements, simplifying control strategies, and improving overall system efficiency to better align with the demands of future renewable energy systems [214–216]. Fig. 18 illustrates the conceptual topology of a modular multilevel converter (MMC) interfacing a three-phase AC system (V_a, V_b, V_c) with a DC source (V_{dc}), suitable for renewable energy applications. Each phase leg consists of upper and lower arms composed of series-connected submodules (SMs) with switches and capacitors. By controlling the insertion and bypassing of submodule capacitors, the MMC generates multilevel voltage waveforms with reduced harmonic distortion. The modular structure enables scalability, improved power quality, and efficient integration of renewable energy sources, although it requires advanced control for capacitor voltage balancing and circulating current suppression.

3.11. Topology-specific requirements for ESS integration

The integration of energy storage systems with multilevel power converters is determined by the structural characteristics of the converter and the electrochemical, electrical, and thermal properties of the

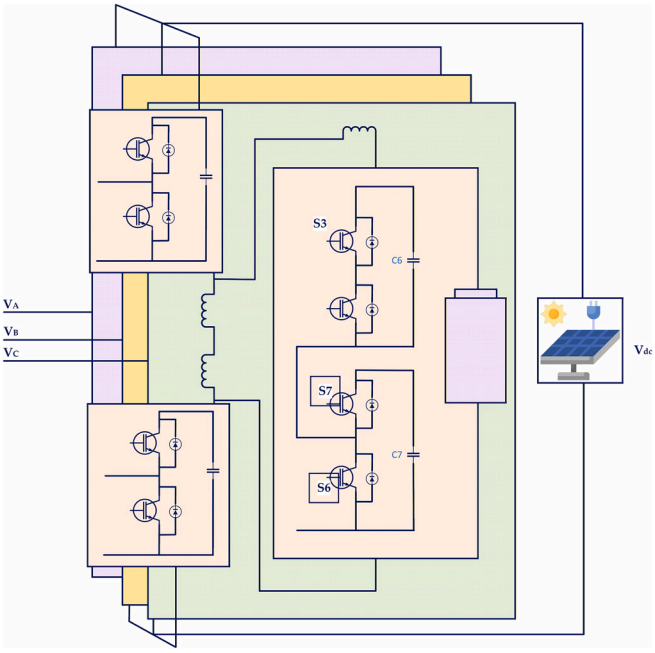

Fig. 18. Conceptual architecture of modular multilevel converter topology.

storage technology. Variations in DC-source configuration, voltage-balancing mechanisms, bidirectional current paths, modularity, galvanic isolation, fault-containment capability, and internal energy-buffering arrangements directly influence storage-current ripple, state-of-charge uniformity, thermal loading, and degradation. Converter selection should therefore be based on compatibility with the storage voltage range, current capability, dynamic response, lifetime requirements, and protection constraints, rather than on conversion efficiency as an isolated performance indicator. Two-level and single-stage converter architectures generally employ a common DC link supplied directly by the storage system. These configurations offer reduced hardware complexity and a comparatively simple control structure. Their principal limitation is the need to accommodate storage-voltage variation over the full state-of-charge range while preserving the modulation margin required by the AC-side interface. The inclusion of a bidirectional DC-DC conversion stage can provide voltage decoupling, independent current regulation, and improved ripple suppression. However, this additional stage increases semiconductor count, control complexity, and conversion losses [217].

Neutral-point-clamped, active-neutral-point-clamped, and T-type converters employ split-DC-link structures and consequently require continuous regulation of the neutral-point or midpoint voltage. During bidirectional operation, asymmetric capacitor currents and rapid transitions between charging and discharging can produce unequal DC-link voltages, non-uniform device stress, and deterioration of the synthesized output waveform [218]. ANPC converters provide redundant switching states that can be utilized for simultaneous neutral-point regulation and redistribution of semiconductor losses [219]. T-type converters reduce the number of devices in the principal conduction path, but their performance remains dependent on effective midpoint-voltage control and coordinated operation of the neutral-point switches [220]. Flying-capacitor converters require active regulation of the intermediate capacitor voltages. These capacitors function as internal energy-balancing elements for voltage-level generation and short-duration buffering, rather than as substitutes for the primary ESS. Their voltage trajectories are influenced by load current, power-flow direction, modulation index, and switching-state selection. Reliable bidirectional operation therefore requires coordinated pre-charge procedures, continuous capacitor-voltage monitoring, and balancing control across

the complete operating range. Cascaded H-bridge converters exhibit a direct structural correspondence between converter cells and modular storage units. This arrangement supports distributed energy storage, independent module control, modular expansion, fault bypass, and scalable voltage synthesis. The principal integration challenge is the maintenance of uniform utilization among storage modules with different states of charge, capacities, temperatures, internal resistances, and degradation levels. CHB-based ESS interfaces therefore require module-condition-dependent power allocation, coordinated state-of-charge balancing, isolation monitoring, and fault-tolerant modulation. Modular multilevel converters permit centralized, arm-level, or submodule-level storage integration. Distributed storage integration can improve redundancy, scalability, and localized power regulation. These advantages are accompanied by substantially greater requirements for sensing, communication, capacitor-voltage balancing, circulating-current suppression, and distributed state-of-charge coordination. The control system must regulate these variables while limiting switching losses, capacitor-voltage ripple, storage-current stress, and thermal imbalance [221].

Hybrid converter configurations can allocate different power-frequency components to storage technologies with complementary dynamic characteristics. Batteries may supply the average and low-frequency energy demand, whereas supercapacitors or other high-power storage devices can compensate rapid transients. This coordinated power allocation can reduce battery RMS current, polarization, thermal loading, and electrochemical degradation. The additional converter stages, sensing infrastructure, and supervisory-control functions must nevertheless be included in system-level energy, exergy, reliability, and lifecycle assessments. Independent of the selected topology, ESS integration requires bidirectional power-conversion capability, controlled pre-charge, overcurrent protection, DC-fault isolation, insulation monitoring, thermal supervision, state-of-charge and state-of-health estimation, and reliable communication with the battery-management system. The selected converter must also provide the required grid-support functions while maintaining the storage device within prescribed current, voltage, temperature, state-of-charge, and degradation limits. A topology should therefore be evaluated according to its ability to coordinate power conversion, storage protection, thermal management, fault response, and lifetime-oriented operation within a unified system architecture. Table 1 presents a comparative synthesis of the principal requirements associated with ESS integration across the selected converter topologies, with particular attention to storage-side configuration, control objectives, and topology-dependent implementation constraints [222].

The comparison shows that converter topologies offering higher modularity and greater internal voltage-control capability can provide increased flexibility for ESS integration. These advantages are generally accompanied by more demanding requirements for sensing, voltage balancing, protection coordination, communication, and control implementation. In contrast, structurally simpler converter configurations reduce hardware and supervisory complexity, but provide less effective decoupling between storage-side dynamics and grid-side power regulation.

Table 1
Topology-specific requirements for energy storage system integration [223].

Converter topology	Typical ESS configuration	Primary integration requirement	Principal technical limitation
Two-level or single-stage VSI	Common DC link supplied directly by the storage system	Accommodation of state-of-charge-dependent storage-voltage variation while limiting converter-induced current ripple	Limited decoupling between storage-side dynamics and grid-side power regulation
Multistage converter	ESS interfaced through a bidirectional DC-DC conversion stage	Independent regulation of storage current and DC-link voltage over a wide operating range	Additional conversion losses, component count, and control complexity
Neutral-point-clamped converter	ESS connected to a split DC-link structure	Neutral-point voltage regulation and balanced loading of the DC-link capacitors	Susceptibility to midpoint-voltage deviation under asymmetric and bidirectional operating conditions
Active-neutral-point-clamped converter	Split DC link with actively controlled clamping paths	Coordinated neutral-point regulation and redistribution of semiconductor losses and thermal stress	Increased switching-state selection complexity and greater control burden
T-type converter	ESS connected to a split DC link	Midpoint-voltage regulation and coordinated operation of the bidirectional neutral-point switches	Sensitivity to DC-link voltage imbalance and unequal capacitor utilization
Flying-capacitor converter	Common ESS with intermediate flying-capacitor cells	Continuous capacitor-voltage balancing, coordinated pre-charge, and reliable voltage monitoring	High capacitor count, increased sensing requirements, and capacitor-aging concerns

3.12. Classification of inverters based on commutation

Inverters can be classified according to the mechanism by which switching devices are commutated. From this perspective, two principal categories are identified: line-commutated inverters (LCIs) and self-commutated inverters (SCIs) [224]. This classification is based on whether the turn-off process of the power devices is naturally enforced by the external circuit conditions or directly controlled by the gate signal. Within the self-commutated category, inverters are further classified as voltage source inverters (VSIs) and current source inverters (CSIs), and VSIs may operate under different modes depending on their regulation strategy [225].

3.12.1. Line-commutated inverters

Line-commutated inverters typically employ semi-controlled devices such as thyristors. In these devices, the gate terminal initiates the turn-on process, whereas turn-off is achieved through natural commutation provided by the external AC system. The reversal of current or voltage polarity forces the device to cease conduction, which means that the inverter relies on the grid or load conditions for successful commutation. For this reason, LCIs are often referred to as load-commutated inverters. Because the turn-off event is not directly controlled by the gate signal, LCIs require an external commutation path or auxiliary circuitry to ensure reliable operation under varying conditions. In half-bridge configurations, antiparallel diodes are frequently incorporated to facilitate forced commutation and to improve switching reliability [226]. Although LCIs are well suited to high-power and medium-frequency applications, their dependence on grid conditions limits switching frequency and dynamic controllability. Consequently, they are less appropriate for applications demanding high-frequency operation, fast transient response, or precise waveform control.

3.12.2. Self-commutated inverters

Self-commutated inverters employ fully controllable semiconductor devices, such as metal–oxide–semiconductor field-effect transistors (MOSFETs) and insulated-gate bipolar transistors (IGBTs). In these devices, both turn-on and turn-off transitions are governed directly by the gate signal, enabling precise and independent switching control [227]. MOSFETs are commonly used in high-frequency applications, often operating in the tens to hundreds of kilohertz range, while IGBTs are preferred in medium-frequency and high-power systems, frequently exceeding 100 kW in rating. The ability to directly control switching transitions allows SCIs to operate at higher switching frequencies and to

implement advanced modulation strategies. Higher switching frequencies contribute to reduced filter size and improved output waveform quality by lowering harmonic distortion [225]. In addition, SCIs provide enhanced power factor regulation, reduced current harmonics, and improved robustness against grid disturbances. With ongoing advancements in semiconductor technology and digital control platforms, SCIs have become the predominant inverter type in modern renewable energy and grid-connected applications. Self-commutated inverters are further subdivided into current source inverters and voltage source inverters.

3.12.3. Current source inverter

In a current source inverter, the DC side is supplied by a stiff current source, typically realized through a large series inductor that maintains nearly constant DC current. The inverter controls the direction and waveform of the output current, while the voltage waveform adjusts according to load conditions. Because the input current polarity is preserved, the power flow pattern is determined primarily by the polarity of the DC source voltage. A significant limitation of CSIs is the requirement for a large DC-link inductor to ensure current stability and continuity [228]. This component increases system volume, cost, and conduction losses, and may reduce overall efficiency [229]. Furthermore, commutation and protection strategies in CSIs are more complex due to the inherent current-source nature of the topology. These factors have limited their widespread use in grid-connected photovoltaic systems, where compactness and high efficiency are essential.

3.12.4. Voltage source inverter

In contrast, a voltage source inverter is supplied by a stiff DC voltage source, typically supported by a large DC-link capacitor connected in parallel with the input. The inverter preserves the polarity of the input voltage and synthesizes an AC output waveform through pulse-width modulation. The amplitude of the AC voltage is primarily determined by the DC-link level, while the switching pattern shapes the output waveform. VSIs are widely adopted in grid-connected photovoltaic applications due to their structural simplicity, relatively low cost, high efficiency, and reduced losses compared with CSIs. The capacitor-based DC link is generally more compact and practical than the large inductor required in CSIs. As a result, VSIs represent the dominant inverter topology in grid-tied renewable energy systems. Voltage source inverters may operate under voltage control mode (VCM) or current control mode (CCM). In VCM operation, the inverter regulates the voltage magnitude, frequency, and phase at the point of common coupling, making this approach suitable for standalone or off-grid systems where the inverter must establish the voltage reference. However, VCM can result in higher short-circuit current during fault conditions. In CCM operation, the inverter directly regulates the injected grid current while synchronizing with the grid voltage. The primary objective of control is to maintain a sinusoidal current waveform with high power factor and low harmonic distortion. CCM is the preferred approach in grid-connected photovoltaic systems because it facilitates effective power factor control, suppresses current harmonics, and improves transient response during grid disturbances [230–232]. Empirical observations indicate that the majority of grid-tied VSIs operate in current control mode, reflecting their suitability for compliance with modern grid codes and dynamic performance requirements. This commutation-based classification reflects the transition from grid-dependent commutation strategies toward fully controllable semiconductor-based inverters, driven by advancements in power electronic devices and digital control technologies.

The comparative evaluation presented in Table 2 provides a comprehensive assessment of prominent multilevel inverter topologies across key structural, operational, and performance parameters. The conventional Neutral Point Clamped (NPC) inverter offers a well-established compromise between efficiency, cost, and implementation complexity; however, its performance remains fundamentally constrained by several inherent limitations. In particular, neutral-point voltage imbalance, arising from unequal capacitor charging and discharging, leads to voltage drift, increased semiconductor stress, and degradation in output waveform quality. Additionally, the NPC topology exhibits non-uniform loss distribution among switching devices, resulting in thermal imbalance and reduced reliability. Its limited scalability beyond three levels, along with dependence on high-voltage semiconductor devices, further restricts its applicability in higher voltage and power domains. In response to these challenges, the Active Neutral Point Clamped (ANPC) topology has emerged as a significant advancement, offering enhanced structural and operational flexibility. By replacing passive clamping diodes with actively controlled switches, the ANPC converter introduces additional switching states that enable direct and dynamic control of the neutral-point voltage, thereby improving voltage balancing under both steady-state and transient conditions. Furthermore, the ANPC configuration allows flexible redistribution of switching and conduction losses across semiconductor devices, leading to improved thermal management, reduced device stress, and enhanced efficiency. The availability of redundant switching states also supports the implementation of advanced modulation techniques, which contribute to lower harmonic distortion and improved dynamic performance. These features, combined with the ability to utilize lower voltage-rated devices in series configurations, make ANPC converters particularly attractive for medium-voltage applications requiring high efficiency and reliability. Other topologies, such as the flying capacitor (FC) and cascaded H-bridge (CHB) converters, provide advantages in terms of voltage redundancy and modular scalability; however, they are associated with increased component count, complex voltage balancing requirements, or the need for multiple isolated DC sources. The cascaded T-type converter offers improved efficiency through reduced conduction losses and enhanced power density, yet it typically requires advanced semiconductor devices and remains sensitive to neutral-point voltage variations. The modular multilevel converter (MMC) represents the most scalable and high-performance solution, offering excellent waveform quality and low dv/dt stress, but at the cost of significantly increased hardware requirements and control complexity. In contrast, the full-bridge single-leg clamped inverter provides a simpler and cost-effective alternative for low-power applications, although its scalability and performance are inherently limited.

Among the evaluated topologies, the ANPC converter demonstrates a particularly favorable balance of efficiency, controllability, and thermal performance, making it a strong candidate for medium-voltage power conversion systems. Nevertheless, significant challenges remain in achieving inherently stable neutral-point voltage balancing under dynamic and unbalanced operating conditions, while simultaneously reducing control complexity and maintaining optimal loss distribution. This indicates a clear research need for the development of simplified control strategies, reduced-switching-state ANPC configurations, and hybrid topological approaches capable of enhancing performance without introducing substantial increases in system complexity or cost.

4. Energy and exergy analysis of ESS-converter systems

The performance of an energy storage system requires evaluation at the integrated system level because the storage medium, bidirectional converter, semiconductor devices, passive components, thermal-management subsystem, sensing infrastructure, and supervisory controller exhibit strong electrical, electrochemical, and thermal interactions [233–235]. These interactions influence conversion efficiency, current ripple, thermal loading, state-of-charge utilization, component degradation, and the quantity of useful energy delivered to the grid or load. Conventional energy analysis quantifies the energy converted, stored, dissipated, and transferred during charging and discharging processes. However, energy analysis alone does not distinguish energy forms according to their capacity to perform useful work. Electrical energy can theoretically be converted entirely into work, whereas thermal energy rejected close to ambient temperature possesses

Table 2
Comparative performance and design evaluation of multilevel inverter topologies.

Parameter	NPC	ANPC	FC	CHB	Cascaded T-Type	FB Single-Leg Clamped	MMC	Two-Level VSI
Basic configuration	Split DC-link with diode-clamping network	NPC-derived structure with active clamping switches	Multilevel structure based on flying capacitors	Series-connected H-bridge power cells	Cascaded arrangement of modified T-type cells	Full-bridge configuration with midpoint-clamping path	Series-connected converter submodules	Conventional two-level voltage-source inverter
Active switches per phase	4	6	4	4 per cell	4–6 per cell	6	2 per half-bridge submodule	2
Clamping elements	Clamping diodes	Active semiconductor switches	Not required	Not required	Not required	Midpoint-clamping branch	Not required	Not required
DC-link and cell capacitors	Two split DC-link capacitors	Two split DC-link capacitors	Multiple flying capacitors and one DC-link capacitor	One isolated DC source or local capacitor per cell	One or more capacitors per cell	Two split DC-link capacitors	One capacitor per submodule	One DC-link capacitor
Nominal voltage stress per switch	Approximately Vdc/2	Approximately Vdc/2	Approximately Vdc/2	Determined by individual cell voltage	Approximately Vdc/2 per cell	Approximately Vdc/2	Approximately Vdc/N, where N is the number of submodules	Vdc
Typical switching-frequency range	1–10 kHz	2–20 kHz	2–15 kHz	1–10 kHz per cell	2–20 kHz	5–20 kHz	0.5–5 kHz per submodule	5–50 kHz
Representative conversion efficiency	96–98%	97–99%	95–97%	96–98%	97–99%	96–98%	97–99.5%	94–97%
Representative THD	3–5%	2–4%	3–5%	2–3%	2–3%	3–5%	Below 2%	5–10% without filtering
dv/dt stress	Moderate	Moderate	Moderate	Low	Low	Moderate	Very low	High
Thermal-stress distribution	Unequal stress between inner and outer devices	Improved loss redistribution through redundant switching states	Distributed across devices, with additional capacitor-related losses	Distributed across converter cells	Relatively uniform across cascaded cells	Moderate concentration in the clamping branch	Highly distributed across submodules	Concentrated in a limited number of devices
Voltage-balancing requirement	Active neutral-point balancing	Neutral-point balancing coordinated with redundant-state selection	Continuous flying-capacitor voltage regulation	Cell-voltage, energy, or state-of-charge balancing	Cell-level and midpoint-voltage balancing	Midpoint-voltage regulation	Continuous submodule-capacitor, arm-energy, and circulating-current regulation	Not required
Fault-tolerance capability	Moderate	Moderate to high	Moderate	High with redundant cells and bypass capability	Moderate to high	Moderate	Very high with redundant submodules	Low to moderate
Power-density potential	High	High to very high	Moderate	Moderate to high	High	High	Moderate	High
Control complexity	Moderate	High	High	Moderate to high	Moderate to high	Moderate	Very high	Low
Implementation complexity	Moderate	High	Very high	High	High	Moderate	Very high	Low
Modularity and scalability	Moderate	Moderate	Moderate	High	High	Limited	Excellent	Limited
Typical power range	Medium	Medium to high	Medium	Low to high, depending on cell count	Medium to high	Low to medium	High to very high	Low to medium
Relative hardware cost	Moderate	Moderate to high	High	Moderate to high	Moderate to high	Moderate	Very high	Low
Relative control cost	Moderate	High	High	Moderate to high	High	Moderate	Very high	Low
Reliability	Moderate	Moderate to high	Moderate to low because of capacitor dependence	High when modular redundancy is available	Moderate to high	High at low and medium power ratings	High with redundant submodules and bypass capability	High because of structural simplicity
Industrial maturity	Mature	Increasing industrial adoption	Limited	Mature	Emerging	Application-specific	Mature in high-power and high-voltage systems	Very mature
Principal advantages	Established structure, reduced device voltage stress, and good	Improved thermal management, flexible switching-state	Redundant switching states and improved waveform quality	High modularity, low dv/dt, and strong fault-tolerance potential	High efficiency, modular expansion, and reduced output-voltage stress	Compact configuration and moderate component count	Excellent scalability, low harmonic distortion, and high redundancy	Low cost, simple control, and compact implementation

(*continued on next page*)

Table 2 (*continued*)

Parameter	NPC	ANPC	FC	CHB	Cascaded T-Type	FB Single-Leg Clamped	MMC	Two-Level VSI
	waveform quality	selection, and high efficiency						
Principal limitations	Neutral-point imbalance and unequal loss distribution	Increased switch count and control complexity	Large capacitor count, difficult voltage balancing, and reduced power density	Requirement for isolated DC sources or coordinated cell-level energy management	Increased balancing and coordination requirements	Limited scalability and midpoint-control requirements	High component count, large capacitor volume, and substantial control burden	High dv/dt, higher harmonic distortion, and full DC-link voltage stress

substantially lower work potential [236]. Exergy analysis addresses this limitation by quantifying the maximum useful work obtainable as a system approaches equilibrium with a defined reference environment. The combined application of energy, exergy, and entropy-generation analyses provides a comprehensive framework for evaluating integrated ESS-converter systems. Energy analysis identifies the magnitude and location of losses, while exergy analysis determines their thermodynamic significance and distinguishes internal irreversibility from exergy discharged to the surroundings. This framework provides a rigorous basis for comparing storage technologies, converter topologies, semiconductor devices, thermal-management strategies, and advanced control methods. Unless otherwise specified, the reference environment is characterized by a constant temperature T_0 and pressure p_0. All energy and exergy balances must be formulated using clearly defined and non-overlapping system boundaries [237].

4.1. Energy efficiency and loss decomposition [238]

The energy efficiency of an ESS-converter system depends on the direction of power flow. During discharge, the system efficiency is defined as

$$\eta_{\mathrm{sys,dis}} = \frac{E_{\mathrm{out}}}{E_{\mathrm{ESS,dis}}} \tag{4}$$

where $E_{\mathrm{ESS,dis}}$ is the energy released by the storage subsystem and E_{out} is the useful electrical energy delivered to the grid or load.

During charging, the corresponding efficiency is

$$\eta_{\mathrm{sys,ch}} = \frac{E_{\mathrm{ESS,ch}}}{E_{\mathrm{in}}} \tag{5}$$

where E_{in} is the electrical energy supplied to the ESS-converter system and $E_{\mathrm{ESS,ch}}$ is the net increase in stored energy.

The round-trip energy efficiency is expressed as

$$\eta_{\mathrm{RT}} = \frac{E_{\mathrm{out}}}{E_{\mathrm{in}}} = \eta_{\mathrm{ch}}\eta_{\mathrm{ret}}\eta_{\mathrm{dis}} \tag{6}$$

where η_{ch}, η_{ret}, and η_{dis} denote the charging, storage-retention, and discharging efficiencies, respectively. The storage-retention efficiency accounts for self-discharge, standby consumption, thermal conditioning, electrolyte circulation, and other losses occurring during the storage interval. These effects become increasingly significant in long-duration storage applications.

For a general control volume containing both the storage and conversion stages, the instantaneous power balance is

$$P_{\mathrm{in}}(t) = P_{\mathrm{out}}(t) + P_{\mathrm{loss,tot}}(t) + \frac{dE_{\mathrm{st}}}{dt} \tag{7}$$

where E_{st} is the energy stored within the control volume. Under the adopted sign convention, $dE_{\mathrm{st}}/dt > 0$ during charging and $dE_{\mathrm{st}}/dt < 0$ during discharging.

During discharge, in the absence of an external electrical input, Eq. (7) becomes

$$-\frac{dE_{\mathrm{st}}}{dt} = P_{\mathrm{out}} + P_{\mathrm{loss,tot}} \tag{8}$$

The total system loss can be decomposed as

$$P_{\mathrm{loss,tot}} = P_{\mathrm{loss,ESS}} + P_{\mathrm{loss,semi}} + P_{\mathrm{loss,mag}} + P_{\mathrm{loss,cap}} + P_{\mathrm{loss,aux}} \tag{9}$$

where the terms represent losses in the storage device, semiconductor devices, magnetic components, capacitors, and auxiliary subsystems, respectively. Additional contributions may be incorporated for cables, busbars, contactors, filters, protection equipment, and transformers when these components are included within the system boundary.

4.1.1. Storage-device losses

For a battery model in which the electrochemical loss mechanisms are represented separately, the irreversible battery loss may be expressed as

$$P_{\mathrm{loss,bat}} = I_{\mathrm{bat}}^2 R_{\Omega} + I_{\mathrm{bat}}(\eta_{\mathrm{act}} + \eta_{\mathrm{conc}}) + P_{\mathrm{side}} \tag{10}$$

where I_{bat} is the battery current, $R_{\Omega}$is the purely ohmic resistance, η_{act} is the activation overpotential, η_{conc} is the concentration overpotential, and P_{side}represents the power associated with irreversible side reactions.

Eq. (10) is applicable only when the ohmic and polarization contributions are identified independently. If an equivalent-circuit model is adopted and its effective resistance already represents the combined ohmic and polarization effects, the loss should instead be expressed as

$$P_{\mathrm{loss,bat}} = I_{\mathrm{bat}}^2 R_{\mathrm{eq}} \tag{11}$$

where R_{eq} is the effective equivalent resistance under the specified operating condition. Eqs. (10) and (11) are alternative formulations and must not be applied simultaneously because doing so would result in partial double counting of the battery losses.

The effective resistance and electrochemical overpotentials depend on state of charge, state of health, temperature, current rate, cell chemistry, and operating history. Consequently, a constant-resistance representation is applicable only within a limited operating range.

4.1.2. Semiconductor losses

The conduction loss of semiconductor device *k*can be evaluated using

$$P_{\mathrm{cond},k} = \frac{1}{T_{\mathrm{s}}}\int_0^{T_{\mathrm{s}}} s_k(t) i_k^2(t) R_{\mathrm{on},k}\left[T_{\mathrm{j},k}(t)\right] dt \tag{12}$$

where T_{s} is the evaluation period, $s_k(t)$ is equal to unity when the device conducts and zero otherwise, $i_k(t)$ is the device current, $R_{\mathrm{on},k}$ is the temperature-dependent on-state resistance, and $T_{\mathrm{j},k}$ is the junction temperature.

When the RMS current is evaluated over the complete period, Eq. (12) reduces to

$$P_{\mathrm{cond},k} = I_{\mathrm{rms},k}^2 R_{\mathrm{on},k} \tag{13}$$

A separate duty-ratio term must not be introduced into Eq. (13), because the conduction interval is already incorporated into the full-

period RMS current.

For semiconductor devices represented by a threshold-voltage model, such as IGBTs and diodes, the conduction loss may be expressed as

$$P_{\mathrm{cond},k} = V_{0,k} I_{\mathrm{avg},k} + R_{\mathrm{d},k} I^2_{\mathrm{rms},k} \tag{14}$$

where $V_{0,k}$ is the threshold voltage, $R_{\mathrm{d},k}$ is the differential resistance, and $I_{\mathrm{avg},k}$ is the average device current over the complete evaluation period.

The total switching loss of a converter containing N_{sw} switching devices may be approximated as

$$P_{\mathrm{sw}} = f_{\mathrm{sw}} \sum_{k=1}^{N_{\mathrm{sw}}} \left[E_{\mathrm{on},k} + E_{\mathrm{off},k} + E_{\mathrm{rr},k} \right] \tag{15}$$

where f_{sw} is the switching frequency, $E_{\mathrm{on},k}$ and $E_{\mathrm{off},k}$ are the turn-on and turn-off energies, and $E_{\mathrm{rr},k}$ is the reverse-recovery energy associated with the corresponding commutation path.

The switching energies depend on the operating conditions and may be represented as

$$E_{\mathrm{on/off},k} = f\left(V_k, I_k T_{\mathrm{j},k} R_{\mathrm{g},k}\right) \tag{16}$$

where V_k, I_k, and $R_{g,k}$ denote the device voltage, current, and gate resistance, respectively.

For GaN HEMTs, conventional diode reverse recovery is generally not the dominant commutation mechanism. A more appropriate engineering representation is

$$P_{\mathrm{sw,GaN}} = f_{\mathrm{sw}} \sum_{k=1}^{N_{\mathrm{sw}}} \left(E_{\mathrm{on},k} + E_{\mathrm{off},k} + E_{\mathrm{oss},k} + E_{\mathrm{dead},k} \right) \tag{17}$$

where $E_{\mathrm{oss},k}$ represents output-capacitance-related loss and $E_{\mathrm{dead},k}$ accounts for dead-time and reverse-conduction losses. Eqs. (15)–(17) are engineering approximations whose accuracy depends on device characteristics, switching trajectories, circuit parasitics, modulation strategy, and converter operating point.

4.1.3. Magnetic-component and capacitor losses

The total loss in an inductor or transformer is

$$P_{\mathrm{mag}} = P_{\mathrm{cu}} + P_{\mathrm{core}} \tag{18}$$

The winding loss may be calculated as

$$P_{\mathrm{cu}} = I^2_{\mathrm{rms}} R_{\mathrm{w,ac}} \tag{19}$$

where $R_{\mathrm{w,ac}}$is the effective AC winding resistance, including skin and proximity effects.

For periodic excitation, the core loss may be approximated using a Steinmetz-type relation:

$$P_{\mathrm{core}} \approx k f^{\alpha} B^{\beta}_{\mathrm{pk}} V_{\mathrm{core}} \tag{20}$$

where k, α, and β are experimentally determined coefficients, f is the excitation frequency, B_{pk} is the peak magnetic flux density, and V_{core} is the core volume. Eq. (20) is empirical and is most accurate under excitation waveform and temperature conditions consistent with those used to determine the coefficients. Generalized Steinmetz formulations are preferable for strongly non-sinusoidal converter waveforms.

The capacitor loss may be estimated as

$$P_{\mathrm{cap}} = I^2_{\mathrm{cap,rms}} R_{\mathrm{ESR}} \tag{21}$$

where $I_{\mathrm{cap,rms}}$ is the RMS capacitor current and R_{ESR} is the frequency- and temperature-dependent equivalent series resistance.

Auxiliary losses include the power consumed by cooling fans, pumps, heaters, battery-management electronics, gate drivers, sensors, communication interfaces, and digital controllers. Although these losses may represent a limited fraction of rated power, they can materially reduce system efficiency during standby and partial-load operation.

The time-averaged system efficiency over the interval from $t_0$to t_1 is

$$\bar{\eta}_{\mathrm{sys}} = \frac{\int_{t_0}^{t_1} P_{\mathrm{out}}(t)\, dt}{\int_{t_0}^{t_1} P_{\mathrm{in}}(t)\, dt} \tag{22}$$

This formulation is preferable to a single rated-point efficiency because it accounts for variations in load, state of charge, temperature, switching frequency, converter operating mode, and auxiliary demand.

4.2. Exergy balance and exergy efficiency

Exergy represents the maximum useful work obtainable as a system reaches equilibrium with the reference environment. In contrast to energy, exergy is not conserved. It may be destroyed by internal irreversibility or transferred across the system boundary without useful recovery [239,240].

Because energy storage systems are inherently transient, the general exergy balance for a control volume is

$$\frac{dEx_{\mathrm{CV}}}{dt} = \sum \dot{E}x_{\mathrm{in}} - \sum \dot{E}x_{\mathrm{out}} - \dot{E}x_{\mathrm{dest}} \tag{23}$$

where Ex_{CV} is the exergy stored within the control volume and $\dot{E}x_{\mathrm{dest}}$ is the exergy-destruction rate.

Under steady-state conditions,

$$\sum \dot{E}x_{\mathrm{in}} = \sum \dot{E}x_{\mathrm{out}} + \dot{E}x_{\mathrm{dest}} \tag{24}$$

The output exergy may be divided into useful product exergy and unrecovered exergy loss:

$$\sum \dot{E}x_{\mathrm{out}} = \dot{E}x_{\mathrm{product}} + \dot{E}x_{\mathrm{loss}} \tag{25}$$

The steady-state exergy balance therefore becomes

$$\sum \dot{E}x_{\mathrm{in}} = \dot{E}x_{\mathrm{product}} + \dot{E}x_{\mathrm{loss}} + \dot{E}x_{\mathrm{dest}} \tag{26}$$

Exergy destruction and exergy loss must be distinguished analytically. Exergy destruction results from irreversible processes occurring within the control volume, whereas exergy loss represents exergy transferred across the system boundary without recovery as a useful product.

Electrical energy is treated as pure work and is therefore entirely exergy:

$$\dot{E}x_{\mathrm{el}} = P_{\mathrm{el}} \tag{27}$$

The exergy transferred with heat across a boundary maintained at a uniform temperature T_{b} is

$$\dot{E}x_{Q} = \left(1 \frac{T_0}{T_{\mathrm{b}}}\right) \dot{Q} \tag{28}$$

where $\dot{Q}$ is the heat-transfer rate. The temperature T_{b} must correspond to the actual heat-transfer boundary and must not automatically be replaced by semiconductor junction temperature or battery-core temperature unless heat crosses the selected boundary at that temperature.

For an electrochemical storage device, the total stored exergy may be represented conceptually as

$$Ex_{\mathrm{ESS}} = Ex_{\mathrm{ph}} + Ex_{\mathrm{ch}} \tag{29}$$

where Ex_{ph} and Ex_{ch} are the physical and chemical exergy contributions, respectively. Physical exergy arises from temperature and pressure differences relative to the reference environment, whereas chemical exergy is associated with the electrochemical state of the active materials.

For a reversible electrochemical reaction at constant temperature and pressure, the maximum reversible electrical work is related to the Gibbs free-energy change:

$$W_{el,rev} = -\Delta G \tag{30}$$

For a cell reaction involving n electrons,

$$\Delta G = -nFE_{eq} \tag{31}$$

where F is Faraday's constant and E_{eq} is the equilibrium cell voltage. Accordingly, when kinetic, potential, and other physical-exergy contributions are negligible, the reversible electrochemical work may be expressed as

$$W_{el,rev} = nFE_{eq} \tag{32}$$

Eqs. (30)–(32) describe the reversible reaction work and must not be interpreted as complete pack-level exergy models without accounting for composition, temperature, pressure, state of charge, and degradation.

The exergy efficiency is defined according to the product-fuel convention:

$$\eta_{ex} = \frac{\dot{E}x_{product}}{\dot{E}x_{fuel}} \tag{33}$$

where $\dot{E}x_{product}$ is the desired exergy output and $\dot{E}x_{fuel}$ is the exergy resource consumed to produce it.

For an electrically charged and discharged ESS,

$$\eta_{ex,RT} = \frac{Ex_{el,dis}}{Ex_{el,ch}} \tag{34}$$

When electricity is the only boundary interaction considered, electrical exergy is identical to electrical energy, and therefore

$$\eta_{ex,RT} = \eta_{RT} \tag{35}$$

Exergy analysis provides additional information when the system boundary includes chemical-exergy variations, heat transfer, standby demand, auxiliary consumption, cooling loads, or other environmental interactions.

A frequently adopted exergy-based sustainability indicator is

$$SI = \frac{1}{1-\eta_{ex}} \tag{36}$$

This expression is a derived comparative indicator rather than a fundamental thermodynamic property. A larger value indicates lower relative irreversibility under the adopted exergy-efficiency definition.

An improvement-potential indicator may be expressed as

$$\dot{IP} = (1\eta_{ex})(\dot{E}x_{in}\dot{E}x_{out}) \tag{37}$$

The interpretation of Eq. (37) depends on the adopted system boundary and the definitions of input and output exergy. These definitions must therefore be stated explicitly when this indicator is applied.

4.3. Entropy generation and exergy destruction

Entropy generation quantifies the irreversibility of real physical processes [239,240]. For a constant reference-environment temperature, the Gouy-Stodola relation connects entropy generation and exergy destruction:

$$\dot{E}x_{dest} = T_0\dot{S}_{gen} \tag{38}$$

with

$$\dot{S}_{gen} \geq 0 \tag{39}$$

The total entropy-generation rate of the integrated system may be decomposed as

$$\dot{S}_{gen,tot} = \dot{S}_{gen,ESS} + \dot{S}_{gen,semi} + \dot{S}_{gen,mag} + \dot{S}_{gen,cap} + \dot{S}_{gen,thermal} + \dot{S}_{gen,aux} \tag{40}$$

provided that the selected subsystem boundaries do not overlap.

For a lumped electrical resistance operating at a uniform temperature T, entropy generation due to Joule heating is

$$\dot{S}_{gen,J} = \frac{I^2R}{T} \tag{41}$$

A more general local representation is

$$\dot{s}'''_{gen,J} = \frac{\mathbf{J}\cdot\mathbf{E}}{T} \tag{42}$$

where J is the current-density vector and Eis the electric-field vector.

For heat transfer from a region at temperature T_h to a region at temperature T_c, the entropy-generation rate is

$$\dot{S}_{gen,ht} = \dot{Q}\left(\frac{1}{T_c}\frac{1}{T_h}\right) \tag{43}$$

where $T_h > T_c$. Eq. (43) demonstrates that larger temperature differences increase thermodynamic irreversibility. This relationship is relevant to battery cells, semiconductor junctions, magnetic cores, thermal-interface materials, heat sinks, cold plates, and coolant circuits.

For a battery model in which irreversible overpotential components are represented separately, entropy generation may be written as

$$\dot{S}_{gen,bat} = \frac{I_{bat}^2R_\Omega}{T_{bat}} + \frac{I_{bat}(\eta_{act}+\eta_{conc})}{T_{bat}} + \dot{S}_{gen,side} \tag{44}$$

where T_{bat} is the battery temperature and $\dot{S}_{gen,side}$ represents the contribution of irreversible side reactions.

An equivalent compact formulation is

$$\dot{S}_{gen,bat} = \frac{I_{bat}\eta_{irr}}{T_{bat}} + \dot{S}_{gen,side} \tag{45}$$

where

$$\eta_{irr} = \eta_\Omega + \eta_{act} + \eta_{conc} \tag{46}$$

and

$$\eta_\Omega = I_{bat}R_\Omega \tag{47}$$

Eqs. (44) and (45) are alternative representations and must not be combined.

The reversible entropic heat of a battery may be represented as

$$\dot{Q}_{rev} = I_{bat}T_{bat}\frac{\partial E_{eq}}{\partial T} \tag{48}$$

The sign of Eq. (48) depends on the adopted current convention, battery chemistry, state of charge, and temperature coefficient of equilibrium voltage. This reversible heat contribution must not be classified as entropy generation or exergy destruction. Current ripple constitutes an important coupling mechanism between converter operation and battery irreversibility. If the battery current is decomposed into average and zero-mean ripple components,

$$i_{bat}(t) = I_{avg} + i_{ripple}(t) \tag{49}$$

with

$$\frac{1}{T}\int_0^T i_{ripple}(t)\,dt = 0 \tag{50}$$

then

$$I_{rms}^2 = I_{avg}^2 + I_{ripple,rms}^2 \tag{51}$$

The corresponding ohmic loss is

$$P_{ohmic} = R_{int}\left(I_{avg}^2 + I_{ripple,rms}^2\right) \tag{52}$$

Eq. (52) indicates that converter-induced ripple increases battery heating even when the average transferred current remains unchanged. This additional thermal loading can increase entropy generation, accelerate resistance growth, and intensify cell-to-cell temperature non-uniformity.

Switching frequency introduces a system-level design trade-off. Increasing the switching frequency generally reduces current ripple and passive-component volume, but it can increase semiconductor switching losses, magnetic AC losses, and cooling demand. The optimal operating range must therefore be identified from the combined energy and exergy behavior of the storage, converter, passive, and thermal subsystems.

4.4. Component-level exergy destruction

Component-level exergy analysis identifies the principal sources of irreversibility and prevents improvements in one subsystem from being achieved at the expense of another [241]. The total exergy destruction is expressed as

$$\dot{E}x_{\mathrm{dest,tot}} = \sum_{i=1}^{N} \dot{E}x_{\mathrm{dest},i} \tag{53}$$

where component boundaries must be non-overlapping and internal exergy transfers must be treated consistently.

The exergy-destruction fraction of component i is

$$y_i = \frac{\dot{E}x_{\mathrm{dest},i}}{\dot{E}x_{\mathrm{dest,tot}}} \tag{54}$$

When the complete system irreversibility is assigned to the selected components,

$$\sum_{i=1}^{N} y_i = 1 \tag{55}$$

Fig. 19 illustrates the component-level distribution of exergy destruction within the integrated converter-storage system. Semiconductor conduction and switching losses constitute the principal sources of irreversibility, followed by passive-component dissipation and storage-related electrochemical losses.

4.4.1. Storage subsystem

In electrochemical storage systems, exergy destruction is principally associated with ohmic resistance, charge-transfer overpotential, mass-transport limitations, concentration gradients, parasitic reactions, and thermal non-uniformity. High C-rates increase current density and polarization, whereas operation near the upper or lower state-of-charge limits can increase resistance and reduce electrochemical reversibility. Non-uniform state of charge, temperature, and state of health across a battery pack further increase irreversibility. Cells with higher resistance experience greater heat generation and can be subjected to disproportionate electrical and thermal stress. Cell balancing, thermal uniformity, and appropriately selected operating windows are therefore essential to exergy-efficient pack operation. For redox-flow batteries, additional exergy destruction may arise from pumping losses, pressure drops, membrane transport, species crossover, shunt currents, and concentration imbalance. In supercapacitor systems, equivalent series resistance and leakage current generally constitute the dominant loss mechanisms. Hybrid storage systems therefore require technology-specific energy and exergy models [242].

4.4.2. Power semiconductor devices

The electrical loss generated within the semiconductor stage is

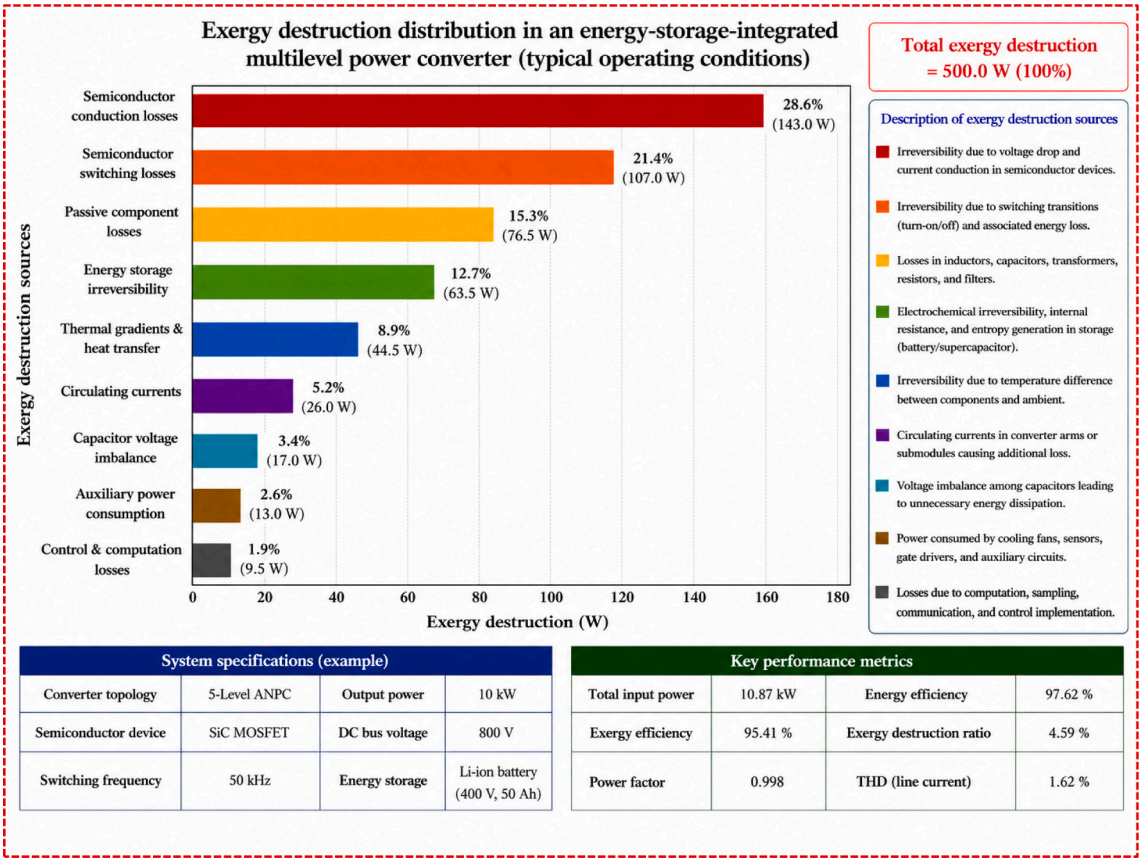

System specifications (example)			
Converter topology	5-Level ANPC	Output power	10 kW
Semiconductor device	SiC MOSFET	DC bus voltage	800 V
Switching frequency	50 kHz	Energy storage	Li-ion battery (400 V, 50 Ah)

Key performance metrics			
Total input power	10.87 kW	Energy efficiency	97.62 %
Exergy efficiency	95.41 %	Exergy destruction ratio	4.59 %
Power factor	0.998	THD (line current)	1.62 %

Fig. 19. Component-level exergy-destruction distribution in an energy-storage-integrated power conversion system.

$$P_{\text{loss,semi}} = P_{\text{cond}} + P_{\text{sw}} + P_{\text{gate}} + P_{\text{leak}} \tag{56}$$

where P_{gate} and P_{leak} represent gate-driving and leakage losses, respectively.

For a steady-state semiconductor control volume in which the electrical loss is converted into heat and rejected at a uniform boundary temperature T_{b}, the thermal exergy leaving the component is

$$\dot{E}x_{\text{Q,out}} = \left(1\frac{T_0}{T_{\text{b}}}\right)P_{\text{loss,semi}} \tag{57}$$

The corresponding semiconductor exergy destruction is

$$\dot{E}x_{\text{dest,semi}} = P_{\text{loss,semi}} - \dot{E}x_{\text{Q,out}} \tag{58}$$

Substitution of Eq. (57) into Eq. (58) yields

$$\dot{E}x_{\text{dest,semi}} = \frac{T_0}{T_{\text{b}}}P_{\text{loss,semi}} \tag{59}$$

Eq. (59) is valid under steady-state conditions, uniform boundary temperature, negligible exergy accumulation, and the absence of additional exergy interactions. In more detailed thermal networks, the semiconductor junction, thermal interface, heat sink, and cooling fluid should be represented as separate control volumes. Wide-bandgap semiconductor devices can produce a measurable reduction in converter exergy destruction by decreasing conduction and switching losses. However, the system-level benefit depends on converter topology, modulation method, switching frequency, parasitic inductance, dynamic on-state resistance, gate-driving conditions, thermal interfaces, and electromagnetic compatibility requirements [243].

4.4.3. Magnetic components and capacitors

Inductors and transformers generate exergy destruction through winding resistance, skin and proximity effects, magnetic hysteresis, eddy-current loss, leakage flux, and finite-temperature heat transfer. Increasing the switching frequency may reduce magnetic-component volume but increase core loss and AC winding resistance. Magnetic-component optimization therefore requires coordinated evaluation with semiconductor and filtering requirements. Capacitors contribute to exergy destruction through equivalent-series-resistance loss, dielectric loss, leakage current, and thermal degradation. High ripple-current density and elevated temperature are particularly significant in compact converters employing reduced passive-component volumes. The exergy benefit associated with increased switching frequency must therefore include its effect on capacitor loading, thermal stress, and service life [244].

4.4.4. Thermal-management subsystem

The electrical exergy supplied to the auxiliary thermal-management and control systems is

$$\dot{E}x_{\text{aux,in}} = P_{\text{fan}} + P_{\text{pump}} + P_{\text{HVAC}} + P_{\text{heater}} + P_{\text{control}} \tag{60}$$

Eq. (60) represents auxiliary exergy input and must not be interpreted directly as auxiliary exergy destruction. The exergy destruction of each auxiliary component must be determined from its corresponding exergy balance. Increased cooling intensity can reduce battery temperature, semiconductor junction temperature, and degradation rate, but it also increases auxiliary energy consumption. The thermal-management strategy should therefore minimize the combined irreversibility of the electrical, electrochemical, and cooling subsystems rather than minimize component temperature independently [245].

4.4.5. Control, sensing, and communication systems

Battery-management systems, sensors, digital controllers, communication devices, and edge-computing platforms generally consume less power than the principal conversion stage. Their contribution nevertheless becomes increasingly significant during standby and low-load operation, particularly in modular or geographically distributed storage systems. Advanced control methods can reduce switching loss, current ripple, and battery stress, but their computational demand must be incorporated into the system-level assessment. This requirement is particularly relevant to model predictive control, digital-twin platforms, reinforcement learning, and real-time artificial intelligence-based optimization [246].

4.5. Exergy optimization pathways

Exergy optimization should be formulated as a coordinated system-level problem. Minimization of an individual component loss is insufficient when the intervention increases irreversibility elsewhere or adversely affects reliability, thermal safety, power quality, or storage lifetime [247].

A representative multi-objective optimization problem may be written as

$$\min_{\text{x}}\left[\dot{E}x_{\text{dest,tot}}, P_{\text{loss,tot}}\Delta T_{\max}D_{\text{deg}}C_{\text{life}}\right] \tag{61}$$

subject to

$$SOC_{\min} \le SOC(t) \le SOC_{\max} \tag{62}$$

$$T_{\text{bat}} \le T_{\text{bat,max}} \tag{63}$$

$$T_{\text{j}} \le T_{\text{j,max}} \tag{64}$$

$$|I_{\text{bat}}| \le I_{\text{bat,max}} \tag{65}$$

$$V_{\text{dc,min}} \le V_{\text{dc}} \le V_{\text{dc,max}} \tag{66}$$

where x contains the design and control variables, $\Delta T_{\max}$ is the maximum relevant temperature difference, D_{deg} is a degradation indicator, and $C_{\text{life}}$is the life-cycle cost.

4.5.1. Pareto-based multi-objective optimization

The design of advanced power-conversion systems requires the simultaneous consideration of competing electrical, thermal, dynamic, reliability, and economic objectives. These objectives are strongly coupled and cannot generally be optimized in isolation. Increasing the switching frequency, for example, may improve waveform quality, control bandwidth, and power density through the reduction of passive-component size. However, it may also increase switching losses, electromagnetic interference, computational demand, and semiconductor thermal cycling. Similarly, aggressive control action can improve transient performance while increasing switching activity, junction-temperature variation, and component degradation [248]. These interactions motivate the adoption of a multi-objective optimization framework capable of identifying balanced converter-control configurations under application-specific constraints.

To ensure dimensional consistency, the relevant performance indicators can be normalized and expressed within a common minimization framework as

$$\min_{\text{x}} \text{F(x)} = \left[1-\eta(\text{x}), \frac{\Delta T_{\text{j}}(\text{x})}{\Delta T_{\text{j,ref}}}, \frac{t_{\text{s}}(\text{x})}{t_{\text{s,ref}}}, \frac{\rho_{\text{P,ref}}}{\rho_{\text{P}}(\text{x})}, 1-R(\text{x}), \frac{C_{\text{LC}}(\text{x})}{C_{\text{ref}}}\right]^{\text{T}} \tag{67}$$

subject to,

$g_i(\text{x}) \le 0, i = 1, \ldots, m,$

$h_j(\text{x}) = 0, j = 1, \ldots, p.$

where, x denotes the design-variable vector;
η is the conversion efficiency;
ΔT_{j} represents the junction-temperature variation;
t_{s} is the control settling time;

ρ_P denotes the converter power density;
R is a normalized reliability index; and
C_{LC}represents the lifecycle cost.

The quantities $\Delta T_{j,ref}$, $t_{s,ref}$, $\rho_{P,ref}$, and C_{ref} are positive reference values introduced to normalize objectives with different physical dimensions and thereby enable consistent comparison within the optimization process. The reliability index is assumed to satisfy $0 \leq R(x) \leq 1$. The design-variable vector may include converter topology, semiconductor technology, switching frequency, passive-component values, modulation strategy, controller parameters, cooling configuration, and computational platform. The associated inequality constraints may represent semiconductor voltage and current limits, maximum junction temperature, harmonic requirements, controller execution time, stability margins, and component-rating restrictions. Equality constraints may represent power-balance relationships, converter-state equations, modulation conditions, and energy-conservation requirements. Because these objectives are mutually conflicting, a single solution that simultaneously optimizes all performance indicators is generally unavailable. The optimization process therefore produces a Pareto front comprising non-dominated solutions. A solution is Pareto optimal when no objective can be improved without degrading at least one other objective. Pareto-front analysis consequently provides a systematic and transparent representation of the trade-offs among conversion efficiency, thermal stress, dynamic response, power density, reliability, and lifecycle cost [249]. Different regions of the Pareto front correspond to distinct design priorities. One region may emphasize high efficiency, reduced junction-temperature cycling, and enhanced reliability, whereas another may favor compactness, rapid dynamic response, and lower initial cost. The final design can then be selected according to the intended application, operating duty, regulatory requirements, and lifecycle considerations. Grid-support converters may prioritize thermal stability, fault tolerance, and long-term reliability, while compact renewable-energy interfaces may place greater emphasis on efficiency, power density, and economic feasibility. Pareto-based optimization therefore supports systematic and traceable design selection without relying solely on arbitrarily assigned weighting factors [250].

4.5.2. Converter topology and semiconductor selection

Converter topology strongly influences conduction paths, switching stress, current ripple, passive-component requirements, and thermal distribution. Multilevel converters, including neutral-point-clamped, active-neutral-point-clamped, T-type, flying-capacitor, cascaded H-bridge, and modular multilevel configurations, can reduce device voltage stress and harmonic distortion. However, additional semiconductor devices, balancing circuits, circulating currents, and control requirements can result in additional mechanisms of exergy destruction. The selection of GaN, SiC, or silicon devices requires systematic evaluation with respect to operating voltage, current, switching frequency, thermal environment, converter topology, and expected load profile. Device-level efficiency improvements must be assessed together with gate-driver loss, passive-component reduction, cooling demand, and electromagnetic compatibility provisions [251].

4.5.3. Switching-frequency and modulation optimization

The optimal switching frequency should be determined as a constrained minimization problem:

$$f_{sw}^{*} = \arg\min_{fsw \in [fmin, fmax]} \dot{E}x_{dest,tot}(f_{sw}) \tag{68}$$

subject to thermal, ripple, harmonic, voltage, current, and control constraints. This formulation is more general than imposing a zero-derivative condition because the optimum can occur at a constraint boundary. Modulation strategies require systematic evaluation according to their influence on switching transitions, neutral-point balancing, common-mode voltage, current ripple, semiconductor utilization, and thermal distribution. Loss-minimizing modulation can reduce the number of commutations or redistribute conduction among devices to limit localized thermal concentration [252].

4.5.4. Current-ripple reduction and hybrid storage

Converter-generated current ripple can be reduced through interleaving, optimized pulse-width modulation, active filtering, improved DC-link design, or increased phase count. A reduction in ripple decreases battery RMS current and the associated ohmic heating. Hybrid battery-supercapacitor systems provide an additional mechanism for performance improvement by assigning rapid power transients to the supercapacitor while the battery supplies the lower-frequency energy component. Appropriately coordinated power allocation can reduce battery polarization, temperature rise, entropy generation, and degradation. However, losses associated with the additional converter stage and supercapacitor must be incorporated into the system-level exergy assessment [253].

4.5.5. Exergy-aware predictive and intelligent control

Model predictive control can incorporate electrical performance, battery stress, converter loss, and exergy destruction within a unified objective function:

$$J = w_1 e_P^2 + w_2 e_Q^2 + w_3 \Delta SOC^2 + w_4 P_{loss,tot} + w_5 \dot{E}x_{dest,tot} + w_6 \Delta T^2 \tag{69}$$

where e_P and e_Q are the active- and reactive-power tracking errors, ΔSOC is the deviation from the desired state of charge, ΔT is a temperature-deviation measure, and w_1 to w_6 are weighting coefficients.

The weighting coefficients must be normalized or selected using a systematic multi-objective procedure because the terms in Eq. (69) possess different units and numerical scales. Without normalization, one term may dominate the optimization because of its magnitude rather than its physical significance. Artificial intelligence-based methods can facilitate adaptive selection of switching frequency, charging rate, cooling intensity, power-sharing commands, and state-of-charge trajectories. Reinforcement learning, neural networks, fuzzy control, and hybrid optimization techniques may identify operating policies under uncertain renewable generation, load demand, ambient temperature, and battery aging. Safety limits and physical constraints must be imposed as explicit operational constraints when data-driven controllers are applied [254].

4.5.6. Thermal and lifetime-oriented optimization

Thermal optimization should minimize both average operating temperature and temperature gradients across battery cells and semiconductor devices. Localized hot spots increase resistance, accelerate aging, and produce non-uniform current distribution. Variable-speed fans, adaptive coolant flow, predictive thermal control, and coordinated converter derating can reduce these effects. At the storage-device level, exergy destruction and degradation can be reduced by limiting operation at extreme states of charge, excessive depth of discharge, prolonged high-voltage exposure, and high C-rates. The optimal operating window depends on storage chemistry, application requirements, ambient conditions, and the economic value of available capacity [255].

4.5.7. Digital-twin-assisted exergy management

A digital twin can combine electrical, electrochemical, thermal, and aging models with real-time measurements to estimate energy loss, entropy generation, and component-level exergy destruction. Model parameters can be updated as the system ages, enabling adaptive optimization rather than dependence on fixed beginning-of-life characteristics. Digital-twin-assisted exergy management can facilitate predictive maintenance, anomaly detection, thermal forecasting, state-of-health estimation, and lifetime-oriented dispatch. The computational energy required for sensing, communication, data processing, and model updating must nevertheless be incorporated into the assessment of net system benefit. Effective exergy optimization requires the

coordinated design and operation of the storage device, converter topology, semiconductor technology, modulation strategy, passive components, thermal-management system, and supervisory controller. The principal objective is to reduce total system irreversibility rather than transfer losses from one subsystem to another, while simultaneously maintaining operational safety, reliability, power quality, and component lifetime. Future investigations should therefore quantify energy efficiency, exergy efficiency, entropy generation, and component-level exergy destruction under representative operating profiles, state-of-charge ranges, ambient conditions, and degradation states. Consistent reporting of these indicators would enable rigorous comparison among energy-storage technologies, converter architectures, semiconductor devices, and advanced control strategies [256].

5. Control technologies and advanced digital controllers

Over the past decade, research has increasingly focused on improving the efficiency, reliability, and grid compatibility of renewable and unconventional energy resources, including solar photovoltaic systems, wind energy, and marine energy conversion [257–261]. The rapid growth of these resources in modern power networks has strengthened the role of power electronic converters as essential enabling technologies. Converters are now fundamental components in a wide range of applications, including renewable energy interfaces, distributed generation, electrified transportation, railway traction, industrial motor drives, and emerging smart grid infrastructures [262–264]. As present-day energy systems integrate multiple sources and storage units with different voltage levels, power ratings, and alternating or direct current formats, power electronic converters provide the critical interface for conditioning, regulating, and integrating these power forms at a common electrical node or point of common coupling [265]. In addition to basic direct current to alternating current and alternating current to direct current conversion, modern converters perform several functions such as direct current voltage regulation, voltage step up and step-down operations, frequency and amplitude control in alternating current systems, waveform shaping, power factor correction, harmonic mitigation, and bidirectional power flow management. A wide range of converter topologies has been proposed to improve energy extraction, reduce losses, and meet increasingly strict requirements for power quality and electromagnetic compatibility [266]. In practical design, converter development is constrained by multiple objectives that often compete with each other, including high conversion efficiency, compact size, reduced component count, low installation cost, manageable thermal design, and scalable control implementation [267–269]. Progress in wide bandgap semiconductor devices, particularly gallium nitride and silicon carbide, has significantly supported these objectives by enabling higher switching frequency operation with reduced switching losses and improved thermal capability, which facilitates higher power density and smaller passive components.

In parallel with advances in hardware, converter control methodologies have evolved considerably over recent decades. Conventional industrial control approaches are predominantly based on linear controllers, typically proportional integral or proportional integral derivative structures, combined with modulation techniques such as pulse width modulation. These methods remain widely adopted due to their simplicity and low computational demand. However, their performance is often limited by reliance on linearized models and restricted closed loop bandwidth, which can reduce robustness under operating point variations, parameter uncertainties, and fast transients commonly observed in renewable energy systems. As renewable penetration increases and grid codes require improved dynamic behavior and power quality, the limitations of purely linear control strategies become more evident. The increasing capability of digital signal processors, field programmable gate arrays, and embedded microcontrollers has enabled the practical implementation of advanced control strategies. Hysteresis based control attracted attention due to its fast transient response and straightforward implementation in digitally controlled power converters. Subsequently, nonlinear and intelligent control methods, including fuzzy logic control and sliding mode control, have been widely investigated for improved robustness and dynamic performance. More recently, model predictive control has gained significant prominence because it provides a systematic framework to address multivariable interactions, nonlinear dynamics, and operational constraints, which are often difficult to treat using classical control structures [270].

Model predictive control was initially developed in the 1960s for constrained control of large-scale industrial processes and later gained acceptance in other sectors due to its effectiveness in multivariable systems [271,272]. Its adoption in fast dynamical applications was historically limited by the need to solve an optimization problem at each sampling instant. Improvements in computing capability and the availability of efficient real time optimization methods have substantially reduced this constraint, enabling increased use of model predictive control in power electronic converters. This has motivated extensive research into predictive control strategies for renewable energy interfaces, where converters must meet stringent requirements on current shaping, voltage regulation, and grid support while operating under variable input conditions [273].

In power electronics, model predictive control is frequently considered a strong alternative to proportional integral and proportional integral derivative based strategies, particularly in applications requiring rapid transient response, coordinated control of multiple variables, and explicit constraint handling [274]. The method relies on a discrete time model of the converter to predict the future behavior of key variables such as currents and voltages over a finite horizon. At each sampling interval, candidate control actions, often represented by feasible switching states, are evaluated using a cost function that penalizes tracking error and may include additional objectives such as reducing switching activity, minimizing losses, balancing internal voltages, or limiting harmonic distortion [275,276]. The switching action that minimizes the cost is applied to the converter, and the process is repeated in a receding horizon manner at the next sampling instant. Despite these advantages, practical implementation still requires careful attention to computational effort, sensitivity to parameter mismatch, selection of sampling time, and systematic tuning of cost function weights, which remain active topics of research [277,278].

Power control is a key functional requirement in grid-connected photovoltaic systems because the inverter must regulate the exchange of active and reactive power with the utility grid while maintaining power quality and satisfying interconnection constraints. The fundamental objective of grid side power control is to ensure that the controlled variables accurately track their reference commands, which are typically specified as active and reactive power setpoints or, equivalently, as grid current references derived from these setpoints. Depending on the control architecture, power control can be formulated in the stationary reference frame or in the synchronously rotating reference frame, with each representation offering different advantages in terms of decoupling, implementation effort, and sensitivity to grid synchronization errors [279]. A stationary frame predictive power control strategy is reported in [280], where active and reactive power regulation is achieved with an additional mechanism to mitigate steady-state tracking error. In [281], a direct model predictive power control method is introduced for a three-phase grid connected inverter, in which the optimal switching state is selected by minimizing a cost function defined over the power tracking error. By directly selecting switching states, such predictive power control schemes can avoid a separate modulation stage and can provide rapid transient response while enabling explicit inclusion of operational constraints. Control techniques become more demanding in three phase four wire systems and in distribution networks where load unbalance and neutral currents are significant. Four-leg grid connected inverters are commonly employed in these cases because the additional leg provides an independent path

for neutral current and allows improved regulation under asymmetric conditions. This structure enhances power control capability by enabling independent management of phase currents and neutral current, which supports higher power quality under unbalanced and nonlinear loading. In [282], model predictive power control is applied to a four-leg grid connected inverter to achieve accurate current tracking under both balanced and unbalanced scenarios, demonstrating improved performance in the presence of neutral current and phase asymmetry. In addition to conventional voltage source inverter structures, impedance source derived topologies have been explored to extend operating flexibility in sola PV conversion, particularly in applications requiring voltage boost without an additional DC-DC stage. The split source inverter has been proposed as an alternative to the Z source inverter to address limitations such as increased component count and elevated voltage stress on the active switches. In contrast to the Z source inverter, the split source inverter can achieve the required boosting behavior without relying on an additional shoot through operating mode, which can reduce switching loss and simplify the associated power control design. A hierarchical power control approach combining proportional integral regulation and predictive power control is described in [283], aiming to retain steady state accuracy while improving dynamic performance and constraint handling during transients.

Within predictive control frameworks for power converters, two main classes are commonly distinguished, namely continuous control set model predictive control and finite control set model predictive control. In continuous control set implementations, the controller produces a continuous valued control input, and a modulator is subsequently used to synthesize the required switching pattern. In finite control set implementations, the discrete switching states are evaluated directly within the optimization stage, and power control is performed by selecting the switching vector that minimizes a defined cost function. Finite control set predictive power control is particularly attractive for power electronic converters because the number of feasible switching states is limited and known as a priority, which allows real time evaluation of candidate actions without requiring an intermediate modulation block [284,285]. Moreover, additional objectives, such as reduction of switching activity, harmonic shaping, or internal voltage balancing, can be incorporated through extra terms in the cost function without reconfiguring a modulator. A recognized limitation, however, is that the switching frequency is not inherently fixed because the selected switching state depends on the optimizer outcome rather than a carrier-based scheme. To reduce switching frequency variability, several approaches have been reported, including expanding the admissible control set, adding switching transition penalties, and adopting constraint-based formulations that indirectly regulate switching activity [286].

5.1. Dead-beat (DB) controller

Dead-beat (DB) control has been widely investigated for the control of three-phase inverters, particularly in distributed generation power systems (DGPSs). In such systems, fast and accurate voltage and current regulation are critical to mitigate disturbances, ensure power quality, and maintain system stability. Due to the increasing penetration of inverter-interfaced renewable energy sources, advanced control strategies capable of delivering high dynamic performance have become essential. Among predictive control approaches, dead-beat control has gained significant attention because of its capability to eliminate tracking errors within a single sampling period under ideal conditions. Dead-beat control belongs to the class of discrete-time predictive controllers. Its fundamental principle is based on predicting the future behavior of system variables and calculating the control action required to force the controlled variable to reach its reference value at the next sampling instant. By directly compensating the forecast error in one control step, the DB controller ensures precise reference tracking without steady-state error, assuming accurate system modeling and parameter knowledge. This predictive mechanism allows the controller to achieve extremely fast dynamic response compared to classical linear controllers. In three-phase inverter applications, DB control has been effectively employed for both current and voltage regulations. The rapid response characteristic of DB control makes it particularly suitable for applications where disturbance rejection and transient performance are critical, such as active power filters and pulse width modulation (PWM) rectifiers [287]. In these applications, the controller can compensate for harmonic currents and reactive components almost instantaneously, thereby improving power quality and reducing total harmonic distortion. Furthermore, DB control has been extended to power control strategies in grid-connected systems. Ma, Li, and Li has proposed a DB-based approach for simultaneous control of active and reactive power, demonstrating its capability to regulate power flow with high accuracy and fast transient response [288,289]. Similarly, Bouzid et al. developed a dead-beat control scheme for inverter-interfaced distributed generation power systems, highlighting its effectiveness in maintaining stable operation under grid disturbances [290]. Additional studies confirm that DB control exhibits superior dynamic characteristics in current and power control applications, making it a preferred choice for high-performance inverter systems [291,292]. Despite its excellent transient performance, the effectiveness of DB control strongly depends on accurate system modeling. Since the control law is derived from the discrete-time model of the inverter and filter, parameter uncertainties, sampling delays, and measurement noise can introduce prediction errors, potentially degrading performance or causing instability. Moreover, implementation requires precise knowledge of system parameters such as inductance, resistance, and DC-link voltage. Therefore, while DB control offers extremely fast dynamic response and precise tracking capability, robustness against parameter variation remains an important consideration in practical applications. In high-performance inverter-interfaced DGPSs, where rapid load changes and grid disturbances are frequent, dead-beat control provides a compelling solution due to its predictive nature and minimal steady-state error. Its suitability for current and power control applications continues to motivate research efforts aimed at enhancing robustness, reducing sensitivity to modeling inaccuracies, and integrating adaptive or intelligent compensation mechanisms.

5.2. PI and PR control

The Proportional–Integral (PI) controller is one of the most widely adopted control strategies in power electronic systems due to its structural simplicity, ease of implementation, and low computational requirements. Its popularity stems from the fact that it does not require an explicit model of the system dynamics for basic tuning, making it attractive for practical industrial applications. PI controllers are commonly employed in both single-phase and three-phase systems for regulating current, voltage, or power variables in inverter-based applications. In synchronous reference frame (dq-frame) control schemes, the PI controller performs effectively because sinusoidal variables are transformed into DC quantities, allowing the integral term to eliminate steady-state error. However, in stationary reference frames (αβ or abc), PI controllers face inherent limitations in tracking sinusoidal reference signals. Under nonlinear load variations or distorted grid conditions, PI control exhibits steady-state tracking errors due to its inability to provide infinite gain at specific AC frequencies. Consequently, harmonic compensation capability is limited unless additional control mechanisms or coordinate transformations are introduced. To address these shortcomings, the Proportional–Resonant (PR) controller was proposed as an alternative solution for AC signal tracking. [293–295]. Unlike PI control, the PR controller operates effectively in the stationary reference frame and introduces a resonant term that provides theoretically infinite gain at a selected resonant frequency. This structure enables precise tracking of sinusoidal reference signals and ensures zero steady-state error at the fundamental frequency [296]. The resonant component

enhances current tracking performance without requiring coordinate transformations, thereby simplifying control architecture in certain applications. An additional advantage of the PR controller is its ability to implement selective harmonic compensation by adding multiple resonant terms tuned to specific harmonic frequencies. This feature allows effective mitigation of lower-order harmonics without requiring extensive computational resources or complex digital filtering algorithms [297]. By achieving high gain at the resonant frequencies, the PR controller provides lower steady-state error and improved harmonic suppression performance compared to conventional PI controllers in stationary frame implementations [298,299].

Despite these benefits, the PR controller exhibits certain practical limitations. Its structure becomes increasingly complex when multiple harmonic compensators are incorporated, which complicates parameter tuning and stability analysis. Furthermore, the performance of the PR controller is strongly dependent on accurate frequency selection. Any deviation in grid frequency reduces the effectiveness of the resonant term and may degrade tracking accuracy. In practical analog and digital implementations, the theoretically infinite gain at the resonant frequency cannot be realized. Instead, a high but finite gain is used, resulting in a finite quality factor (Q-factor). Excessively high Q-factors may amplify noise, introduce sensitivity to parameter variations, and reduce system robustness [300]. Additionally, digital discretization introduces approximation errors that may affect stability margins. Therefore, while PI controllers offer simplicity and robustness in DC-based control frameworks and PR controllers provide superior sinusoidal tracking capability in stationary frames, both approaches present trade-offs in terms of harmonic compensation, robustness to frequency variations, and implementation complexity. These characteristics motivate the exploration of advanced control strategies that combine the simplicity of PI control with the harmonic rejection capabilities of PR-based approaches, while improving robustness and dynamic performance under nonlinear load conditions.

5.3. Direct power control (DPC)

Direct power control (DPC) is a converter control methodology derived from the direct-regulation concept established in Direct Torque Control (DTC) for AC machine drives. While DTC directly manipulates inverter switching states to regulate torque and stator flux, DPC reformulates the objective in terms of the instantaneous active and reactive power exchanged between a voltage source converter and the AC system. A defining feature of conventional DPC is the direct selection of converter switching states based on power-tracking requirements, thereby avoiding the cascaded current-control structure and modulation stage typically used in vector-controlled converters. This direct switching decision mechanism can provide fast power response and a comparatively compact control architecture [301]. In a standard DPC implementation for an AC/DC voltage source converter, the instantaneous active power $P$and reactive power $Q$are computed from measured grid voltages and converter currents, commonly in the stationary reference frame. These estimated powers are compared with reference commands $P_{ref}$and Q_{ref}, and the corresponding errors are processed using hysteresis comparators or equivalent decision logic. The discrete outputs indicate whether $P$and Qshould be increased or decreased. In parallel, the position of the grid voltage vector is used to determine the operating sector in the voltage vector plane. Using the power error states together with the identified sector, a switching table is employed to select an appropriate converter voltage vector. The selected vector is applied directly to the converter, so that the resulting current dynamics drive the instantaneous powers toward their reference values. The control action in DPC is enabled by the coupling between the applied converter voltage vector and the evolution of the grid-side current through the interface filter. Since instantaneous active and reactive power are functions of grid voltage and current, and current dynamics are governed by the difference between the converter output voltage and the grid voltage, an appropriate switching vector can be chosen to impose the desired change in $P$and Q. This mechanism provides high dynamic performance during step changes in active power demand, variations in DC-link loading, and grid disturbances. Because the switching decision is taken directly from the power errors, DPC can exhibit strong transient response without requiring high-bandwidth inner current loops, provided that the power estimation and grid voltage angle detection remain accurate [302].

The conventional direct power control (DPC) structure applied to an AC/DC converter, as illustrated in Fig. 20, regulates the instantaneous active and reactive power exchanged with the grid. In many grid-connected applications, reactive power reference is set to $Q_{ref} = 0$to ensure unity power factor operation and minimize reactive power exchange. The active power reference $P_{ref}$is typically generated by an outer DC-link voltage control loop, where a proportional–integral (PI) controller processes the DC-link voltage error to produce the required active power command. This control strategy maintains the DC-link voltage at its reference value while ensuring proper power balance between the DC and AC sides. Several implementation aspects influence the practical performance of conventional DPC. The hysteresis-based switching logic generally produces a variable switching frequency because switching events depend on the trajectory of the power errors within the hysteresis bands and on the transitions between voltage vector sectors. This characteristic can complicate filter design and may increase the difficulty of meeting electromagnetic compatibility requirements. In addition, discrete switching-table operation can increase current ripple relative to fixed-frequency modulation approaches, particularly when hysteresis bands are wide or when sampling, computation, and gating delays become significant. DPC performance also depends on the accuracy of voltage and current measurement and on the quality of grid synchronization, since errors in the vector voltage can lead to inappropriate sector identification and suboptimal vector selection. These limitations have motivated several refinements, including constant switching frequency DPC using space vector modulation, predictive DPC formulations that explicitly evaluate candidate vectors over a sampling interval, and hybrid approaches that retain the direct power regulation principle while improving harmonic performance and switching regularity.

5.4. Hysteresis current control

Hysteresis current control is a widely used nonlinear control technique for generating gating signals in single phase and three phase power electronic converters. Owing to its simple structure and ease of implementation, it has been extensively applied in voltage source inverters, active power filters, motor drive systems, and grid connected converters. The operating principle of hysteresis current control is based

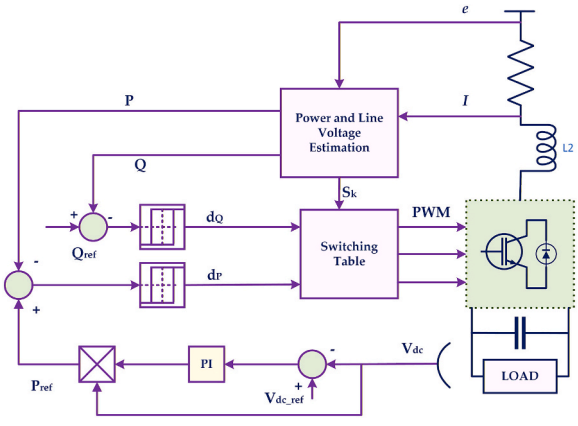

Fig. 20. Block diagram of DPC control technique [303].

on maintaining the actual converter output current within a predefined tolerance band around a reference current. Two boundary limits, referred to as the upper and lower hysteresis bands, are defined symmetrically around the reference waveform, which is typically sinusoidal in grid connected applications. The switching states of the semiconductor devices are determined directly from the instantaneous current error. When the measured current exceeds the upper limit, the controller changes the switching state to force the current to decrease. Similarly, when the current falls below the lower limit, the switching state is modified to increase the current. As a result, the output current oscillates within the hysteresis band and closely follows the reference signal. One of the main advantages of hysteresis current control is its fast dynamic response. Because the switching action is directly driven by the current error, the controller responds immediately to disturbances, changes in reference, and parameter variations. This property makes the method highly robust with respect to uncertainties in load parameters, supply voltage variations, and modeling inaccuracies. In addition, the control strategy does not require an accurate mathematical model of the system, coordinate transformations, or complex tuning procedures, which significantly simplifies practical implementation [304–306].

Another important feature is its inherent stability. Since the current error is continuously restricted within predefined limits, the tracking performance remains bounded during both steady state and transient conditions. The direct relationship between the current error and switching decision eliminates the need for external modulation techniques, resulting in a straightforward control structure. However, hysteresis current control also presents several limitations. The most significant drawback is the variable switching frequency. The switching frequency is not constant and depends on operating conditions such as the direct current link voltage, supply voltage magnitude, filter inductance, load impedance, and instantaneous current slope. Consequently, the switching frequency varies over the fundamental cycle. This behavior complicates filter design, increases electromagnetic interference, and may introduce resonance issues in grid connected systems. Moreover, the irregular and potentially high switching frequency leads to increased switching losses, reduced efficiency, and greater thermal stress on power semiconductor devices. Although the hysteresis band limits the instantaneous current error within a specified range, it does not allow precise control of harmonic distortion or switching spectrum distribution. Therefore, total harmonic distortion performance is influenced by the selected hysteresis bandwidth and operating conditions [307–311].

In practical implementations, factors such as sampling delay, dead time effects, finite switching speed, and measurement inaccuracies may further affect tracking accuracy. For these reasons, hysteresis current control is generally preferred in applications where simplicity, robustness, and fast transient performance are more critical than strict control of switching frequency. In applications requiring predictable switching behavior and optimized efficiency, alternative control methods such as sinusoidal pulse width modulation, space vector modulation, or model predictive control are often employed.

5.5. Repetitive control

Repetitive Control (RC) has been extensively recognized as an effective control strategy for disturbance rejection and reference tracking in systems subjected to periodic signals. The theoretical foundation of RC is derived from the Internal Model Principle (IMP), which states that perfect tracking of a reference signal or complete rejection of a disturbance can be achieved if a mathematical model of that signal is embedded within the control loop. By incorporating a delay element equivalent to one fundamental period of the target signal, RC effectively reconstructs the periodic behavior of the system and compensates errors iteratively from one cycle to the next. This structure enables the controller to generate theoretically infinite gain at the fundamental frequency and its integer harmonics, thereby achieving zero steady-state error for periodic references and disturbances [312]. When implemented as a high-order harmonic compensator, RC provides exceptional harmonic suppression capability. In power electronic systems, particularly grid-connected converters and UPS applications, harmonic distortion significantly affects voltage quality and overall system performance. The frequency-selective nature of RC allows it to attenuate specific harmonic components without requiring complex filter designs. By embedding multiple harmonic models implicitly within its delay-based structure, RC ensures high-quality voltage tracking while maintaining low total harmonic distortion (THD) levels [313,314]. This makes RC especially attractive in applications where periodic nonlinear loads introduce repetitive disturbances. An additional advantage of RC lies in its inherent frequency adaptability. Advanced implementations incorporate mechanisms that adjust the delay length according to estimated grid frequency, enabling the controller to cope with moderate frequency variations. This adaptive feature enhances robustness under practical grid conditions, where slight deviations from nominal frequency are common. Consequently, RC can maintain harmonic compensation performance even in the presence of small synchronization deviations.

Despite these significant benefits, conventional RC exhibits several limitations that restrict its performance in high-dynamic environments. A major concern is its strong dependence on the accuracy of the phase-locked loop (PLL). Since the internal delay must precisely match the fundamental period of the grid or reference signal, any frequency estimation error directly affects phase alignment. Even minor mismatches between the actual and estimated frequency can degrade harmonic suppression performance and reduce disturbance rejection effectiveness [312]. In weak grid scenarios or under severe frequency fluctuations, this sensitivity may compromise overall stability margins. Another inherent drawback of RC is its relatively slow dynamic response. Because the control action relies on error information from the previous period, compensation is inherently delayed by one cycle. While this structure guarantees superior steady-state harmonic rejection, it limits the controller's ability to respond rapidly to non-periodic disturbances or sudden load variations. During transient events, such as abrupt load steps, RC may exhibit temporary overshoot or oscillatory behavior before achieving steady-state correction [315]. This delay-induced trade-off between steady-state precision and transient speed represents a fundamental characteristic of repetitive control systems. Nevertheless, RC remains widely implemented in uninterruptible power supply (UPS) systems due to its relatively simple structure, straightforward digital implementation, and limited number of tuning parameters. In such systems, where the output voltage is inherently periodic and disturbances are often repetitive, the strengths of RC outweigh its limitations. To improve transient performance and robustness, RC is frequently combined with conventional controllers such as proportional–integral (PI) or proportional–resonant (PR) regulators, forming hybrid control architectures that balance harmonic suppression with improved dynamic response. These characteristics position RC as a highly effective solution for periodic disturbance rejection in power electronic applications, while also highlighting the necessity for enhanced or adaptive variants in systems requiring faster transient performance and reduced sensitivity to synchronization inaccuracies.

5.6. Model predictive direct power control

Model Predictive Control (MPC) is an optimization-based control framework that employs an explicit discrete-time model of the plant to predict the future evolution of controlled variables over a finite prediction horizon. At each sampling instant, the controller evaluates the predicted response of the system under a set of admissible control actions and selects the action that minimizes a predefined cost function. The cost function is formulated to reflect the control objectives by quantifying the deviation between predicted variables and their reference values, while constraints can be incorporated either explicitly or

through penalty terms. In power electronic converters, the control actions typically correspond to the finite set of available switching states, which makes MPC particularly suitable for direct switching control. In predictive model direct power control, the predictive control principle is applied directly to the regulation of instantaneous active and reactive power. Unlike conventional direct power control, which commonly relies on hysteresis comparators and a switching table, the predictive formulation determines the optimal converter switching vector by forecasting the resulting power trajectories [316–319]. Specifically, for each candidate switching state, the converter model is used to predict the grid-side current evolution and, consequently, the active and reactive power at the next sampling instant $k+1$. The optimal switching state is selected by minimizing a cost function commonly defined in terms of active and reactive power tracking, for example,

$$J = \left(P_{ref} - P(k+1)\right)^2 + \lambda\left(Q_{ref} - Q(k+1)\right)^2 \tag{70}$$

where $P_{ref}$and Q_{ref}denote the active and reactive power references, $P(k+1)$and $Q(k+1)$are the predicted powers for the next sampling period, and $\lambda$is a weighting factor that sets the relative emphasis between active and reactive power regulation. The switching state that yields the minimum value of $J$is then applied during the subsequent sampling interval T_s, and the optimization is repeated in a receding-horizon manner at the next control step using updated measurements.

The block diagram of a single step predictive power control strategy for a converter is presented in Fig. 21. In this method, measured grid voltages and converter currents are used to determine the instantaneous active and reactive power, which are then compared with their respective reference values. A discrete time predictive model is employed to estimate the future power response associated with each possible switching state. An optimization stage evaluates a cost function for all admissible switching vectors and selects the switching state that minimizes the predicted tracking error, with the corresponding gating signals applied directly to the converter. This predictive control formulation removes the need for a separate modulation stage and offers several advantages in power converter operation. It enables simultaneous control of active and reactive power within a unified framework, while additional control objectives such as current limitation, switching loss reduction, and internal voltage regulation can be incorporated through appropriate cost function design. In comparison with hysteresis based direct power control, predictive methods provide improved flexibility in dynamic response and enhanced steady state performance. Although this approach requires higher computational effort than conventional linear control techniques, advances in digital processing allow real time implementation, supporting its application in high performance grid connected power conversion systems.

5.7. Model-based predictive sliding mode control

In conventional predictive control architectures for grid-connected converters, the active power reference is commonly generated by an outer-loop proportional–integral (PI) controller responsible for regulating the DC-link voltage, as illustrated in Fig. 22. Although this approach is structurally simple and widely implemented, its dynamic performance is highly dependent on appropriate tuning of the PI gains. Under parameter variations, load disturbances, or abrupt changes in operating conditions, fixed PI coefficients may result in overshoot, undershoot, extended settling times, and non-negligible steady-state error. Furthermore, systematic gain tuning that guarantees robust performance across a wide operating range is challenging, particularly in systems characterized by nonlinear behavior and time-varying parameters. To address these limitations, sliding mode control (SMC) has been incorporated into predictive control frameworks, leading to the development of Model Predictive Sliding Mode Control (MPSMC). In this strategy, the conventional PI-based outer loop is replaced by a sliding mode regulator designed to enforce a predefined sliding surface that captures the desired system dynamics. The sliding surface is typically defined as a function of the DC-link voltage error and its derivative, or equivalently in terms of active power error dynamics. By driving the system state toward this surface and maintaining it within a bounded neighborhood, the controller achieves enhanced robustness against parameter uncertainty and external disturbances [320–325].

The principal advantage of sliding mode control lies in its inherent robustness properties. Once the system trajectory reaches the sliding surface, the closed-loop dynamics become largely insensitive to certain modeling inaccuracies and perturbations. This characteristic is particularly beneficial in power electronic converters subjected to fluctuations in output voltage demand, variations in load resistance, or grid-side disturbances. However, classical sliding mode implementations may

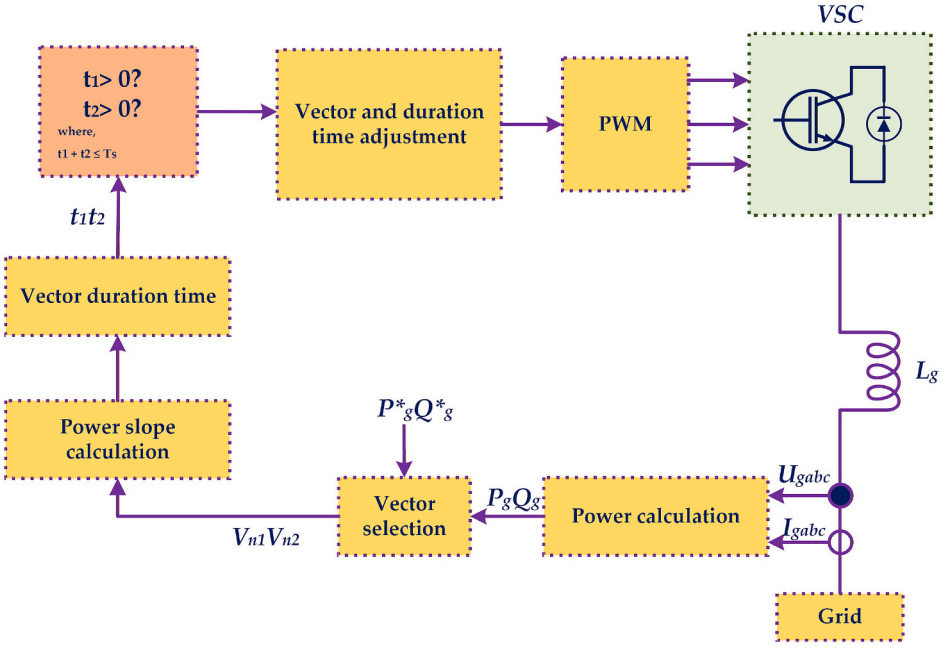

Fig. 21. Control structure of model predictive direct power controller.

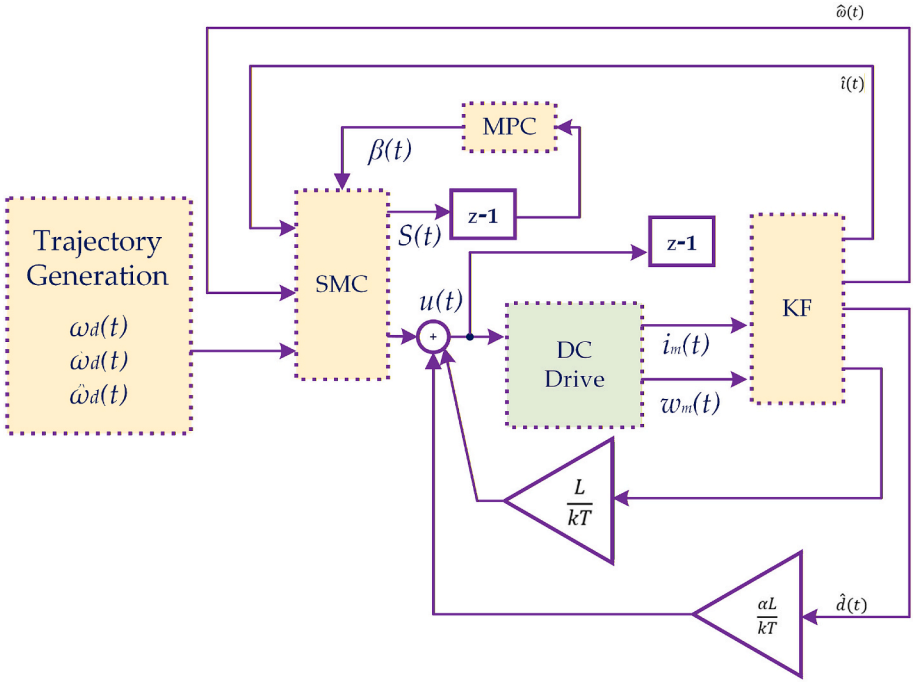

Fig. 22. Model-based predictive sliding mode control technique.

exhibit chattering due to high-frequency switching near the sliding surface, which can increase switching losses and stress on semiconductor devices. In the MPSMC framework, the sliding mode controller generates a reference or control action that reflects the desired robust dynamics, while the predictive control layer evaluates the finite set of admissible switching states using a discrete-time converter model. At each sampling instant, the predictive algorithm selects the switching state that minimizes a cost function incorporating both power tracking objectives and sliding surface constraints. By embedding the sliding condition within the predictive optimization process, the controller preserves robustness while reducing the chattering typically associated with conventional SMC. Moreover, additional objectives such as current limitations, switching frequency regulation, or neutral-point voltage balancing can be incorporated into the cost function, providing enhanced flexibility [326–328].

The integration of sliding mode control with predictive optimization combines the disturbance rejection capability of SMC with the constraint-handling and multivariable coordination features of model predictive control. This hybrid approach offers improved transient performance, reduced steady-state error under disturbances, and enhanced robustness compared with conventional PI-based predictive schemes, making it suitable for high-performance AC/DC converter applications operating under dynamic and uncertain conditions.

5.8. Predictive sliding mode control

Predictive sliding mode control (PSMC) represents an advanced nonlinear control approach that integrates the robustness of sliding mode control with the anticipatory capability of model-based predictive strategies. This combined framework preserves the inherent advantages of sliding mode control, including strong disturbance rejection and fast transient response, while improving control accuracy through predictive evaluation of system behavior. Consequently, PSMC is well suited for power electronic converters operating under variable conditions and parameter uncertainties [329,330].

Within this framework, a sliding surface is defined to characterize the desired closed-loop dynamics. For discrete-time implementation, the tracking error is expressed as,

$$e(k) = V_{dc}(k) - V_{dc,ref} \tag{71}$$

where $V_{dc}(k)$ denotes the measured DC-link voltage at the sampling instant k, and $V_{dc,ref}$represents its reference value. Based on this error, the sliding surface is formulated as,

$$s(k) = e(k) + \lambda[e(k) - e(k-1)] \tag{72}$$

where $\lambda > 0$ is a design parameter that determines the convergence characteristics and dynamic response of the system. This formulation ensures that the system trajectory is driven toward the desired operating condition and maintained within a bounded region around the sliding surface.

In contrast to conventional sliding mode control, which relies on discontinuous switching laws, PSMC employs a discrete-time predictive model to estimate the future evolution of system states for each admissible control input. The predicted behavior of the sliding surface is evaluated at the next sampling instant, and a cost function is defined to quantify control performance. A commonly used formulation is

$$J = s^2(k+1) + \alpha\,\Delta u \tag{73}$$

where $s(k+1)$represents the predicted value of the sliding surface, Δudenotes the control variation or switching transition, and $\alpha$is a weighting factor that balances tracking accuracy and switching activity. The optimal control action is determined by minimizing this cost function over the finite set of possible switching states.

This predictive selection mechanism enables the direct generation of gating signals for the converter, eliminating the requirement for an intermediate modulation stage. As a result, faster dynamic response and reduced implementation complexity can be achieved. In addition, system constraints such as voltage limits, current bounds, and switching frequency restrictions can be incorporated into the cost function, providing a flexible and comprehensive control framework. Through continuous feedback of system measurements, the controller maintains closed-loop operation and adapts to disturbances and parameter variations in real time. The resulting control strategy achieves accurate DC-link voltage regulation, maintains power balance between the DC and AC domains, and ensures stable converter operation. These

characteristics make predictive sliding mode control a suitable candidate for high-performance grid-connected power electronic systems [331–333]. The schematic diagram of the predictive sliding mode control (PSMC) strategy is presented in Fig. 23, where the robust characteristics of sliding mode control are combined with the predictive capability of model-based control. The control process begins with the acquisition of reference trajectories and measured system variables, such as currents and voltages. These signals are used to compute the tracking error, which forms the basis for constructing the sliding surface. The sliding surface defines the desired system dynamics and ensures convergence of the system states toward the reference trajectory. A discrete-time system model is employed to predict the future behavior of the controlled variables for each admissible control input. This predictive stage evaluates the evolution of both the system states and the sliding surface over the next sampling interval. The predicted values are then processed within a cost function that incorporates multiple performance criteria, including tracking accuracy, sliding surface deviation, switching effort, and operational constraints such as current and voltage limits. An optimization procedure evaluates the cost function across all possible control actions and selects the optimal switching state that minimizes the defined objective. The selected control input is directly applied to the power converter in the form of gating signals, eliminating the need for a separate modulation stage. This direct control approach enhances dynamic response and simplifies implementation compared to conventional modulation-based methods. Furthermore, system constraints and boundary conditions are explicitly incorporated into the control framework, ensuring safe and reliable operation under varying conditions. The closed-loop structure is maintained through continuous feedback of system measurements, enabling real-time correction of deviations and adaptation to disturbances or parameter uncertainties. This control strategy provides fast transient response, improved steady-state accuracy, and strong robustness against external disturbances and model uncertainties, making it well suited for high-performance power electronic converter applications [334–336].

5.9. Discussion

A comprehensive assessment of control strategies for power converters, as summarized in Table 3, demonstrates a clear transition from conventional linear methods to advanced predictive and nonlinear control techniques. Classical controllers such as proportional–integral and proportional–resonant structures remain attractive due to their simplicity, low computational requirements, and well-established theoretical foundations. However, their limited capability to address nonlinear behavior, parameter variations, and rapidly changing operating conditions restricts their effectiveness in modern renewable energy systems. Repetitive control offers improved tracking of periodic signals and effective harmonic compensation, yet its applicability is inherently limited to systems with well-defined periodicity. Fast acting methods such as hysteresis current control and direct power control provide rapid transient response and strong disturbance rejection. Nevertheless, their variable switching frequency introduces challenges related to switching losses, electromagnetic interference, and filter design. Deadbeat control achieves very fast dynamic response under ideal conditions, but its strong dependence on an accurate system model reduces robustness in practical implementations. Nonlinear control approaches, including sliding mode control and its model based and predictive variants, exhibit strong robustness to uncertainties and disturbances. These methods provide excellent dynamic performance and nonlinear handling capability, as reflected in Table 3. However, practical issues such as chattering, sensitivity to measurement noise, and increased implementation complexity limit their suitability for high performance renewable energy converters. Predictive control techniques represent a significant advancement in this context. Model predictive control offers a systematic framework based on the prediction of future system behavior and the optimization of control actions over a finite horizon. As indicated in Table 3, it combines fast dynamic response, low steady state error, and good harmonic performance while maintaining controllable switching frequency. A key advantage of this approach lies in its ability to explicitly incorporate system constraints,

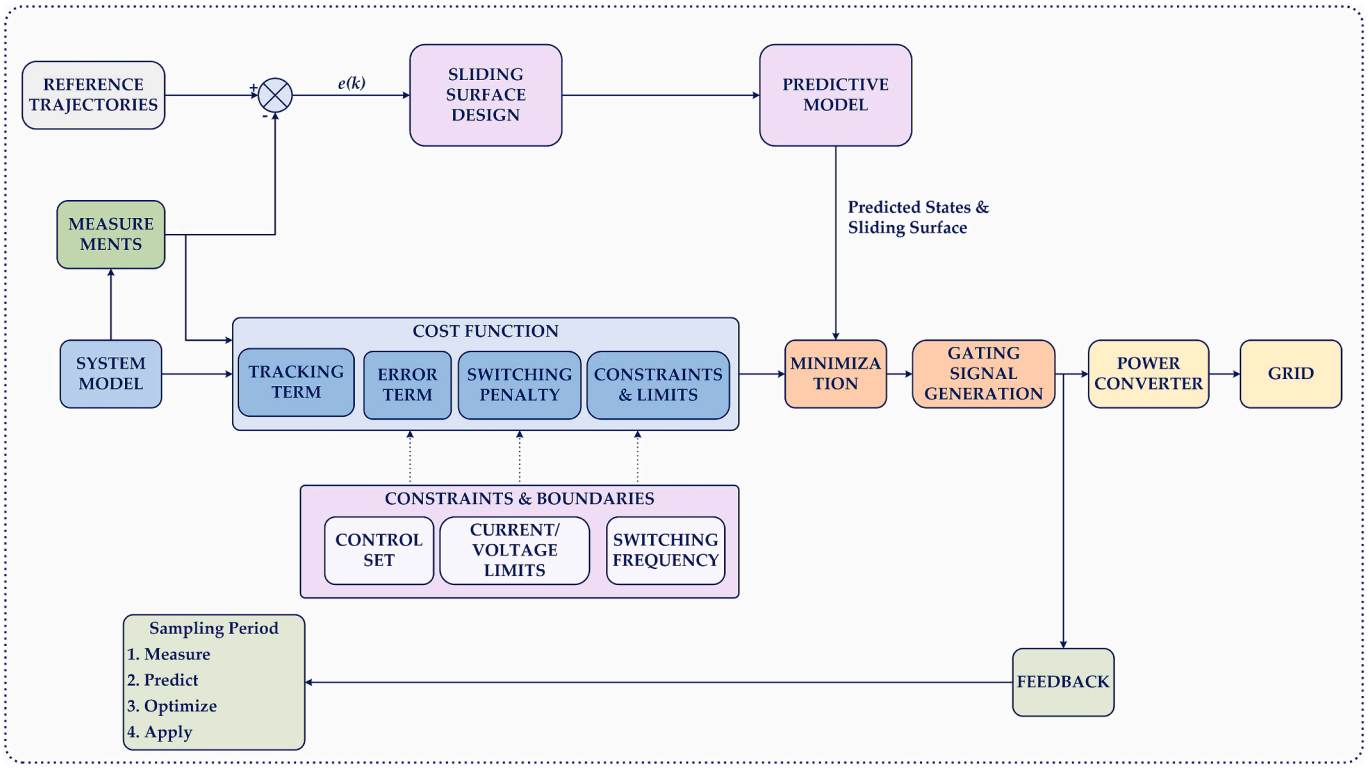

Fig. 23. Schematic diagram of predictive sliding mode control technique [335].

Table 3
Comparative analysis of advanced control strategies for power electronic systems based on performance and robustness criteria.

Technical Criterion	Deadbeat (DB) Control	Direct Power Control (DPC)	PI / PR Control	Repetitive Control (RC)	Hysteresis Current Control	Model Predictive Control (MPC)	Model-Based Predictive Sliding Mode	Predictive Sliding Mode Control
Control Law Structure	Discrete-time state prediction with one-step reference tracking	Direct regulation of instantaneous active and reactive power vectors	Linear feedback regulation using proportional–integral or proportional–resonant compensation	Internal model principle with periodic error memory	Nonlinear relay switching with hysteresis band	Finite-horizon optimization using predicted states	Sliding surface design with predictive plant dynamics	Predictive state estimation combined with sliding mode switching
System Model Dependency	Strong dependence on accurate discrete-time model	Moderate model dependence on power estimation	Low model dependency	Low model dependency	Minimal model requirement	High dependence on accurate system model	Requires accurate plant model	Moderate dependence on system model
Nonlinear System Handling Capability	Limited; typically requires linearization	Moderate nonlinear tolerance	Limited for strongly nonlinear systems	Limited	Moderate nonlinear tolerance	Strong nonlinear handling via predictive optimization	Very strong due to sliding invariance	Very strong via predictive sliding dynamics
Transient Dynamic Response	Very fast; typically, ≈1 sampling cycle under ideal conditions	Fast power dynamics ≈10–25 ms typical	Moderate response ≈20–40 ms typical	Moderate ≈20–50 ms typical	Very fast due to switching action ≈10–20 ms typical	Very fast ≈5–20 ms typical	Very fast ≈5–15 ms typical	Very fast ≈5–15 ms typical
Steady-State Error Characteristics	Near-zero error under accurate model conditions	Low steady-state power error	Zero steady-state error with integral or resonant action	Near-zero periodic error	Small error bounded by hysteresis band	Very low steady-state error	Very low	Very low
Harmonic Mitigation (Typical THD)	Moderate ≈3–5%	Moderate ≈3–5%	High ≈2–4% with PR control	Excellent periodic rejection ≈1–3%	Moderate ≈3–6%	Good ≈2–4% depending on cost function	Good ≈2–3%	Good ≈2–3%
Switching Frequency Regulation	Fixed switching frequency	Typically variable switching frequency	Fixed switching frequency	Fixed switching frequency	Variable switching frequency	Fixed or controlled variable frequency	Typically fixed switching frequency	Typically fixed switching frequency
Robustness to Parameter Variations	Low due to model mismatch sensitivity	Moderate	Moderate	Moderate	High	Moderate	High	High
Robustness under Grid Disturbances	Moderate	High	Moderate	High	High	High	Very high	Very high
Constraint Handling (Current / Voltage Limits)	Not explicitly handled	Limited	Not explicitly handled	Not explicitly handled	Implicit via hysteresis band	Explicit constraint handling through optimization	Partial constraint enforcement	Partial constraint enforcement
Computational Complexity	Low O(n) arithmetic operations	Low	Very low	Moderate	Very low	High optimization computation per cycle	High	Moderate–high
Control Update Time	≈1–5 μs	≈2–10 μs	≈1–5 μs	≈5–20 μs	≈1–3 μs	≈20–100 μs depending on solver	≈20–80 μs	≈10–50 μs
Memory Requirement	Low (<50 kB typical)	Low (<50 kB typical)	Very low (<20 kB typical)	Moderate (≈50–200 kB)	Very low (<20 kB)	Moderate–high (≈100 kB – 1 MB)	Moderate (≈100–500 kB)	Moderate (≈100–500 kB)
Real-Time DSP / FPGA Implementation	Highly feasible	Highly feasible	Very easy	Feasible	Very easy	Requires high-performance processors	Challenging without hardware acceleration	Feasible with optimized implementation
Stability Verification	Classical discrete-time control theory	Analytical methods available	Extensive linear control theory tools	Internal model stability analysis	Guaranteed within hysteresis bounds	Complex stability analysis due to optimization	Lyapunov-based stability methods	Lyapunov-based analysis
Suitability for High-Frequency GaN Converters	Good due to low computational delay	Good	Very good	Moderate	Good	Challenging due to computational latency	Moderate	Moderate
Typical Application Domain	Fast current regulation in converters	Grid-connected inverter power regulation	Voltage and current control loops	Harmonic compensation and grid synchronization	Motor drives and current control	High-performance converter and inverter control	Robust control under system uncertainties	Robust predictive inverter control

including current and voltage limits, within the control formulation. This feature is essential for ensuring safe and reliable operation in renewable energy systems subject to strict grid requirements. In addition, model predictive control provides a flexible structure capable of handling multivariable interactions and nonlinear system dynamics without the need for cascaded control loops. Compared to other predictive and nonlinear methods, it enables a more direct and unified treatment of performance objectives, including efficiency, power quality, and switching behavior. Although it requires higher computational resources and memory compared to conventional techniques, ongoing developments in digital control hardware and optimization algorithms have significantly improved its real time feasibility. Based on the comparative evaluation presented in Table 3, model predictive control demonstrates superior overall performance across key technical criteria, including dynamic response, steady state accuracy, harmonic mitigation, robustness under disturbances, and constraint handling capability. These characteristics make it particularly well suited for renewable energy applications, where operating conditions are inherently variable and system performance requirements are increasingly stringent. Future work should focus on reducing computational burden, improving robustness to model uncertainties, and enhancing scalability for high frequency converter systems. Such developments will further strengthen the applicability of model predictive control as a leading solution for advanced power electronic systems in renewable energy applications.

6. Role of artificial intelligence in power conversion

Artificial intelligence has recently emerged as a significant enabler in the advancement of grid connected power conversion systems. The rapid integration of renewable energy sources, along with the ongoing transition toward decentralized and digitally managed power networks, has introduced substantial variability and operational uncertainty into modern electrical grids. These evolving conditions impose stringent requirements on inverter control systems in terms of stability, adaptability, and power quality, thereby challenging the effectiveness of conventional control methodologies. Grid connected inverters are required to operate under diverse and dynamic conditions, including variations in grid impedance, frequency deviations, intermittent generation, and the presence of nonlinear and unbalanced loads. In addition, compliance with increasingly strict grid codes necessitates enhanced performance in terms of harmonic mitigation, voltage regulation, and transient response. Conventional control approaches, typically based on fixed parameter tuning and simplified system models, often exhibit limited robustness when subjected to such complex and time varying environments. In this context, artificial intelligence provides a paradigm shift by enabling data driven and adaptive control capabilities. Rather than relying exclusively on predefined analytical models, intelligent control frameworks can interpret system behavior in real time and adjust control actions accordingly. This capability is particularly advantageous in power conversion systems where accurate modeling is inherently difficult due to parameter uncertainties, component aging, and external disturbances. A key contribution of artificial intelligence in power conversion lies in enhancing system awareness and operational intelligence. Modern inverter systems can incorporate advanced monitoring layers that continuously assess electrical variables and grid conditions, allowing for improved state estimation and early detection of abnormal operating scenarios. This facilitates proactive control actions, enhances system reliability, and reduces the risk of instability or performance degradation.

Artificial intelligence also contributes significantly to improving dynamic performance and power quality. By enabling real time adaptation to transient disturbances such as voltage fluctuations and load variations, intelligent control frameworks support stable operation while minimizing harmonic distortion and maintaining waveform integrity. These capabilities are particularly critical in weak grid environments and microgrid configurations, where system interactions are highly nonlinear and sensitive to disturbances. Furthermore, artificial intelligence enables coordinated management of multiple performance objectives in power converters. In practical applications, inverter operation involves tradeoffs among efficiency, thermal stress, switching behavior, voltage regulation, and grid compliance. Intelligent control structures provide a unified framework for addressing these competing requirements, thereby enhancing overall system performance and enabling more efficient utilization of power electronic hardware. The integration of artificial intelligence with emerging digital technologies further extends its capabilities. The use of digital twins allows for virtual representation and continuous evaluation of converter performance, supporting predictive maintenance and system optimization. In addition, the deployment of intelligent functionalities on edge computing platforms facilitates low latency decision making and real time control at the converter level. These developments contribute to the realization of intelligent, interconnected, and autonomous power electronic systems. In practical implementations, artificial intelligence is generally incorporated within hierarchical control architecture. The primary control loop is typically maintained using established control principles to ensure stability and compliance with grid standards, while higher level intelligent layers provide adaptive tuning, supervisory control, and performance enhancement. This hybrid approach enables the system to leverage the reliability of conventional control while benefiting from the flexibility and adaptability of artificial intelligence. From a broader perspective, the application of artificial intelligence in power conversion aligns with the evolution of smart grids and intelligent energy systems. As power networks continue to transition toward distributed generation, bidirectional power flow, and active grid participation, power converters are increasingly required to perform advanced functionalities. Artificial intelligence enables these converters to operate as active and intelligent components within the grid, supporting stability, improving power quality, and facilitating autonomous operation. In conclusion, artificial intelligence represents a transformative advancement in the control of grid connected power converters. Its ability to provide adaptive, robust, and intelligent control in complex and uncertain environments makes it a critical component of next generation power systems. Continued developments in computational platforms, digital integration, and system level design are expected to further enhance its practical applicability and impact. The subsequent section presents a detailed discussion of representative intelligent control approaches and their implementation in grid connected inverter systems.

6.1. *Fuzzy logic control*

Fuzzy Logic control is a knowledge-based control methodology developed to manage uncertainty, imprecision, and nonlinear system behavior. Unlike classical Boolean logic, which restricts variables to binary values, fuzzy logic allows variables to take values within a continuous range between zero and one, representing degrees of membership. This characteristic enables the controller to describe system behavior using linguistic variables rather than relying strictly on precise mathematical expressions. A fuzzy logic control system is generally composed of four major components: fuzzification, knowledge base, inference engine, and defuzzification. The knowledge base consists of a database defining membership functions and a rule base containing a set of linguistic if then rules derived from expert knowledge or empirical system observations. These rules establish relationships between input variables and desired control actions. During the fuzzification stage, crisp input signals, such as voltage error and change of error, are transformed into fuzzy variables through membership functions. Common membership function shapes include triangular, trapezoidal, and Gaussian functions, each selected based on desired smoothness and computational efficiency. The inference engine then evaluates the activated rules using logical operations and combines their outputs to generate a fuzzy control signal. Finally, the defuzzification process converts the aggregated fuzzy output into a crisp numerical value,

typically using centroid or weighted average methods, which can be directly applied to the power converter. In grid connected inverter applications, nonlinear characteristics arise from switching actions, semiconductor device behavior, saturation effects, and grid disturbances. Additionally, system parameters such as inductance, resistance, and grid impedance may vary over time. Developing an accurate mathematical model under these conditions is often challenging. Fuzzy logic control mitigates this limitation by avoiding strict dependence on precise system models. Instead, it captures system dynamics using rule-based reasoning, effectively integrating locally linearized behaviors into a unified global nonlinear control strategy. The ability of fuzzy logic controllers to handle uncertainties makes them particularly suitable for systems operating under fluctuating grid conditions, voltage distortions, and load variations. Furthermore, FL controllers typically exhibit strong robustness and smooth control behavior without requiring complex parameter identification procedures. However, performance depends heavily on appropriate rule design and membership function selection. Poorly designed rule bases may degrade system performance, and systematic tuning methods are often required to achieve optimal results [337–339]. Fig. 24 illustrates the architecture of a fuzzy logic controller (FLC)-based control strategy for inverter-based microgrid operation. The input data are first processed through a fuzzification stage, where crisp signals are converted into fuzzy variables. These variables are then evaluated using a fuzzy inference system, which relies on a predefined rule base and database derived from expert knowledge. The resulting fuzzy outputs are converted back into crisp control signals through defuzzification and applied to the microgrid model. A feedback loop using measured signals ensures continuous system monitoring and adaptive control for stable microgrid operation.

6.2. Neural network control

Neural Networks are computational frameworks inspired by biological neural systems and are widely used for nonlinear modeling and adaptive control applications. The basic processing element of a neural network is the artificial neuron, which receives multiple input signals, multiplies each input by an associated weight, and sums the weighted inputs along with a bias term. This aggregated signal is then passed through a nonlinear activation function that determines the neuron output [343]. The activation function introduces nonlinearity into the network, enabling it to model complex system behavior. Neural networks are organized into layered architectures consisting of an input layer, one or more hidden layers, and an output layer. The input layer receives measured system variables, such as current, voltage, or power error. Hidden layers perform nonlinear transformations through weighted interconnections, and the output layer produces the control signal applied to the converter. The weights and biases are adjusted during a training process, which can be performed offline using historical data or online through adaptive learning algorithms. One of the most significant theoretical properties of neural networks is their universal approximation capability. A properly structured neural network with sufficient neurons can approximate any continuous nonlinear function within a bounded domain to an arbitrary degree of accuracy [344]. This property makes neural networks particularly suitable for power electronic systems, where nonlinearities arise from switching devices, magnetic components, and grid interactions. In grid connected inverter control, neural networks can be employed for system identification, adaptive parameter estimation, disturbance rejection, and direct control signal generation. For example, a neural network can learn the inverse dynamics of a converter and generate appropriate switching commands to minimize tracking error. Additionally, neural networks can compensate for modeling inaccuracies and parameter uncertainties by continuously updating their internal weights based on observed performance [345–347]. Neural network-based controllers demonstrate strong adaptability under varying operating conditions and can improve transient response and harmonic performance. However, their effectiveness depends on appropriate network architecture selection, sufficient training data, and computational capability for real time implementation. Excessive network complexity may increase computational burden, while insufficient training may result in poor generalization and instability. When properly designed, neural network control provides a powerful tool for addressing nonlinear and uncertain dynamics in modern power electronic converters. Its integration with conventional control strategies can further enhance robustness, stability, and overall system performance [348,349]. Fig. 25 illustrates the architecture of a neural network (NN)-based control strategy for power converters. The reference voltage/current and measured converter output are compared to generating an error signal, which serves as an input to the neural network controller. The NN processes these inputs through its hidden layers to produce appropriate control signals for the power converter. The converter output is continuously monitored and fed back to the controller, forming a closed-loop system. This approach enables adaptive and nonlinear control, improving dynamic performance and robustness of the converter under varying operating conditions.

6.3. Adaptive neuro fuzzy inference system control

The Adaptive Neuro Fuzzy Inference System (ANFIS) combines the linguistic reasoning capability of fuzzy logic with the learning and

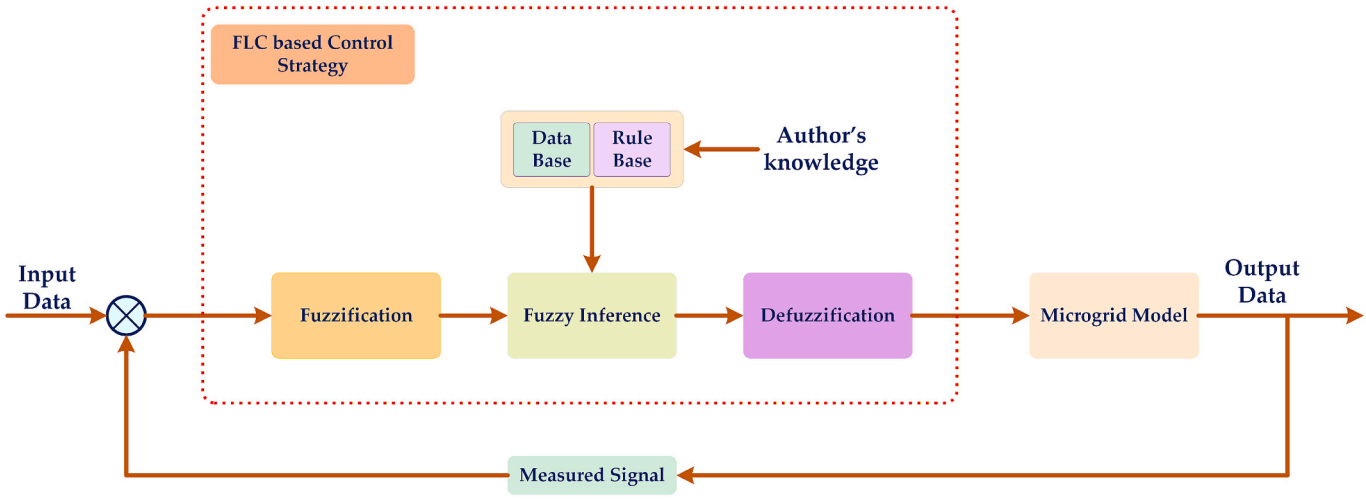

Fig. 24. Architecture of the fuzzy logic controller (FLC)-based control strategy for inverter based microgrid operation [340–342].

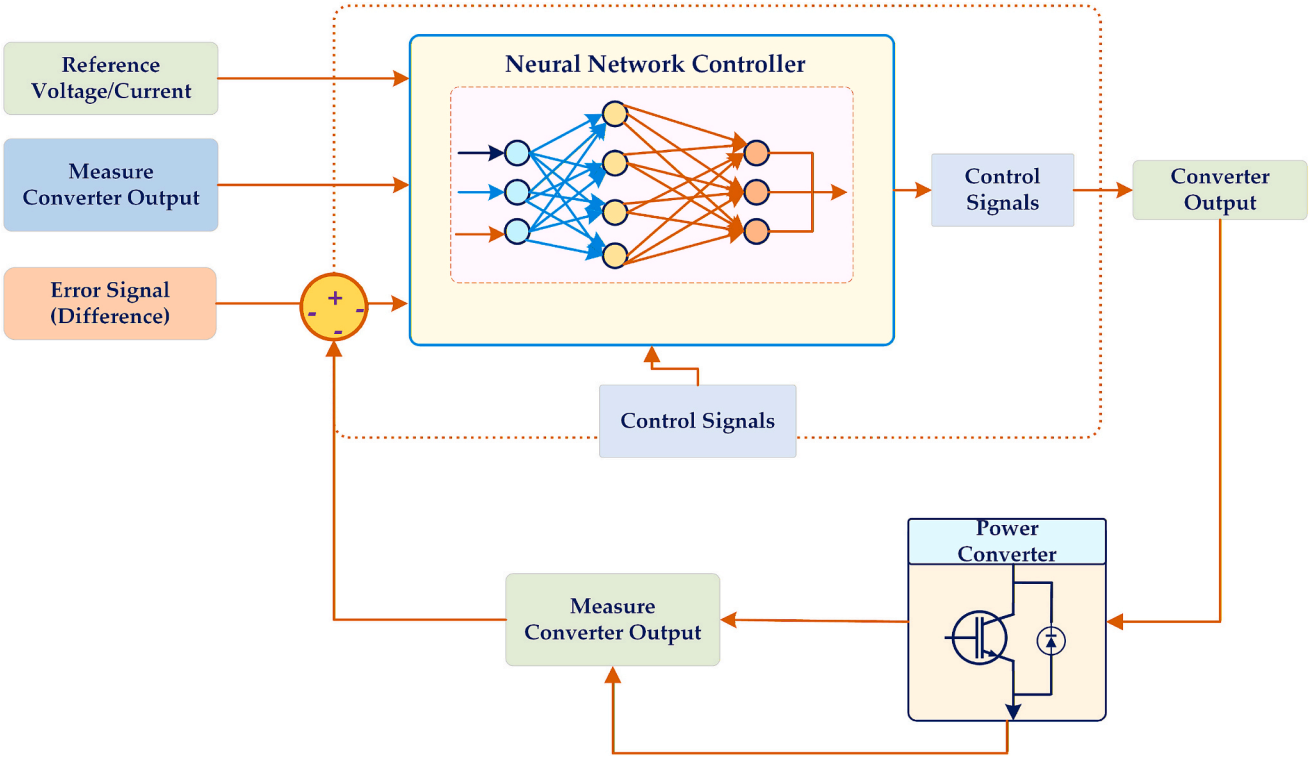

Fig. 25. Neural Network based control strategy for power converters [343,348,349].

approximation ability of neural networks. It is designed to overcome the limitations of conventional fuzzy logic control, particularly dependence on manually designed membership functions and rule bases. By integrating neural network learning mechanisms into a fuzzy inference structure, ANFIS enables automatic tuning of membership functions and rule parameters based on input output training data. An ANFIS architecture typically consists of multiple layers that represent fuzzification, rule evaluation, normalization, defuzzification, and output summation processes. In the first layer, input variables are mapped into fuzzy sets using parameterized membership functions. Unlike classical fuzzy systems, these membership parameters are adjustable. The second layer computes the firing strength of each fuzzy rule by applying logical operations to the fuzzified inputs. The third layer normalizes these firing strengths, while subsequent layers calculate rule outputs and aggregate

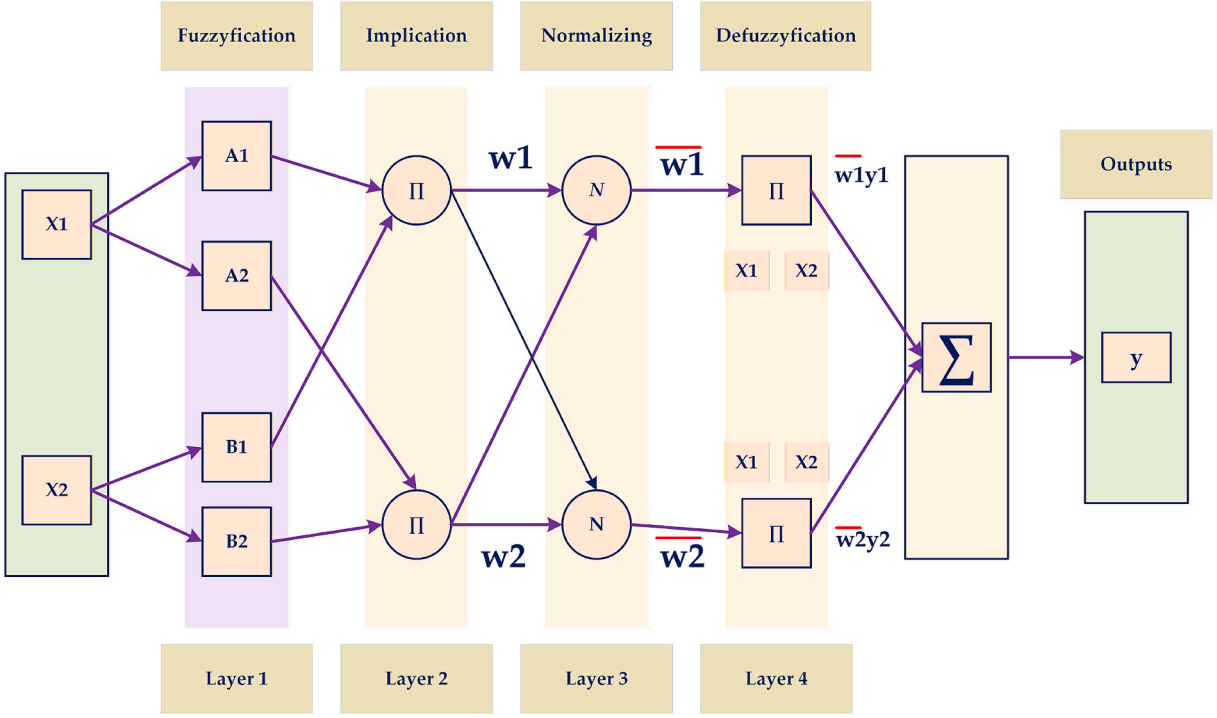

Fig. 26. Schematic diagram of ANFIS control technique.

them to produce the final crisp control signal. The learning process in ANFIS is generally achieved through hybrid training algorithms that combine gradient descent and least squares estimation. During training, the system minimizes the error between the predicted output and the desired output by iteratively adjusting the premise and consequent parameters of the fuzzy rules. This learning capability enables ANFIS to adapt to nonlinear system behavior and time varying operating conditions without requiring extensive manual tuning. In grid connected inverter applications, ANFIS offers significant advantages for handling nonlinearities, parameter uncertainties, and fluctuating grid conditions. It can approximate complex nonlinear mappings between system states and control signals with high accuracy. Moreover, the adaptive nature of ANFIS improves robustness against disturbances and grid variations. Compared to standalone fuzzy logic control, ANFIS provides enhanced precision and systematic parameter optimization. However, its performance depends on adequate training data and proper initialization, and computational complexity may increase with the number of rules and inputs [350–352]. Fig. 26 illustrates the schematic architecture of the adaptive neuro-fuzzy inference system (ANFIS) control technique. The input variables (X_1, X_2) are first processed through the fuzzification layer, where membership functions (e.g., A_1,A_2,B_1,B_2) map crisp inputs into fuzzy sets. In the second layer, fuzzy rules are applied, and the firing strengths (w_1, w_2) are computed. These firing strengths are then normalized in the third layer to ensure proper weighting of each rule. In the fourth layer, consequent parameters are applied to generate rule outputs, which are weighted by the normalized firing strengths. Finally, the outputs are aggregated in the summation layer to produce the overall system output (y). This layered structure enables ANFIS to combine the learning capability of neural networks with the reasoning of fuzzy logic for effective nonlinear control.

6.4. Reinforcement learning control for inverters

Reinforcement Learning (RL) represents a data driven control paradigm in which an agent learns optimal control policies through interaction with the environment. Unlike supervised learning methods, RL does not require labeled input output datasets. Instead, it relies on a reward-based mechanism, where the controller continuously adjusts its actions to maximize cumulative reward over time. In inverter control applications, the RL agent observes system states such as voltage error, current error, switching states, or grid conditions. Based on these observations, the agent selects control actions, such as modifying switching patterns, adjusting modulation indices, or tuning controller gains. After executing an action, the system provides feedback in the form of a reward signal, typically defined according to performance objectives such as minimizing tracking error, reducing harmonic distortion, lowering switching losses, or improving stability margins. Through iterative exploration and exploitation, the RL algorithm learns an optimal control policy that maps system states to control actions. Advanced RL methods, including Q learning, policy gradient methods, and deep reinforcement learning, have demonstrated strong potential for handling nonlinear, high dimensional control problems. In power electronic converters, RL can optimize multi objective performance criteria under uncertain and dynamic operating conditions. The main advantage of RL in inverter control lies in its ability to adapt autonomously to changing system conditions without requiring an explicit mathematical model. This feature is particularly beneficial in systems with parameter uncertainties or complex grid interactions. However, practical implementation presents challenges such as ensuring system stability during learning, managing computational requirements, and defining appropriate reward functions. Safe learning strategies and hybrid approaches are often employed to ensure reliable real time operation [353,354]. Fig. 27 presents the proposed reinforcement learning (RL)-based control architecture for a grid-connected inverter. The controller receives reference active and reactive power signals (P^*Q^*)and system state observations, including inverter output voltage (V_{abc}), inverter current (I_{abc}), and grid frequency. These measured variables are provided to the RL agent to represent the system state. Based on the observed states, the RL agent generates control actions, such as voltage reference or duty cycle commands, to regulate the inverter operation. The inverter interacts with the grid environment, and its performance is evaluated using a reward function defined by control objectives such as power tracking error, total harmonic distortion

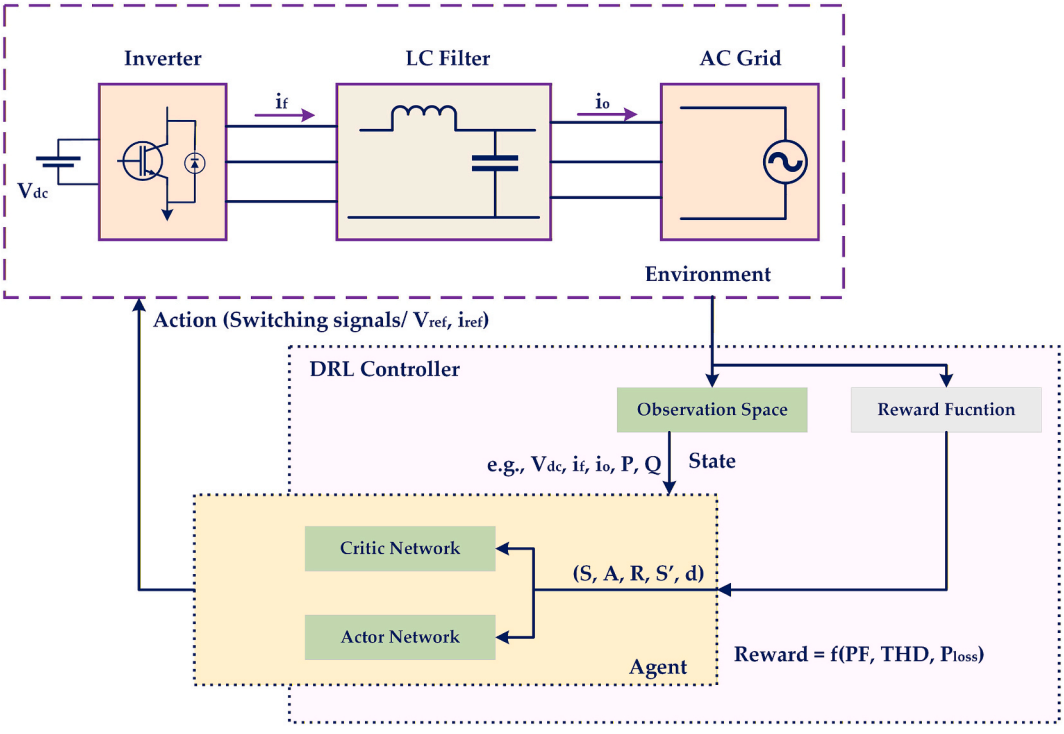

Fig. 27. Reinforcement learning–based control architecture for a grid-connected inverter system.

(THD), and power factor. The reward signal is fed back to the RL agent to update its control policy through continuous learning. This closed-loop learning mechanism enables adaptive control, improved power quality, and enhanced dynamic performance of the grid-connected inverter under varying operating conditions [355].

6.5. Hybrid fuzzy logic and neural network control strategy

Hybrid control strategies combining fuzzy logic and neural networks aim to exploit the complementary strengths of both approaches. While fuzzy logic provides intuitive rule-based reasoning and robustness under uncertainty, neural networks offer powerful nonlinear approximation and adaptive learning capabilities. Integrating these methods results in improved adaptability, precision, and performance compared to stand-alone implementations [356]. One common hybrid approach involves using neural networks to optimize the membership functions or rule parameters of a fuzzy logic controller. In this configuration, the fuzzy structure provides interpretability and stability, while the neural network performs online tuning to adapt to changing operating conditions. Another approach utilizes fuzzy logic to generate initial control decisions and neural networks to refine or compensate these outputs based on learned system behavior. In grid connected inverter systems, hybrid FL-NN control can significantly enhance dynamic response and harmonic suppression under nonlinear load conditions and grid disturbances. The fuzzy component ensures robust baseline control even when system knowledge is limited, while the neural network component continuously improves performance by learning from real time data. This synergy allows the controller to handle parameter variations, nonlinearities, and transient disturbances more effectively than either method alone. Despite these advantages, hybrid control strategies increase design complexity and computational requirements. Proper coordination between the fuzzy and neural components is necessary to maintain stability and avoid conflicting control actions. Careful selection of network architecture, training algorithms, and rule base design are essential to achieve optimal performance [357–360]. Fig. 28 illustrates the proposed hybrid fuzzy logic and neural network–based control architecture for inverter-based power systems. The control framework integrates fuzzy logic reasoning with neural network learning to enhance the dynamic response, adaptability, and robustness of the inverter under varying operating conditions. The control process begins with the reference active and reactive power signals (P^*Q^*), which define the desired operating point. The difference between the reference and measured outputs produces power error signals that serve as inputs to the hybrid controller. In addition, a state observation module collects real-time system variables, including inverter output voltage (V_{abc}), inverter current (I_{abc}), and grid frequency. Within the hybrid controller, the fuzzy logic controller processes the error signals using predefined membership functions and rule-based reasoning to generate an initial control action. The neural network controller subsequently refines this action by learning nonlinear system dynamics, thereby improving control accuracy and adaptability. The resulting control signals are applied to the inverter to regulate power exchange with the grid. System performance is continuously assessed through an evaluation and feedback mechanism based on metrics such as power tracking accuracy, power factor, and harmonic distortion. This feedback enables continuous adjustment of the controller, ensuring improved stability, power quality, and overall system efficiency.

6.6. Artificial intelligence assisted control techniques

The increasing complexity of modern power electronic systems, particularly grid connected converters operating under variable renewable energy sources and nonlinear loads, has motivated the integration of artificial intelligence into conventional control frameworks. Artificial intelligence assisted control refers to strategies in which learning, optimization, or adaptive mechanisms are embedded within classical controllers to enhance their performance. Unlike fully AI based control schemes, these approaches preserve the analytical structure of traditional controllers while augmenting them with data driven adaptability. In grid connected inverter systems, control objectives often include voltage and current regulation, harmonic mitigation, DC link stabilization, power factor correction, and constraint handling under uncertain grid conditions. Conventional controllers, although effective in well-modeled environments, may suffer from degraded performance when system parameters vary, operating conditions change, or disturbances occur. AI assisted methods address these challenges by introducing adaptive parameter tuning, nonlinear approximation, and real time optimization capabilities. The principal advantage of AI assisted control lies in its ability to transform fixed controller parameters into adaptive variables optimized through learning or evolutionary processes. This enhances disturbance rejection capability, reduces steady state error, and improves transient response. However, these benefits come at the cost of increased computational burden and the need for reliable training data or real time learning stability. Consequently, careful implementation and hardware selection are required to ensure

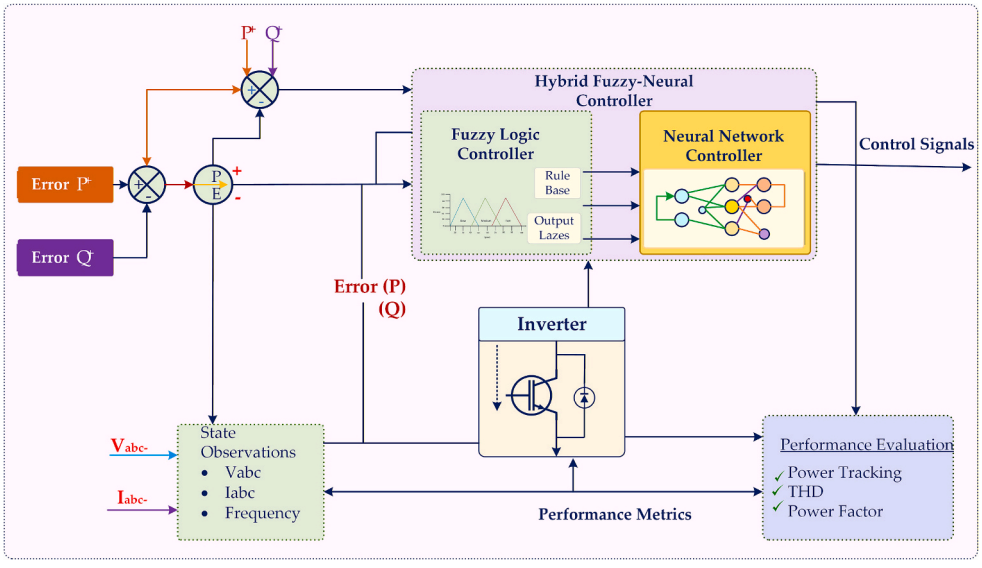

Fig. 28. Architecture of the hybrid fuzzy logic and neural network–based control strategy for inverter systems [358].

practical feasibility in high frequency switching applications.

6.6.1. AI assisted proportional integral control

The proportional–integral (PI) controller continues to be one of the most extensively employed control strategies in power electronics due to its structural simplicity, ease of implementation, and effectiveness in eliminating steady-state error in DC quantities. These characteristics make PI control particularly suitable for applications such as grid-connected converters, motor drives, and power conditioning systems. However, despite its widespread adoption, the performance of a conventional PI controller is highly dependent on the proper selection of proportional and integral gains. Fixed-gain PI controllers are inherently sensitive to variations in system parameters, nonlinear dynamics, and external disturbances, which can lead to degraded dynamic performance, increased settling time, oscillations, and reduced robustness under changing operating conditions. To overcome these limitations, artificial intelligence (AI)-assisted PI control has emerged as an advanced control paradigm that enhances the classical PI structure by introducing adaptive and data-driven mechanisms. In this approach, the controller gains are no longer static but are dynamically adjusted based on system behavior, thereby improving performance in the presence of uncertainties and nonlinearities [361–363]. AI-assisted PI control leverages computational intelligence techniques to provide optimal tuning, real-time adaptability, and improved disturbance rejection capabilities. One of the fundamental approaches in AI-assisted PI control involves the optimization of controller gains using intelligent algorithms. Evolutionary optimization techniques, such as genetic algorithms (GA), particle swarm optimization (PSO), differential evolution, and other heuristic search methods, are widely applied to determine optimal proportional and integral gains. These algorithms explore the search space iteratively to minimize predefined performance indices, including integral of absolute error (IAE), integral of squared error (ISE), total harmonic distortion (THD), rise time, and settling time. By formulating the tuning process as an optimization problem, these methods enable the identification of gain values that provide improved transient and steady-state performance without requiring an accurate analytical model of the system. As a result, the controller becomes more robust to parameter variations and modeling uncertainties. In addition to offline optimization, real-time adaptive control can be achieved through neural network-based PI control strategies. In these configurations, artificial neural networks (ANNs) are trained to capture the nonlinear relationship between system states and optimal controller parameters. During operation, the neural network continuously monitors system error signals and dynamically updates the proportional and integral gains to maintain optimal performance. This adaptive mechanism allows the controller to respond effectively to rapid changes in operating conditions, such as load variations, grid disturbances, and fluctuations in renewable energy sources. The incorporation of neural networks significantly enhances transient response characteristics, reduces overshoot, and improves stability margins [364–366]. In grid-connected inverter systems, particularly those integrated with energy storage units, neural network-based PI controllers have demonstrated superior current tracking accuracy, faster dynamic response, and reduced voltage ripple compared to conventional dual-loop PI control schemes. Furthermore, hybrid intelligent control techniques have been developed to further enhance PI controller performance in nonlinear and uncertain environments. Among these, neuro-fuzzy systems represent a prominent approach that combines the learning capability of neural networks with the reasoning mechanism of fuzzy logic. In neuro-fuzzy PI control structures, fuzzy inference systems are employed to handle nonlinearities, parameter uncertainties, and external disturbances by generating compensatory control actions based on linguistic rules and membership functions. Meanwhile, the PI controller provides baseline regulation and ensures steady-state accuracy. The integration of these techniques results in improved harmonic suppression, enhanced reactive power compensation, and better overall power quality, particularly in systems operating under nonlinear load conditions [367,368].

Fig. 29 illustrates the proposed AI-assisted proportional–integral (PI) control architecture for inverter-based power systems. The control framework integrates artificial intelligence with a conventional PI controller to achieve enhanced control accuracy, adaptability, and dynamic performance. The control process begins with the generation of reference active and reactive power signals (P^*Q^*), which define the desired operating point of the inverter. These reference signals are compared with the measured active and reactive power outputs to produce error signals that represent the deviation from the desired operating conditions. These error signals are subsequently processed by an AI-based optimization module, which utilizes system data, learned patterns, and performance evaluation criteria to determine appropriate adjustments to the PI controller gains. Depending on the implementation, this module may employ optimization algorithms, neural networks, or hybrid intelligent techniques to perform adaptive tuning. The updated proportional and integral gains are then applied to the PI controller, which generates control signals required for inverter switching and modulation. A state observation module plays a critical role in the control architecture by continuously acquiring real-time system measurements, including inverter output voltage (V_{abc}), inverter current (I_{abc}), grid frequency, and other relevant electrical variables. These measurements provide essential feedback for both the PI controller and the AI module, enabling accurate monitoring of system dynamics and facilitating adaptive decision-making. The control signals generated by the PI controller regulate the inverter operation, ensuring controlled power exchange between the energy source, such as a renewable energy system or storage unit, and the electrical grid. To ensure optimal performance, a performance evaluation module continuously assesses system behavior using key performance indicators, including power tracking accuracy, total harmonic distortion, power factor, and dynamic response characteristics. The results of this evaluation are fed back into the AI module, forming a closed-loop learning mechanism that allows continuous refinement of controller parameters. This iterative adaptation enhances system stability, improves disturbance rejection, and maintains high power quality under a wide range of operating conditions.

6.6.2. AI assisted sliding mode control

Sliding Mode Control is inherently robust against matched uncertainties and external disturbances due to its discontinuous control law and sliding surface design. However, practical implementation of classical sliding mode control is often limited by chattering effects and sensitivity to parameter uncertainties. Artificial intelligence assisted sliding mode control enhances the conventional structure by introducing adaptive approximation and intelligent parameter tuning. In AI assisted sliding mode schemes, neural networks or fuzzy logic systems are commonly used to approximate the equivalent control component. The sliding mode mechanism then compensates for residual approximation errors, ensuring robustness and stability. This configuration reduces chattering amplitude while maintaining strong disturbance rejection capability. In DC nano-grid and distributed generation applications, AI enhanced sliding mode control has demonstrated improved tracking precision and reduced control effort compared with traditional two loop sliding mode architectures. Reinforcement learning based tuning of sliding mode parameters represents another advanced enhancement strategy. In such approaches, deep neural networks learn optimal switching gains or boundary layer parameters through interaction with the converter system. This adaptive adjustment enables the controller to maintain performance under varying operating conditions without requiring precise system models. Although these techniques increase computational requirements, they provide superior adaptability and improved performance in systems subject to nonlinear dynamics and uncertain grid conditions. Fig. 30 presents the proposed AI-

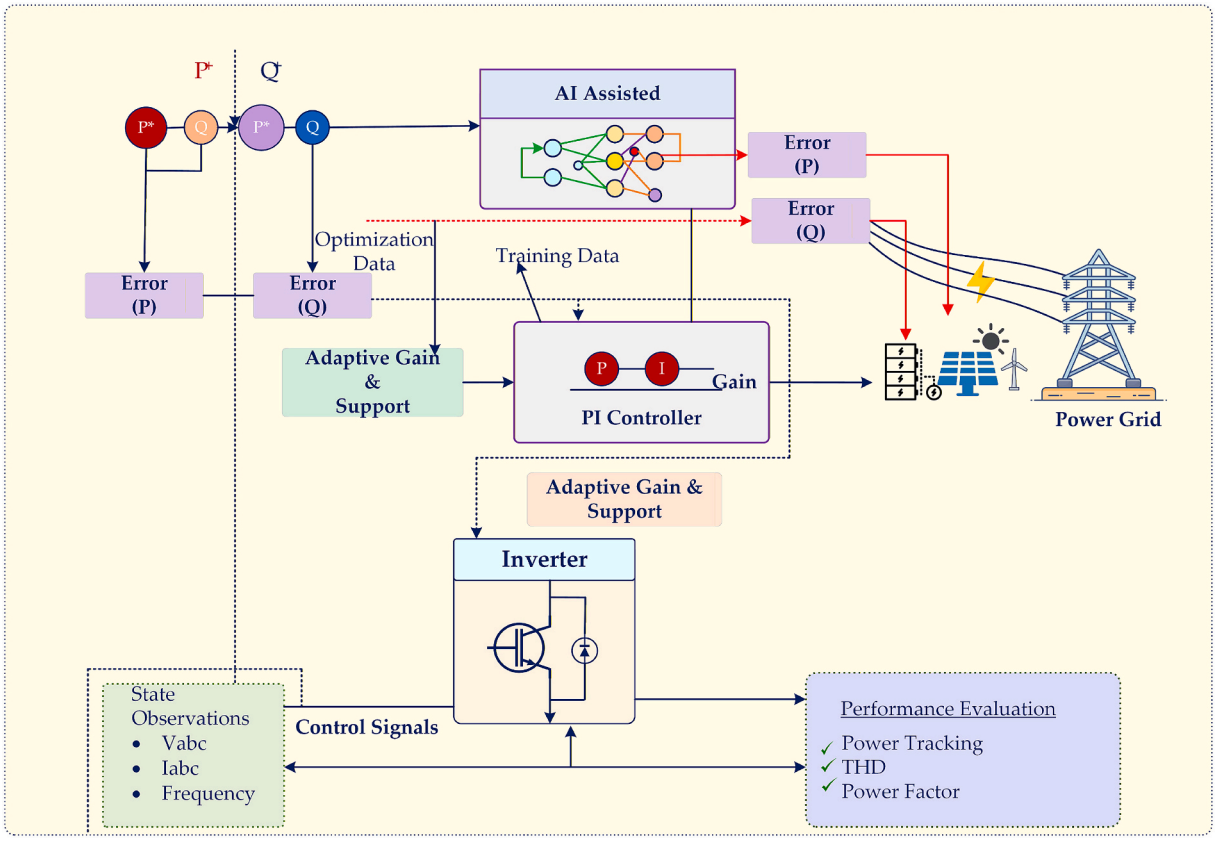

Fig. 29. Architecture of the proposed AI-assisted proportional–integral (PI) control strategy for inverter-based power systems [369].

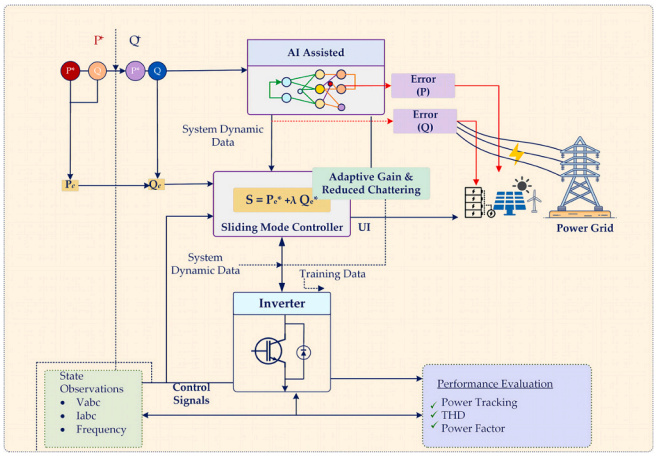

Fig. 30. Architecture of the proposed AI-assisted sliding mode control (SMC) scheme for inverter-based power systems [370].

assisted sliding mode control (SMC) framework for inverter-based power systems. The control architecture integrates artificial intelligence with conventional sliding mode control to enhance robustness, reduce chattering, and improve dynamic performance under varying grid conditions. The control process begins with the reference active and reactive power signals (P^*Q^*), which specify the desired power injection into the grid. These reference values are compared with the measured outputs to generate power error signals, which are used to construct the sliding surface of the controller. The sliding surface is defined as $S = P_e + kQ_e$, where $P_e$and $Q_e$represent the active and reactive power errors, respectively. An AI-assisted module is incorporated to provide adaptive parameter tuning based on system dynamics and training data. This module analyzes operating conditions and adjusts controller parameters to improve control accuracy and mitigate the chattering effect typically associated with traditional sliding mode control. A state observation module collects real-time system measurements, including inverter output voltage (V_{abc}), inverter current (I_{abc}), and grid frequency. These measurements are used to monitor system behavior and provide feedback to the control system. The resulting control signals are applied to the inverter, enabling controlled power transfer to the grid. System performance is continuously evaluated through a performance evaluation module, which assesses metrics such as power tracking accuracy, total harmonic distortion (THD), and power factor. This evaluation enables continuous refinement of the AI-assisted controller, ensuring improved stability, power quality, and disturbance rejection capability. The integration of artificial intelligence with sliding mode control provides an adaptive and robust control solution, making it well suited for advanced inverter applications in modern power systems [370–372]. Fig. 30 illustrates the architecture of the proposed AI-assisted sliding mode control (SMC) scheme for inverter-based power systems. The reference active and reactive powers (P^*, Q^*) are compared with measured values to generate error signals, which are processed by an AI-assisted module. This module utilizes dynamic data to enhance control accuracy and adaptability. The sliding mode controller employs a composite sliding surface ($S = P_e + \lambda Q_e$) and incorporates adaptive gain mechanisms to mitigate chattering effects. The resulting control signals are applied to the inverter, which interfaces with the power grid. System states, including voltage, current, and frequency, are continuously monitored, while performance metrics such as power tracking, total harmonic distortion (THD), and power factor are evaluated. This integrated approach improves robustness, dynamic response, and stability under varying operating conditions

6.6.3. AI assisted model predictive control

Model Predictive Control is particularly attractive in power converter applications due to its ability to handle multivariable systems and incorporate system constraints directly within the optimization problem. However, the effectiveness of MPC strongly depends on accurate system modeling and appropriate weighting factor selection. Artificial intelligence assisted by MPC enhances predictive control by addressing these two critical aspects. First, AI techniques can be employed to construct accurate system models for predictive control. Neural networks are capable of learning nonlinear converter dynamics from operational data, thereby reducing modeling errors associated with parameter uncertainties. Incorporating such learned models into the predictive framework improves reference tracking performance and dynamic response under step variations. In multilevel converters, neural network-based sensor less predictive control strategies have also been proposed to reduce sensor count while preserving regulation accuracy. Second, AI methods can optimize internal MPC parameters, particularly the weighting factors within the cost function. The selection of weighting coefficients significantly influences the tradeoff between tracking accuracy, switching frequency, and DC link stability. Reinforcement learning algorithms provide an adaptive mechanism for adjusting these weighting factors in real time according to predefined performance objectives. Neural network inference models have also been developed to predict optimal weighting parameters without requiring manual tuning. In advanced applications such as resonant converters and multi-input multi output systems, deep learning enhanced predictive strategies enable improved efficiency and power density while satisfying complex operational constraints [373–375].

Fig. 31 illustrates the AI-assisted model predictive control (MPC) framework developed for inverter-based power systems. The control architecture integrates artificial intelligence with model predictive control to enhance prediction accuracy, adaptive capability, and overall control performance under varying operating conditions. The control process begins with the reference active and reactive power signals (P^*Q^*), which represent the desired power injection into the grid. These reference signals are compared with the measured system outputs to generate power error signals $(e_P e_Q)$. The error signals are provided as inputs to the AI-assisted MPC controller, which performs predictive optimization of the control actions. Within the controller, a prediction model estimates the future behavior of the system over a defined prediction horizon. The AI module supports adaptive tuning by learning system dynamics and improving the accuracy of the predictive model. Based on the predicted system response, the controller evaluates a cost function subject to system constraints and determines the optimal control signals (U_i)that minimize the tracking error while maintaining system stability. A state observation module collects real-time measurements from the inverter and grid, including inverter output voltage (V_{abc}), inverter current (I_{abc}), and grid frequency. These measures provide updated system information for the predictive model and ensure accurate control decisions. The resulting control signals are applied to the inverter, enabling regulated power transfer to the power grid. System performance is continuously assessed through a performance evaluation module, which evaluates key indicators such as power tracking accuracy, total harmonic distortion (THD), and power factor. The evaluation results are used as feedback to refine the AI-assisted predictive control strategy. By combining artificial intelligence with model predictive control, the proposed approach provides improved prediction capability, adaptive optimization, and enhanced dynamic performance, making it well suited for advanced inverter control applications in modern power systems.

Artificial intelligence assisted control represents a balanced approach between purely classical and fully AI based control strategies. By embedding intelligent adaptation within well-established control frameworks, these methods preserve theoretical stability properties while enhancing performance under nonlinear and uncertain conditions. Compared with conventional controllers, AI assisted techniques demonstrate improved harmonic mitigation capability, enhanced dynamic response, and stronger robustness to parameter variation. However, implementation challenges must be carefully considered. Increased computational complexity may limit real time feasibility in high switching frequency converters unless dedicated digital signal processors or field programmable gate arrays are employed. Additionally, ensuring stable learning behavior and avoiding overfitting or unstable adaptation remains a critical research topic. Despite these challenges, AI assisted control provides a promising pathway for next generation power electronic systems, particularly in applications requiring high power density, fast dynamic response, and superior power quality. As switching devices such as wide bandgap semiconductors enable higher frequency operation, intelligent augmentation of classical control strategies is expected to play a central role in

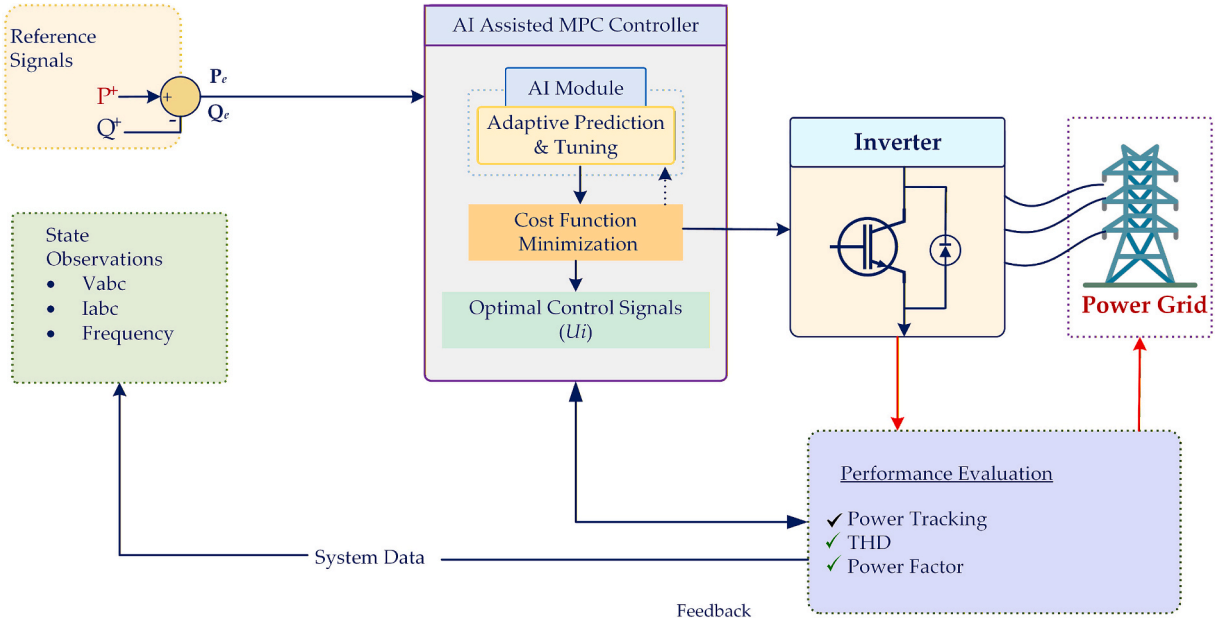

Fig. 31. Architecture of the proposed AI-assisted model predictive control (MPC) strategy for grid-connected inverter systems.

achieving optimal system performance.

Table 4 presents a comparative analysis of conventional control, AI-assisted control, and fully AI-based control strategies across key technical criteria relevant to power electronic systems. Conventional control methods are predominantly deterministic and model-based, relying on analytical formulations derived from system dynamics. These approaches provide strong theoretical stability guarantees, low computational requirements, and high interpretability, which make them suitable for real-time implementation in digital controllers. However, their performance can be constrained in the presence of nonlinear dynamics, parameter variations, and uncertain operating conditions. AI-assisted control integrates data-driven adaptation within traditional control architectures. In this hybrid framework, artificial intelligence techniques are typically employed to adjust controller parameters, enhance disturbance rejection, or improve transient performance while maintaining an underlying analytical structure. Such approaches offer improved robustness to system uncertainties and nonlinearities while retaining partial interpretability and established stability analysis methods. Fully AI-based control strategies derive control policies directly from data through machine learning techniques such as neural networks or reinforcement learning. These methods are capable of capturing complex nonlinear relationships and supporting multi-objective optimization and constraint handling. Nevertheless, they introduce higher computational and memory demands and present challenges in formal stability verification. Consequently, practical deployment in high-frequency power electronic systems often requires hardware acceleration and extensive validation to ensure reliable real-time operation.

6.7. Comparative evaluation of conventional and AI-based control strategies

A systematic comparison of conventional and artificial-intelligence-based control approaches is presented in Table 5. The evaluation encompasses prediction capability, dynamic response, computational requirements, dependence on training data, robustness against parameter variations and operating uncertainties, interpretability, real-time implementation feasibility, and constraint-handling capability. In addition, the comparative framework examines the applicability of each method to converter-level regulation, state estimation, energy-management functions, degradation-aware operation, and coordinated control of power-conversion systems.

Conventional model predictive control is particularly appropriate for high-bandwidth converter regulation because it provides rapid transient response, coordinated control of multiple variables, and explicit enforcement of operational constraints within the control formulation. Its effectiveness, however, remains dependent on model fidelity, parameter accuracy, prediction-horizon selection, and the computational capability of the embedded control platform. AI-assisted MPC extends this framework through data-driven prediction, online parameter estimation, and model-error compensation, thereby improving adaptability under nonlinear, uncertain, and time-varying operating conditions. These benefits are accompanied by increased dependence on representative training data, greater implementation complexity, and the need for rigorous assessment of stability, generalization, and real-time reliability. Reinforcement learning is more suitable for supervisory control, power allocation, and long-term energy-management functions, where adaptive sequential decision-making is required. Its use in safety-critical inner control loops remains constrained by limited interpretability, training instability, and uncertain behavior outside the trained operating region. Artificial neural networks are effective for nonlinear state estimation, fault diagnosis, parameter identification, and predictive modeling, although their performance is strongly influenced by the quality, diversity, and representativeness of the available data. Fuzzy-logic and adaptive control methods provide comparatively transparent and computationally efficient solutions for systems affected

Table 4
Comparison of conventional, AI-assisted, and AI-based control methods [376–379].

Technical Criterion	Conventional Control	AI-Assisted Control	AI-Based Control
Control Law Formulation	Deterministic, model-based analytical design	Analytical controller with adaptive or data-driven parameter tuning	Fully data-driven or learned control policy obtained from training
Mathematical Model Dependency	Strong; requires accurate plant model	Moderate; base model compensated by adaptive learning	Minimal or none; model-free learning possible
Nonlinear Dynamics Handling	Limited; requires linearization or gain scheduling	Improved through nonlinear approximation or adaptive tuning	Intrinsic nonlinear mapping capability
Parameter Uncertainty Tolerance	Low–moderate (typically tolerates ≈10–20% variation)	High (≈20–35% variation with adaptive tuning)	High (≈30–50% variation depending on training)
Disturbance Rejection Bandwidth	Limited by controller bandwidth (typically <200 Hz)	Improved through adaptive parameter adjustment (≈100–400 Hz)	Potentially high depending on training and policy design
Harmonic Suppression (THD)	2–5% depending on controller type	1.5–3.5% with adaptive compensation	≈1–3% depending on training quality
Constraint Handling (Current / Voltage Limits)	Explicit only in predictive control methods	Improved through adaptive constraint weighting	Can be embedded directly into cost or reward functions
Multi-Objective Optimization	Limited; manual tuning required	Moderate; achievable through adaptive parameter tuning	Strong; optimized through objective or reward functions
Dynamic Response (Settling Time)	1–2 grid cycles (≈20–40 ms at 50 Hz)	Improved transient response (≈10–30 ms typical)	Potentially fast (≈10–25 ms typical) but training dependent
Overshoot	5–10%	3–7%	1–5% depending on policy optimization
Steady-State Error	Near zero with integral action	Reduced further through adaptive compensation (≈0–1%)	Very low (<1%) if training converges properly
Disturbance Recovery Time	30–60 ms	15–40 ms	10–30 ms depending on training
Converter Efficiency Impact	Baseline performance	Often improves efficiency by ≈1–3%	Potential improvement of ≈2–5% depending on optimization
Stability Guarantee	Strong analytical tools available (Lyapunov, frequency domain)	More complex due to adaptive elements	Difficult to formally guarantee; often validated experimentally
Robustness under Weak Grid Conditions	Moderate	High due to adaptive compensation	High if trained under diverse grid scenarios
Sensitivity to Model Parameter Drift	High	Reduced via real-time adaptation	Low if learning remains stable
Switching Frequency Impact	Minimal computational delay	Moderate processing requirement	Higher computational burden at high sampling frequencies

(continued on next page)

Table 4 (*continued*)

Technical Criterion	Conventional Control	AI-Assisted Control	AI-Based Control
Computational Complexity	Low, typically O (n) operations	Moderate, O (n + m) including adaptation updates	High, O(k·n) depending on network depth
Control Update Time	≈1–5 μs	≈5–30 μs	≈30–150 μs depending on model complexity
Memory Requirement	Low (<50 kB typical)	Moderate (≈50–200 kB)	High (≈0.5–5 MB depending on network size)
Convergence Requirement	Not applicable	Required for adaptive tuning	Required for training or learning stability
Real-Time Implementation (DSP/FPGA)	Highly feasible even at MHz switching frequencies	Feasible with optimized implementation	Challenging at very high frequencies unless hardware accelerated
Interpretability	High; parameters physically meaningful	Moderate; hybrid interpretability	Low; black-box behavior
Design and Tuning Effort	Moderate manual tuning	Higher due to hybrid design and training	High due to training, architecture selection, and validation
Scalability to MIMO Systems	Moderate	High	Very high
Suitability for Wide-Bandgap High-Frequency Converters	High due to low computational latency	Moderate depending on hardware capability	Limited unless computational latency is minimized

by uncertainty, parameter drift, and gradual variations in operating conditions. Hybrid control architectures offer the most comprehensive functionality by combining model-based constraint handling with adaptive and data-driven capabilities. Nevertheless, their practical implementation requires careful controller coordination, substantial computational resources, robust real-time execution, and extensive experimental validation.

6.8. Coupled hardware-software design and experimental validation

The growing interdependence among converter topology, semiconductor characteristics, control algorithms, thermal behavior, and embedded implementation necessitates an integrated hardware-software design methodology. In contrast to conventional sequential development, in which the power stage and controller are designed largely as independent subsystems, a coupled workflow enables electrical, thermal, computational, and reliability constraints to be considered concurrently. This approach reduces the likelihood that a control strategy exhibiting satisfactory numerical performance becomes impractical because of switching constraints, sensing and communication delays, limited numerical precision, processor capability, or excessive thermal loading. Model-based design provides the foundation for this integrated methodology by representing the converter, grid interface, control architecture, thermal network, and operating constraints within a unified simulation environment. MATLAB/Simulink can support system-level modeling, control development, parameter optimization, software-in-the-loop verification, and automatic code generation. PLECS complements this process through detailed switched-converter simulation, semiconductor-loss calculation, and electro-thermal analysis. Finite-element analysis may further be employed to investigate magnetic-component behavior, electromagnetic-field distribution, current density, insulation stress, and heat-transfer mechanisms. The combined use of these tools supports a systematic progression from system-level control formulation to device- and component-level verification. Rapid-control prototyping provides an intermediate stage between offline simulation and final embedded deployment. Control algorithms developed within the simulation environment can be executed on real-time processing platforms to evaluate sampling delay, signal quantization, computational latency, switching synchronization, and communication timing. Digital signal processors are generally appropriate for control schemes with moderate computational requirements, whereas field-programmable gate arrays offer deterministic parallel execution for high-frequency switching, multichannel data acquisition, and computationally intensive predictive-control implementations. Hardware-in-the-loop testing further strengthens the validation process by interfacing the physical controller with a real-time digital representation of the converter and its associated electrical network. This configuration enables operating-point variations, grid disturbances, sensor faults, abnormal switching states, and protection events to be reproduced without exposing a full-scale prototype to excessive electrical or thermal risk. Hardware-in-the-loop evaluation is therefore particularly valuable for assessing controller stability, execution timing, fault response, protection coordination, and real-time feasibility before laboratory implementation. Digital-twin-assisted optimization extends model-based development by continuously updating the virtual representation using measured operational data. A digital twin can estimate unmeasured electrical and thermal states, detect parameter drift, predict component degradation, and evaluate alternative control actions under changing operating conditions. It can therefore support online controller adaptation, thermal management, predictive maintenance, and lifecycle-oriented operation. Its effectiveness, however, depends on model fidelity, data quality, synchronization accuracy, system observability, and available computational resources. Data-driven surrogate modeling can further reduce the computational burden associated with repeated high-fidelity simulation. Neural networks, Gaussian-process models, polynomial response surfaces, and reduced-order models can approximate the relationships between design variables and performance indicators, including converter losses, thermal stress, harmonic distortion, reliability, and cost. These surrogate models may then be integrated with multi-objective optimization algorithms to accelerate the exploration of large design spaces. Their application should nevertheless be supported by representative training data, uncertainty quantification, and validation against detailed simulation or experimental measurements. A representative coupled design workflow therefore comprises system specification and constraint definition, converter and semiconductor selection, electrical and thermal modeling, controller development, multi-objective optimization, software-in-the-loop verification, rapid-control prototyping, hardware-in-the-loop testing, laboratory validation, and digital-twin-assisted operational monitoring. The coordinated use of MATLAB/Simulink, PLECS, finite-element tools, real-time digital simulation, FPGA- or DSP-based control, and experimental testing provides a systematic pathway from conceptual design to experimentally validated implementation.

6.9. Discussion

A systematic evaluation of multilevel converter topologies and their associated control strategies demonstrates that converter hardware and control architecture should be designed in a coordinated manner. Their interaction directly influences conversion efficiency, waveform quality, dynamic response, thermal-stress distribution, reliability, and real-time implementation feasibility. Conventional control methods, including proportional-integral, proportional-resonant, deadbeat, and hysteresis control, remain widely adopted because of their established theoretical foundations, modest computational requirements, and relatively straightforward implementation. Although these methods generally provide satisfactory performance under nominal operating conditions, their effectiveness may deteriorate in the presence of nonlinear dynamics, parameter variations, grid disturbances, and rapidly changing renewable-generation profiles. Advanced nonlinear and predictive

Table 5
Comparative performance and implementation characteristics of advanced control and artificial-intelligence-based methods.

Control approach	Prediction capability	Dynamic response	Computational burden	Training-data requirement	Robustness	Interpretability	Real-time feasibility	Constraint handling	Principal applications	Principal advantages	Principal limitations
Conventional MPC	High, based on an explicit system model	Very fast, typically within microsecond-to-millisecond timescales	Moderate to high	Not required	Moderate and dependent on model accuracy	High	High with optimized algorithms and suitable hardware	Explicit	Current, voltage, and power control	Fast response and explicit constraint handling	Model sensitivity and computational demand
AI-assisted MPC	Very high through data-driven prediction, model correction, or online parameter estimation	Very fast	High	Moderate to high	High	Moderate	Moderate to high	Explicit or hybrid	Nonlinear and degradation-aware control	Improved prediction and adaptability	Data dependence and validation complexity
Reinforcement learning	High through interaction-based policy optimization	Fast after training, generally within millisecond timescales	High during training and moderate during execution	High	Moderate to high within the trained operating region	Low	Moderate to high	Limited unless safe or constrained RL is employed	Supervisory control and energy management	Adaptive model-free optimization	Training instability and safety concerns
Artificial neural networks	High for nonlinear approximation, estimation, and prediction	Fast during online inference	High during training and low to moderate during execution	High	Moderate	Low	High with compact network architectures	Indirect	Estimation, diagnosis, and predictive support	Strong nonlinear approximation	Limited interpretability and extrapolation risk
Fuzzy-logic control	Moderate and primarily rule-based	Fast	Low to moderate	Low, although expert knowledge is required	High under bounded uncertainty	High	High	Indirect	Nonlinear and supervisory regulation	Simple and robust implementation	Rule-base tuning and scalability limitations
Adaptive control	Moderate to high through online parameter adjustment	Fast	Moderate	Generally not required	High against gradual parameter variation	High	High	Limited to moderate	Parameter and operating-point compensation	Online adaptation to system variation	Limited response to abrupt nonlinear changes
Hybrid control approaches	Very high through integration of model-based, adaptive, and data-driven methods	Fast to very fast	High to very high	Moderate to high	High	Moderate	Moderate	Explicit, learned, or combined	Coordinated and fault-tolerant control	Combined prediction, robustness, and adaptability	High design and implementation complexity

Note: The reported response characteristics are representative and may vary with converter topology, sampling interval, processor architecture, model complexity, and control implementation. Qualitative ratings indicate relative performance among the compared methods.

control methods provide greater flexibility for addressing these operating challenges. Model predictive control is particularly relevant to multilevel converters because it evaluates candidate switching states using a predefined cost function and selects the control action that best satisfies the specified objectives. Depending on the adopted formulation, MPC can simultaneously address current tracking, voltage regulation, capacitor-voltage balancing, switching-frequency limitation, semiconductor-loss reduction, and thermal-stress redistribution. Predictive sliding-mode control can offer improved robustness against disturbances and parameter uncertainties, although its practical effectiveness depends on accurate system representation, appropriate switching implementation, and mitigation of chattering-related effects. AI-assisted predictive control may further improve disturbance forecasting, online parameter estimation, and adaptation to changing operating conditions. However, these advantages are accompanied by increased computational demand, dependence on representative data, limited interpretability, and the need for rigorous assessment of stability and generalization. From a topological perspective, NPC, ANPC, flying-capacitor, T-type, CHB, and MMC configurations offer several advantages over conventional two-level converters, including reduced semiconductor voltage stress, improved output-waveform quality, lower harmonic distortion, and enhanced scalability. Nevertheless, their relative suitability depends on the voltage level, power rating, source configuration, balancing requirements, fault-tolerance objectives, and acceptable implementation complexity. NPC converters are technologically mature and well suited to medium-voltage applications. However, they require effective neutral-point-voltage regulation, and non-uniform semiconductor loss distribution may introduce thermal imbalance and reduce long-term reliability. CHB converters provide modularity, scalability, and cell-level redundancy, although they commonly require multiple isolated DC sources or independently regulated modules. MMCs are particularly attractive for high-voltage and high-power systems because of their modular structure and high-quality output-voltage synthesis, but impose substantial requirements for circulating-current suppression, submodule-capacitor balancing, distributed sensing, and computational coordination.

The ANPC topology provides additional control flexibility through actively controlled clamping paths and redundant switching states. These characteristics can be exploited to regulate neutral-point voltage, redistribute semiconductor losses, and mitigate thermal imbalance without changing the required output-voltage level. ANPC converters are therefore attractive for applications in which internal voltage regulation, device utilization, and thermal management are important design criteria. However, these benefits depend strongly on the selected modulation and control strategy. The increased number of switching states also enlarges the control search space and introduces additional sensing, gate-signal coordination, and protection requirements. Accordingly, ANPC converters should not be regarded as universally superior to other multilevel topologies, but rather as a suitable option when their switching-state redundancy can be effectively utilized. The coordinated implementation of ANPC converters and MPC is particularly promising because the predictive controller can exploit redundant switching states to satisfy multiple objectives within a unified framework. In addition to current and voltage regulation, the cost function can incorporate neutral-point-voltage deviation, switching losses, harmonic distortion, junction-temperature variation, and switching-transition penalties. AI-assisted MPC may further improve model adaptation, state estimation, and prediction under uncertain and time-varying operating conditions. Nevertheless, the achievable benefits depend strongly on the prediction horizon, cost-function formulation, sampling frequency, processor capability, training-data quality, and stability-assurance mechanism. Comparative claims should therefore be based on equivalent converter ratings, operating profiles, switching frequencies, thermal conditions, and validation procedures. Real-time implementation remains one of the principal limitations of advanced predictive and AI-assisted control strategies. Increasing the number of voltage levels and candidate switching states substantially expands the computational search space, particularly when electrical, thermal, reliability, and degradation-related objectives are considered simultaneously. The high switching frequencies enabled by SiC and GaN devices further reduce the time available for signal acquisition, prediction, optimization, and gate-signal generation. Although DSP platforms are adequate for many control applications, more computationally intensive formulations may require FPGA-based parallel processing, reduced-order prediction models, restricted switching-state evaluation, or optimized embedded-code implementation. Wide-bandgap devices also introduce additional challenges associated with electromagnetic interference, parasitic effects, gate-drive design, insulation stress, and high-frequency measurement accuracy. These factors should be addressed jointly through converter-control and hardware-software co-design. The reviewed evidence indicates that no single converter topology or control method is universally optimal for renewable-energy applications. Converter and controller selection should therefore be based on a coordinated evaluation of conversion efficiency, harmonic performance, voltage and current stress, thermal loading, reliability, scalability, computational burden, hardware cost, and lifecycle requirements. ANPC converters coordinated with MPC, including appropriately constrained AI-assisted variants, represent a promising solution for applications that prioritize neutral-point regulation, rapid dynamic response, thermal-stress redistribution, and adaptive operation. Their practical viability, however, depends on computationally efficient implementation, rigorous and interpretable stability guarantees, reproducible validation, and demonstrable advantages over less complex alternatives. An integrated hardware-software design methodology is therefore essential for translating advanced converter-control concepts into reliable, scalable, and economically viable power-conversion systems for renewable-energy-integrated storage applications.

7. Future research directions

The increasing deployment of renewable energy sources and battery energy storage systems (BESSs) is imposing more stringent operational requirements on power electronic converters. Converter control systems must ensure efficient bidirectional energy conversion, accurate power regulation, and stable grid interaction under variations in renewable generation, load demand, battery state of charge, temperature, component aging, and grid conditions. Artificial intelligence (AI) offers considerable potential for addressing these requirements through adaptive, predictive, and data-driven control methodologies. A significant research direction involves the development of hybrid control architectures that integrate AI methods with established model-based control techniques. These architectures could retain the stability, transparency, and predictable behavior of conventional controllers while improving adaptability to nonlinear dynamics, parameter uncertainty, and rapidly changing operating conditions. The practical implementation of AI-based converter control remains constrained by computational complexity, memory requirements, execution latency, and energy consumption. These limitations are particularly significant in BESS applications, in which control algorithms are commonly implemented using resource-constrained embedded hardware and must operate at high switching frequencies. Research should therefore concentrate on lightweight neural network architectures, model compression, pruning, quantization, knowledge distillation, and hardware-aware optimization. The suitability of these techniques for implementation on digital signal processors, microcontrollers, and field-programmable gate arrays should be evaluated using practical criteria, including inference time, memory utilization, computational burden, energy consumption, control accuracy, and switching-frequency compatibility. Experimental implementation and hardware-in-the-loop validation are required to establish whether the performance observed in numerical simulations can be maintained under realistic operating and hardware constraints.

The robustness and generalization capability of AI-based converter controllers require further investigation. Models trained using data obtained from a restricted range of operating conditions may exhibit inadequate performance when subjected to battery degradation, parameter variations, sensor inaccuracies, grid disturbances, extreme temperatures, or previously unobserved faults. Future studies should therefore employ comprehensive datasets representing different battery chemistries, converter topologies, aging conditions, environmental conditions, and grid events. Physics-informed learning, transfer learning, online adaptation, and uncertainty-aware modeling may reduce dependence on extensive application-specific datasets while improving performance under unfamiliar operating conditions. The establishment of open benchmark datasets, standardized converter models, and consistent performance indicators is also necessary to support reproducibility and objective comparison among alternative control strategies. Safety, stability, and operational constraint enforcement must be incorporated throughout the development of AI-based controllers. In energy storage applications, inaccurate control actions may violate current, voltage, temperature, state-of-charge, or state-of-health limits, potentially accelerating battery degradation or compromising grid stability. Further research is required to establish formal procedures for stability assessment, constraint satisfaction, uncertainty quantification, and verification of AI-generated control actions. Explainable AI techniques may improve the transparency of controller decisions and facilitate fault diagnosis, regulatory evaluation, and operator acceptance. Hybrid supervisory architectures incorporating conventional fallback controllers may provide additional protection when an AI model encounters abnormal measurements, communication failures, cyberattacks, or operating conditions outside its training domain. The systematic integration of power converter control and battery management constitutes another important area for future investigation. Converter dynamics, battery electrochemical characteristics, thermal behavior, degradation mechanisms, and energy-management decisions are inherently interdependent; however, these aspects are frequently investigated as separate research domains. Integrated AI-based frameworks could enable the simultaneous optimization of power conversion efficiency, charging performance, thermal management, power quality, and battery lifetime. Multi-timescale control architectures may be particularly suitable for this purpose, with high-speed control layers regulating converter dynamics and supervisory control layers optimizing energy flow, battery degradation, and operating costs. Digital-twin frameworks could further facilitate this integration by supporting continuous condition monitoring, virtual validation, controller adaptation, and predictive analysis without subjecting physical equipment to unsafe operating conditions.

AI-assisted predictive maintenance represents an additional opportunity to improve the technical reliability and economic performance of converter-interfaced energy storage systems. Future investigations should consider the combined analysis of electrical, thermal, environmental, and operational data to identify early indications of degradation in battery cells, semiconductor devices, capacitors, and magnetic components. Predictive models should provide uncertainty estimates and remaining useful life assessments in addition to fault detection and classification. Long-term experimental investigations and validation using field data will be essential for determining whether these approaches can consistently reduce unplanned downtime, maintenance expenditure, and component replacement costs. The increasing deployment of distributed BESSs also necessitates scalable coordination among multiple converter-interfaced units. Distributed learning and multi-agent optimization may contribute to improved power sharing, voltage and frequency regulation, harmonic mitigation, congestion management, and grid-forming operation. However, the practical performance of these methods must be evaluated under communication delays, bandwidth restrictions, data loss, cyberattacks, and changes in network topology. Communication-efficient and decentralized algorithms capable of preserving local operational autonomy while satisfying system-level objectives therefore require further investigation. Cybersecurity, interoperability, and regulatory compliance must also be incorporated into the design and validation of AI-based converter controllers. Continuous sensing, remote monitoring, and communication between controllers create vulnerabilities associated with corrupted measurements, adversarial inputs, unauthorized commands, and communication failures. Secure communication protocols, anomaly-detection mechanisms, resilient control strategies, and privacy-preserving learning should consequently be regarded as fundamental design requirements. Standardized testing procedures, interoperability requirements, and certification frameworks will also be necessary to support the safe deployment of AI-based control systems in large-scale energy storage applications. Progress in these research areas is expected to contribute to the development of converter-interfaced energy storage systems characterized by improved efficiency, adaptability, security, and operational reliability.

8. Conclusion

This review provides a critical synthesis of energy and exergy optimization in energy-storage-integrated multilevel power conversion systems, with particular emphasis on converter-control co-design and advanced control implementation. The findings demonstrate that converter topology, semiconductor technology, modulation strategy, control architecture, storage characteristics, thermal management, and auxiliary consumption are strongly interdependent and should be evaluated within a unified system-level framework. Multilevel converter structures, including neutral-point-clamped, active-neutral-point-clamped, T-type, flying-capacitor, cascaded H-bridge, and modular multilevel converters, offer important advantages in voltage-stress distribution, waveform quality, harmonic performance, and scalability. Their practical effectiveness, however, depends on topology-specific requirements such as capacitor-voltage balancing, circulating-current suppression, switching-state coordination, fault management, and semiconductor thermal-stress distribution. The analysis further indicates that conventional energy-efficiency metrics alone are insufficient for assessing integrated storage-converter systems. Exergy analysis provides an additional basis for quantifying the degradation of useful energy potential associated with semiconductor conduction and switching losses, passive-component dissipation, electrochemical irreversibility, thermal gradients, auxiliary cooling demand, circulating currents, capacitor-voltage imbalance, and control-dependent switching activity. System optimization should therefore extend beyond the minimization of isolated electrical losses, since a control action that improves converter efficiency may simultaneously increase storage degradation, thermal loading, auxiliary consumption, or lifecycle cost. A comprehensive optimization framework should incorporate energy loss, exergy destruction, entropy generation, storage degradation, thermal constraints, power quality, reliability, and economic performance. The interaction between the converter and the energy-storage system is particularly significant. Converter-induced current ripple, rapid power reversals, elevated charge and discharge rates, wide state-of-charge excursions, and high operating temperatures can accelerate internal resistance growth, capacity fade, and electrochemical aging. Degradation-aware control should therefore extend beyond current tracking and DC-link regulation by incorporating storage-side ripple, state-of-charge limits, state-of-health indicators, thermal conditions, and service-life objectives. Coordinated thermal management of the converter and storage system is equally important because semiconductor losses, battery heating, enclosure conditions, and cooling demand collectively determine the net energy and exergy performance of the integrated system.

The comparative assessment of semiconductor technologies indicates that silicon carbide and gallium nitride devices can reduce switching losses, increase feasible switching frequency, enhance power density, and reduce passive-component volume relative to conventional

silicon-based solutions. These advantages remain application dependent. High-speed switching increases sensitivity to parasitic elements, electromagnetic interference, insulation stress, gate-driver design, common-mode effects, and thermal packaging. Gallium nitride is particularly attractive for high-frequency, low- and medium-voltage applications, whereas silicon carbide remains more suitable for many high-voltage and high-power systems. Semiconductor selection should therefore be based on operating voltage, switching frequency, thermal limits, control requirements, reliability targets, and system-level cost. Advanced control approaches, including model predictive control, AI-assisted predictive control, neural-network-based estimation, and reinforcement learning, provide increased flexibility for multi-objective operation. These methods can support current regulation, capacitor-voltage balancing, thermal-stress redistribution, degradation prediction, fault diagnosis, and adaptive operation under uncertain renewable-generation and grid conditions. Their practical implementation, however, remains constrained by computational demand, training-data quality, model interpretability, limited generalization, stability verification, memory requirements, and control latency. Physics-informed and constraint-aware control methods provide a more suitable basis for safety-critical converter applications because they combine adaptive capability with explicit electrical, thermal, storage, and grid-code constraints. The review also identifies the absence of consistent benchmarking as a major limitation in the available literature. Reported values of efficiency, harmonic distortion, thermal performance, transient response, degradation reduction, and computational burden are frequently obtained under different converter ratings, topologies, semiconductor devices, switching frequencies, operating profiles, and validation platforms. Direct comparison is therefore difficult, and reported numerical ranges should not be interpreted as universal design limits. Standardized datasets, representative duty cycles, clearly defined operating conditions, reproducible controller implementations, and common electrical, thermal, electrochemical, reliability, and exergy-based performance indicators are required to support rigorous assessment.

Future investigations should prioritize exergy-aware and degradation-conscious predictive control, Pareto-based hardware-software optimization, digital-twin-assisted monitoring, physics-informed artificial intelligence, and coordinated management of converter, storage, and cooling subsystems. Further research is also required in grid-forming storage converters, fault-tolerant multilevel architectures, scalable distributed control, lifecycle-oriented design, and experimentally validated electrothermal and exergy models. Hardware-in-the-loop testing, power-hardware-in-the-loop validation, accelerated aging studies, and long-duration experiments under representative grid-service conditions are necessary to establish practical applicability. The advancement of renewable-energy-integrated power conversion systems requires a transition from isolated component optimization toward coordinated converter-control-storage design. Such an approach provides a rigorous basis for improving efficiency, reducing exergy destruction, limiting electrochemical and thermal stress, enhancing reliability, and extending service life in intelligent power conversion systems intended for renewable-energy integration and advanced grid-support applications.

Key Takeaways

- Energy-storage-integrated multilevel converters should be assessed through coordinated converter-control-storage design that incorporates topology, semiconductor technology, modulation, storage characteristics, thermal management, and auxiliary consumption.
- Exergy analysis extends conventional efficiency assessment by quantifying useful-energy degradation associated with semiconductor losses, passive-component dissipation, electrochemical irreversibility, thermal gradients, and auxiliary power demand.
- Degradation-aware control should incorporate converter-induced current ripple, charge-discharge rates, state-of-charge limits, state-of-health indicators, and thermal conditions to preserve storage lifetime and improve long-term reliability.
- Silicon carbide and gallium nitride devices enable higher switching frequencies, reduced losses, increased power density, and smaller passive components, although their system-level benefits depend on electromagnetic compatibility, parasitic-aware design, gate-drive implementation, insulation coordination, and thermal packaging.
- Advanced predictive and AI-assisted control methods provide strong multi-objective capabilities, but their practical deployment requires standardized benchmarking, physics-informed constraints, real-time validation, and experimentally verified converter-control-storage co-design procedures.

Declaration of generative AI and AI-assisted technologies in the manuscript preparation process

The authors wish to acknowledge the use of ChatGPT (OpenAI) during manuscript preparation to assist with linguistic refinement and improve the clarity and readability of the text. All AI-assisted material was carefully reviewed, verified, and revised by the authors, who accept full responsibility for the accuracy, originality, and integrity of the final manuscript.

CRediT authorship contribution statement

Gowthamraj Rajendran: Writing – review & editing, Writing – original draft, Validation, Methodology, Investigation, Formal analysis, Data curation, Conceptualization. **Darius Andriukaitis:** Visualization, Validation, Supervision, Resources, Project administration, Investigation, Formal analysis, Data curation, Conceptualization. **Reiko Raute:** Writing – review & editing, Visualization, Validation, Supervision. **Vytautas Markevičius:** Writing – review & editing, Writing – original draft, Visualization, Validation, Supervision. **Dangirutis Navikas:** Writing – review & editing, Visualization, Validation, Supervision. **Mindaugas Žilys:** Writing – review & editing, Visualization, Validation, Supervision. **Algimantas Valinevičius:** Writing – review & editing, Visualization, Validation, Supervision. **Roman Šotner:** Writing – review & editing, Visualization, Validation, Supervision. **Jan Jerabek:** Writing – review & editing, Visualization, Validation, Supervision. **Ladislav Polak:** Writing – review & editing, Visualization, Validation, Supervision.

Declaration of competing interest

The authors declare that they have no known competing financial interests or personal relationships that could have appeared to influence the work reported in this article.

Acknowledgment

This project has received funding from the European Union's Horizon Europe research and innovation programme under the Marie Skłodowska-Curie grant agreement No. 101244571 (REnCon). Funded by the European Union. Views and opinions expressed are however those of the author(s) only and do not necessarily reflect those of the European Union or the European Research Executive Agency (REA). Neither the European Union nor the granting authority can be held responsible for them.

Data availability

No data was used for the research described in the article.

References

[1] J. Jasiūnas, P.D. Lund, J. Mikkola, Energy system resilience–a review, Renew. Sustain. Energy Rev. 150 (2021) 111476.
[2] A. Gholami, T. Shekari, M.H. Amirioun, F. Aminifar, M.H. Amini, A. Sargolzaei, Toward a consensus on the definition and taxonomy of power system resilience, IEEE Access 6 (2018) 32035–32053.
[3] I. P. O. C. Change, Climate change 2014: synthesis report, in: Core Writing Team, R.K. Pachauri, L.A. Meyer (Eds.)Contribution of working groups I," II and III to the Fifth Assessment Report of the Intergovernmental Panel on Climate Change 151, IPCC, Geneva, Switzerland, 2014.
[4] J. Rockström, et al., Safe and just earth system boundaries, Nature 619 (7968) (2023) 102–111.
[5] F. Food, Agriculture Organisation, The Future of Food and Agriculture: Trends and challenges, FAO, Rome, 2017.
[6] M. Kummu, M. Heino, M. Taka, O. Varis, D. Viviroli, Climate change risks pushing one-third of global food production outside the safe climatic space, One Earth 4 (5) (2021) 720–729.
[7] P.R. Shukla, et al., Climate Change and Land: An IPCC Special Report on Climate Change, Desertification, Land Degradation, Sustainable Land Management, Food Security, and Greenhouse Gas Fluxes in Terrestrial Ecosystems, 2019.
[8] P.R. Shukla, et al., Climate Change and Land: An IPCC Special Report on Climate Change, Desertification, Land Degradation, Sustainable Land Management, Food Security, and Greenhouse Gas Fluxes in Terrestrial Ecosystems, 2019.
[9] R.M. Elavarasan, et al., A comprehensive review on renewable energy development, challenges, and policies of leading Indian states with an international perspective, Ieee Access 8 (2020) 74432–74457.
[10] U. C. Change, The Paris Agreement, United Nations, 2015.
[11] W. Confirms, "as Warmest Year on Record at About 1.55° C Above Pre-industrial Level," *World Meteorological* Organization, 2025.
[12] U. Nations, The Sustainable Development Goals Report 2019, New York, 2019.
[13] M. Child, O. Koskinen, L. Linnanen, C. Breyer, Sustainability guardrails for energy scenarios of the global energy transition, Renew. Sustain. Energy Rev. 91 (2018) 321–334.
[14] C. Breyer, et al., On the history and future of 100% renewable energy systems research, IEEe Access 10 (2022) 78176–78218.
[15] K. Hansen, C. Breyer, H. Lund, Status and perspectives on 100% renewable energy systems, Energy 175 (2019) 471–480.
[16] T.W. Brown, T. Bischof-Niemz, K. Blok, C. Breyer, H. Lund, B.V. Mathiesen, Response to 'Burden of proof: a comprehensive review of the feasibility of 100% renewable-electricity systems, Renew. Sustain. Energy Rev. 92 (2018) 834–847.
[17] W. IEA and O. Special, Africa Energy Outlook 2019, International Energy Agency, 2019.
[18] B.K. Bose, Power electronics, smart grid, and renewable energy systems, Proc. IEEE 105 (11) (2017) 2011–2018.
[19] F.J. De Haan, B.C. Ferguson, R.C. Adamowicz, P. Johnstone, R.R. Brown, T. H. Wong, The needs of society: a new understanding of transitions, sustainability and liveability, Technol. Forecast. Soc. Change 85 (2014) 121–132.
[20] R. Kemp, J. Schot, R. Hoogma, Regime shifts to sustainability through processes of niche formation: the approach of strategic niche management, Tech. Anal. Strat. Manag. 10 (2) (1998) 175–198.
[21] S. Jacobsson, A. Johnson, The diffusion of renewable energy technology: an analytical framework and key issues for research, Energy Policy 28 (9) (2000) 625–640.
[22] "Renewable Capacity Highlights." IRENA – International Renewable Energy Agency, Accessed: Jan. 12, 2025. [Online]. Available: https://www.irena.org/-/media/Files/IRENA/Agency/Publication/2025/Mar/IRENA_DAT_RE_Capacity_Highlights_2025.pdf, Mar. 26, 2025.
[23] C. Caiafa, T. Hattori, H. Nam, H. de Coninck, International technology innovation to accelerate energy transitions: the case of the international energy agency technology collaboration programmes, Environ. Innov. Soc. Trans. 48 (2023) 100766.
[24] M.Z. Jacobson, et al., 100% clean and renewable wind, water, and sunlight all-sector energy roadmaps for 139 countries of the world, Joule 1 (1) (2017) 108–121.
[25] O. Edenhofer, N. Bauer, E. Kriegler, The impact of technological change on climate protection and welfare: insights from the model MIND, Ecol. Econ. 54 (2–3) (2005) 277–292.
[26] C. Breyer, et al., Solar photovoltaics demand for the global energy transition in the power sector, Prog. Photovolt. Res. Appl. 26 (8) (2018) 505–523.
[27] D. Keiner, et al., Global-local heat demand development for the energy transition time frame up to 2050, Energies 14 (13) (2021) 3814.
[28] K. Zhu, M. Victoria, T. Brown, G.B. Andresen, M. Greiner, Impact of CO2 prices on the design of a highly decarbonised coupled electricity and heating system in Europe, Appl. Energy 236 (2019) 622–634.
[29] C. Breyer, S. Khalili, D. Bogdanov, Solar photovoltaic capacity demand for a sustainable transport sector to fulfil the Paris agreement by 2050, Progress in Photovoltaics: Research and Applications 27 (11) (2019) 978–989.
[30] M. Reuß, P. Dimos, A. Léon, T. Grube, M. Robinius, D. Stolten, Hydrogen road transport analysis in the energy system: a case study for Germany through 2050, Energies 14 (11) (2021) 3166.
[31] R.M. Johannsen, B.V. Mathiesen, K. Kermeli, W. Crijns-Graus, P.A. Østergaard, Exploring pathways to 100% renewable energy in European industry, Energy 268 (2023) 126687.
[32] J. Haas, et al., Copper mining: 100% solar electricity by 2030? Appl. Energy 262 (2020) 114506.
[33] U. Caldera, D. Bogdanov, S. Afanasyeva, C. Breyer, Role of seawater desalination in the management of an integrated water and 100% renewable energy based power sector in Saudi Arabia, Water 10 (1) (2017) 3.
[34] M. Heihsel, S.M.H. Ali, J. Kirchherr, M. Lenzen, Renewable-powered desalination as an optimisation pathway for renewable energy systems: the case of Australia's Murray–Darling Basin, Environ. Res. Lett. 14 (12) (2019) 124054.
[35] M. ElSayed, A. Aghahosseini, U. Caldera, C. Breyer, Analysing the techno-economic impact of e-fuels and e-chemicals production for exports and carbon dioxide removal on the energy system of sunbelt countries–case of Egypt, Appl. Energy 343 (2023) 121216.
[36] F. Ueckerdt, R. Pietzcker, Y. Scholz, D. Stetter, A. Giannousakis, G. Luderer, Decarbonizing global power supply under region-specific consideration of challenges and options of integrating variable renewables in the REMIND model, Energy Econ. 64 (2017) 665–684.
[37] M. Elkadeem, S. Wang, S.W. Sharshir, E.G. Atia, Feasibility analysis and techno-economic design of grid-isolated hybrid renewable energy system for electrification of agriculture and irrigation area: a case study in Dongola, Sudan, Energy Convers. Manag. 196 (2019) 1453–1478.
[38] M.Z. Jacobson, et al., Impacts of green new deal energy plans on grid stability, costs, jobs, health, and climate in 143 countries, One Earth 1 (4) (2019) 449–463.
[39] D. Bogdanov, A. Gulagi, M. Fasihi, C. Breyer, Full energy sector transition towards 100% renewable energy supply: integrating power, heat, transport and industry sectors including desalination, Appl. Energy 283 (2021) 116273.
[40] T. Brown, D. Schlachtberger, A. Kies, S. Schramm, M. Greiner, Synergies of sector coupling and transmission reinforcement in a cost-optimised, highly renewable European energy system, Energy 160 (2018) 720–739.
[41] J. Gea-Bermúdez, et al., The role of sector coupling in the green transition: a least-cost energy system development in northern-Central Europe towards 2050, Appl. Energy 289 (2021) 116685.
[42] B.V. Mathiesen, et al., Smart energy systems for coherent 100% renewable energy and transport solutions, Appl. Energy 145 (2015) 139–154.
[43] Sector coupling in facilitating integration of variable renewable energy in cities, IRENA – International Renewable Energy Agency, World Bank, Mar. 12, 2021. Accessed: Mar. 12, 2025. [Online]. Available: https://www.irena.org/Publications/2021/Oct/Sector-Coupling-in-Cities.
[44] T. Galimova, et al., Global trading of renewable electricity-based fuels and chemicals to enhance the energy transition across all sectors towards sustainability, Renew. Sustain. Energy Rev. 183 (2023) 113420.
[45] F. Ueckerdt, C. Bauer, A. Dirnaichner, J. Everall, R. Sacchi, G. Luderer, Potential and risks of hydrogen-based e-fuels in climate change mitigation, Nat. Clim. Chang. 11 (5) (2021) 384–393.
[46] G.T. Chala, S.M. Al Alshaikh, Solar photovoltaic energy as a promising enhanced share of clean energy sources in the future—a comprehensive review, Energies 16 (24) (2023) 7919.
[47] N.S.M.N. Izam, Z. Itam, W.L. Sing, A. Syamsir, Sustainable development perspectives of solar energy technologies with focus on solar photovoltaic—a review, Energies 15 (8) (2022) 2790.
[48] M.N. AlMallahi, Y. Al Swailmeen, M.A. Abdelkareem, A.G. Olabi, M. Elgendi, A path to sustainable development goals: a case study on the thirteen largest photovoltaic power plants, Energ. Conver. Manage.: X 22 (2024) 100553.
[49] IRENA, Renewable Capacity Highlights 2025 [Online]. Available: https://www.irena.org/-/media/Files/IRENA/Agency/Publication/2025/Mar/IRENA_DAT_RE_Capacity_Highlights_2025.pdf, 2025.
[50] L. Fernández, Cumulative solar PV capacity installed worldwide from 2000 to 2024 [Online]. Available: https://www.statista.com/statistics/280220/global-cumulative-installed-solar-pv-capacity/, 2025.
[51] M. Kharrich, O.H. Mohammed, N. Alshammari, M. Akherraz, Multi-objective optimization and the effect of the economic factors on the design of the microgrid hybrid system, Sustain. Cities Soc. 65 (2021) 102646, https://doi.org/10.1016/j.scs.2020.102646.
[52] M.B. Kahsay, J. Lauwaert, Excess energy from PV-battery system installations: a case of rural health center in Tigray, Ethiopia, Energies 15 (12) (2022) 4355, https://doi.org/10.3390/en15124355.
[53] M.A. Vaziri Rad, A. Kasaeian, X. Niu, K. Zhang, O. Mahian, Excess electricity problem in off-grid hybrid renewable energy systems: a comprehensive review from challenges to prevalent solutions, Renew. Energy 212 (2023) 538–560, https://doi.org/10.1016/j.renene.2023.05.073.
[54] P. Bastida-Molina, Y. Rivera, C. Berna-Escriche, D. Blanco, L. Álvarez-Piñeiro, Challenges and opportunities in electric vehicle charging: harnessing solar photovoltaic surpluses for demand-side management, Machines 12 (2) (2024) 144, https://doi.org/10.3390/machines12020144.
[55] J. Hoon, R.H.G. Tan, Grid-connected solar PV plant surplus energy utilization using battery energy storage system, in: 2020 IEEE student conference on Research and Development (SCOReD), Sep. 2020, https://doi.org/10.1109/SCOReD50371.2020.9250977, pp. 1–5.
[56] B. Baah, et al., Analysis and hypothesis testing of redundant energy of solar home systems without net-metering, Renew. Energy 220 (2024) 119736, https://doi.org/10.1016/j.renene.2023.119736.
[57] L. Šriupša, M. Vaitkūnas, A. Baronas, J. Dosinas, Analysis of self-generated PV energy consumption profiles in prosumers microgrid, International Journal of Sustainable Energy 42 (1) (2023) 1583–1602, https://doi.org/10.1080/14786451.2023.2290302.
[58] G. Zhu, G. Yan, D. Garmroudi, Optimizing solar-wind hybrid energy systems for sustainable charging stations and commercial applications: a two-stage framework with ebola-inspired optimization, Expert Syst. Appl. 246 (2024) 123180, https://doi.org/10.1016/j.eswa.2024.123180.

[59] A. Elsanabary, K. Khairullah, N.F.A. Aziz, S. Mekhilef, Power management and optimized control of hybrid PV-BESS-grid integrated fast EV charging stations, J. Energy Storage 90 (2024) 111802, https://doi.org/10.1016/j.est.2024.111802.
[60] N. Niveditha, M.M. Rajan Singaravel, Optimal sizing of hybrid PV–wind–battery storage system for net zero energy buildings to reduce grid burden, Appl. Energy 324 (2022) 119713, https://doi.org/10.1016/j.apenergy.2022.119713.
[61] B. Zhang, W. Hu, X. Xu, T. Li, Z. Zhang, Z. Chen, Physical-model-free intelligent energy management for a grid-connected hybrid wind-microturbine-PV-EV energy system via deep reinforcement learning approach, Renew. Energy 200 (2022) 433–448, https://doi.org/10.1016/j.renene.2022.09.125.
[62] G. Rajendran, R. Raute, C. Caruana, A comprehensive review of solar PV integration with smart-grids: challenges, standards, and grid codes, Energies 18 (9) (2025) 2221, https://doi.org/10.3390/en18092221.
[63] Z. Mirza, H. Jain, From challenges to solutions: review and analysis of grid-supportive technologies in sustainable power systems, Appl. Energy 403 (2026) 127111, https://doi.org/10.1016/j.apenergy.2025.127111.
[64] M. Amir, et al., Energy storage technologies: an integrated survey of developments, global economical/environmental effects, optimal scheduling model, and sustainable adaption policies, J. Energy Storage 72 (2023) 108694, https://doi.org/10.1016/j.est.2023.108694.
[65] N. Naval, J.M. Yusta, R. Sánchez, F. Sebastián, Optimal scheduling and management of pumped hydro storage integrated with grid-connected renewable power plants, J. Energy Storage 73 (2023) 108993, https://doi.org/10.1016/j.est.2023.108993.
[66] G. De Carne, et al., The role of energy storage systems for a secure energy supply: a comprehensive review of system needs and technology solutions, Electr. Pow. Syst. Res. 236 (2024) 110963, https://doi.org/10.1016/j.epsr.2024.110963.
[67] X. Liu, et al., Advancements in energy-storage technologies: a review of current developments and applications, Sustainability 17 (18) (2025) 8316, https://doi.org/10.3390/su17188316.
[68] Q. Ma, W. Wei, S. Mei, Health-aware coordinate long-term and short-term operation for BESS in energy and frequency regulation markets, Appl. Energy 356 (2024) 122363, https://doi.org/10.1016/j.apenergy.2023.122363.
[69] A. Selänniemi, M. Hellström, M. Björklund-Sänkiaho, Long-duration energy storage—a literature review on the link between variable renewable energy penetration and market creation, Energies 17 (15) (2024) 3779, https://doi.org/10.3390/en17153779.
[70] K.R. Ngoy, et al., Lithium-ion batteries and the future of sustainable energy: a comprehensive review, Renew. Sustain. Energy Rev. 223 (2025) 115971, https://doi.org/10.1016/j.rser.2025.115971.
[71] S.H. Khan, Energy storage systems for deep decarbonization: a critical review, J. Energy Storage 150 (2026) 120485, https://doi.org/10.1016/j.est.2026.120485.
[72] S. Hemavathi, A. Arun Kumar, R. AkashKumar, J. Vinoth Kumar, Advancements in thermal management and safety of Li-ion batteries for electric vehicles: addressing thermal runaway and fire risk mitigation, Thermal Science and Engineering Progress 71 (2026) 104561, https://doi.org/10.1016/j.tsep.2026.104561.
[73] J.S. Menye, M.-B. Camara, B. Dakyo, Lithium battery degradation and failure mechanisms: a state-of-the-art review, Energies 18 (2) (2025) 342, https://doi.org/10.3390/en18020342.
[74] M. Faizan, M.N. Siddiqui, Advancing sodium-ion batteries for sustainable energy storage, J. Power Sources 679 (2026) 240162, https://doi.org/10.1016/j.jpowsour.2026.240162.
[75] R. Li, H. Yan, Y. Guo, Z. Yan, S. Yuan, M. Lin, Research on the current development status of redox flow batteries, Molecules 31 (6) (2026) 943, https://doi.org/10.3390/molecules31060943.
[76] C.V.M. Gopi, R. Ramesh, Review of battery-supercapacitor hybrid energy storage systems for electric vehicles, Results Eng. 24 (2024) 103598, https://doi.org/10.1016/j.rineng.2024.103598.
[77] Z. Dong, et al., A survey of battery–supercapacitor hybrid energy storage systems: concept, topology, control and application, Symmetry 14 (6) (2022) 1085, https://doi.org/10.3390/sym14061085.
[78] E. Enasel, G. Dumitrascu, Storage solutions for renewable energy: a review, Energy Nexus 17 (2025) 100391, https://doi.org/10.1016/j.nexus.2025.100391.
[79] S. Bielecki, T. Skoczkowski, M. Wołowicz, Microgrids as a tool for energy self-sufficiency, Sensors 25 (21) (2025) 6707, https://doi.org/10.3390/s25216707.
[80] J. Oladigbolu, M.S. Bakare, S.G. Motlagh, A. Mujeeb, L. Li, A review on transport and power systems planning-operation integrating electric vehicles, energy storage, and other distributed energy resources, J. Energy Storage 135 (2025) 118419, https://doi.org/10.1016/j.est.2025.118419.
[81] Í. de la Parra, J. Marcos, J. Pascual, M. García, L. Marroyo, Determining the optimal size of energy storage systems for wind farm ramp-rate control, J. Energy Storage 154 (2026) 121136, https://doi.org/10.1016/j.est.2026.121136.
[82] A. Atif Abdalla, M.S. El Moursi, T.H.M. El-Fouly, K.H. Al Hosani, A state-of-the-art review of adaptive, predictive, synergistic, and degradation-aware power variability smoothing techniques in photovoltaic power plants, Renew. Sustain. Energy Rev. 230 (2026) 116687, https://doi.org/10.1016/j.rser.2025.116687.
[83] Z. Zheng, G. Chen, Z. Shen, Z. Dong, Data-driven robust optimization for energy and reserve scheduling considering multi-uncertainty, International Journal of Electrical Power & Energy Systems 169 (2025) 110751, https://doi.org/10.1016/j.ijepes.2025.110751.
[84] A.G. Papakonstantinou, S.A. Papathanassiou, Battery energy storage participation in automatic generation control of island systems, coordinated with state of charge regulation, Appl. Sci. 12 (2) (2022), https://doi.org/10.3390/app12020596, p. 596.
[85] J. Yang, T.K. Saha, M.R. Alam, W. Tushar, Transactive control of community batteries for voltage regulation in distribution systems, J. Energy Storage 90 (2024) 111798, https://doi.org/10.1016/j.est.2024.111798.
[86] I. Manamperi, I. Ahmad, D. Habibi, A. Aziz, Optimising grid-forming inverters to prevent under-frequency load shedding with minimal energy storage, J. Energy Storage 98 (2024) 112842, https://doi.org/10.1016/j.est.2024.112842.
[87] N. Khosravi, D. Çelik, H. Bevrani, S. Echalih, Microgrid stability: a comprehensive review of challenges, trends, and emerging solutions, International Journal of Electrical Power & Energy Systems 170 (2025) 110829, https://doi.org/10.1016/j.ijepes.2025.110829.
[88] M. Tostado-Véliz, M. Gómez-González, H.M. Hasanien, F. Jurado, Resilience-oriented siting and sizing of storage systems in active distribution networks: a worst-case-driven approach, Sustainable Energy, Grids and Networks 47 (2026) 102336, https://doi.org/10.1016/j.segan.2026.102336.
[89] B. Zakeri, K. Surana, J.D. Hunt, V. Krey, K. Riahi, The AI–energy storage nexus: opportunities for clean energy transitions, Energy Clim. Change (Jul. 2026) 100259, https://doi.org/10.1016/j.egycc.2026.100259.
[90] E. Villa-Ávila, D. Ochoa-Correa, P. Arévalo, Advancements in power converter technologies for integrated energy storage systems: optimizing renewable energy storage and grid integration, Processes 13 (6) (2025) 1819, https://doi.org/10.3390/pr13061819.
[91] B. Wang, H. Tang, An analytical model for DC-link capacitor ripple current in multi-phase H-bridge inverters, Processes 14 (7) (2026) 1059, https://doi.org/10.3390/pr14071059.
[92] Z. Dong, X. Shen, L. Wei, A. Iranzo, J.I. Leon, Control strategies for alkaline water electrolysis hydrogen production: a comprehensive review and future perspectives, Global Energy Interconnection 9 (1) (2026) 1–28, https://doi.org/10.1016/j.gloei.2025.10.008.
[93] M.A. Islam, K.N. Hasan, G. Lamb, M. Datta, Energy storage functions and technological developments of vehicle-to-everything enabled electric vehicle chargers: converter designs, control strategies, services, and market readiness, J. Energy Storage 159 (2026) 121778, https://doi.org/10.1016/j.est.2026.121778.
[94] I. Hussain, Y. He, M.M. Khan, A.U. Khan, A.A. Samejo, A. Annuk, Optimal design and sensitivity analysis of a dual active bridge converter for electrolyzer-based hydrogen production, J. Power Sources 676 (2026) 239923, https://doi.org/10.1016/j.jpowsour.2026.239923.
[95] R. Maakestad, F. Hyder, G. Ramnarase, B. Yan, Review of degradation models of battery energy storage for potential integration into unit commitment problems, Energies 19 (6) (2026) 1425, https://doi.org/10.3390/en19061425.
[96] A.M. Soomar, S. Shaikh, P. Musznicki, Power semiconductor technologies for renewable energy systems: performance, integration, and deployment challenges, Comput. Electr. Eng. 138 (2026) 111294, https://doi.org/10.1016/j.compeleceng.2026.111294.
[97] A. Aleksic, C. Terlizzi, S. Bifaretti, State-of-the-art of hybrid energy storage Systems for Electric Vehicles, IEEE Open Journal of Industry Applications 7 (2026) 191–215.
[98] L.P.R. K, V.K. M, Novel partial power converter topologies for renewable-integrated ultra-fast electric vehicle charging stations, Results Eng. 29 (Mar. 2026) 109665, https://doi.org/10.1016/j.rineng.2026.109665.
[99] N.I. Shchurov, et al., Degradation of lithium-ion batteries in an electric transport complex, Energies 14 (23) (2021) 8072, https://doi.org/10.3390/en14238072.
[100] A. Keerthi, C. Dhanamjayulu, A thorough review of energy management and an advanced control techniques for bi-directional DC-DC converters in electric vehicle applications, Results Eng. 27 (2025) 106726, https://doi.org/10.1016/j.rineng.2025.106726.
[101] M.A. Hossain, Experimental validation of DC-link based voltage control framework for islanded hydrogen DC microgrids, Int. J. Hydrogen Energy 189 (2025) 152033, https://doi.org/10.1016/j.ijhydene.2025.152033.
[102] S. Yuvaraja, V. Khandelwal, X. Tang, X. Li, Wide bandgap semiconductor-based integrated circuits, Chip 2 (4) (2023) 100072, https://doi.org/10.1016/j.chip.2023.100072.
[103] S.S. Alharbi, S.S. Alharbi, A. Bubshait, H. Alharbi, A. Alateeq, Effects of wide bandgap devices on the inverter performance and efficiency for residential PV applications, Electronics 14 (6) (2025) 1061, https://doi.org/10.3390/electronics14061061.
[104] M.H. Nguyen, S. Kwak, Enhance reliability of semiconductor devices in power converters, Electronics 9 (12) (2020) 2068, 2020, https://doi.org/10.3390/electronics9122068.
[105] T. Qoria, X. Wang, R. Kadri, Grid-forming control VSC-based including current limitation and re-synchronization functions to deal with symmetrical and asymmetrical faults, Electr. Pow. Syst. Res. 223 (2023) 109647, https://doi.org/10.1016/j.epsr.2023.109647.
[106] S.M. Parsa, Physics-informed machine learning meets renewable energy systems: a review of advances, challenges, guidelines, and future outlooks, Appl. Energy 402 (2025) 126925, https://doi.org/10.1016/j.apenergy.2025.126925.
[107] V. Vega–Garita, M. Heydarzadeh, A.H. Dadash, E. Immonen, The need for aging-aware control methods in lithium-ion batteries: a review, J. Energy Storage 132 (Oct. 2025) 117653, https://doi.org/10.1016/j.est.2025.117653.
[108] M. Pan, et al., Coordinated thermal–energy management for battery energy storage systems in hybrid electric vehicles: architecture, modeling, control strategies, and engineering validation, J. Energy Storage 164 (2026) 121939, https://doi.org/10.1016/j.est.2026.121939.

[109] H.A. Soomro, M.H.B.M. Khir, S.A.B.M. Zulkifli, G.E.M. Abro, M.M. Abualnaeem, Applications of wide bandgap semiconductors in electric traction drives: current trends and future perspectives, Results Eng. 26 (2025) 104679, https://doi.org/10.1016/j.rineng.2025.104679.
[110] A. Korompili, A. Monti, Review of modern control technologies for voltage regulation in DC/DC converters of DC microgrids, Energies 16 (12) (2023) 4563, https://doi.org/10.3390/en16124563.
[111] A.S. Abdelwahab, I. Vokony, Beyond synchronization: the evolution of grid-following to grid-forming inverters and the quest for power system stability, Energy Rep. 15 (2026) 109221, https://doi.org/10.1016/j.egyr.2026.109221.
[112] Z. Hu, Y. Hai, X. Liang, H. Wu, Artificial intelligence and data-driven approaches in renewable energy: a review of achievements and challenges, Energ. Strat. Rev. 64 (2026) 102093, https://doi.org/10.1016/j.esr.2026.102093.
[113] E. Arpaci, The place and future of AI in thermal analysis processes: from prediction to foresight, Neural Comput. Appl. 38 (12) (2026) 497, https://doi.org/10.1007/s00521-026-12232-7.
[114] S. Mabuwa, K. Moloi, Physics-informed neural networks for real-time control of grid-forming inverters: embedding physical system laws into deep learning architectures, Energies 19 (11) (2026) 2690, https://doi.org/10.3390/en19112690.
[115] Z. Du, R. Lu, Physics-informed neural networks for advanced thermal management in electronics and battery systems: a review of recent developments and future prospects, Batteries 11 (6) (2025) 204, https://doi.org/10.3390/batteries11060204.
[116] F. Roccaforte, et al., Emerging trends in wide band gap semiconductors (SiC and GaN) technology for power devices, Microelectron. Eng. 187 (2018) 66–77.
[117] M. Buffolo, et al., Review and outlook on GaN and SiC power devices: industrial state-of-the-art, applications, and perspectives, IEEE Trans. Electron Devices 71 (3) (2024) 1344–1355.
[118] B.M. Bryant, A.N. Lemmon, B.T. DeBoi, C.D. New, S.J. Jimenez, Improved methodology for estimating switching losses of wide-bandgap semiconductors using Gaussian curve fitting, IEEE Trans. Power Electron. 39 (5) (2024) 5590–5601.
[119] A. Waheed, et al., Hybrid multimodule DC–DC converters accelerated by wide bandgap devices for electric vehicle systems, Sci. Rep. 14 (1) (2024) 4746.
[120] J. Ballestín-Fuertes, J. Muñoz-Cruzado-Alba, J.F. Sanz-Osorio, E. Laporta-Puyal, Role of wide bandgap materials in power electronics for smart grids applications, Electronics 10 (6) (2021) 677.
[121] S.S.H. Rafin, R. Ahmed, O.A. Mohammed, "Wide band gap semiconductor devices for power electronic converters," presented at the 2023 Fourth international symposium on 3D power electronics integration and manufacturing (3D-PEIM), IEEE, 2023, pp. 1–8.
[122] S. Yuvaraja, V. Khandelwal, X. Tang, X. Li, Wide bandgap semiconductor-based integrated circuits, Chip 2 (4) (2023) 100072.
[123] K.C. Lee, M. Weis, Charge traps in wide-bandgap semiconductors for power electronics applications, Inorganics 12 (10) (2024) 257.
[124] Y. Wang, Y. Ding, Y. Yin, Reliability of wide band gap power electronic semiconductor and packaging: a review, Energies 15 (18) (2022) 6670.
[125] A. Kumar, et al., Wide band gap devices and their application in power electronics, Energies 15 (23) (2022) 9172.
[126] I.C. Kizilyalli, E.P. Carlson, D.W. Cunningham, J.S. Manser, Y.A. Xu, A.Y. Liu, "Wide band-gap semiconductor based power electronics for energy efficiency," US Department of Energy (USDOE), Washington DC (United States). Advanced …, 2018.
[127] B. Zhang, S. Wang, "An overview of wide bandgap power semiconductor device packaging techniques for EMI reduction," presented at the 2018 IEEE symposium on electromagnetic compatibility, signal integrity and power integrity (EMC, SI & PI), IEEE, 2018, pp. 297–301.
[128] I.N. Jiya, R. Gouws, Overview of power electronic switches: a summary of the past, state-of-the-art and illumination of the future, Micromachines 11 (12) (2020) 1116.
[129] G. Iannaccone, C. Sbrana, I. Morelli, S. Strangio, Power electronics based on wide-bandgap semiconductors: opportunities and challenges, IEEE access 9 (2021) 139446–139456.
[130] K. Ravinchandra, T.K.S. Freddy, V. Thiruchelvam, Review of electrical characteristics for wide bandgap power devices, in: presented at the 2021 IEEE 12th energy conversion congress & exposition-Asia (ECCE-Asia)IEEE, 2021, pp. 963–966.
[131] A. Castellazzi, E. Gurpinar, Z. Wang, A. Suliman Hussein, P. Garcia Fernandez, Impact of wide-bandgap technology on renewable energy and smart-grid power conversion applications including storage, Energies 12 (23) (2019) 4462.
[132] N. Keshmiri, D. Wang, B. Agrawal, R. Hou, A. Emadi, Current status and future trends of GaN HEMTs in electrified transportation, IEEE access 8 (2020) 70553–70571.
[133] L. Zhang, Z. Zheng, X. Lou, A review of WBG and Si devices hybrid applications, Chinese Journal of Electrical Engineering 7 (2) (2021) 1–20.
[134] K. Ravinchandra, et al., Review of wide band-gap technology: power device, gate driver, and converter design, Journal of Power Electronics 22 (8) (2022) 1398–1413.
[135] I.C. Kizilyalli, O.B. Spahn, E.P. Carlson, Recent progress in wide-bandgap semiconductor devices for a more electric future, ECS Trans. 109 (8) (2022) 3.
[136] M. Kanechika, T. Uesugi, T. Kachi, Advanced SiC and GaN power electronics for automotive systems, in: presented at the 2010 International electron devices meetingIEEE, 2010, pp. 13–5.
[137] T. Kachi, D. Kikuta, T. Uesugi, GaN power device and reliability for automotive applications, in: presented at the 2012 IEEE International Reliability Physics Symposium (IRPS)IEEE, 2012, pp. 3D–1.
[138] E.A. Jones, F.F. Wang, D. Costinett, Review of commercial GaN power devices and GaN-based converter design challenges, IEEE journal of emerging and selected topics in power electronics 4 (3) (2016) 707–719.
[139] S. Dargahi, P. Valizadeh, S.S. Williamson, Proof-of-concept gallium-nitride power electronic converter design for HEV energy management application, in: presented at the 2011 IEEE Vehicle Power and Propulsion ConferenceIEEE, 2011, pp. 1–5.
[140] H. Shen, J. Yang, Z. Yuan, N. Ye, J. Di, J. Mo, Research of optimal parameters in MOSFET structure based on wide band gap semiconductor material GaN, in: presented at the 2016 Chinese control and decision conference (CCDC)IEEE, 2016, pp. 6086–6089.
[141] D. Han, C.T. Morris, W. Lee, B. Sarlioglu, A case study on common mode electromagnetic interference characteristics of GaN HEMT and Si MOSFET power converters for EV/HEVs, IEEE Trans. Transp. Electrif. 3 (1) (2016) 168–179.
[142] R. Semiconductor, Physical Properties and Characteristics of Sic, 2019.
[143] F.M. Shah, H.M. Xiao, R. Li, M. Awais, G. Zhou, G.T. Bitew, Comparative performance evaluation of temperature dependent characteristics and power converter using GaN, SiC and Si power devices, in: 2018 IEEE 12th International Conference on Compatibility, Power Electronics and Power Engineering (CPE-POWERENG 2018), Apr. 2018, pp. 1–7, https://doi.org/10.1109/CPE.2018.8372523.
[144] D. Ueda, et al., Present and future prospects of Gan-based power electronics, Presented at the 2008 9th International Conference on Solid-State and Integrated-Circuit Technology, IEEE, 2008, pp. 1078–1081.
[145] J. Roberts, Lateral GaN Transistors-A Replacement for IGBT devices in Automotive Applications, ," presented at the PCIM Europe 2014; International exhibition and conference for power electronics, Intelligent Motion, Renewable Energy and Energy Management,, VDE, 2014, pp. 1–8.
[146] S. Chowdhury, GaN electronics for next generation cars, IEEE Transp. Electrific. Community (2014).
[147] R. Mitova, R. Ghosh, U. Mhaskar, D. Klikic, M.-X. Wang, A. Dentella, Investigations of 600-V GaN HEMT and GaN diode for power converter applications, IEEE Trans. Power Electron. 29 (5) (2013) 2441–2452.
[148] A. Note, "Design considerations of paralleled gan hemt-based half bridge power stage," GaN Systems, [Online] Available at www.gansystems.com, 2016.
[149] D. Han, A. Ogale, S. Li, Y. Li, B. Sarlioglu, "Efficiency characterization and thermal study of GaN based 1 kW inverter," presented at the 2014 IEEE applied power electronics conference and exposition-APEC 2014, IEEE, 2014, pp. 2344–2350.
[150] A.S. Abdelrahman, Z. Erdem, Y. Attia, M.Z. Youssef, Wide bandgap devices in electric vehicle converters: a performance survey, Can. J. Elect. Comput. Eng. 41 (1) (2018) 45–54.
[151] A. Lidow, M. De Rooij, J. Strydom, D. Reusch, J. Glaser, GaN Transistors for Efficient Power Conversion, John Wiley & Sons, 2019.
[152] J. Xu, D. Chen, A Performance Comparison of GaN E-HEMTs versus SiC MOSFETs in Power Switching Applications [Online]. Available: https://eepower.com/technical-articles/a-performance-comparison-of-gan-e-hemts-versus-sic-mosfets-in-power-switching-applications/#, 2017.
[153] R. Hou, J. Lu, D. Chen, Parasitic capacitance Eqoss loss mechanism, calculation, and measurement in hard-switching for GaN HEMTs, in: presented at the 2018 IEEE applied power electronics conference and exposition (APEC)IEEE, 2018, pp. 919–924.
[154] C.-H. Lin, S.A. Farooqui, H.-D. Liu, A. Sarwar, M. Zaid, J. Ahmad, Performance enhancement of a multilevel inverter in renewable energy systems using equilibrium optimizer, Electr. Pow. Syst. Res. 243 (2025) 111538, https://doi.org/10.1016/j.epsr.2025.111538.
[155] A. Azizi, M. Akhbari, S. Danyali, Z. Tohidinejad, M. Shirkhani, A review on topology and control strategies of high-power inverters in large- scale photovoltaic power plants, Heliyon 11 (3) (2025) e42334, https://doi.org/10.1016/j.heliyon.2025.e42334.
[156] M. Manivel, L. Kaliappan, Analysis and implementation of switched capacitor-based multi-level inverter for electric vehicles applications, Elektronika Ir Elektrotechnika 29 (1) (2023) 21–32.
[157] G. Han, J. Kim, S. Park, W. Bae, Thermal management of wide-bandgap power semiconductors: strategies and challenges in SiC and GaN power devices, Electronics 14 (21) (2025) 4193, https://doi.org/10.3390/electronics14214193.
[158] B.M. Bile, A. CHERIFI, H.A. Barkad, K. MEGHRICHE, New multilevel inverter with the elimination of successive low-rank harmonics using PWHM for integration into the distribution grid, Results Eng. 27 (Sep. 2025) 106544, https://doi.org/10.1016/j.rineng.2025.106544.
[159] V. K. N. V. and G. T, A comprehensive survey on reduced switch count multilevel inverter topologies and modulation techniques, J. Electr. Syst. Inf. Technol. 10 (1) (2023) 3, https://doi.org/10.1186/s43067-023-00071-8.
[160] S. Gangavarapu, M. Verma, A.K. Rathore, A novel transformerless single-stage grid-connected solar inverter, IEEE J. Emerg. Sel. Top. Power Electron. 11 (1) (2020) 970–980.
[161] R. Attanasio, M. Cacciato, F. Gennaro, G. Scarcella, Review on single-phase PV inverters for grid-connected applications, in: presented at the 4th IASME/WSEAS, International Conference on Energy, Environment, Ecosystems and Sustainable Development (EEESD'08), Algarve, Portugal, 2008.
[162] R.O. Caceres, I. Barbi, A boost DC-AC converter: analysis, design, and experimentation, IEEE Trans. Power Electron. 14 (1) (2002) 134–141.

[163] N. Vázquez, J. Almazán, J. Álvarez, C. Aguilar, J. Arau, Analysis and experimental study of the buck, boost and buck-boost inverters, ," Presented at the 30th Annual IEEE Power Electronics Specialists Conference. Record.(vol. Cat. No. 99CH36321),, IEEE, 1999, pp. 801–806.
[164] Y. Gu, W. Li, Y. Zhao, B. Yang, C. Li, X. He, Transformerless inverter with virtual DC bus concept for cost-effective grid-connected PV power systems, IEEE Trans. Power Electron. 28 (2) (2012) 793–805.
[165] Z. Ozkan, A. HAVA, Classification of grid connected transformer less PV inverters with a focus on the leakage current characteristics and extension of topology families, J. Power Electron. 15 (1) (2015).
[166] J. Madouh, N.A. Ahmed, A.M. Al-Kandari, Advanced power conditioner using sinewave modulated buck–boost converter cascaded polarity changing inverter, International Journal of Electrical Power & Energy Systems 43 (1) (2012) 280–289.
[167] P. Chaudhary, M. Rizwan, Voltage regulation mitigation techniques in distribution system with high PV penetration: a review, Renew. Sustain. Energy Rev. 82 (2018) 3279–3287.
[168] P. Kala, S. Arora, A comprehensive study of classical and hybrid multilevel inverter topologies for renewable energy applications, Renew. Sustain. Energy Rev. 76 (2017) 905–931.
[169] J.M. Myrzik, Novel inverter topologies for single-phase stand-alone or grid-connected photovoltaic systems, in: Presented at the 4th IEEE International Conference on Power Electronics and Drive Systems. IEEE PEDS 2001-Indonesia. Proceedings (Cat. No. 01TH8594)IEEE, 2001, pp. 103–108.
[170] H. Shinohara, et al., "Development of a residential use, utility interactive PV inverter with isolation transformer-less circuit-development aspects," presented at the Proceedings of 1994 IEEE 1st World Conference on Photovoltaic Energy Conversion-WCPEC (A Joint Conference of PVSC, PVSEC and PSEC), IEEE, 1994 (pp. 1216–1218).
[171] J.-S. Lai, F.Z. Peng, Multilevel converters-a new breed of power converters, IEEE Trans. Ind. Appl. 32 (3) (1996) 509–517.
[172] Y. Gu, W. Li, Y. Zhao, B. Yang, C. Li, X. He, Transformerless inverter with virtual DC bus concept for cost-effective grid-connected PV power systems, IEEE Trans. Power Electron. 28 (2) (2012) 793–805.
[173] P.M. Bhagwat, V. Stefanovic, Generalized structure of a multilevel PWM inverter, IEEE Trans. Ind. Appl. 6 (1983) 1057–1069.
[174] S.B. Kjaer, J.K. Pedersen, F. Blaabjerg, "Power inverter topologies for photovoltaic modules-a review," presented at the Conference Record of the 2002 IEEE industry applications conference. 37th IAS Annual Meeting (Cat. No. 02CH37344), IEEE, 2002, pp. 782–788.
[175] B.K. Bose, P.M. Szczesny, R.L. Steigerwald, Microcomputer control of a residential photovoltaic power conditioning system, IEEE Trans. Ind. Appl. 5 (1985) 1182–1191.
[176] A. Draz, A.M. Othman, A.A. El-Fergany, State-of-the-art with numerical analysis on electric fast charging stations: infrastructures, standards, techniques, and challenges, Renewable Energy Focus 47 (2023) 100499, https://doi.org/10.1016/j.ref.2023.100499.
[177] V.N. Hoang, D.P. Hong, Predictive current control with selection vector table scheme for 3L-NPC inverter, Elektron. Elektrotech. 31 (4) (2025) 30–39.
[178] H. Boumaaraf, A. Talha, O. Bouhali, A three-phase NPC grid-connected inverter for photovoltaic applications using neural network MPPT, Renew. Sustain. Energy Rev. 49 (2015) 1171–1179.
[179] F. Faraji, A. Hajirayat, A.A.M. Birjandi, K. Al-Haddad, Single-stage single-phase three-level neutral-point-clamped transformerless grid-connected photovoltaic inverters: topology review, Renew. Sustain. Energy Rev. 80 (2017) 197–214.
[180] S.A.O. da Silva, L.B.G. Campanhol, G.M. Pelz, V. de Souza, Comparative performance analysis involving a three-phase UPQC operating with conventional and dual/inverted power-line conditioning strategies, IEEE Trans. Power Electron. 35 (11) (2020) 11652–11665.
[181] E. Akbari, A.Z.G. Seyyedi, Power quality enhancement of distribution grid using a photovoltaic based hybrid active power filter with three level converter, Energy Rep. 9 (2023) 5432–5448.
[182] C. Dietrich, S. Gediga, M. Hiller, R. Sommer, and H. Tischmacher, "A new 7.2 kV medium voltage 3-Level-NPC inverter using 6.5 kV-IGBTs," Presented at the 2007 European Conference on Power Electronics and Applications, IEEE, 2007, pp. 1–9.
[183] L.B.G. Campanhol, S.A.O. da Silva, A.A. de Oliveira, V.D. Bacon, Single-stage three-phase grid-tied PV system with universal filtering capability applied to DG systems and AC microgrids, IEEE Trans. Power Electron. 32 (12) (2017) 9131–9142.
[184] P. Ramasamy, V. Krishnasamy, A 3D-space vector modulation algorithm for three phase four wire neutral point clamped inverter systems as power quality compensator, Energies 10 (11) (2017), p. 1792.
[185] S. Madhusoodhanan, et al., Harmonic analysis and controller design of 15 kV SiC IGBT-based medium-voltage grid-connected three-phase three-level NPC converter, IEEE Trans. Power Electron. 32 (5) (2016) 3355–3369.
[186] T. Meynard, H. Foch, Multi-level choppers for high voltage applications, EPE J. 2 (1) (1992) 45–50.
[187] S.T. Meraj, N.Z. Yahaya, K. Hasan, A. Masaoud, A hybrid T-type (HT-type) multilevel inverter with reduced components, Ain Shams Eng. J. 12 (2) (2021) 1959–1971.
[188] G. Karmiris, G. Tsengenes, G. Adamidis, A multifunction control scheme for current harmonic elimination and voltage sag mitigation using a three phase three level flying capacitor inverter, Simul Model Pract Theory 24 (2012) 15–34.
[189] M. Humayun, M.M. Khan, M.U. Hassan, W. Zhang, Analysis of hybrid switches symmetric flying capacitor multilevel inverter based STATCOM, International Journal of Electrical Power & Energy Systems 131 (2021) 107054.
[190] M. Humayun, M.M. Khan, A. Muhammad, J. Xu, W. Zhang, Evaluation of symmetric flying capacitor multilevel inverter for grid-connected application, International Journal of Electrical Power & Energy Systems 115 (2020) 105430.
[191] A. Falehi, M. Rafiee, Enhancement of DFIG-wind turbine's LVRT capability using novel DVR based odd-nary cascaded asymmetric multi-level inverter, Eng. Sci. Technol. Int. J. 20 (3) (2017) 805–824.
[192] S.A. González, M.I. Valla, UPQC implemented with cascade asymmetric multilevel converters, Electr. Power Syst. Res. 124 (2015) 144–151.
[193] A. Bughneda, M. Salem, A. Richelli, D. Ishak, S. Alatai, Review of multilevel inverters for PV energy system applications, Energies 14 (6) (2021) 1585.
[194] M. Marchesoni, M. Mazzucchelli, S. Tenconi, A nonconventional power converter for plasma stabilization, IEEE Trans. Power Electron. 5 (2) (1990) 212–219.
[195] F.Z. Peng, H. Akagi, A. Nabae, A combined system of shunt passive and series active filters stability and compensation characteristics, IEEJ Transactions on Industry Applications 110 (5) (1990) 542–550.
[196] J.R. Espinoza, G. Joós, State variable decoupling and power flow control in PWM current-source rectifiers, IEEE Trans. Ind. Electron. 45 (1) (2002) 78–87.
[197] S. Badawi, et al., Utilization of a reduced switch-count topology in regenerative cascaded H-bridge (CHB) medium-voltage drives, IEEE J. Emerg. Sel. Top. Power Electron. 10 (6) (2021) 6938–6949.
[198] L. Liu, H. Li, Y. Xue, W. Liu, Decoupled active and reactive power control for large-scale grid-connected photovoltaic systems using cascaded modular multilevel converters, IEEE Trans. Power Electron. 30 (1) (2014) 176–187.
[199] F.V. Amaral, T.M. Parreiras, G.C. Lobato, A.A.P. Machado, I.A. Pires, B. de Jesus Cardoso Filho, Operation of a grid-tied cascaded multilevel converter based on a forward solid-state transformer under unbalanced PV power generation, IEEE Trans. Ind. Appl. 54 (5) (2018) 5493–5503.
[200] H. Mhiesan, J. Umuhoza, K. Mordi, C. Farnell, H.A. Mantooth, Evaluation of 1.2 kV SiC MOSFETs in multilevel cascaded H-bridge three-phase inverter for medium-voltage grid applications, Chinese Journal of Electrical Engineering 5 (2) (2019) 1–13.
[201] Y. Zhang, X. Yuan, M. Al-Akayshee, A reliable medium-voltage high-power conversion system for MWs wind turbines, IEEE Trans. Sustain. Energy 11 (2) (2019) 859–867.
[202] V. Muneer, A. Bhattacharya, G. Biju, Second-order sliding-mode control for three-level H-bridge-based unified power quality conditioner with vanilla feedforward neural network, IEEE J. Emerg. Sel. Top. Ind. Electron. 4 (2) (2022) 514–524.
[203] R. Chakrabarty, R. Adda, DSTATCOM implementation using reduced switch single DC source cascaded H-bridge multilevel inverter, Electr. Pow. Syst. Res. 199 (2021) 107373, https://doi.org/10.1016/j.epsr.2021.107373.
[204] B.K. Bose, P.M. Szczesny, R.L. Steigerwald, Microcomputer control of a residential photovoltaic power conditioning system, IEEE Trans. Ind. Appl. 5 (1985) 1182–1191.
[205] T.A. Meynard, H. Foch, "Multi-level conversion: high voltage choppers and voltage-source inverters," in *PESC '92 Record. 23rd Annual IEEE Power Electronics Specialists Conference*, Jul. 1992, pp. 397–403, vol. 1. https://doi.org/10.1109/PESC.1992.254717.
[206] A. Chen, X. He, Research on hybrid-clamped multilevel-inverter topologies, IEEE Trans Ind Electron 53 (6) (2006) 1898–1907, https://doi.org/10.1109/TIE.2006.885154.
[207] A. Nabae, I. Takahashi, H. Akagi, A new neutral-point-clamped PWM inverter, IEEE Trans. Ind. Appl. IA-17 (5) (1981) 518–523, https://doi.org/10.1109/TIA.1981.4503992.
[208] V. Jayakumar, B. Chokkalingam, J.L. Munda, A comprehensive review on space vector modulation techniques for neutral point clamped multi-level inverters, IEEE Access 9 (2021) 112104–112144, https://doi.org/10.1109/ACCESS.2021.3100346.
[209] N.S. Hasan, N. Rosmin, Dygku.A.Awg. Osman, A.H. Musta'amal@Jamal, Reviews on multilevel converter and modulation techniques, Renew. Sustain. Energy Rev. 80 (2017) 163–174, https://doi.org/10.1016/j.rser.2017.05.163.
[210] T.A. Meynard, H. Foch, "Multi-level conversion: High voltage choppers and voltage-source inverters," Presented at the PESC'92 Record. 23rd Annual IEEE Power Electronics Specialists Conference, IEEE, 1992, pp. 397–403.
[211] P. Duan, L. Yang, X. Luo, Y. Zhou, T. Yan, and S. Yang, "Response-function framework for evaluating converter topologies in renewable energy integration," Front. Energy Res., vol. Volume 13-2025, 2025, doi:https://doi.org/10.3389/fenrg.2025.1734909.
[212] L. Zhang, Q. Zhu, H. Xiao, Topology, control, and applications of MMC with embedded energy storage: a brief review, Electronics 14 (5) (2025) 949, https://doi.org/10.3390/electronics14050949.
[213] L. Zhang, Multilevel Converters for Renewable Energy Systems, in: Recent Advancements and Emerging Technologies in Multi-level Inverters, River Publishers, 2025, pp. 277–301.
[214] M. Marchesoni, M. Mazzucchelli, "Multilevel converters for high power AC drives: A review," presented at the ISIE'93-Budapest: IEEE International Symposium on Industrial Electronics Conference Proceedings, IEEE, 1993, pp. 38–43.
[215] F. Deng, Z. Chen, Voltage-balancing method for modular multilevel converters switched at grid frequency, IEEE Trans. Ind. Electron. 62 (5) (2014) 2835–2847.
[216] H. Saad, X. Guillaud, J. Mahseredjian, S. Dennetiere, S. Nguefeu, MMC capacitor voltage decoupling and balancing controls, IEEE Trans. Power Deliv. 30 (2) (2014) 704–712.
[217] E. Villa-Ávila, D. Ochoa-Correa, P. Arévalo, Advancements in power converter technologies for integrated energy storage systems: optimizing renewable energy storage and grid integration, Processes 13 (6) (2025) 1819, 2025, https://doi.org/10.3390/pr13061819.

[218] S. Alepuz, et al., A survey on capacitor voltage control in neutral-point-clamped multilevel converters, Electronics 11 (4) (2022), https://doi.org/10.3390/electronics11040527, p. 527.
[219] J. Li, L. Min, W. Tang, Y. Zhai, Modulation optimization and load power boundary condition for a five-level ANPC converter under DC-side unbalanced loads, Energies 19 (6) (2026) 1576, https://doi.org/10.3390/en19061576.
[220] C.-D. Le, Performance evaluation of a single-phase three-level F-type PFC converter with FOPI-based current regulation for enhanced DC-link capacitor voltage balancing, Results Eng. 31 (2026) 111454, https://doi.org/10.1016/j.rineng.2026.111454.
[221] M.A. Islam, K.N. Hasan, G. Lamb, M. Datta, Energy storage functions and technological developments of vehicle-to-everything enabled electric vehicle chargers: converter designs, control strategies, services, and market readiness, J. Energy Storage 159 (2026) 121778, https://doi.org/10.1016/j.est.2026.121778.
[222] A. El Aoumari, H. Ouadi, H. Rafia, J. El-Bakkouri, Y. Boumaalif, Hybrid energy management strategy combining adaptive frequency separation and deep reinforcement learning for fuel-cell hybrid electric vehicles, Results Eng. 29 (2026) 109433, https://doi.org/10.1016/j.rineng.2026.109433.
[223] P. Ranjbaran, J. Ebrahimi, A. Bakhshai, P. Jain, A comprehensive review of topologies and energy management methods for hybrid energy storage systems in electric vehicle applications, IEEE Trans. Power Electron. 41 (2025) 6149–6178, https://doi.org/10.1109/TPEL.2025.3625535.
[224] S. Alatai, et al., A review on state-of-the-art power converters: bidirectional, resonant, multilevel converters and their derivatives, Appl. Sci. 11 (21) (2021) 10172, https://doi.org/10.3390/app112110172.
[225] M. Calais, V.G. Agelidis, "Multilevel converters for single-phase grid connected photovoltaic systems-an overview," in *IEEE International Symposium on Industrial Electronics. Proceedings. ISIE'98 (Cat. No.98TH8357)*, Jul. 1998, pp. 224–229, 1, https://doi.org/10.1109/ISIE.1998.707781.
[226] J. Rodriguez, S. Bernet, P.K. Steimer, I.E. Lizama, A survey on neutral-point-clamped inverters, IEEE Trans Ind Electron 57 (7) (2010) 2219–2230, https://doi.org/10.1109/TIE.2009.2032430.
[227] M. Calais, J. Myrzik, T. Spooner, V.G. Agelidis, Inverters for single-phase grid connected photovoltaic systems-an overview, in: 2002 IEEE 33rd Annual IEEE Power Electronics Specialists Conference. Proceedings (Cat. No.02CH37289), Jun. 2002, pp. 1995–2000, vol. 4, https://doi.org/10.1109/PSEC.2002.1023107.
[228] M.H. Mohamed Hariri, M.K. Mat Desa, S. Masri, M.A. Mohd Zainuri, Grid-connected PV generation system—components and challenges: a review, Energies 13 (17) (2020) 4279, https://doi.org/10.3390/en13174279.
[229] T. Ishikawa, Grid-Connected Photovoltaic Power Systems: Survey of Inverter and Related Protection Equipments, 2002.
[230] S. Azmi, K. Ahmed, S. Finney, B. Williams, "Comparative analysis between voltage and current source inverters in grid-connected application," presented at the IET conference on renewable power generation (RPG 2011), IET, 2011, p. 101.
[231] K. Zeb, et al., A comprehensive review on inverter topologies and control strategies for grid connected photovoltaic system, Renew. Sustain. Energy Rev. 94 (2018) 1120–1141, https://doi.org/10.1016/j.rser.2018.06.053.
[232] M.I. Ali, M.A.A.M. Zainuri, A.A. Ibrahim, A.H.M. Hashim, M.S. Ali, Performance analysis of a secondary-side resonance 1 MHz GaN-based active-clamp Flyback DC-DC converter in CCM, Elektron. Elektrotech. 31 (6) (2025) 13–22.
[233] G. De Carne, et al., The role of energy storage systems for a secure energy supply: a comprehensive review of system needs and technology solutions, Electr. Pow. Syst. Res. 236 (2024) 110963, https://doi.org/10.1016/j.epsr.2024.110963.
[234] Y. Chen, X. Liu, Y. Fu, State-of-health predictive energy management and grid-forming control for battery energy storage systems, Batteries 12 (1) (2026) 15, https://doi.org/10.3390/batteries12010015.
[235] S. Kazemian, T. Geury, O. Hegazy, A review of battery systems and power electronics interfaces in electrified maritime transportation: topologies, control techniques and future trends, Energy Rep. 15 (2026) 109396, https://doi.org/10.1016/j.egyr.2026.109396.
[236] A.B. Ahmad, et al., Renewable integration and energy storage management and conversion in grid systems: a comprehensive review, Energy Rep. 13 (2025) 2583–2602, https://doi.org/10.1016/j.egyr.2025.02.008.
[237] N. Salehi, M. Mahmoudi, A. Bazargan, G. McKay, Exergy and life cycle-based analysis, in: C.M. Hussain (Ed.), Handbook of Environmental Materials Management, Springer International Publishing, Cham, 2019, pp. 1057–1078, https://doi.org/10.1007/978-3-319-73645-7_84.
[238] R. Khwanrit, Y. Lim, S. Javaid, S. Kittipiyakul, Y. Tan, Study of energy loss for distributed power-flow assignment in a smart home environment, Designs 6 (6) (2022) 99, https://doi.org/10.3390/designs6060099.
[239] Y. Demirel, Entropy and exergy, in: Nonequilibrium Thermodynamics, Elsevier Science, Amsterdam, 2002, pp. 102–123, https://doi.org/10.1016/B978-044450886-7/50005-9.
[240] Y. Demirel, Balance equations and entropy generation, in: Nonequilibrium Thermodynamics, Elsevier Science, Amsterdam, 2002, pp. 84–101, https://doi.org/10.1016/B978-044450886-7/50004-7.
[241] I. Dincer, M.A. Rosen, M. Al-Zareer, Exergoenvironmental analysis, in: I. Dincer (Ed.), Comprehensive Energy Systems, Elsevier, Oxford, 2018, pp. 377–421, https://doi.org/10.1016/B978-0-12-809597-3.00108-5.
[242] H. Zhang, Y. Song, L. li, Optimization of heat exchanger design for third generation centralized solar power generation system: CFD and thermoeconomic coupling method for improving thermal performance and reducing storage costs of batteries, Case Stud. Therm. Eng. 81 (May 2026) 107866, https://doi.org/10.1016/j.csite.2026.107866.
[243] K. Wei, P. Shi, P. Bao, C. Liu, Y. Qin, Analysis of key factors affecting case-to-ambient thermal resistance in thermal modeling of power devices, Energies 17 (22) (2024) 5692, https://doi.org/10.3390/en17225692.
[244] S. Mikulić, D. Žarko, Stray losses in structural components of power transformers, Energies 19 (2) (2026) 322, https://doi.org/10.3390/en19020322.
[245] M.C. Ignuta-Ciuncanu, Thermodynamic rating of active cooling in battery thermal management, International Communications in Heat and Mass Transfer 178 (2026) 111832, https://doi.org/10.1016/j.icheatmasstransfer.2026.111832.
[246] M. Mahmood, P. Chowdhury, R. Yeassin, M. Hasan, T. Ahmad, N.-U.-R. Chowdhury, Impacts of digitalization on smart grids, renewable energy, and demand response: an updated review of current applications, Energy Conversion and Management: X 24 (2024) 100790, https://doi.org/10.1016/j.ecmx.2024.100790.
[247] C. James, T.Y. Kim, R. Jane, A review of exergy based optimization and control, Processes 8 (3) (2020) 364, https://doi.org/10.3390/pr8030364.
[248] M.A. Elseify, S. Kamel, Pareto front-based multi-objective optimization of renewable DGs in distribution networks using an enhanced Newton-Raphson algorithm with techno-economic and environmental assessment, Computers and Electrical Engineering 128 (2025) 110637, https://doi.org/10.1016/j.compeleceng.2025.110637.
[249] S. Giannelos, X. Zhang, T. Zhang, G. Strbac, Multi-objective optimization for Pareto frontier sensitivity analysis in power systems, Sustainability 16 (14) (2024) 5854, https://doi.org/10.3390/su16145854.
[250] R.K. Behara, A.K. Saha, Artificial intelligence techniques framework in the design and optimisation phase of the doubly fed induction generator's power electronic converters: a review of current status and future trends, Renew. Sustain. Energy Rev. 215 (2025) 115573, https://doi.org/10.1016/j.rser.2025.115573.
[251] S. Alepuz, J. Nicolás-Apruzzese, G. García-Rojas, S. Busquets-Monge, M. Grespan, X. Yuan, Thermal stress reduction in neutral-point-clamped multilevel converters through a switching-cell array-based implementation and active thermal control, Electronics 15 (5) (2026) 1099, https://doi.org/10.3390/electronics15051099.
[252] W. Cheng, P. Wang, W. Wang, D. Xu, Parameter design method of variable frequency modulation for grid-tied inverter considering loss optimization and thermal and harmonic constraints, Energies 19 (4) (2026) 1032, https://doi.org/10.3390/en19041032.
[253] A.A. Khan, N.A. Zaffar, M.J. Ikram, DC-link ripple reduction for parallel inverter systems by a novel formulation using multiple space vector-based interleaving schemes, Electronics 12 (6) (2023), https://doi.org/10.3390/electronics12061496, p. 1496.
[254] K. Salahshoor, M.H. Asheri, A new exergy-based model predictive control methodology for energy assessment and control, J. Nat. Gas Sci. Eng. 21 (2014) 489–495, https://doi.org/10.1016/j.jngse.2014.08.024.
[255] J. He, C. Wang, Y. Huang, Thermal management and performance optimization in high-power-density Lithium-ion battery modules, Energies 18 (9) (2025) 2294, https://doi.org/10.3390/en18092294.
[256] L. Ba, F. Tangour, I. El Abbassi, R. Absi, Analysis of digital twin applications in energy efficiency: a systematic review, Sustainability 17 (8) (2025), https://doi.org/10.3390/su17083560, p. 3560.
[257] M.S. Uddin, S. Kumar, Energy, emissions and environmental impact analysis of wind turbine using life cycle assessment technique, J. Clean. Prod. 69 (2014) 153–164.
[258] A. Darwish, A. Abdelsalam, Massoud, and S. Ahmed,—Single phase grid connected curent source inverter: Mitigation of oscillating power effect on the grid current, in: presented at the Proc. IET Conf. Renewable Power Generation, 2011, pp. 1–7.
[259] Y. Li, X. Ruan, D. Yang, F. Liu, C.K. Tse, Synthesis of multiple-input DC/DC converters, IEEE Trans. Power Electron. 25 (9) (2010) 2372–2385.
[260] L. Solero, A. Lidozzi, J.A. Pomilio, Design of multiple-input power converter for hybrid vehicles, IEEE Trans. Power Electron. 20 (5) (2005) 1007–1016.
[261] B. Karanayil, M. Ciobotaru, V.G. Agelidis, Power flow management of isolated multiport converter for more electric aircraft, IEEE Trans. Power Electron. 32 (7) (2016) 5850–5861.
[262] X. Wu, S. Gao, Y. Liu, R. Li, X. Jiang, X. Cai, Battery cluster fault-tolerant control for high voltage transformerless grid-tied battery energy storage system, CPSS Trans. Power Electron. Appl. 10 (2025) 141–152.
[263] J. Kienast, S. Bernet, G. Sturm, Operation, design, and losses of the modular multilevel matrix converter in a flywheel energy storage system, IEEE Open Journal of Industry Applications 4 (2023) 336–345.
[264] F. Blaabjerg, Z. Chen, S.B. Kjaer, Power electronics as efficient interface in dispersed power generation systems, IEEE Trans. Power Electron. 19 (5) (2004) 1184–1194.
[265] K. Hasan, M.M. Othman, S.T. Meraj, Md.S. Rahman, M.S. Hossain Lipu, M. R. Sarker, Emerging power quality improvement technology: recent advances on topologies, control schemes, issues and prospects towards grid decarbonization, Results Eng. 29 (Mar. 2026) 109256, https://doi.org/10.1016/j.rineng.2026.109256.
[266] J. Iwaszkiewicz, P. Mysiak, A. Muc, Current controlled AC/DC converter and its performance—a mathematical model, Energies 18 (2) (2025), https://doi.org/10.3390/en18020419, p. 419.
[267] M. Abolghasemi, I. Soltani, M. Shivaie, H. Vahedi, Recent advances of step-up multi-stage DC-DC converters: a review on classifications, structures and grid applications, Energy Rep. 13 (2025) 3050–3081, https://doi.org/10.1016/j.egyr.2025.02.025.
[268] R.A. Acosta-Rodríguez, J. Rosero-García, M. Rivera, K. Chaimanekorn, Recent advances in non-isolated DC/DC converter topologies: a review and future

perspectives, Appl. Sci. 15 (24) (2025), https://doi.org/10.3390/app152412868, p. 12868.
[269] B. Ejaz, R. Zamora, C. Reusser, X. Lin, A comprehensive review of partial power converter topologies and control methods for fast electric vehicle charging applications, Electronics 14 (10) (2025) 1928, https://doi.org/10.3390/electronics14101928.
[270] H.A. Mosallam, E.A. Badran, A systematic review of DC–DC converter technologies: traditional, bidirectional, and impedance-source topologies, Discover Electronics 3 (1) (2026) 16, https://doi.org/10.1007/s44291-026-00168-0.
[271] S. Kouro, P. Cortés, R. Vargas, U. Ammann, J. Rodríguez, 2009, Model predictive control—a simple and powerful method to control power converters, IEEE Trans. Ind. Electron. 56 (6) (2008) 1826–1838.
[272] A. Dekka, B. Wu, V. Yaramasu, R.L. Fuentes, N.R. Zargari, Model predictive control of high-power modular multilevel converters—an overview, IEEE J. Emerg. Sel. Top. Power Electron. 7 (1) (2018) 168–183.
[273] T. Geyer, Model Predictive Control of High Power Converters and Industrial Drives, John Wiley & Sons, 2016.
[274] Q. Ullah, E. Costa Resende, L. Carlos Gomes Freitas, H. Laaksonen, M. Godoy Simões, Enhancing voltage stability of grid forming power converters based on model predictive controller, Int. J. Electr. Power Energy Syst. 163 (2024) 110317, https://doi.org/10.1016/j.ijepes.2024.110317.
[275] T. Rigaut, A. Nassiopoulos, F. Bourquin, P. Giroux, A. Pény, Model predictive control for energy and climate management of a subway station thermo-electrical microgrid, Transportation Research Procedia 14 (2016) 926–935.
[276] G. Serale, M. Fiorentini, A. Capozzoli, D. Bernardini, A. Bemporad, Model predictive control (MPC) for enhancing building and HVAC system energy efficiency: problem formulation, applications and opportunities, Energies 11 (3) (2018) 631.
[277] S.R. Mohapatra, V. Agarwal, Model predictive control for flexible reduction of active power oscillation in grid-tied multilevel inverters under unbalanced and distorted microgrid conditions, IEEE Trans. Ind. Appl. 56 (2) (2019) 1107–1115.
[278] M. Wu, H. Tian, Y.W. Li, G. Konstantinou, K. Yang, A composite selective harmonic elimination model predictive control for seven-level hybrid-clamped inverters with optimal switching patterns, IEEE Trans. Power Electron. 36 (1) (2020) 274–284.
[279] T. Cao, Z. Ye, Q. Wu, X. Wan, J. Wang, D. Li, A review of adaptive control methods for grid-connected PV inverters in complex distribution systems, Energies 18 (3) (2025) 473, https://doi.org/10.3390/en18030473.
[280] A. Villalón, M. Rivera, Y. Salgueiro, J. Muñoz, T. Dragičević, F. Blaabjerg, Predictive control for microgrid applications: a review study, Energies 13 (10) (2020) 2454, https://doi.org/10.3390/en13102454.
[281] Z. Guo, et al., An enhanced model predictive control method for single-stage three-phase transformerless grid-connected photovoltaic inverter, International Journal of Electrical Power & Energy Systems 172 (2025) 111239, https://doi.org/10.1016/j.ijepes.2025.111239.
[282] M.M. Fayyaz, I.M. Syed, Y. Meng, M.N. Aman, Comprehensive predictive control model for a three-phase four-legged inverter, Energies 16 (6) (2023) 2650, https://doi.org/10.3390/en16062650.
[283] I. Grgić, D. Vukadinović, M. Bašić, M. Bubalo, Efficiency boost of a quasi-Z-source inverter: a novel shoot-through injection method with dead-time, Energies 14 (14) (2021) 4216, https://doi.org/10.3390/en14144216.
[284] C.-H. Lin, S.A. Farooqui, H.-D. Liu, J.-J. Huang, M. Fahad, Finite control set model predictive control (FCS-MPC) for enhancing the performance of a single-phase inverter in a renewable energy system (RES), Mathematics 11 (21) (2023) 4553, https://doi.org/10.3390/math11214553.
[285] A. Kardamaki, T. Protoulis, A. Alexandridis, H. Sarimveis, An explicit model predictive control framework based on physics-informed neural networks, J. Process Control 158 (2026) 103634, https://doi.org/10.1016/j.jprocont.2026.103634.
[286] Y. Fang, J. Gu, F. Liu, Y. Liu, S. Shi, Voltage balancing control strategy for hybrid MMC based on BADS-optimized second harmonic injection, Energies 18 (22) (2025) 5904, https://doi.org/10.3390/en18225904.
[287] S. Dalapati, C. Chakraborty, Dynamic performance of a dead-band controlled capacitor charging type inverter, Simul Model Pract Theory 17 (5) (2009) 911–934, https://doi.org/10.1016/j.simpat.2009.02.010.
[288] Mengchao Ma, Peng Li, Botao Li, Study on deadbeat control strategy for grid-connected distributed generation system, in: *2008 Third International Conference on Electric Utility Deregulation and Restructuring and Power Technologies*, Apr. 2008, pp. 2553–2557, https://doi.org/10.1109/DRPT.2008.4523841.
[289] H. Ma, X. Yao, J. Wang, X. Luo, S. Huang, Improved deadbeat predictive direct power control for three-phase PWM rectifier based on LADRC, Journal of Marine Science and Engineering 13 (3) (2025) 402, https://doi.org/10.3390/jmse13030402.
[290] A.E.M. Bouzid, H. Chaoui, M. Zerrougui, S. Ben Elghali, M. Benbouzid, Robust control based on linear matrix inequalities criterion of single phase distributed electrical energy systems operating in islanded and grid-connected modes, Appl. Energy 292 (2021) 116776, https://doi.org/10.1016/j.apenergy.2021.116776.
[291] Y. Daili, J.-P. Gaubert, L. Rahmani, M. Bouzid, An improved voltage control scheme based on deadbeat-repetitive techniques of a single distributed generation unit in island mode, in: *IECON 2013 - 39th Annual Conference of the IEEE Industrial Electronics Society*, Nov. 2013, pp. 424–429, https://doi.org/10.1109/IECON.2013.6699173.
[292] M. Majstorović, V. Nougain, L. Ristić, A. Lekić, Deadbeat-based control for MMC-HVDC power systems, International Journal of Electrical Power & Energy Systems 167 (2025) 110583, https://doi.org/10.1016/j.ijepes.2025.110583.
[293] S.B. Joseph, E.G. Dada, A. Abidemi, D.O. Oyewola, B.M. Khammas, Metaheuristic algorithms for PID controller parameters tuning: review, approaches and open problems, Heliyon 8 (5) (2022) e09399, https://doi.org/10.1016/j.heliyon.2022.e09399.
[294] K. Alluhydan, A.T. EL-Sayed, F.T. El-Bahrawy, The effect of proportional, proportional-integral, and proportional-integral-derivative controllers on improving the performance of torsional vibrations on a dynamical system, Computation 12 (8) (2024) 157, https://doi.org/10.3390/computation12080157.
[295] D. Selisteanu, M. Roman, L. Mandache, R. Prejbeanu, S. Ivanov, A. Radu, Three-level inverter control techniques: design, analysis, and comparisons, Elektronika Ir Elektrotechnika 27 (3) (2021) 26–37.
[296] M. Nowak, T. Binkowski, S. Piróg, Proportional-resonant controller structure with finite gain for three-phase grid-tied converters, Energies 14 (20) (2021) 6726, https://doi.org/10.3390/en14206726.
[297] M. Parvez, M.F.M. Elias, N.A. Rahim, N. Osman, Current control techniques for three-phase grid interconnection of renewable power generation systems: a review, Sol. Energy 135 (2016) 29–42, https://doi.org/10.1016/j.solener.2016.05.029.
[298] M. Dai, M.N. Marwali, J.-W. Jung, A. Keyhani, A three-phase four-wire inverter control technique for a single distributed generation unit in island mode, IEEE Trans. Power Electron. 23 (1) (2008) 322–331, https://doi.org/10.1109/TPEL.2007.911816.
[299] F. Blaabjerg, R. Teodorescu, M. Liserre, A.V. Timbus, Overview of control and grid synchronization for distributed power generation systems, IEEE Trans Ind Electron 53 (5) (2006) 1398–1409, https://doi.org/10.1109/TIE.2006.881997.
[300] A.M. Bouzid, J.M. Guerrero, A. Cheriti, M. Bouhamida, P. Sicard, M. Benghanem, A survey on control of electric power distributed generation systems for microgrid applications, Renew. Sustain. Energy Rev. 44 (2015) 751–766, https://doi.org/10.1016/j.rser.2015.01.016.
[301] I. Nouira, B. El Badsi, Direct power control of grid-connected DC/AC converters, in: I. Nouira, B. El Badsi (Eds.), Control Strategies of Electric Drives: MATLAB/Simulink Modeling and dSPACE 1104 Validation: A Practical Approach, Springer Nature Switzerland, Cham, 2025, pp. 55–72, https://doi.org/10.1007/978-3-031-81332-0_3.
[302] N. Muangruk, S. Nungam, Direct power control of three-phase voltage source converters using feedback linearization technique, Procedia Computer Science 86 (2016) 365–368, https://doi.org/10.1016/j.procs.2016.05.100.
[303] M. Bouzidi, A. Benaissa, S. Barkat, Hybrid direct power/current control using feedback linearization of three-level four-leg voltage source shunt active power filter, Int. J. Electr. Power Energy Syst. 61 (2014) 629–646.
[304] C. Jaen, J. Pou, R. Pindado, V. Sala, J. Zaragoza, "A linear-quadratic regulator with integral action applied to pwm dc-dc converters," Presented at the IECON 2006-32nd Annual Conference on IEEE Industrial Electronics, IEEE, 2006, pp. 2280–2285.
[305] B.K. Bose, Power Electronics and Motor Drives: Advances and Trends, 2010.
[306] A. Shukla, A. Ghosh, A. Joshi, Hysteresis modulation of multilevel inverters, IEEE Trans. Power Electron. 26 (5) (2010) 1396–1409.
[307] J. Rodriguez, P. Cortes, Predictive Control of Power Converters and Electrical Drives, John Wiley & Sons, 2012.
[308] B. Wu, M. Narimani, High-Power Converters and AC Drives, John Wiley & Sons, 2017.
[309] J. Hu, Z. Zhu, Investigation on switching patterns of direct power control strategies for grid-connected DC–AC converters based on power variation rates, IEEE Trans. Power Electron. 26 (12) (2011) 3582–3598.
[310] A. Bouafia, J.-P. Gaubert, F. Krim, Predictive direct power control of three-phase pulsewidth modulation (PWM) rectifier using space-vector modulation (SVM), IEEE Trans. Power Electron. 25 (1) (2009) 228–236.
[311] M.P. Kazmierkowski, M. Jasinski, G. Wrona, DSP-based control of grid-connected power converters operating under grid distortions, IEEE Trans. Industr. Inform. 7 (2) (2011) 204–211.
[312] A.M. Bouzid, J.M. Guerrero, A. Cheriti, M. Bouhamida, P. Sicard, M. Benghanem, A survey on control of electric power distributed generation systems for microgrid applications, Renew. Sustain. Energy Rev. 44 (2015) 751–766, https://doi.org/10.1016/j.rser.2015.01.016.
[313] M. Parvez, M.F.M. Elias, N.A. Rahim, N. Osman, Current control techniques for three-phase grid interconnection of renewable power generation systems: a review, Solar Energy 135 (2016) 29–42, https://doi.org/10.1016/j.solener.2016.05.029.
[314] Q.-C. Zhong, T. Hornik, Control of Power Inverters in Renewable Energy and Smart Grid Integration, John Wiley & Sons, 2012.
[315] D.D. Rasolomampionona, M. Połecki, K. Zagrajek, W. Wróblewski, M. Januszewski, A comprehensive review of load frequency control technologies, Energies 17 (12) (2024) 2915, https://doi.org/10.3390/en17122915.
[316] T. Geyer, Model predictive direct current control: formulation of the stator current bounds and the concept of the switching horizon, IEEE Ind. Appl. Mag. 18 (2) (2011) 47–59.
[317] T. Geyer, G. Papafotiou, M. Morari, Model predictive direct torque control—part I: concept, algorithm, and analysis, IEEE Trans. Ind. Electron. 56 (6) (2008) 1894–1905.
[318] G. Papafotiou, J. Kley, K.G. Papadopoulos, P. Bohren, M. Morari, Model predictive direct torque control—part II: implementation and experimental evaluation, IEEE Trans. Ind. Electron. 56 (6) (2008) 1906–1915.
[319] T. Geyer, Generalized model predictive direct torque control: Long prediction horizons and minimization of switching losses, in: presented at the Proceedings of

the 48h IEEE Conference on Decision and Control (CDC) held jointly with 2009 28th Chinese Control ConferenceIEEE, 2009, pp. 6799–6804.
[320] I. Lee, Y. Lee, D. Shin, C.C.C. hung, A sliding mode based model predictive control structure for permanent magnet synchronous motor, in: 2015 15th International Conference on Control, Automation and Systems (ICCAS), Oct. 2015, pp. 550–555, https://doi.org/10.1109/ICCAS.2015.7364979.
[321] In-Cheol Baik, Kyeong-Hwa Kim, Myung-Joong Youn, Robust nonlinear speed control of PM synchronous motor using boundary layer integral sliding mode control technique, IEEE Trans. Control Syst. Technol. 8 (1) (2000) 47–54, https://doi.org/10.1109/87.817691.
[322] Yoon-Seok Han, Jung-Soo Choi, Young-Seok Kim, Sensorless PMSM drive with a sliding mode control based adaptive speed and stator resistance estimator, IEEE Trans. Magn. 36 (5) (2000) 3588–3591, https://doi.org/10.1109/20.908910.
[323] X. Zhang, L. Sun, K. Zhao, L. Sun, Nonlinear speed control for PMSM system using sliding-mode control and disturbance compensation techniques, IEEE Trans. Power Electron. 28 (3) (2013) 1358–1365, https://doi.org/10.1109/TPEL.2012.2206610.
[324] C.-K. Lai, Kuo-Kai Shyu, A novel motor drive design for incremental motion system via sliding-mode control method, IEEE Trans. Ind. Electron. 52 (2) (Apr. 2005) 499–507, https://doi.org/10.1109/TIE.2005.844230.
[325] S. Li, M. Zhou, X. Yu, Design and implementation of terminal sliding mode control method for PMSM speed regulation system, IEEE Trans. Industr. Inform. 9 (4) (2013) 1879–1891, https://doi.org/10.1109/TII.2012.2226896.
[326] Q. Liu, A. Thul, K. Hameyer, A robust model reference adaptive controller for the PMSM drive system with torque estimation and compensation, in: *2014 International Conference on Electrical Machines (ICEM)*, Sep. 2014, pp. 665–671, https://doi.org/10.1109/ICELMACH.2014.6960252.
[327] S. Li, Z. Liu, Adaptive speed control for permanent-magnet synchronous motor system with variations of load inertia, IEEE Trans. Ind. Electron. 56 (8) (2009) 3050–3059, https://doi.org/10.1109/TIE.2009.2024655.
[328] S.N.M. Isa, Z. Ibrahim, F. Patkar, Comparative study of fuzzy logic speed controller in vector controlled PMSM drive: Minimum number of fuzzy rule-base, in: 2009 Innovative Technologies in Intelligent Systems and Industrial Applications, Jul. 2009, pp. 112–118, https://doi.org/10.1109/CITISIA.2009.5224229.
[329] S.A. Hamad, F.F.M. El-Sousy, M.M. Ismail, M.F. Elmorshedy, D. Almakhles, Mohamed.A. Ghalib, Improved terminal sliding mode control based on MPC for LIM applied to linear metro, Sci. Rep. 15 (1) (2025) 37346, https://doi.org/10.1038/s41598-025-22191-z.
[330] K.K. Ayten, A. Dumlu, Implementation of a pid type sliding-mode controller design based on fractional order calculus for industrial process system, Elektronika ir Elektrotechnika 27 (6) (2021) 4–10.
[331] S. Kanthalakshmi, W.P. Annal, Predictive sliding mode controller for continuous bio-fermenter systems, J. Control Eng. Appl. Inform. 22 (2) (2020) 33–42.
[332] P. Song, Q. Yang, D. Li, G. Wen, Z. Zhang, J. Peng, Disturbance-compensation-based predictive sliding mode control for aero-engine networked systems with multiple uncertainties, IEEE Trans. Autom. Sci. Eng. 22 (2024) 276–292.
[333] X. Bu, Prescribed performance control approaches, applications and challenges: a comprehensive survey, Asian J. Control 25 (1) (2023) 241–261.
[334] H. Karami, F. Bayat, S. Mobayen, A. Fekih, Robust model-predictive sliding mode control for disturbed linear systems with actuator constraint and measurement noise, IEEE Access 13 (2025) 169490–169503, https://doi.org/10.1109/ACCESS.2025.3614465.
[335] K.M. Abo-Al-Ez, A. Elaiw, X. Xia, A dual-loop model predictive voltage control/sliding-mode current control for voltage source inverter operation in smart microgrids, Electric Power Components and Systems 42 (3–4) (2014) 348–360.
[336] F. Bayat, Model predictive sliding control for finite-time three-axis spacecraft attitude tracking, IEEE Trans. Ind. Electron. 66 (10) (2018) 7986–7996.
[337] V. Vartika, S. Singh, S. Das, S.K. Mishra, S.S.S. ahu, A review on intelligent pid controllers in autonomous vehicle, in: M.J.B. Reddy, D.Kr. Mohanta, D. Kumar, D. Ghosh (Eds.), Advances in Smart Grid Automation and Industry 4.0, Springer Singapore, Singapore, 2021, pp. 391–399.
[338] G. San, W. Zhang, X. Guo, C. Hua, H. Xin, F. Blaabjerg, Large-disturbance stability for power-converter-dominated microgrid: a review, Renew. Sustain. Energy Rev. 127 (2020) 109859, https://doi.org/10.1016/j.rser.2020.109859.
[339] S. Zhao, F. Blaabjerg, H. Wang, An overview of artificial intelligence applications for power electronics, IEEE Trans. Power Electron. 36 (4) (2021) 4633–4658, https://doi.org/10.1109/TPEL.2020.3024914.
[340] C. Dumitrescu, P. Ciotirnae, C. Vizitiu, Fuzzy logic for intelligent control system using soft computing applications, Sensors 21 (8) (2021) 2617, https://doi.org/10.3390/s21082617.
[341] M. Versaci, S. Calcagno, M. Cacciola, F.C. Morabito, I. Palamara, D. Pellicanò, Innovative fuzzy techniques for characterizing defects in ultrasonic nondestructive evaluation, in: P. Burrascano, S. Callegari, A. Montisci, M. Ricci, M. Versaci (Eds.), Ultrasonic Nondestructive Evaluation Systems: Industrial Application Issues, Springer International Publishing, Cham, 2015, pp. 201–232, https://doi.org/10.1007/978-3-319-10566-6_7.
[342] M.S. Raboaca, C. Dumitrescu, I. Manta, Aircraft trajectory tracking using radar equipment with fuzzy logic algorithm, Mathematics 8 (2) (2020) 207, https://doi.org/10.3390/math8020207.
[343] D.E. Babatunde, A. Anozie, J. Omoleye, Artificial neural network and its applications in the energy sector – an overview, IJEEP 10 (2) (2020) 250–264.
[344] K. Przystalski, M.J. Ogorzałek, J.K. Argasiński, W. Chmielnicki, Neural networks, in: K. Przystalski, M.J. Ogorzałek, J.K. Argasiński, W. Chmielnicki (Eds.), Pattern Recognition Primer, Springer Nature Switzerland, Cham, 2026, pp. 205–254, https://doi.org/10.1007/978-3-031-91816-2_8.
[345] S. Rehimi, H. Bevrani, C.T. Urabe, T. Kato, T. Kato, Smart tuning of control system parameters for a grid connected converter: a robust artificial neural network approach, Electronics 14 (4) (2025) 699, https://doi.org/10.3390/electronics14040699.
[346] M.T. Hossain, et al., Next generation power inverter for grid resilience: technology review, Heliyon 10 (21) (2024) e39596, https://doi.org/10.1016/j.heliyon.2024.e39596.
[347] Md.K. Hossain, P. Chowdhury, I. Nowshin, Md.R. Islam, A. Al-Hysam, O. Farrok, Grid-connected inverter for photovoltaic energy harvesting: advances in topologies and control techniques, Energy Conversion and Management: X 29 (2026) 101422, https://doi.org/10.1016/j.ecmx.2025.101422.
[348] Y.-J. Liu, W. Zhao, L. Liu, D. Li, S. Tong, C.L.P. Chen, Adaptive neural network control for a class of nonlinear systems with function constraints on states, IEEE Trans. Neural Netw. Learn. Syst. 34 (6) (2023) 2732–2741, https://doi.org/10.1109/TNNLS.2021.3107600.
[349] F. Renhai, et al., A deep recurrent neural network-based droop control strategy for frequency stabilization in low-inertia power systems with high renewable energy penetration, Results Eng. 28 (2025) 107443, https://doi.org/10.1016/j.rineng.2025.107443.
[350] M.S. Rahman, Mohd.H. Ali, Adaptive neuro fuzzy inference system (ANFIS)-based control for solving the misalignment problem in vehicle-to-vehicle dynamic wireless charging systems, Electronics 14 (3) (2025) 507, https://doi.org/10.3390/electronics14030507.
[351] Y.L. Loukas, Adaptive neuro-fuzzy inference system: an instant and architecture-free predictor for improved QSAR studies, J. Med. Chem. 44 (17) (2001) 2772–2783, https://doi.org/10.1021/jm000226c.
[352] S. Arslankaya, Comparison of performances of fuzzy logic and adaptive neuro-fuzzy inference system (ANFIS) for estimating employee labor loss, J. Eng. Res. 11 (4) (2023) 469–477, https://doi.org/10.1016/j.jer.2023.100107.
[353] Y.M. Alginahi, O. Sabri, W. Said, Reinforcement learning for industrial automation: a comprehensive review of adaptive control and decision-making in smart factories, Machines 13 (12) (2025) 1140, https://doi.org/10.3390/machines13121140.
[354] X. Lai, Z. Yang, J. Xie, Y. Liu, Reinforcement learning in transportation research: Frontiers and future directions, Multimodal Transportation 3 (4) (2024) 100164, https://doi.org/10.1016/j.multra.2024.100164.
[355] M. Nicola, C.-I. Nicola, and D. Selișteanu, "Improvement of the control of a grid connected photovoltaic system based on synergetic and sliding mode controllers using a reinforcement learning deep deterministic policy gradient agent," Energies, vol. 15, no. 7, p. 2392, 2022, doi:https://doi.org/10.3390/en15072392.
[356] J. Lin, R.-J. Lian, Hybrid fuzzy-logic and neural-network controller for MIMO systems, Mechatronics 19 (6) (2009) 972–986, https://doi.org/10.1016/j.mechatronics.2009.07.002.
[357] W. Li, Q. Tan, "A method for design of a hybrid neuro-fuzzy control system based on behaviour classification," presented at the Proceedings of ICNN'95-International Conference on Neural Networks, IEEE, 1995, pp. 2275–2280.
[358] R. Trach, I. Chupryna, M. Mykhalova, O. Khomenko, Y. Trach, R. Stepaniuk, A hybrid fuzzy logic and artificial neural network approach for engineering structure condition assessment based on long-term inspection data, Appl. Sci. 16 (2) (2026) 794, https://doi.org/10.3390/app16020794.
[359] Rongguang Chen, Chunsheng Li, Xia Meng, Yongguang Yu, The application of fuzzy-neural network on control strategy of hybrid vehicles, in: *2008 27th Chinese Control Conference*, Jul. 2008, pp. 281–284, https://doi.org/10.1109/CHICC.2008.4604992.
[360] S. Kalyankar-Narwade, R.K. Chidambaram, S. Patil, Neural network- and fuzzy control-based energy optimization for the switching in parallel hybrid two-wheeler, World Electr. Veh. J. 12 (1) (2021) 35, https://doi.org/10.3390/wevj12010035.
[361] M. Nour, O. Bouketir, C.E. Yong, Self-tuning of PI speed controller gains using fuzzy logic controller, Mod. Appl. Sci. 2 (6) (2008) 55–65.
[362] M. Azman, J. Aris, Z. Hussain, A. Samat, A.M. Nazelan, "A comparative study of fuzzy logic controller and artificial neural network in speed control of separately excited DC motor," Presented at the 2017 7th IEEE International Conference on Control System, Computing and Engineering (ICCSCE), IEEE, 2017, pp. 336–341.
[363] E. Joseph, O. Olaiya, Cohen-coon PID tuning method; a better option to Ziegler Nichols-PID tuning method, ENginerring Research 2 (11) (2017) 141–145.
[364] P.K. Khanke, S.D. Jain, "Comparative analysis of speed control of BLDC motor using PI, simple FLC and fuzzy-PI controller," Presented at the 2015 International Conference on Energy Systems and Applications, IEEE, 2015, pp. 296–301.
[365] I.D. Díaz-Rodríguez, S. Han, L. Keel, S. Bhattacharyya, Advanced tuning for Ziegler-Nichols plants, IFAC-PapersOnLine 50 (1) (2017) 1805–1810.
[366] A.I. Glushchenko, "Neural tuner development method to adjust PI-controller parameters on-line," presented at the 2017 IEEE conference of Russian young researchers in electrical and electronic engineering (EIConRus), IEEE, 2017, pp. 849–854.
[367] M. Abu-Zaher, et al., Power quality enhancement in grid-tied photovoltaic systems through artificial neural network-based current control strategies, Int. J. Electr. Power Energy Syst. 172 (2025) 111362, https://doi.org/10.1016/j.ijepes.2025.111362.
[368] C.-T. Chao, N. Sutarna, J.-S. Chiou, C.-J. Wang, Equivalence between fuzzy PID controllers and conventional PID controllers, Appl. Sci. 7 (6) (2017) 513, https://doi.org/10.3390/app7060513.
[369] D. Somwanshi, M. Bundele, G. Kumar, G. Parashar, Comparison of fuzzy-PID and PID controller for speed control of DC motor using LabVIEW, Procedia Computer Science 152 (2019) 252–260, https://doi.org/10.1016/j.procs.2019.05.019.

[370] S. Cai, Q. Dong, P. Asef, M. Salimi, AI-assisted adaptive sliding mode control for pseudo-resonance suppression in dynamic capacitive wireless charging systems, Energies 18 (22) (2025) 6052, https://doi.org/10.3390/en18226052.
[371] C.E. Castañeda, AI-based optimization of a neural discrete-time sliding mode controller via Bayesian, particle swarm, and genetic algorithms, Robotics 14 (9) (2025) 128, https://doi.org/10.3390/robotics14090128.
[372] Y. Shtessel, F. Plestan, C. Edwards, Adaptive sliding mode and second order sliding mode control with applications: a survey, IFAC-PapersOnLine 56 (2) (2023) 761–772, https://doi.org/10.1016/j.ifacol.2023.10.1658.
[373] D. Zhuang, V.J. Gan, Z.D. Tekler, A. Chong, S. Tian, X. Shi, Data-driven predictive control for smart HVAC system in IoT-integrated buildings with time-series forecasting and reinforcement learning, Appl. Energy 338 (2023) 120936.
[374] K. Bamdad, N. Mohammadzadeh, M. Cholette, S. Perera, Model predictive control for energy optimization of HVAC systems using energyplus and ACO algorithm, Buildings 13 (12) (2023) 3084.
[375] H. Zhang, S. Seal, D. Wu, F. Bouffard, B. Boulet, Building energy management with reinforcement learning and model predictive control: a survey, IEEE Access 10 (2022) 27853–27862.
[376] E.R. Fernández Mareco, D. Pinto-Roa, Application of artificial intelligence in control systems: trends, challenges, and opportunities, AI 6 (12) (2025), https://doi.org/10.3390/ai6120326, p. 326.
[377] D.B. Raven, et al., Machine learning & conventional approaches to process control & optimization: industrial applications & perspectives, Comput. Chem. Eng. 189 (2024) 108789, https://doi.org/10.1016/j.compchemeng.2024.108789.
[378] M. Trigka, E. Dritsas, Control theory in the era of intelligent systems: applications, trends, and future directions, Annu. Rev. Control. 61 (2026) 101049, https://doi.org/10.1016/j.arcontrol.2026.101049.
[379] S.D. Lalitha, C. Danamaraju, M.P. Raj, D. Kumar, R. Sethuraman, M. V, AI-driven control strategies for power electronics converters, in: 2024 Ninth International Conference on Science Technology Engineering and Mathematics (ICONSTEM), Apr. 2024, pp. 1–6, https://doi.org/10.1109/ICONSTEM60960.2024.10568766.